EXPERIMENTAL CHARACTERIZATION OF THE PRESSURE BUILDUP IN THE INTRAMEDULLARY CANAL DURING ORTHOPAEDIC REAMING USING A SYNTHETIC BONE ANALOGUE

By

Azar Hojabr, BASc.

University of Toronto, 2004

A thesis

Presented to Ryerson University

In partial fulfillment of the requirements for the degree of

Master of Applied Science

In the program of

Mechanical Engineering

Toronto, Ontario, Canada, 2006

AUTHOR'S DECLARATION

I hereby declare that I am the sole author of this thesis

I authorize Ryerson University to lend this thesis to other institutions or individuals for the purpose of scholarly research.

I further authorize Ryerson University to reproduce this thesis by photocopying or by other means, in total or in part, at the request of other institutions or individuals for the purpose of scholarly research.

BORROWER'S PAGE

Ryerson University requires the signatures of all persons using or photocopying this thesis. Please sign below and give the address and date.

ABSTRACT

Experimental Characterization of the Pressure Buildup in the Intramedullary Canal during Orthopaedic Reaming using a Synthetic Bone Analogue

Master of Applied Science, Mechanical Engineering, 2006, Azar Hojabr

School of Graduate Studies, Ryerson University

During certain orthopaedic procedures such as total hip or total knee arthroplasty, it is necessary to ream the intramedullary canal of long bones prior to the insertion of the implant. This reaming procedure can generate significant intramedullary pressure elevations, potentially leading to the release of embolic fat into the blood stream, and thus increasing the risk of a potentially fatal complication, i.e., fat embolism syndrome. In this thesis, a two layer synthetic bone analogue with open cell porosity and mechanical properties similar to that of real bone was developed and used to evaluate the effect of reaming parameters such as RPM, advancement speed, reamer size, bone marrow viscosity and clogged reamer on resulting intramedullary pressure elevations. All the aforementioned parameters, except the reamer size, were found to significantly influence the medullary pressure. It was found that increases in the reamer advancement speed increased the pressure, whereas increases in the reamer RPM decreased the pressure. The correlation between the simulated intramedullary pressure, imposed forces to the bone and applied torque to the reamer was also assessed. No significant correlations between these variables could be established.

AKNOWLEDGEMENTS

I would like to express my gratitude to all those who gave me the possibility to complete this thesis. In particular, I would like to acknowledge the enthusiastic supervision of Dr. Marcello Papini during the past two years whose tremendous guidance, aid in editing and endless support enabled me to complete this work. I thank him for his time, encouragement and utmost provision to strive for perfection.

I would also like to thank my co-supervisors Dr. Kamran Behdinan and Dr. Ziad Saghir for their valuable advice and guidance. Special thanks to medical supervisors Dr. Paul Zalzal and Dr. Justin DeBeer for their stimulating suggestions and support during this work. Special gratitude is also due to my colleagues Daniel Dobrjanski, Omar Gaber, Jon Bahen, Sherry Towfighian and Paul Saadetian.

I owe my most sincere gratitude to Joseph Amankrah for his indispensable technical support in the design and fabrication of the experimental set up. I will always be grateful to his constructive work and ideas. I would also like to acknowledge the technical support and friendly help of Andrew Heim and Devin Ostrom.

I wish to express my warm and sincere thanks to Touchstone Research Laboratory for the generous contribution with the raw material. Thank you Patrick Steingroewer and Rick Lucas. Without your kind support this project would not be possible.

I am forever indebted to my parents Kafieh and Ebrahim Hojabr for their sympathetic, unconditional patience and encouragement when it was most required. My heartfelt acknowledgement is to my friends Goli, Kaz, Tom, Sara, Sai, Hamid, Randy, Simon, Helen, Alex, Brian, Sonia, Yashar and Hummed for the emotional support. Especially, I would like to give my special thanks to my boyfriend Matthew Saiedfar for his love, support and encouragement, and for believing in me even when I did not.

Azar Hojabr

This Research was supported with funding from the Natural Sciences and Engineering Research Council of Canada (NSERC).

TABLE OF CONTENTS

LIST OF FIGURES

LIST OF TABLES

NOMENCLATURE

The definition of symbols will be done in alphabetical order:

F : Ronald Fisher number; Ratio of effect variance to error variance

F_x : Force in x-direction [N]

F_y : Force in y-direction [N]

F_z : Force in z-direction, axial force [N]

H_o : Null Hypothesis

k : Number of factor in a factorial design

L : Number of levels associated with each factor in a factorial design

N : Number of pairs in measurement sample in correlation analysis

n : Total number of experimental observations

P : Pressure [mmHg]

p : Level of significance

R : Correlation coefficient

R^2 : Correlation of determination

SS : Sum of squares

S^2 : Variance

t : (or t-test) Test of significance established based on analysis of t distribution

X : Experimental observation, variable

$\overline{X}$: Mean of experimental observations

Y : Experimental observation, variable

Greek symbol

α_t : Quantitative effect of each treatment

1 Introduction

1.1 Motivation

Fat Embolism, FE, refers to the presence of fat globules within the blood circulation that can produce embolic phenomena. Fat Embolism Syndrome, FES, refers to clinical symptoms associated with FE that can cause potentially life threatening complications after long bone trauma, blunt trauma, and intramedullary canal manipulations[1,2]. The intramedullary canal is the internal hollow cavity in the long bone containing bone marrow, blood vessels, nerve fibers, and soft tissues[3]. Complications such as fat embolism syndrome are reported in many orthopaedic procedures involving breaching of the intramedullary canal, such as, for example, Total Knee or Hip Arthroplasty procedures, TKA or THA. Given the increasing age of the population, the number of such procedures is also increasing, so that even the 1% reported occurrence of FES in patients having undergone THA represents a large number of cases.[1] It is thus of interest to study ways of decreasing its occurrence.

In orthopaedic procedures, the intramedullary canal often needs to be reamed to a larger size in order to accommodate the insertion of the implant. A number of studies have shown evidence of elevated intramedullary pressure due to the penetration of orthopaedic reamers. This elevated pressure is generally accepted to increase the probability of the release of bone marrow contents into the blood circulation, and thus the probability of FES occurring.[1,2,4,5,6,7]To reduce the intramedullary pressure, a modification of standard orthopaedic techniques by adjusting the reaming parameters is

required. The focus of the present work is thus to assess the reaming parameters and propose modifications to reduce the intramedullary pressure.

Previous studies on this subject are mainly based on observations from orthopaedic surgeries on human and animal (*in-vivo*) or cadaveric long bones (*in-vitro*). Such studies, however, suffer from significant specimen to specimen variability since the bone composition and properties vary depending on age, gender and health. Some studies instead have used synthetic bone analogues, made of, for example, Polyurethane foam[8], Silicon shells[9], Plexiglas cylinders[10], Teflon cylinders and porous ceramics[11] (see Section 2.6.3). These existing bone analogues, however, generally utilize a one layer closed-cell structure, which only mimics the outer layer of the bone. As a result, they generally lead to unrealistically high measured pressures. In the present work, these difficulties were avoided by developing a new two layer open cell structure synthetic bone analogue with similar structural and mechanical properties to a human femur.

1.2 Thesis Objective

The objective of this work is to assess the effect of reaming parameters leading to elevated intramedullary pressure during orthopaedic procedures, as well as to provide recommendations on how to alter them, to prevent the risk of FES. To meet this primary objective, two secondary objectives were necessary: 1) To design and construct a synthetic bone analogue that mimics intramedullary pressure buildup in a human femur when being reamed, and to assess its performance by conducting reaming experiments and comparing the measured pressures to cadaveric data from the literature. 2) To perform parametric studies to evaluate the factors leading to elevated intramedullary pressure and recommend an optimized technique to reduce the risk of FES.

2 Literature Review

2.1 Fat Embolism Syndrome (FES)

Fat Embolism Sydrome (FES) is a collection of respiratory, neurological, and haematological symptoms associated with long bone trauma, blunt trauma, and intramedullary manipulation[1,2]. Fat embolism itself, i.e., fat globules within the blood circulation, is quite common and reported in 90% of patients with long bone fracture. However, the incidence of fat embolism syndrome is reported to be 0.5% to 2% in patients with single long bone fracture and 5% to 10% in those with multiple long bone fractures[4]. The syndrome occurs more in adults than children because adults have a higher fat content and a different fat composition in their bone marrow than children[5]. Investigation of the causes and origin of FES reveals the multi-factorial nature of this clinical syndrome. This makes it difficult to establish methods to prevent or treat FES.[1]

2.2 Early history of Fat Embolism Syndrome

Fat embolism has been recognized since 1862, when Zencker first reported the presence of fat droplets in the lungs of patients with severe abdominal crush injury at an autopsy. In 1873, Bergmann clinically diagnosed fat embolism for the first time in a patient with a fractured femur.[6] The study of the pathophysiology and pathogenesis of fat embolism continued throughout the early twentieth century when Peltier published his work on the pulmonary consequences and treatment of fat embolism in 1969.[1] In 1970, Gurd described and classified fat embolism syndrome by collecting similar clinical

manifestations. He found that FES is a pulmonary dysfunction that affects the lungs, brain, heart, eyes, and skin.[1]

2.3 *Pathophysiology of Fat Embolism Syndrome*

There are two different theories regarding the mechanisms causing FES: the mechanical theory and the biochemical theory.

2.3.1 *Mechanical Theory of FES*

Fat droplets from the intramedullary canal are ejected into the bloodstream after bone trauma and enter the venous system. The large fat droplets between 20-40 μm block the small pulmonary vascular branches, while the small fat cells are deposited in the capillary beds and travel through arteriovenous shunts and enter the circulation system into the brain.[6] The mechanical theory hypothesizes that the fat from the bone marrow is physically forced into the circulation blood system following the trauma. Normally, the bone marrow pressure is between 30-50 mmHg. Animal studies show that the threshold pressure for the passage of bone marrow into the capillary bed, and thus possibly result in fat embolism syndrome, is >50mmHg. Large amounts of marrow resulting in pulmonary impairment[7], i.e., configured emboli, begin to appear at pressure elevations of over 200mmHg. Some literature has reported intramedullary pressure increases of up to 1000 mmHg during reaming of an intact (unbroken) long bone.[7]

2.3.2 *Biochemical Theory of FES*

This theory states that FES occurs due to chemical reaction of tissues where blood lipids eventually grow into embolic fat in a series of non-traumatic conditions such as diabetes mellitus, burns, liposuction, decompression sickness and alcoholism. Embolic

fat in this theory refers to large fat globules with diameters of up to 40 μm that are capable of causing capillary closure.[12]

While the pathophysiology and etiology of FES are very important, the focus of the present work is on the mechanical operative parameters that increase intramedullary pressure, generally accepted to lead to FES.[1,13, 14]

2.4 Early History of Intramedullary Fixation

Intramedullary fixation was originally introduced in Mexico in the 16th century, and followed by four centuries of development of implants and techniques. Early implants used in intramedullary fixations were organic-based, made of material such as wood, ivory, or bone. In mid twentieth century, during World War II, intramedullary fixation was introduced to North Americans when American soldiers returned from Germany with metallic implants in their medullary canals. Further developments involved introduction of intramedullary reaming techniques in 1942, which led to investigation of problems associated with fat embolism during intramedullary reaming. Introduction of bio-resorbable materials for implants are a more recent breakthrough in the intramedullary fixation techniques in the 21th century.[14] However, these do not exclude the use of reamers, which will tend to raise the pressure inside the intramedullary canal.

2.5 Intramedullary Reaming

Intramedullary reaming is an orthopaedic procedure used in TKA, THA, and certain orthopaedic trauma surgeries (e.g., intramedullary nails to treat fracture) to prepare the canal for implant insertion. Previous studies from the literature show

evidence that this intramedullary reaming is a risk factor for FES incidence. Timing of the operation appears to be very important. Complications are generally increased in patients with multiple fractures when the surgery is delayed more than 24 hours or the surgery takes longer than usual.[2] The relationship between FES and intramedullary complications has previously been examined experimentally in the literature[1,2] under the generally accepted assumption that pressure buildup in the intramedullary canal leads to FES.

2.6 *Elevated Intramedullary Pressure during Orthopaedic Procedures*

Parameters such as reamer rotational speed (RPM), advancement speed, reamer design, and the force applied to the reamer can affect the intramedullary pressure, and as such are candidates for studies aimed at minimizing the occurrence of FES in orthopaedic procedures. Such studies can generally be classified into three main categories: 1) Human studies 2) Animal studies 3) Studies based on synthetic bone analogues.

2.6.1 Human Studies

2.6.1.1 In Vivo[i]

In 1990, Fahmy et al.[15] monitored the blood-gas and circulatory changes during TKA's in 35 patients to examine the effect of insertion of an 8 mm solid alignment rod versus a fluted alignment rod into the distal femur. After insertion of both rods, they found traces of marrow content in the blood sample from the right atrium of the heart. It was concluded that the presence of embolism marrow content in the blood was associated

[i] *In vivo is the Latin word for "in the living". It is used to indicate the presence of a living organism*

with the significant increase in intramedullary pressure due to insertion of rods in the femur. Further, they examined the possibility of inserting the fluted rod through a 12.7 mm drill hole entry site. They found that the pressure buildup could be prevented by making the entry hole diameter at least 4.7 mm larger than the fluted rod diameter. The reason for this large offset is that the highest intramedullary pressure was reached during insertion of the guide wire or rod. By making a larger diameter hole as the entry site, a larger portion of marrow could leave the channel, thus preventing further pressure buildup within the intramedullary cavity.

Herndon et al.[16] studied 34 patients who underwent THA by monitoring the femoral vein using ultrasounic probes. According to this study, in almost every cemented THA, fat embolic events were observed, albeit of various intensities. Later, Hofmann et al.[17] postulated that these cases were likely to cause less than 0.1% of fatal FES cases. Herndon[16] also concluded that using a suction method to remove all the bone marrow and debris from the cavity during or after the reaming could prevent them from entering the blood circulation system.

Parvisi et al.[18] noted that FES is mostly reported after cemented THA, in which the marrow cavity is reamed and the implant is placed in the cavity using surgical cement. In a recent report of 38,488 THA patients at the Mayo clinic between 1969 and 1997, no deaths were reported among 15,411 uncemented arthroplasty surgeries, but 23 deaths were reported in 23,077 cemented arthroplasty surgeries, in which the bone cavity is reamed. [18]

Peter et al.[19] found that the advancement speed of the reamer can influence the pressure buildup in the medullary canal. They monitored the intramedullary pressure in

nine patients with long bone fractures undergoing prophylactic nailing of femora. In these experiments, the intramedullary pressure was monitored using a pressure transducer device inserted through the distal canal. Maximum pressures in a range of 300 to 450 mmHg were recorded during insertion of the smaller reamer diameters (9-9.5 mm) at high penetration speeds. They found that rapid reamer advancement increased the pressure within the intramedullary canal, whereas a slow reamer advancement prevented such excessive pressure buildups. Due to technical difficulties, their study was unable to report the actual reamer advancement rate used by the surgeons, but they reported a maximum pressure of 100 mmHg during 'slow' reamer advancement.

2.6.1.2 In vitro[ii]

Muller et al.[20] studied the variation of compression force (axial force) applied to the bone during intramedullary reaming. Five cadaveric human femurs, hydrogenated in physiological saline solution for 24 hours, were used in these experiments. This study reported a compression force of 59 N concurrent with the diaphyseal and metaphyseal maximum pressures of respectively 206 and 367 mmHg.

Johnson et al.[8] used six pairs of preserved human cadaveric femurs to study the correlation between the intramedullary pressures and axial forces during reaming. The bones were filled with albumin and maintained at physiological temperature of 37°C during their experiments. They reported no significant correlation between these two variables at the distal canal (R^2=0.191, p=0.048).

[ii] *In vitro is the Latin word for "within glass". In the current work, it is used to indicate experimental technique where the experiment is performed on cadaveric bones.*

Heim et al.[21]used twenty human cadaver bones with intact (unbroken) medullary canal to compare reamed and undreamed nailing of the femur. They found no significant difference in pressure elevations within the femoral shaft between these two methods. The maximum intramedullary pressure during reamed nailing of femoral canal was reported as 511mmHg in this study. They also used venting holes to decrease the medullary pressure, but no significant effect due to introduction of a venting hole was reported by Heim et al. The reason was explained due to the fact that the venting hole becomes blocked by bone debris created during clearance of the cancellous bone.[21]

2.6.2 Animal Studies

Mousavi et al.[22] conducted controlled reaming experiments to assess the influence of reaming parameters such as RPM, advancement rate, and reamer size on the intramedullary pressure of twenty-four sheep. They reported higher pressure elevations due to high advancement speed and low RPM.

Kropfl et al.[23], studied the intramedullary pressure elevations and embolization of bone marrow comparing unreamed and reamed femoral nailing using sixteen baboons. They established a statistically significant difference between the two methods ($p<0.001$), reporting peak intramedullary pressures ranging from 420 to 1510mmHg.

2.6.3 Studies Based on Synthetic Bone Analogues

Plexiglas tubes filled with a mixture of paraffin and petroleum jelly were used by Muller et al.[10]to study the effect of different reamer designs using hollow flexible reamers. Hollow reamers are designed to allow the marrow to escape through their hollow cavity and are expected to produce lower pressure than the solid ones; however,

the hole of the hollow cavity was reported to quickly become blocked by bone debris during reaming.[10]The investigators reported that hollow reamers only lead to pressure reduction in combination with a thin flexible drive. The reason was explained on the basis of the fact that penetration of the reamer can be compared to a piston entering a cylinder filled with viscous fluid. In a piston and cylinder system, the flow-rate is directly proportional to the cube of the gap (h) between the reamer and Plexiglas tube ($flowrate \propto h^3$)[24]. Thus, a larger gap for a thinner flexible drive results in a higher flow rate of the escaping marrow, leading to a lower pressure buildup. [10]

Silicon cylindrical shells (350 mm long with 3 mm thickness) filled with a 1:2 ratio of paraffin/petroleum jelly mixture were used by Mousavi et al.[9]to represent the femoral shaft. A controlled reaming design was used to study the effect of the reaming parameters. They reported the driving speed as the most significant variable influencing the pressure elevations. They showed that increases in the driving speed (advancement) increased the pressure, whereas increases in the reamer RPM decreased the pressure.

3 Background

3.1 Bone Structure

Bone is a specialized tissue that has two functions in the body: physiological and mechanical. The physiological function, together with the kidneys and intestines, is the regulation of calcemia. Calcium ions are diversified into the bone matrix during its mineralization to reduce the excessive calcium content of the blood. Similarly, calcium ions can be sent into the bloodstream to increase the calcium level during the bone resorption. Besides this metabolic function, bone has vital mechanical properties such as hardness, modulus of elasticity, brittleness, and limited plasticity that provide enough strength for daily activities, i.e., movement and standing.[3]

3.1.1 Basic Components of Bone Matrix

Bone consists of two main components: the organic matrix and inorganic mineral components. The organic material provides flexibility, whereas the inorganic material provides resilience. Together, these components provide mechanical and physiological support to various parts of the body.[25]

3.1.1.1 Organic Matrix

The organic matrix of the bone consists of collagen and non-collagen proteins distributed as 90% and 10%, respectively. Collagen is a fibrous protein that provides flexibility and strength. Collagen molecules contain three long chains of over a thousand amino acids. Bundles of these molecules are arranged into fibrils that are twisted into a right handed coil or fibre. Depending on the orientation of the collagen fibres, two types

of bone tissues are recognized: cortical bone (also referred as compact or lamellar) and cancellous bone (also referred as trabecular, spongy, or non-lamellar).[26] Cancellous bone is always surrounded by cortical bone.

The non-collagen components of the organic matrix include phospholipids, glycoproteins, and phosphoproteins. The distribution and amount of non-collagen component varies depending on the type of bone and the zone of the bone at which they are located. Non-collagenous proteins have a regulatory effect on the calcification process. [3]

3.1.1.2 Mineral Component

The mineral component of bone is a calcium phosphate hydroxyapatite. It consists of calcium, phosphate, calcium carbonate, calcium fluoride, calcium hydroxide and citrate, comprising approximately 65 to 70% of the bone's dry weight. The remaining of the bone's dry weight is composed of collagen fibers, making up approximately 95% of the organic extracellular matrix.[25]

The inorganic substances of bone appear as needlelike crystals or tablets. Their crystal structure allows them to fit exactly into the holes and fibrils without disrupting their structure.[3]

3.1.2 Whole Bone

A variable assembly of the basic components forms the bone as a tissue. Whole bone, i.e., bone as an organ, includes the bone tissue matrix as well as blood vessels, nerves, and bone marrow whose properties change with age and type of the bone. In a skeleton, bones may appear as long bones (tubular), short bones (irregular prismatic) or

flat bones (bilaminar plates). Long bones are the long tubular segments (e.g., femur, tibia, etc.), which are the focus of this thesis.

Three regions are distinguished in a long bone: diaphysis, epiphyses, and metaphyses (Figure 3-1). Diaphysis is the central shaft representing the longest part. Epiphyses are the two ends of the bone. Metaphyses are the regions that lie between the diaphysis and epiphysis.

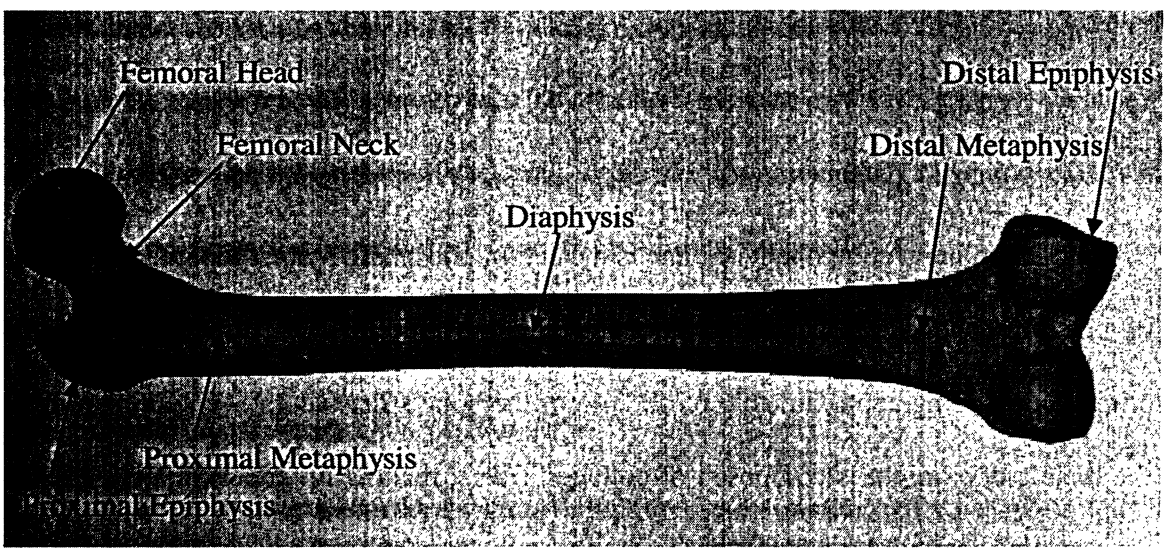

Figure 3-1-Schematic representation of human femur

Three types of cavities exist in a long bone: haversian canals, marrow cavities, and the lacuna[27]. Haversian canals are typically located in the cortical bone. They consist of blood vessels and nerves supplying nutrients and blood to osteocytes, bone cells, which are surrounded by lamellae and lacunae. Lamellae are concentric layers of a mineralized matrix that are found in cancellous bone. Lacunae are small cavities bordering the concentric layers of lamellae. The lamellae are connected via numerous small channels called canaliculi. The *intramedullary canal* is a hollow channel within the cancellous bone, in which sits the bone marrow, whose primary purpose is to generate

blood cells. Osteocytes receive nutrients through canaliculi from blood vessels located in bone marrow[28].

3.1.3 Porous Properties of Bone

Cortical bone and cancellous bone are distinguished based on their collagen fibre orientations and degree of porosity even though they have similar basic compositions. To be more precise, the real difference of cortical and cancellous bone is in their organization and porosity.[3]

Porosity is defined as the ratio of void volume to total volume. Porosity of cortical bone ranges from 5% to 30%, mainly due to voids created by osteon canals and lacuna. Porosity of cancellous bone, due to vascular and bone marrow spaces, varies from 30% to 90%.[3,29] For human femurs, Wang and Oingwen recently studied the relationship between age and changes in bone porosity and pore size, using the pulsed nuclear magnetic resonance (NMR) process[30]. Their findings suggest that cortical porosity ranges from 8%, for young individuals, to 24-28% for elderly individuals. Typical values for Haversian canal pore size and osteocytic lacunae size were reported as 58 μm, and 4 μm, respectively.[30] The osteocytic lacunae pore sizes are of less importance, because Haversian canals make up most of the cortical bone structure. Table 3.1, compiled from the literature, shows the porosity and pore size which a reasonable cortical and cancellous bone analogue must possess.

The material density of the cortical bone is defined as the wet weight divided by the total volume. It is a function of porosity and mineral content. The apparent density for cortical bone is the same as its material density as, unlike cancellous bone, there are no spaces within cortical bone for bone marrow elements. The apparent density of the

cancellous bone, on the other hand, is related to its mechanical properties such as compressive stiffness and strength.[31] The apparent densities of cortical and cancellous bone reported by Carter et al. are 1.8 $\frac{g}{cm^3}$ and 0.1 to 0.9 $\frac{g}{cm^3}$, respectively. [32]

3.1.4 Mechanical Properties of Bone

Bone structural properties are greatly dependent on the loading, disease and aging parameters.[33] In order to be able to simulate reaming operations, the bone analogue material must not only have similar porous properties, but also similar mechanical properties. Two important mechanical properties to be simulated are modulus of elasticity and strength. The modulus of elasticity measures the ability of a material to sustain elastic deformations due to an applied force, while strength provides a measure of the resistance of a material to plastic deformation and fracture.

Mechanical properties of the bone are determined utilizing mechanical testing procedures; i.e., the application of compressive, tensile, torsional, or shear loads to the bone, and measurement of the response. The results of compression tests are more reliable estimations for long bones as they are mostly loaded in compression, in order to support the body. Table 3.1 shows average estimates of the mechanical properties of cortical and cancellous bone based on compression testing of cadaver bones. To properly represent the mechanical properties, the materials representing cancellous and cortical bone should have material properties approximately matching those shown in this table.

Bone Type	Porosity [%]	Apparent Density [kg/m^3]	Pore Size [μm]	Modulus of Elasticity [MPa]	Ultimate Strength [MPa]
Cortical	5 - 30	1810	3 – 78	14700-34300	133-295
Cancellous	30 - 90	320	100 – 400	74 - 522	1.8 - 9.4

Table 3.1-Properties of long bone compiled from the literature

3.2 Bone Marrow Properties

Bone marrow is a soft, sponge-like, fatty tissue that houses immature cells known as hematopoietic or stem cells, found inside long bones. These stem cells transform themselves into three types of blood cells: white and red blood cells and platelets. White blood cells fight infection, red blood cells carry oxygen and platelets help the blood to clot. There are two types of bone marrow: red marrow and yellow marrow. Red marrow is highly vascularized and contains stem cells; whereas the yellow marrow, which is not vascularized and contains a large amount of fat cells.[34]

Structural properties of bone marrow follow the properties of those of a non-Newtonian fluid, in which the shear stress is not linearly proportional to the deformation rate. The purpose of bone marrow is twofold: to create hydraulic resistance and hydraulic strengthening, which are, respectively, resistance of fluid flow through the porous media and viscous interaction between the bone and fluid.[35]

Unfortunately, there has been very little study on the rheology of bone marrow. Bryant et al.[36] measured the viscosity of bone marrow in the distal and proximal regions of long bone in bovines. They found a very large difference in marrow viscosity due to changes in temperature. They reported a viscosity change of 50 cP to 1000cP for the temperature range of 20°C to approximately 40°C. They also found a large difference in the viscosity of bone marrow between the distal and proximal portions of the bone,

respectively 50cP and 600cP.[36] This viscosity has been considered in a number of previous studies[11,37,38,39,40,41] as being representative of that found in human long bones, and is thus considered in the present work as well.

3.3 Reaming

Reaming is a machining process used to create an accurate hole size with a smooth surface finish on a previously existing hole. Reamers thus are used to enlarge holes, typically created by a drilling or boring machine, accurately to the desired size. Typically, a reamer is a multi-edge fluted cutting tool in which the edges cut simultaneously to create a round hole[42]. However, the accuracy of the hole roundness in reaming has been a subject of investigation in the literature. For example, Kiyota et al.[43] and Friedman et al.[44] reported the phenomenon of multi corner-profiled hole in reaming, and Bayly et al.[45] investigated the effect of tool oscillations and hole roundness error using a quasi-static model of reaming. The experimental measurements (Chapter 6) from the present work has been used by another Ryerson graduate student to establish stability analysis and hole roundness error due to tool vibrations.[46,47]

3.3.1 Reamer Types

To investigate the reamer behavior for the present application, one needs to be familiar with the structure of reamers. There are three types of standard reamer shapes available in the market: straight flute, right-hand spiral, and left hand spiral. Orthopedic reamers are mostly available in straight flute and right-hand spiral shape.

3.3.1.1 Straight Flute

Straight flute reamers are the most common reamer type. They have two or more flutes with cutting edges that are parallel to the tool axis. The straight shape of the flutes allows the cutting material to flow back as the reamer advances. These reamers are mostly used when there are no keyways or interruptions in the hole. In the present work, solid six-fluted straight orthopaedic reamers are used (Figure 3-2). Refer to Appendix E for detailed reamer specifications.

Figure 3-2-Pictorial schematic of orthopaedic reamers used in this study

3.3.1.2 Right-hand Spiral

The right-hand spiral reamers have two or more flutes in a right helix to the tool axis. These reamers tend to push the cutting material out of the hole. They are not suitable to ream soft materials as they tend to pull down into the hole[42]. These reamers are mostly used in the hollow flexible drive reamers, described in Section 2.6.3.

3.3.1.3 Left-hand Spiral

The left-hand spirals have a tendency to pull out of the hole, hence to push down the cutting material. They require a higher advancement force to feed smoothly. This type is more conveniently used on soft materials[42]. These reamers are not as common in orthopaedic applications due to the fact that they push down the cutting material in the bone cavity.

3.3.2 Reaming Parameters

The *reaming parameters* are the operational conditions which may change the hole finish quality or the hole accuracy. The two most important reaming parameters in a reaming process are the rotational and advancement speeds of the reamer.

3.3.2.1 Rotational Speed

Rotational speed is defined as the spindle speed of the reaming device in the form of number of revolutions per minute (RPM). Reamer RPM has been shown to affect the intramedullary pressure during orthopaedic procedures; a number of investigators have reported that low RPM increases the pressure elevation during orthopaedic reaming.[9,22]

3.3.2.2 Advancement Speed

Advancement speed is the rate of penetration of the reamer into the work piece defined in terms of distance the reamer moves forward every second, e.g., millimeters per second. A low advancement speed may wear out the reamer blades; however, a very high advancement speed may result in a lower hole accuracy or a lower surface finish quality. Advancement rate should be high enough to allow the cutting blades to cut the

working material rather than to rub the hole surface. In practice, reaming should thus be at high enough speed to prevent rubbing while creating a good quality hole finish[42].

The effect of advancement speed on elevation of intramedullary pressure during orthopaedic reaming is evident in the literature. It is seen that a higher advance speed increases the marrow pressure within the bone.[9,19,22]

3.3.2.3 Alignment

Alignment can also affect the finish and accuracy of the hole. Ideally, the axis of the spindle, reamer, and hole should be aligned in a reaming process. Any misalignments may result low hole accuracy, which might lead to excessive intramedullary pressure.[42]

3.3.2.4 Chatter

Chatter is a self-excited violent relative vibration between work piece and tool. The presence of chatter in a reaming process is undesirable, as it may cause dull blades and low quality holes, potentially leading to high pressure buildups during orthopaedic procedures. Generally, chatter occurs at rotational speeds higher than 500 RPM.[45] In the current work, the maximum rotational speed of the reamer was 200 RPM, and it was thus assumed that chatter was not a problem.

4 Experimental Apparatus and Procedures

4.1 Preliminary Considerations Regarding Synthetic Bone Analogue

Previous studies in the literature on the parameters leading to pressure buildup in the intramedullary canal have mostly used cadaveric specimens. In the present work, the aim was to find a synthetic bone analogue which would have a relatively simple geometry and would have a lower specimen to specimen variability than that found in cadaveric bones.

It would be very difficult to construct a bone analogue which possesses the detailed structure and network of the bone. However, for the purposes of biomechanical parametric studies which, above all, require comparative rather than absolute measurements, a reasonable first approximation would be to assume that bone has an approximately homogeneous porous open cell structure. With this approximation in mind, for study of fluid flow, the properties of human long bone that an analogue must match are porosity and pore size, strength and modulus of elasticity. Variation of these properties causes major differences in fluid flow and indeed can be used to distinguish between the cortical and cancellous material.

4.1.1 Geometry

For the purposes of this thesis, i.e., in order to approximate the mechanical and fluid dynamics behavior of a human femur during orthopaedic reaming procedures, the shape of human femur was represented as a simplified two layer (outer layer is cortical, and the inner layer is cancellous bone) cylindrical analogue (Figure 4-1 and 4-2) based on

an average femur size. A 10 mm diameter cylindrical void at the center represented the intramedullary canal. This geometry, without the cancellous component (i.e., with only the cortical 32 mm outer diameter, 16 mm inner diameter cortical layer), has been previously used to experimentally study the pressure buildup due to hammering of orthopaedic implants into long bones.[11,37]The cortical geometry has also been used as a base for numerical models of pressure buildup in the intramedullary canal, due to orthopaedic implant hammering.[38,39,40,41]

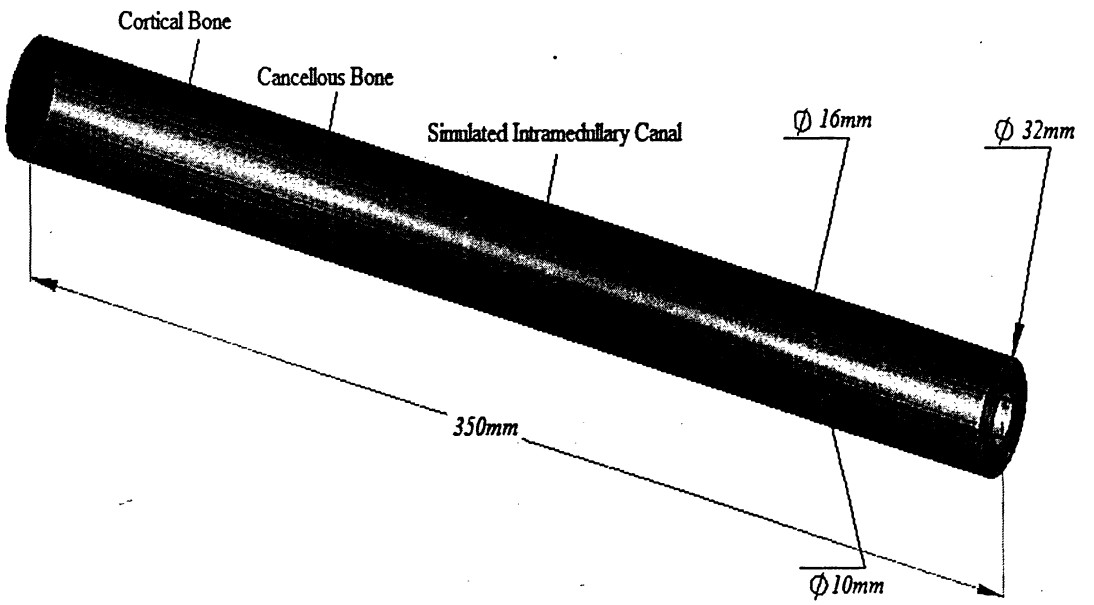

Figure 4-1- Approximation for the geometry of human long bone

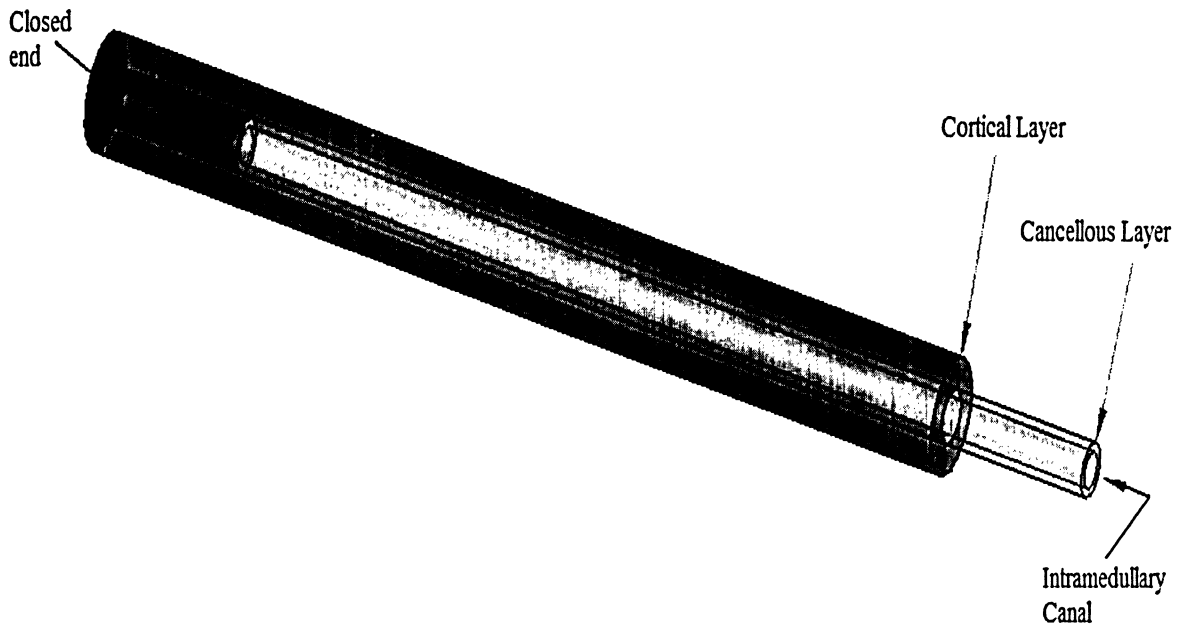

Figure 4-2-Schematic of cortical and cancellous layers in the long bone

4.1.2 Choice of Representative Materials for Cancellous and Cortical Bone Simulation

Generally, in an orthopedic reaming process, the cancellous bone is reamed, and significant amounts of cortical bone are rarely reamed. Thus, the porous properties of human cortical bone should be accurately simulated, while simulation of the mechanical properties is less important. The cortical bone analogue is only used to ensure that a realistic resistance to fluid flow is provided when the intramedullary pressure is increased. The present study thus utilized the cortical substitute used with success in previous work.[11,37] Thus, the outer shell in Figure 4-1, was made of 22.5% porous and 40-60 microns pore size open-cell ultra high molecular weight Polyethylene (UHMW-

PE) (Porex Porous Products Group, Fairburn, GA, USA), meeting the porous requirements outlined in Table 3.1.

In order to find an appropriate substitute for the cancellous bone, both the structural and mechanical properties needed to be met, as it would be reamed, and also have to transmit fluid to the cortical shell. It thus had to have similar porosity, pore size, density, strength, and modulus of elasticity as human cancellous bone (Table 3.1). It proved extremely difficult to find a material matching all these requirements that could also be manufactured in a hollow thin walled tube form. Table 4.1 summarizes the candidate materials for a cancellous type structure. Three categories of porous materials were considered: carbon, metallic and polyurethane foams.

Material/Trade Name	Supplier	Available Porosity	Available Pore Size	Modulus	Strength	Composition	Common Use	Suitability as a cancellous analogue
CFOAM17	Touchstone Research Laboratory (Triadelphia, WV USA)	85%	700-1000μm	550 MPa	6.2MPa	Open cell porous carbon foam	Used in the manufacture of Total Hip Replacement (THR) implants.	Mechanical properties and porosity suitable. Pore size too high.
Reticulated Vitreous Carbon (RVC) Foam	ERG Materials and Aerospace Corp.(Oakland, CA, USA)	88-91%	~ 85 µm	69 – 275.8 MPa	0.69-1.38 MPa	Open cell Duocel Reticulated Vitreous Carbon (9-12% dense compressed 300 PPI (pore per inch))	Insulation, filtration, and acoustic control	Foam properties such as modulus of elasticity and strength can be adjusted for specific application by independently changing porosity and pore size respectively ranging from 88%-97% and 254-5080 µm. - Well suited for cancellous bone but not cost effective.
Doucel Aluminum Foam	ERG Materials and Aerospace Corp.(Oakland, CA, USA)	85-88%	~282μm	393-620.53 MPa	3.79-5.52 MPa	Open cell porous aluminum foam (6101-T6, 12-15% density, 90 PPI (pores per inch))	Currently used for fluid flow control devices, energy absorption, heat exchangers, and orthopedic applications such as bio-mimicking of cancellous bone structure	-The material properties can be adjusted to match the mechanical and physical properties of cancellous bone more precisely with pore size independently varying from 635-5080 µm and independently variable porosity of 88%-97%. - Suited for cancellous bone but not cost effective.
Open Cell Urethane Foam	Pacific Research Laboratories (Seattle, WA, USA)	90%	1.5-2.5 mm	18.6 MPa	0.28 MPa	Urethane foam with a 95% open cell structure (7.5 pcf (pores per cubic feet))	Used for applications that require open celled structure, such as cement injection and modeling osteoporotic cancellous bone	Only the structure resembles the cancellous bone, but not the mechanical properties.

Table 4.1-Cancellous bone analogue candidates

Open cell metallic foams (e.g., aluminum foam) were considered due to their ability to duplicate the cancellous bone porous and mechanical properties. Also, the physical and mechanical properties could be varied independently of each other. The strength and modulus of elasticity of these foams depend on their relative density and the properties of the base material.[48] Porosity and pore size can be adjusted by applying higher pressure to the base material during the manufacturing process. ERG Materials and Aerospace Corp. (Oakland, CA, USA) can custom manufacture 12-15 % dense 6101-T6 alloy with 85-88% porosity and 282 μm pore size. The mechanical properties such as elastic modulus of 393-620.53 MPa and compressive yield strength of 3.79-5.52 MPa closely match the requirement for the cancellous bone[iii].[49] Although this material closely resembles cancellous bone properties, a more cost effective material was selected for the present application.

Open cell rigid polyurethane foams from Pacific Research Laboratory (Vashon, WA, USA) were considered due to their ability to duplicate the cancellous bone porous properties. However, these porous foams have very low strength and are very brittle, and are thus impractical for experimental purposes. Also, the large pore size of a few millimeters made the manufacture of the thin wall tube suitable for cancellous bone simulation virtually impossible.

The most promising material for an analogue of cancellous bone suitable for fluid flow study is carbon foam. These foams can be tailor manufactured to the specifications by adjusting the foam density and pore size to match porosity and mechanical properties. Reticulated carbon (RVC) foam manufactured by ERG Materials and Aerospace Corp.

[iii] These are compressed foams in which the cells are no longer isotropic. The mechanical properties are approximations based on uncompressed foams with isotropic cells.

(Oakland, CA, USA) can be tailored to have reasonably close properties to the cancellous bone such as 88-91% porosity, 85 μm pore size, 69 – 275.8 MPa elastic modulus, and 0.69-1.38 MPa yield strength. The mechanical properties of these foams are strongly related to the foam relative density, defined as the foam density divided by the solid base material density. The available relative density ranges from 3% to 15% (97% and 85% porosity, respectively[50]). RVC was thus an excellent option for the cancellous bone in terms of both physical and mechanical properties.

CFOAM 17, manufactured by Touchstone Research Laboratory (Triadelphia, WV, USA), was an alternative, and more cost efficient porous open-cell carbon foam. It has a porosity of 85%, density of 270 kg/m^3, pore diameters in the range of 700-1000 μm, modulus of elasticity of 550 MPa, and strength of 6.2 MPa.[51] With the exception of the relatively large pore size, all the other properties reasonably match those of cancellous bone (Table 3.1). For the purposes of the present study, which aims to measure pressures inside simulated bone analogues, this higher pore size should not pose much of a problem. Most of the resistance to fluid flow is expected to occur in the less porous cortical layer, and thus the influence of the thin (3 mm) cancellous layer should not affect the results significantly. This carbon foam was thus chosen as the cancellous bone analogue.

4.2 Chosen Synthetic Bone Analogue Model

The simplified axi-symmetric geometry discussed in Section 4.1.1 (Figure 4-1 and 4-2), was chosen for both ease of manufacture and to ensure that future computational fluid dynamic and finite element modeling would be greatly simplified. Thus, the outer layer of cortical bone was represented by a Porex porous plastic tube having an inner and outer diameter of 16 mm and 32 mm, respectively. Rigidly attached to the inner surface of the cortical tube was a CFOAM17 tube representing the cancellous bone, having an outer and inner diameter of 16 and 10 mm (representing the intramedullary canal), respectively. The length of the cortical/cancellous bone construct was chosen as 350 mm to represent a large human femur.

Since the cancellous analogue was tightly fit into the cortical analogue, the two were only fixed to each other at the open entrance using silicon sealant (LePage, All-purpose White Silicon Sealant, North York, ON. Canada). Although originally some sealant was also applied at the closed end of the cortical analogue, further modifications resulted in elimination of sealant at the closed end to ensure no interruption in the marrow flow through the porous walls. The resulting model is shown schematically in Figure 4-1, and pictorially in Figure 4-3.

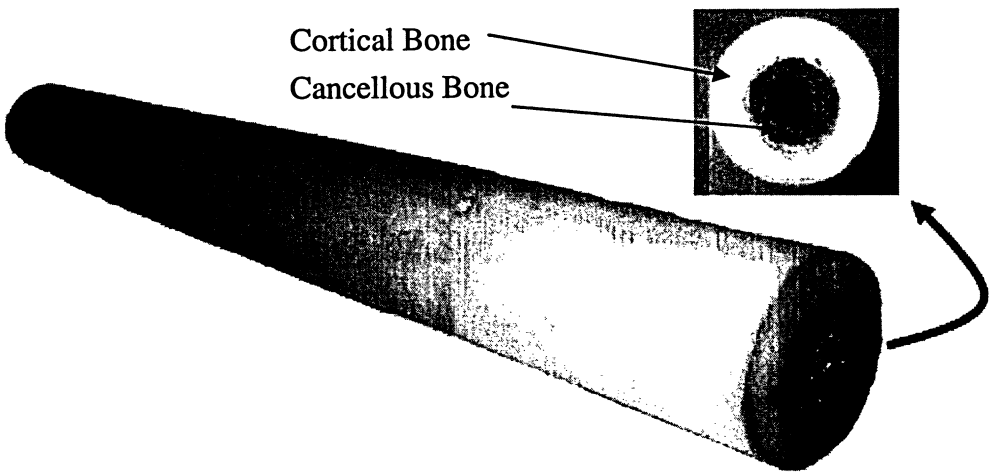

Figure 4-3- Picture of the bone analogue used to represent a human femur

Use of the proposed synthetic model eliminates the need for cadaver bone storage, greatly reduces the specimen to specimen variability, and allows for simplified comparison to numerical models. The model has the additional advantage that properties such as geometry, porosity, pore size and mechanical properties can be fairly easily accommodated as the manufacturer can change these parameters on demand. This would allow for parametric studies which aim to establish, for example, the effect of aging on the resulting pressures generated in the intramedullary canal during reaming.

4.3 Bone Marrow Analogue

To reproduce the bone marrow, a petroleum jelly and liquid paraffin mixture has been proposed in the literature by Mousavi et al.[9] and Miller et al.[10] They used a 1:2 ratio of paraffin/petroleum jelly at 20°C, which was found to have similar viscoelastic properties of bone marrow at approximately 36°C. [10]

A more realistic behavior that allowed more easy flow through the porous cortical bone substitute was proposed by Dobrjanski[11]; i.e., use of a 45/55% petroleum

jelly/paraffin mixture. This mixture, having a measured viscosity of 82.6 cP[11], was adapted as the standard for the experiments in the present work. Experiments that required a higher marrow viscosity were conducted using a 65/35% petroleum jelly/paraffin mixture, having a measured viscosity of 396 cP[11].

It was noted that overnight exposure of petroleum jelly/paraffin mixture to open air caused excessive evaporation of liquid paraffin, leading to increases in the mixture viscosity. It was also noted that preserved mixtures, in air-tight bottles, also experienced an increase in viscosity after a longer period of time. The reason for this viscosity increase was not clear, but may have been due to separation and layering of the two components of the mixture in the bottle, when left for some time. In any case, the following precautions were used to avoid experiment to experiment changes in viscosity:

1. The bone marrow mixture was always freshly made prior to each experiment.
2. While heating the mixture components, the temperature never exceeded 60°C. It was noted that the paraffin tended to evaporate and escape in a gas form at a temperature higher than 60°C.
3. The mixture temperature was usually cooled down to 20°C either by using an ice-water bath or letting it sit at room temperature until it slowly reached room temperature (20°-22°C) . Cooling speed did not appear to affect the resulting viscosity of the mixture.

4.4 Experimental Apparatus

A controlled reaming system was designed and developed (Figure 4-4) to generate controlled and repeatable reaming parameters such as RPM and advancement speed, and to help ensure alignment of the bone with the reamer was maintained as best

as possible. The experimental apparatus was capable of measuring simulated intramedullary pressure, load components at the closed end of the bone, and reamer torque, in response to penetration of reamer into the synthetic bone analogue.

A variable speed surgical spindle (Stryker Instruments, Bucharest, Romania) generated the required rotational speed in the reamer. A torque transducer (Lorenz DR2207, Lorenz Messtechnik GmbH, Alfdorf, Germany) was attached in-line between the reamer and spindle to measure the applied torque to the reamer. The in-line spindle, torque transducer and reamer set-up was placed on a sliding linear stage that allowed smooth movement, which was advanced forward/backward utilizing a variable speed 12" stroke DC linear actuator (Firgelli Automations, Bellingham, WA, USA). A DC variable power supply was used to vary the speed of the linear actuator while the direction of movement was controlled using the back/forth switch.

Three pressure transducers (Kulite XTM-190, Kulite Semiconductor Products Inc., Leonia, USA) were tapped into the synthetic bone analogue to measure the simulated pressure within the intramedullary canal. The closed end of the bone was attached to a dynamometer (AMTI MC3A-6-500, Advanced Mechanical Technology Inc., Watertown, MA, USA) that allowed measurements of the loads applied to the bone.

All instruments and transducers were calibrated by corresponding manufacturers and distributed by A-Tech Instruments (Scarborough, ON, Canada), and are discussed in detail in Sections 4.4.1-4.4.8

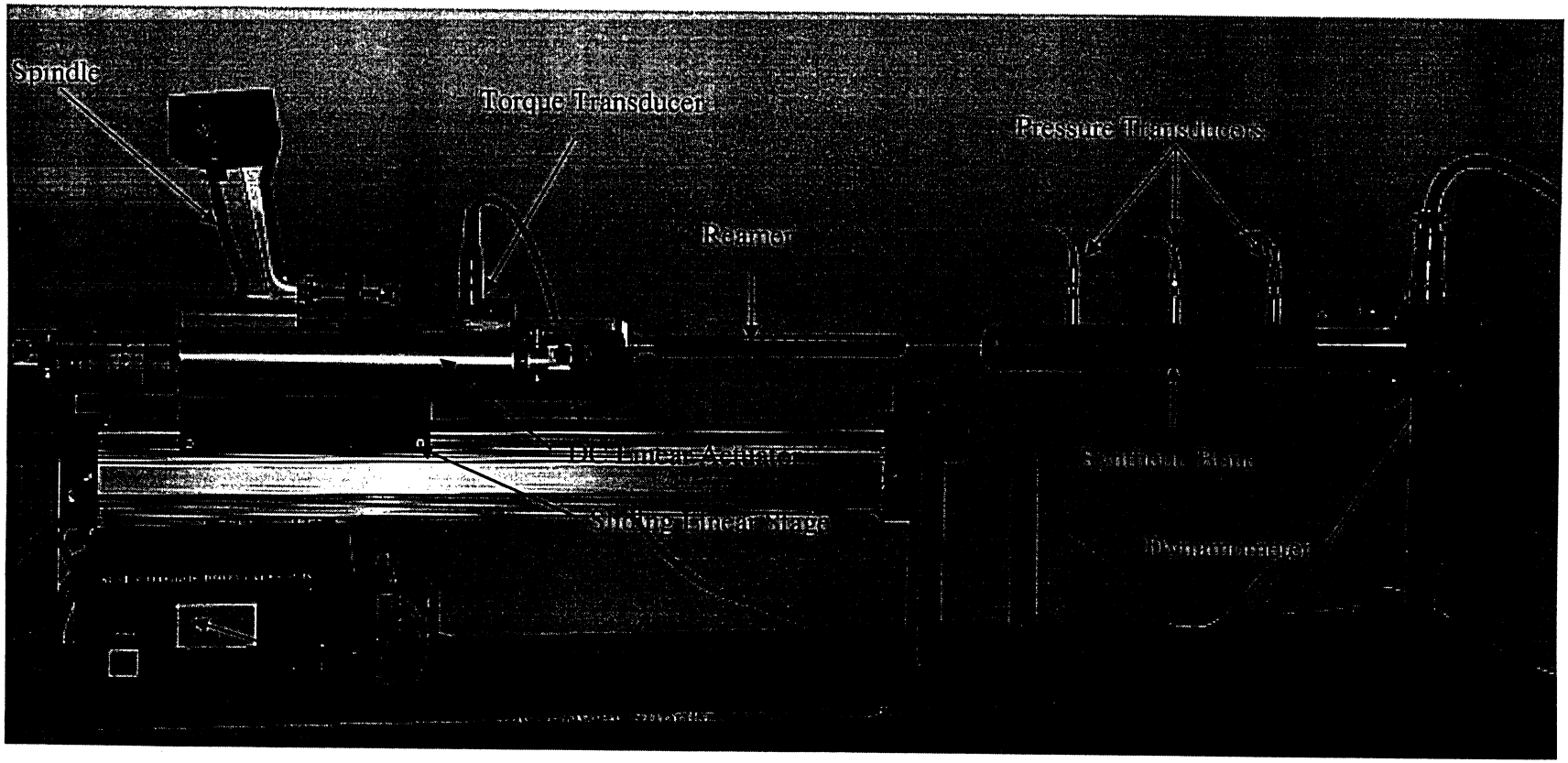

Figure 4-4-Experimental Set-up

4.4.1 Configuration of Synthetic Bone Cylinder on the Set-up

The synthetic bone was placed horizontally in the set-up. The closed end of the bone was attached to a dynamometer (load cell) using a rigid metal holder, as shown in Figure 4-5. The purpose of the metal holder was to create a stable connection between the bone and the dynamometer and to distribute the forces applied to the bone evenly onto the load cell.

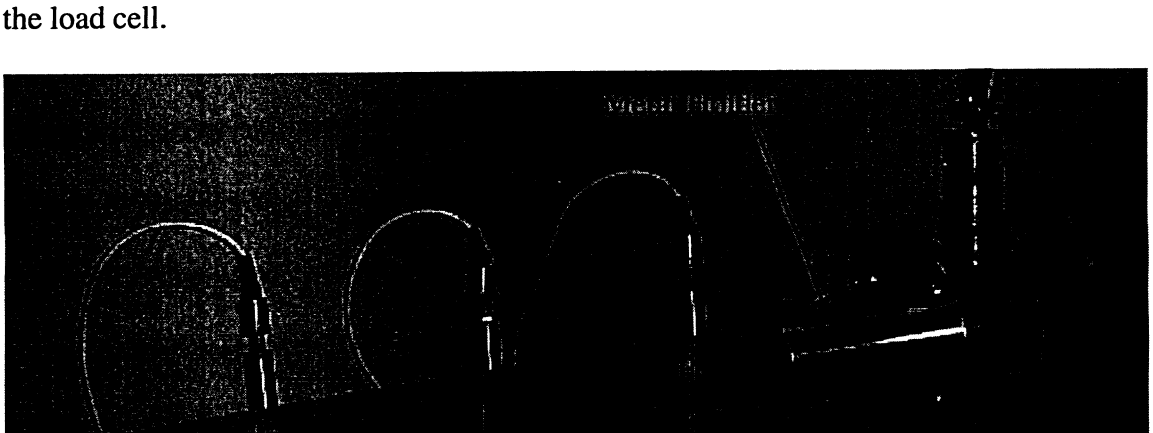

Figure 4-5- Synthetic bone attached to the apparatus

4.4.2 Spindle

A 4103 orthopaedic reamer spindle (Stryker Instruments, Hamilton, Ontario, Canada), Figure 4-6, was used to generate constant RPM for the reamers. This cordless battery powered spindle can generate a maximum rotational speed of 220 RPM.

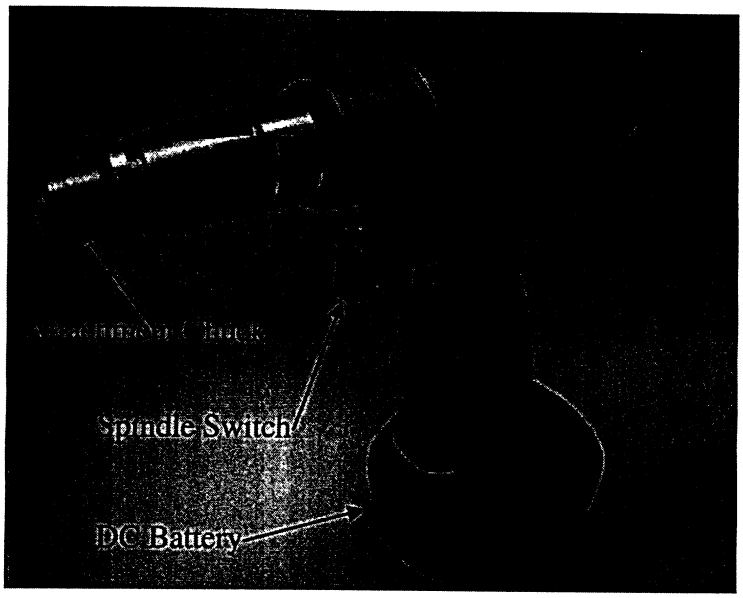

Figure 4-6-Stryker spindle

The spindle speed (RPM) was set to the desired rotational speed using a small trigger jig seen in Figure 4-7. A DT-105A contact tachometer (Electromatic Equip't Co., Cedarhurst, NY, USA) was used to measure the rotational speed of the reamer. The spindle was coupled to a torque transducer, which was connected to the reamer. The rotational motion generated by spindle was transmitted to the reamer through the rotary torque transducer, detailed in Section 4.4.7.

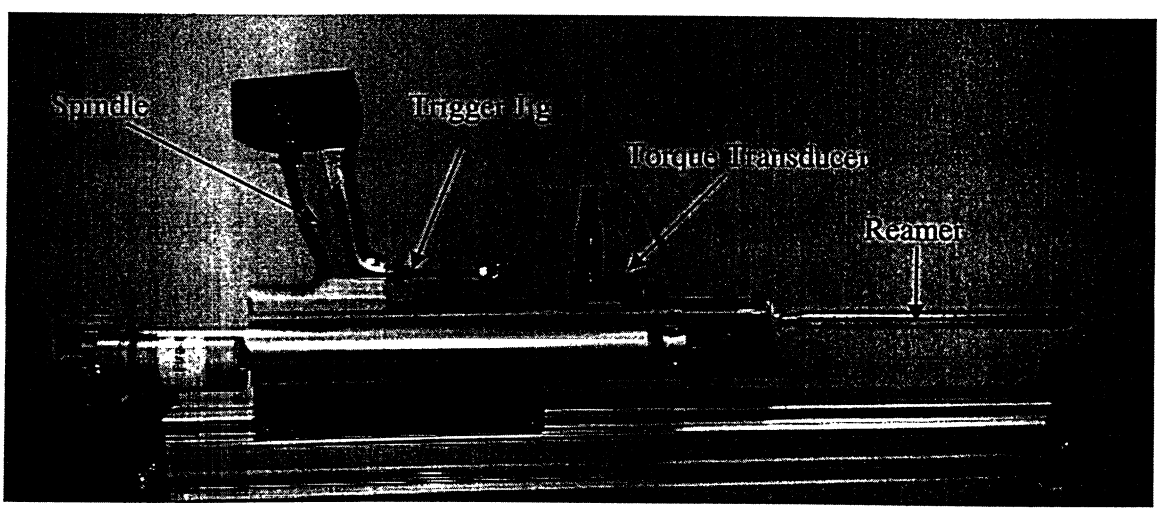

Figure 4-7- Location of spindle on the apparatus

4.4.3 DC Linear Actuator

Two 12" stroke linear actuators (Firgelli Automations, Bellingham, WA, USA), Figure 4-8, were used to advance or retract the reamer set-up attached to the sliding linear stage. Each linear actuator was used to generate a different advancement speed range. One generated low speeds and the other generated high speeds. Together, the two actuators allowed generation of advancement speeds in the range of 8-50 $\frac{mm}{sec}$.

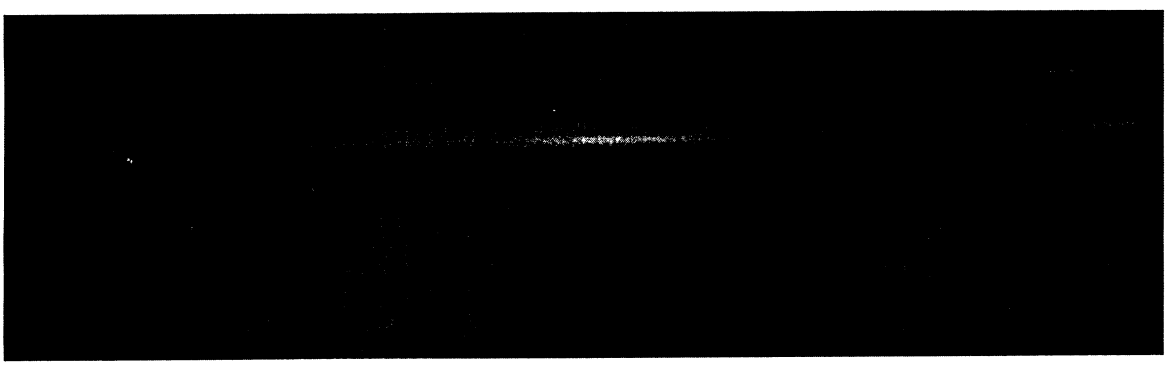

Figure 4-8- DC Linear Actuator

4.4.4 Data Acquisition System

The IOtech DaqBook2000 (IOtech Inc., Cleveland, OH, USA), was used as an external module Data Acquisition (DAQ) to collect data during experiments (Figure 4-9). This 32-channel DAQ system was connected via the parallel port to a Pentium 4 2.6 GHz computer, where the raw data were acquired by the data acquisition and logging software, DaqView 2000 (DASYTEC USA Incorporated, Bedford, NH, USA). This DAQ system is capable of collecting the raw data at a maximum sample rate of 200 kHz.

The analog input module, Figure 4-9, was composed of two 16-channel isolated analog signal conditioning and expansion boards (DBK207, IOtech Inc., Cleveland, OH, USA). The analog module was connected to DaqBook2000 allowing the simultaneous

use of all 32 channels. In the present work, only seven channels were used to collect data at a sample rate of 20 kHz from transducers, (three pressure transducers, three orthogonal force components from the dynamometer, and one rotary torque transducer). Note that this 20 kHz sampling rate is much higher than the expected Nyquist frequency (twice as large as the reamer spindle frequency, 3.33 Hz.)

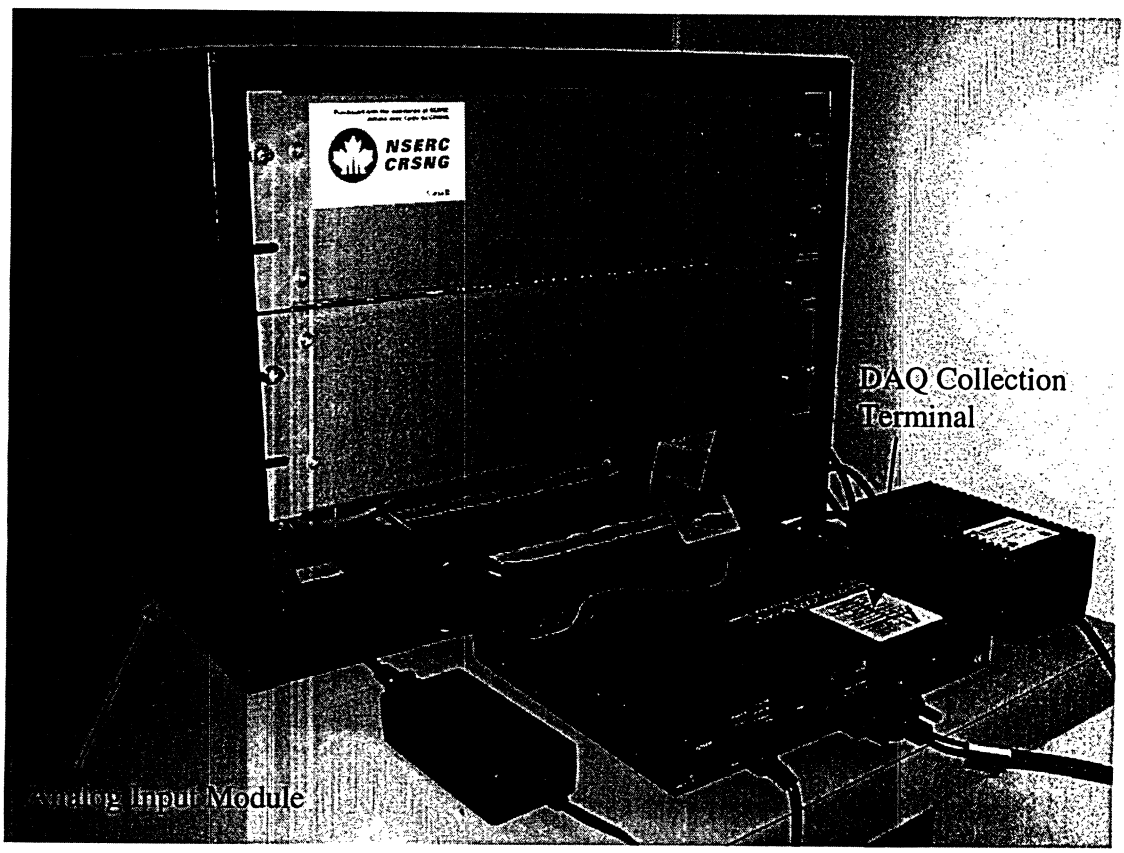

Figure 4-9-DAQ System

4.4.5 Pressure Transducers

Miniature pressure transducers (Model XTM-190, Kulite Semiconductor Products Inc., Leonia, USA), shown in Figure 4-10, were used to measure the simulated pressure buildup within the intramedullary canal. These transducers utilize a flush metal

diaphragm as a force collector with a piezo-resistive sensor as the sensing element where the sensing principle is a fully isolated four arm Wheatstone bridge. The transducer measures the gage pressure, so that zero output is at atmospheric pressure.

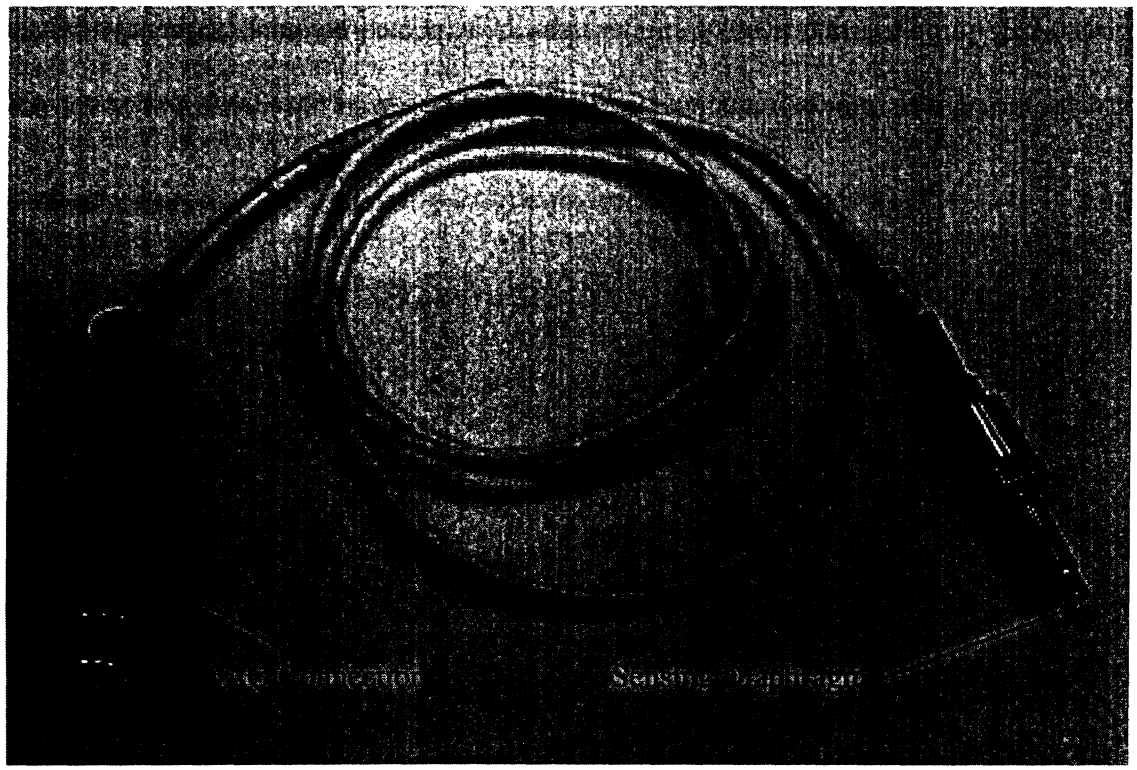

Figure 4-10- Pressure Transducer

4.4.5.1 Implementation of Pressure Transducers on the Bone

As mentioned previously, the synthetic bone analogue described in Section 4.2, was tapped at three locations along the bone to allow placement of the pressure transducers at the intervals shown in Figure 4-11. Originally, the self tapping tips of the pressure transducers were placed tightly in the bone without any connecting adaptors. Data inconsistencies such as the occasional random high frequency pressure spike (see Section 5.2) were observed when the pressure transducer diaphragm and the rotating reamer were in close proximity. Due to the random occasional nature of these spikes, it

was postulated that these high frequency spikes were not a true reflection of the actual intramedullary pressure within the bone, but due to vibrations of the pressure transducer diaphragms. To test this hypothesis, modifications were made to keep the sensing diaphragms away from the passage of the reamers. For this purpose, stainless steel connecting adaptors (Figure 4-11) were designed to indirectly connect the pressure transducers to the bone, and found to eliminate these apparent random pressure spikes. The connecting adaptors, discussed in more detail in Section 5.2, were used in most of the subsequent experiments.

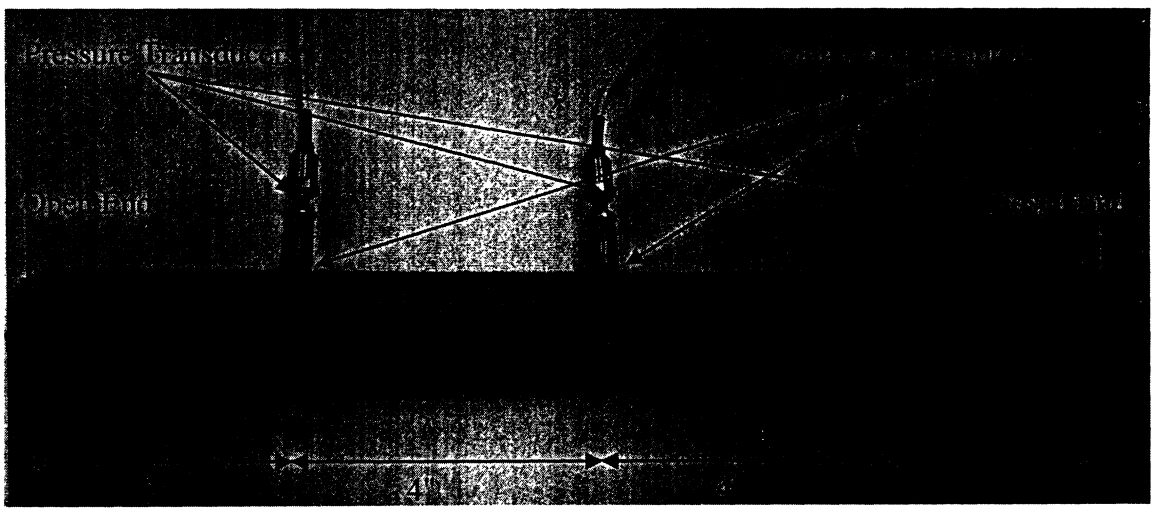

Figure 4-11- Bone analogue with the location of pressure transducers. Note that the reamer enters the bone from the left hand side.

4.4.6 Dynamometer

A single element multi-component dynamometer (Model MC3A-6-500, Advanced Mechanical Technology Inc., Watertown, MA, USA), shown in Figure 4-12, was used to measure the applied forces at the end of the bone. It is a force/torque transducer specially designed for simultaneous measurement of three orthogonal force

and moment components. The sensing principle incorporates a single cylindrical strain element on which the strain gages are mounted.

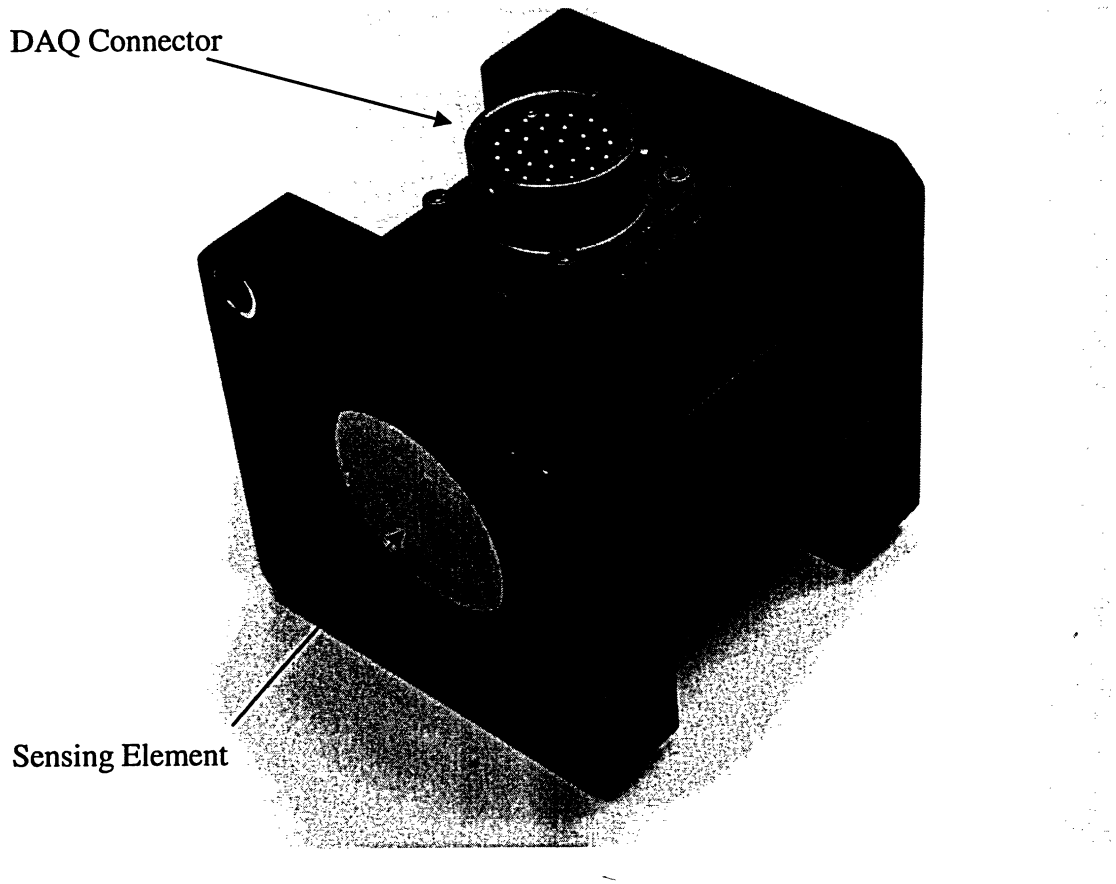

Figure 4-12-Dynamometer

4.4.7 Torque Transducer

A rotary torque transducer (Model DR2207, Lorenz Messtechnik GmbH, Alfdorf, Germany), was used to measure the applied torque to the reamer (Figure 4-13). It is a contact-type torque transducer with slip rings, used to apply power to and retrieve the signal from strain gages mounted on the rotating shaft.

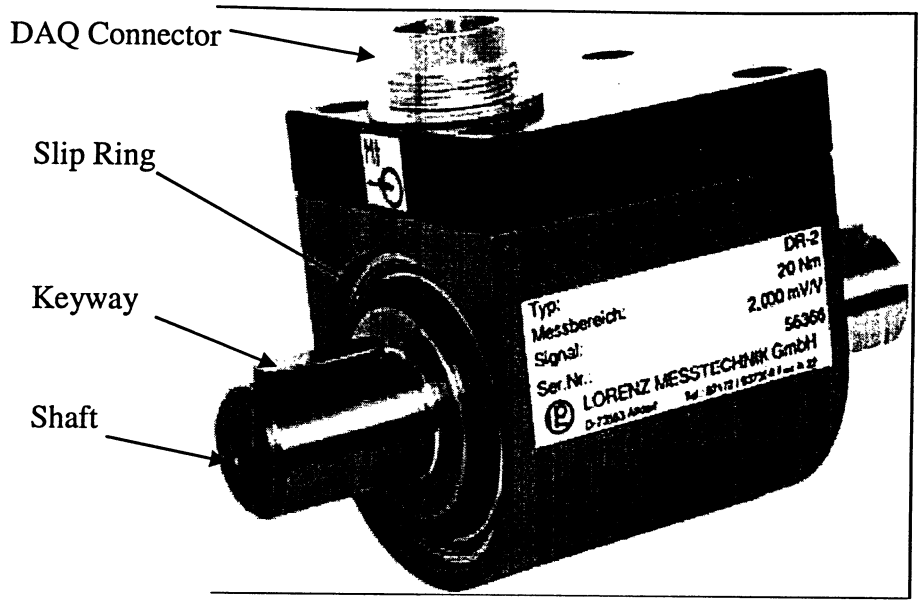

Figure 4-13- Rotary Torque Transducer

4.5 Experimental Procedure

A number of experiments were conducted in order to carry out an experimental parametric study aimed at verifying the effect of different parameters on intramedullary pressure (Chapter 5) and to establish a correlation analysis between the imposed forces, torque and peak intramedullary pressures (Chapter 6). Parametric studies were performed to verify the effect of factors such as rotational speed (RPM), reamer advancement speed, and bone marrow viscosity, as well as the effect that a clogged reamer would have on simulated intramedullary pressure within the bone.

Each experiment involved the advancement of a rotating reamer at a constant speed into the two layer cylindrical synthetic bone to a depth of 235mm, equal to the length of the reamer (see Appendix E for reamer specifications). The reamer was mounted, aligned to the axis of the bone, on a sliding rail, which could be advanced with a constant desired velocity using a linear actuator. In each experiment the reamer was

advanced then retracted back with the same RPM, rotational direction and retraction speed as that of the advancement. The open end of the bone was free to move, whereas the closed end was attached to a dynamometer to measure the applied force components in three dimensions during the reaming process. During each experiment, data were collected, using the DAQ system, from the pressure transducers, the torque transducer and the dynamometer. Reaming RPM and advancement speed were changed for each specific experiment.

In each of the experiments, the cancellous part of each bone analogue, i.e., the inner layer, was to be reamed using eleven reamers starting from the smallest to the largest (11-16 mm in diameter) with 0.5 mm incremental increase of diameter between each successive reamer size. This is a similar procedure to that used by orthopaedic surgeons when reaming long bones.

Prior to each experimental run, the bone analogue was tilted upward to a vertical position, and completely filled with the synthetic bone marrow. However, the reaming took place with the bone in the horizontal position, with the pressure transducers located at the top surface of the bone, and facing downward. Prior to reaming, the bone analogue was required to be saturated with bone marrow, in order to ensure that the marrow was evenly distributed into the pores of cancellous bone, as well as fully penetrated into the connecting adaptors between the bone and the pressure transducers. To accomplish this, a 240 mm long rod with a 10 mm diameter was inserted into the bone with an advancement speed of $20\frac{mm}{s}$, whilst recording the resulting intramedullary pressure within the bone. It was found that after six consecutive insertions at ten minute time intervals, the pressure began to stabilize and the pressure transducers showed repeatable behavior. During this

ten minute wait time between the insertions, the bone was refilled with marrow to make sure the marrow filled up the pores completely. This procedure was carefully repeated before each bone was reamed using eleven reamers. After the bone was saturated with marrow, the actual reaming experiments began at five minute time intervals. Between each two reaming experiments, there was enough time to change the reamer to another size and fill up the bone with bone marrow.

The reason the bone was filled with marrow previous to every reaming step was to simulate the realistic condition of blood and intramedullary contents refilling the intramedullary canal in a real orthopaedic procedure. A similar refilling procedure was also implemented by Johnson et al.[8], who used albumin to refill the cadaveric femoral canal before each reaming step.

In most reaming experiments, it was observed that the bone marrow tended to escape through the open cell structure of the bone. There were attempts to calculate the amount of marrow escaping the bone, but it was almost impossible since the escaping marrow mostly created a thin layer on the outer layer of bone, which was then sucked back in during the retraction of the reamer. Although eventually the thin layer of simulated marrow started to drip down from the bone, it was still considered negligible compared to the amount of marrow trapped inside the bone cavity.

Depending on the time required for full advancement and retraction of the reamer, based on the particular advancement speed value, the experiments took between 20 and 60 seconds to complete. This resulted in the collection of 400,000 to 1,200,000 data samples per transducer for each experiment.

5 Parametric Study: Analysis of Intramedullary Pressure Elevation during Reaming Procedures

5.1 Typical Pressure Data

A typical pressure curve, collected from one of the pressure transducers during reaming of the synthetic bone at spindle rotational speed of 200 RPM, is shown in Figure 5-1. Due to the rotational speed of the spindle, fluctuation was observed in the pressure signals. It was observed that data collected by pressure transducers during reaming procedures are a combination of periodic signals with frequencies of those of the tool vibration. The data thus should consist of two periodic signals with one frequency corresponding to the revolution of the spindle speed and the other to that of the blade-pass (e.g., six cycles corresponding to the six reamer blades).[52]

In the data of Figure 5-1, the periodic behaviour associated with the frequency of one revolution of the spindle (3.33 Hz) was present in the pressure signals. However, the blade-pass frequency, which was one sixth of the spindle frequency for a six blade reamer, was not evident in the pressure signal. The reason is probably due to the fact that the reamers were slightly warped, and this was dominant over the smaller fluctuations due to the blade pass.

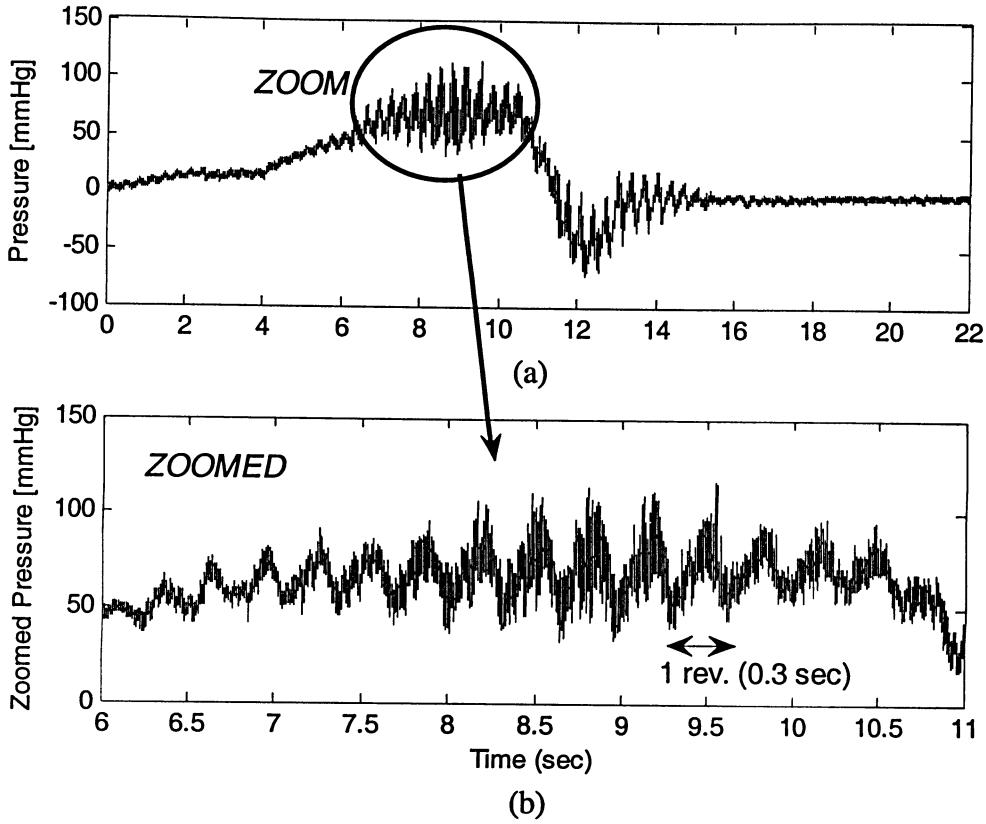

Figure 5-1- Typical pressure curve. Data are taken from transducer #2 while reaming with unclogged 12.5 mm reamer at 200 rpm and 20 mm/sec advancement speed using low viscosity marrow (82.6 cP).

Figure 5-2 shows the location of three pressure transducers tapped into the synthetic bone cylinder used in all experiments. A comparison of the pressure signals observed by the three pressure transducers is shown in Figure 5-3, which also shows at what point each of the transducers was passed. As the reamer advanced in the bone, the vibrations increased in the transducer closest to the tip of the reamer; and as the reamer passed the transducer, the vibrations died out. Note that the reamer never reached pressure transducer #3 as it was located too far away from the open end of the bone. This was the reason that pressure transducer #3 experienced fewer vibrations.

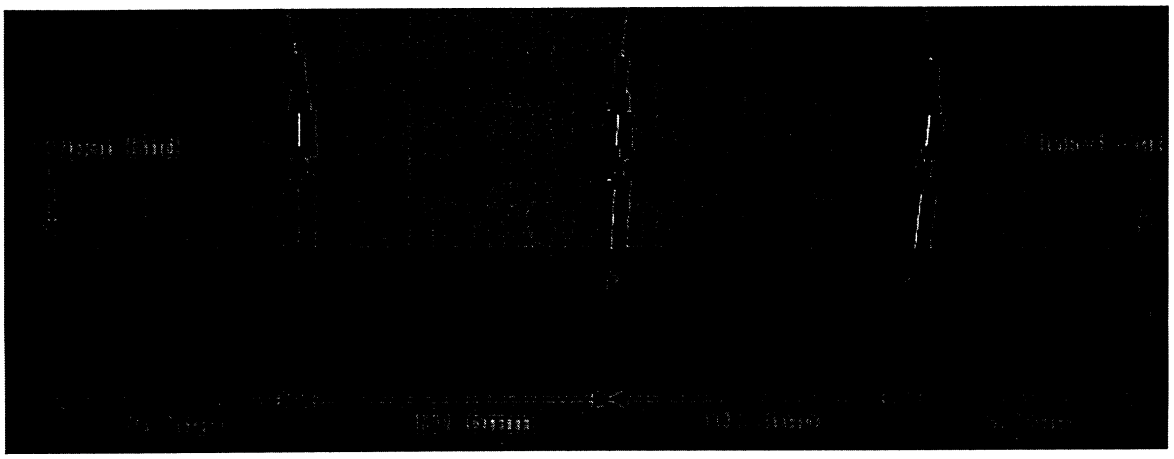

Figure 5-2- Location of pressure transducers on the bone analogue.

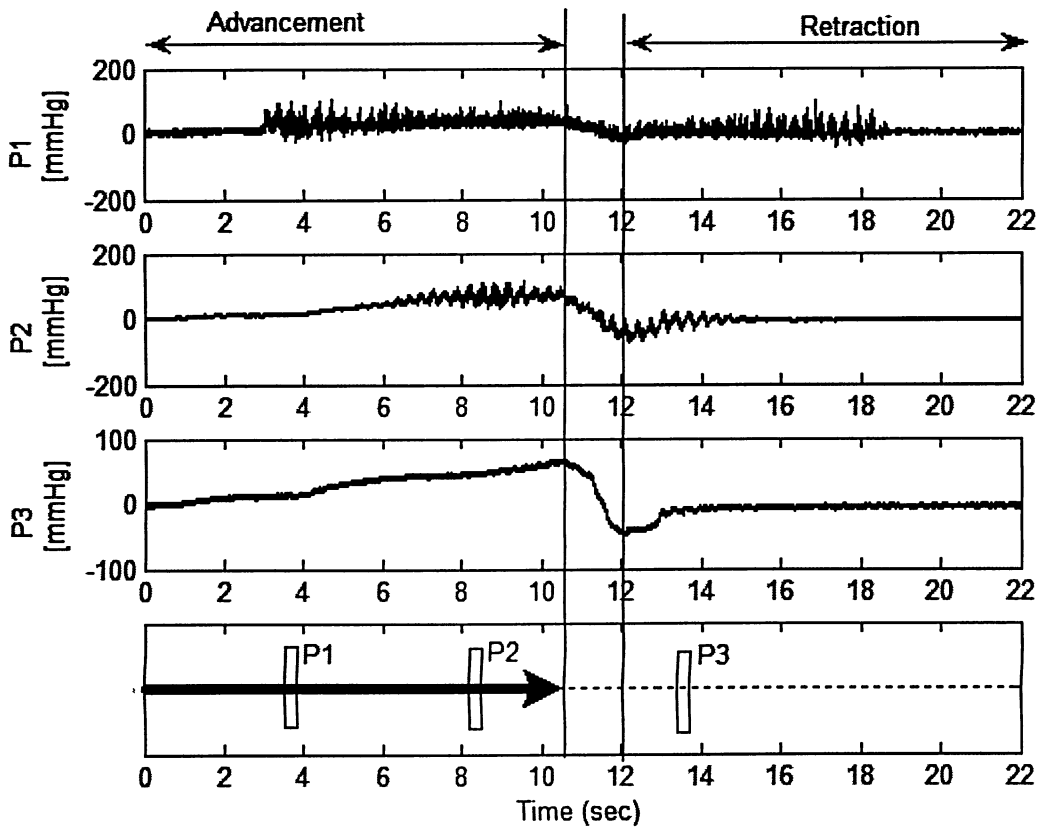

Figure 5-3- Comparison of vibration experienced by the three pressure transducers. Data were taken from unclogged 13mm reamer at 200 rpm and 20 mm/sec advancement speed using low viscosity marrow (82.6 cP).

5.2 Repeatability

A number of tests were conducted in an attempt to evaluate the experimental repeatability of the setup. As mentioned in Section 4.4, the original experimental set-up, in which the pressure transducers were directly tapped into the bone, experienced occasional high frequency pressure spikes (Figure 5-4) in a random manner. Because of the pressure spikes, the peak pressures in consecutive trials under the same conditions did not follow a repeatable pattern, although the mean pressures were observed to fall within 5% of each other. It was later concluded that the high frequency pressure spikes were not a true representative of the marrow pressure elevation within the bone. They were found to be the result of mechanical vibrations between the reamer and the transducer diaphragm that caused the random spikes. These random spikes in peak pressure made it difficult to establish repeatability, and thus modifications were made to the pressure transducer set-up by adding one inch stainless steel connecting adaptors between the bone and the transducers (see Figure 5-2).

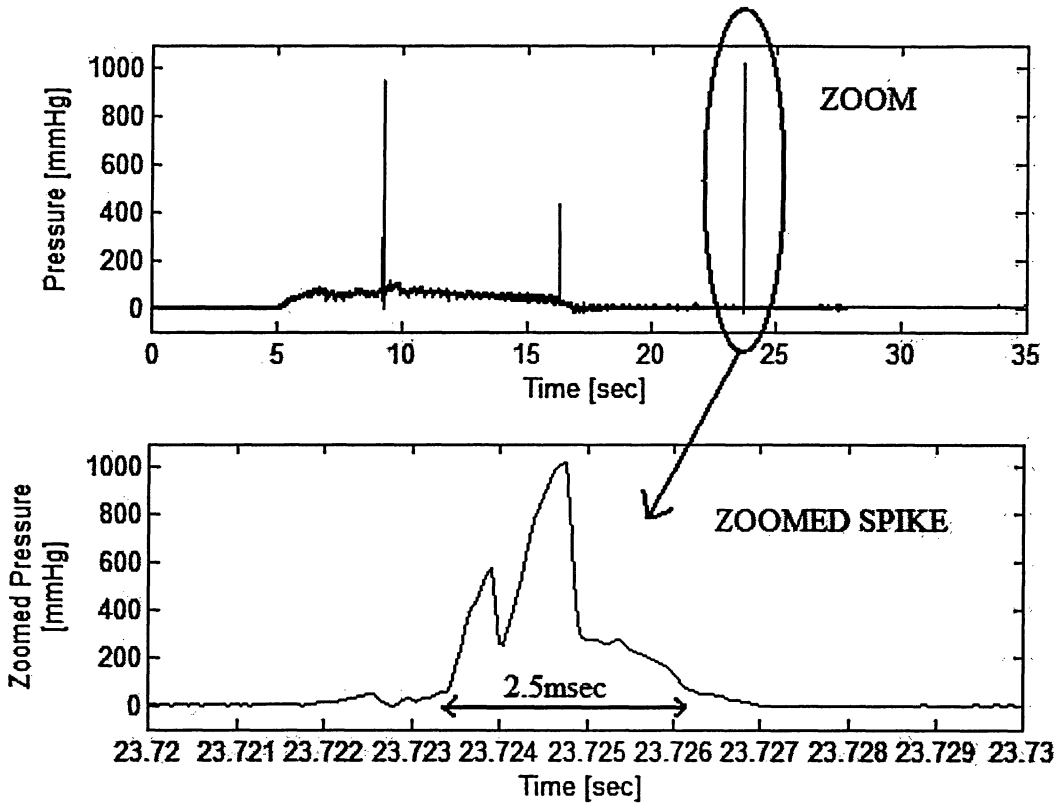

Figure 5-4-Close up of one spike observed during a reaming experiment at 200 RPM and 20 mm/sec with reamer size of 13.5mm in diameter. Data was collected by pressure transducer # 1.

Experimental repeatability in peak pressures improved when these connectors were used. Various tests were carried out to evaluate the performance of the connecting adaptors to meet two main goals: The primary goal was to show that the pressure spikes were eliminated where adaptors were utilized. For this purpose, one bone analogue was reamed starting from the 11 mm diameter reamer up to 16 mm diameter with 0.5 mm increments. All the experiments were conducted utilizing the adaptor, except for reamer sizes 14 and 14.5 mm. From Figure 5-5, it is clearly observed that the runs with 'No Adaptors' both experienced high frequency spikes (Figure 5-5(c) & (d)), whereas the ones with adaptors attached (Figure 5-5(a), (b), (e) &(f)) did not experience the spikes.

The secondary goal was to verify that the data recorded with the adaptors in place showed the actual pressure elevation within the bone. In other words, to verify that addition of adaptors did not change the signature and magnitude of the pressure signals detected by the transducers without use of the adaptors. To test this, a five inch long clear plastic tube was filled with water; where two tests were performed, one with the aforementioned stainless adaptor and one without, attached to a pressure transducer. The inner diameter of the plastic tube was the same as the diameter of the pressure transducer threads so that the transducer could be tightly tapped into the plastic tube, while preventing any leaks. The tube was carefully filled with water using a syringe to avoid air bubbles. The pressure applied by the small column of water was measured with the pressure transducers. Taking into consideration that 5 inH_2O is equivalent to 9.34 mmHg; both tests generated repeatable results within 5%. Hence, it was concluded that the stainless adaptor did not interfere with the pressure readings nor did they change the signature of the pressure signal.

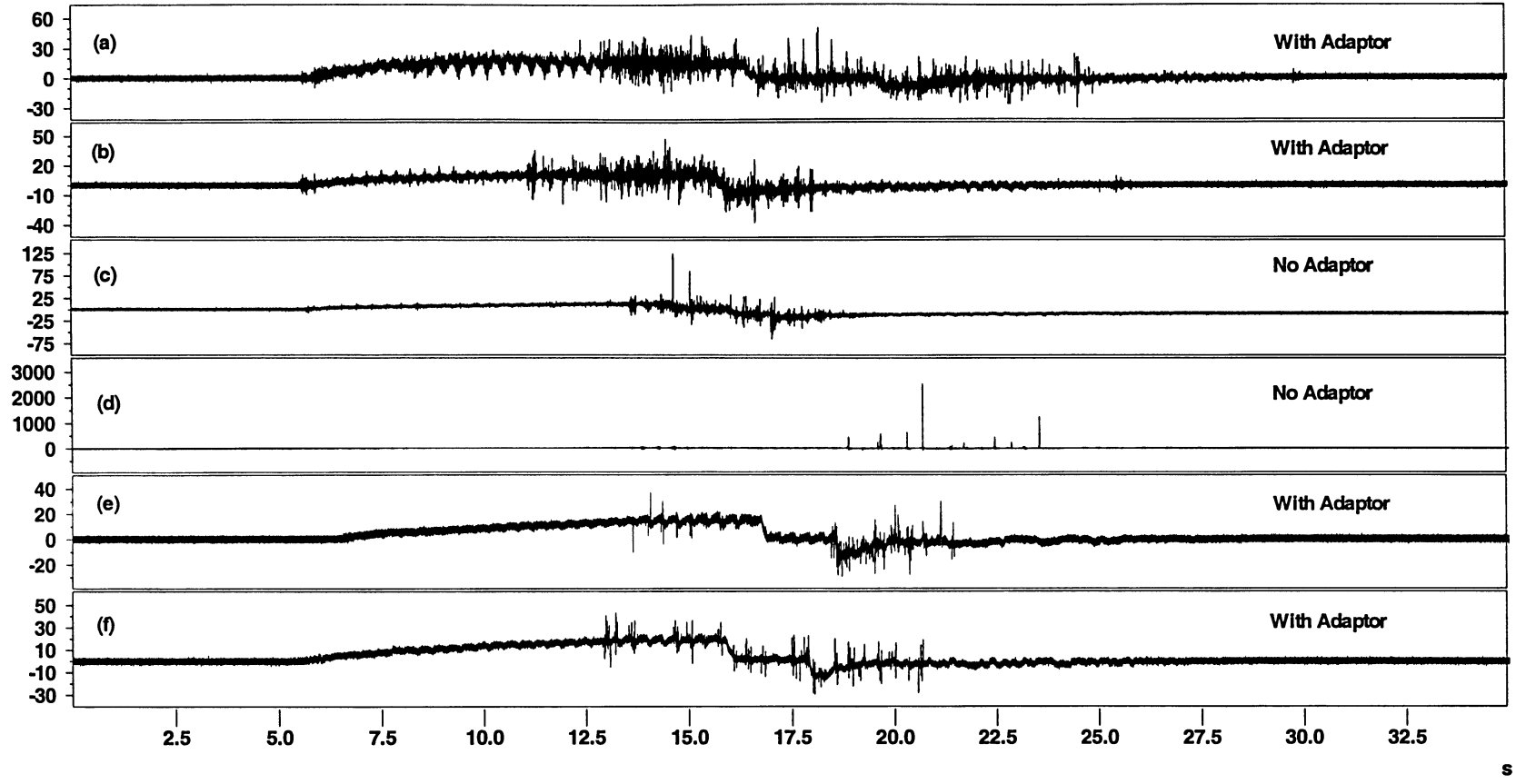

Figure 5-5- Results from verification tests to evaluate the performance of connecting adaptors. All experiments were conducted consecutively on one bone analogue at 200 RPM with an advancement rate of 20 mm/sec. Curves (a) to (f) correspond to reamer size 13mm to 15mm respectively.

5.3 *Statistical Analysis*

Statistical analysis was conducted to examine the extent to which the effect of change in the reaming parameters (independent variables) was a major contributor to the pressure buildup within the bone (dependent variable). Analysis of Variance, ANOVA, was the primary statistical method employed in the present work to determine the level of significance of such parameters. ANOVA is a widely used powerful statistical technique which allows examination of the influence of two or more independent variables on a dependent variable.[53,54]

5.3.1 *Factorial Design*

Prior to the application of ANOVA to the experimental data, a factorial design plan needs to be established. In general, a factorial design includes one or more independent factors (variables) along with the number of levels for each factor. The concept of factorial design allows the effects attributed to separate factors to be estimated, as well as those attributed to combination of factors. The estimated effect from each individual factor is referred to as the *main effect*, whereas the *factor interaction effect* is associated with the effect of a combination of factors.[53] The total number of experiments required to conduct a factorial design is calculated by Equation (5-1), where L_1, L_2... L_k are the number of levels associated with each factor and k is the number of total factors available for the analysis.

$$\textit{Total}\ \text{Number of experiments} = L_1 \times L_2 \times \cdots \times L_k \quad (5\text{-}1)$$

In the present work, five independent factors were considered:

1) Rotational speed of the reamer (RPM)

2) Advancement speed of the reamer

3) Reamer diameter

4) Viscosity of the bone marrow

5) Whether the reamer flutes were clogged or not

Because each of the experiments was a destructive test (i.e., the bone analogue was reamed and thus could not be re-used), and the bones were quite expensive and time-consuming to manufacture, the number of experiments was kept to a minimum. Thus, the five factors were incorporated into two three-factor designs (parametric studies) where their effect was estimated using ANOVA. A three-factor design means that three sources of variance can be investigated in an experiment.

The parametric studies were divided into two separate portions, as shown in Table 5.1. Parametric study #1 evaluated the effect of Reamer diameter, RPM and advancement speed assuming there were no complications due to variations of bone marrow viscosity or clogged reamer. Parametric study #2 examined the influence of factors such as bone marrow variation and degree of clogged reamer as well as the effect of the reamer diameter in such cases.

Parametric Study	Reamer Size [mm]	Rotational Speed [RPM]	Advancement Speed $[\frac{mm}{sec}]$	Viscosity [cP]	Reamer Clogging Factor
1	11-16	200,50	50,10	82.6	Unclogged
2	11,11.5,12,15	200	50	82.6, 396	Clogged, Unclogged

Table 5.1- Summary of parameter variation in the parametric studies.

5.3.2 F-test

The statistical test used in ANOVA is called the *F*-test, named after the statistician who developed it, Ronald A. Fisher. *F* is defined as the ratio of *effect variance* to *error variance*. Effect variance represents systematic variation due to the *effect* of different factors. Error variance represents random variations due to *chance* that are not due to the effect of factors. The higher this ratio is (*F*-value), the higher is the significance of the effect of the corresponding factor.[54] The mathematical definition of the *F*-value is presented in Equation (5-2). Further details on calculation of the variances are explained in Section 5.3.5.

$$F = \frac{\text{Variance of the factor of interest}}{\text{Variance of the error}} \qquad (5\text{-}2)$$

In a three-factor design, a total of six *F*-values are calculated: three for the main effects of the factors and three for the interaction between each two factors. Based on the *F*-value, a level of significance can be found from *F*-tables. The level of significance is represented by a *p*-value.

5.3.3 p-value

A *p*-value represents how likely it is that an experimental observation could have occurred by chance. A small *p*-value, $p < 0.05$, means that there is less than 5% probability that the experimental results only occurred by chance. In other words, there is $100(1-p)\%$ confidence that the results did not occur by chance. This result is said to be significant at the $p < 0.05$ level of significance. [54]

5.3.4 *Null Hypothesis*

The statistical significance of factors is tested based on rejection of the null hypothesis, H_o, shown by Equation (5-3), where t is the number of treatments and α_t is the quantitative effect of each treatment.[55] Note that a treatment is defined as an application of different levels of factors to estimate the effect of that factor on the dependent variable (i.e., pressure, in the present work).

$$H_o : (\alpha_t = 0, \text{for } t = 1, 2, 3, \ldots) \qquad (5\text{-}3)$$

The null hypothesis states that the effect of each treatment is zero. In other words, every treatment is the same. If the p-value found, based on the F-value, is small enough (e.g., $p<0.05$ or $p<0.01$), the null hypothesis can be rejected. Rejection of H_o means that the effect of treatments are NOT the same; hence, the corresponding factor is statistically significant and can have a significant effect on the pressure (dependent variable).[55]

5.3.5 *Variance*

Variance is a fundamental concept in ANOVA and most statistical analysis. Variance reflects the total deviation of all experimental observations from the overall mean. The general mathematical definition of variance is shown in Equation (5-4), where $\sum (X - \overline{X})^2$ is the sum of the squares (SS) of the deviation of each experimental observation (X) from the mean ($\overline{X}$). The mean is defined as the sum of all the observations divided by the total number of observations (n), Equation (5-5). [54]

$$Varianvce\,(S^2) = \frac{\sum (X - \bar{X})^2}{n-1} \qquad (5\text{-}4)$$

$$Mean\,(\bar{X}) = \frac{\sum X}{n} \qquad (5\text{-}5)$$

The quantity $n-1$ is known as the Degrees of Freedom (*DOF*). In ANOVA, the degree of freedom for each factor represents the number of levels associated with that factor minus one. Therefore, in ANOVA, the total number of observations (n) for each factor is equal to the number of levels corresponding to that factor.

5.4 Parametric Study 1: Effect of Reamer Size, RPM and Advancement Speed on Intramedullary Pressure Elevation

5.4.1 Methodology

The factorial experimental design established to verify the effect of factors such as reamer diameter (factor A), rotational speed (factor B) and advancement speed (factor C) is summarized in Table 5-2. Factor A had eleven levels and factors B and C had two levels each. A total number of forty four experiments were conducted in which four synthetic bones were each reamed eleven times using reamer sizes from 11 mm to 16 mm, increased in diameter by 0.5 mm steps. In each bone, all eleven reamers were inserted at a constant RPM and advancement speed, as shown in Table 5.2.

Bone #	Reamer Size [*mm*] (Factor A)	Rotational Speed [*rpm*] (Factor B)	Advancement Speed [$\frac{mm}{sec}$] (Factor C)	Bone Marrow Viscosity [cP]	Reamer Clogging Factor
1	11-16	200	10	82.6	Unclogged
2		50	10		
3		200	50		
4		50	50		

Table 5.2-Parametric study#1-Summary of factors and levels.

In each experiment, only the peak pressures (maximum pressures from each run) recorded by the transducers were used for the analysis; as these are the most likely to cause ejection of bone marrow fat into the bloodstream in a real bone. The effect of the parameters was analyzed separately for each of the three pressure transducers, as they are positioned at different locations throughout the bone (Figure 5-2). Appendix A (Figures A.1 to A.44) contains pressure profiles from which the maximum pressures were used in parametric study #1.

5.4.2 Results and Discussion

Table 5.3, 5.4 and 5.5 show the peak pressures recorded during each run by pressure transducers #1 (proximal), 2 (middle) and 3 (distal), respectively. To observe the trend of pressure variations with different reaming parameters, these pressures are also presented using bar graphs in Figure 5-6, 5-7 and 5-8.

P_1 [mmHg]	Rotational Speed (B)			
	50 [RPM]		200 [RPM]	
Reamer Size (A) [mm]	Advancement Speed (C)		Advancement Speed (C)	
	$10\,[\frac{mm}{sec}]$	$50\,[\frac{mm}{sec}]$	$10\,[\frac{mm}{sec}]$	$50\,[\frac{mm}{sec}]$
11	63.8	23.3	9.1	28.8
11.5	26.3	36.1	17.6	27.3
12	24.5	52.1	18.8	43.4
12.5	23.4	36.7	22.0	38.9
13	26.1	49.1	20.3	53.9
13.5	25.9	35.6	18.1	39.1
14	15.6	34.1	19.1	33.9
14.5	11.3	39.8	12.9	33.2
15	14.3	45.3	12.8	19.3
15.5	12.7	33.1	11.4	20.9
16	18.2	27.0	27.1	21.9

Table 5.3- Parametric study #1-Peak pressures recorded by pressure transducer #1

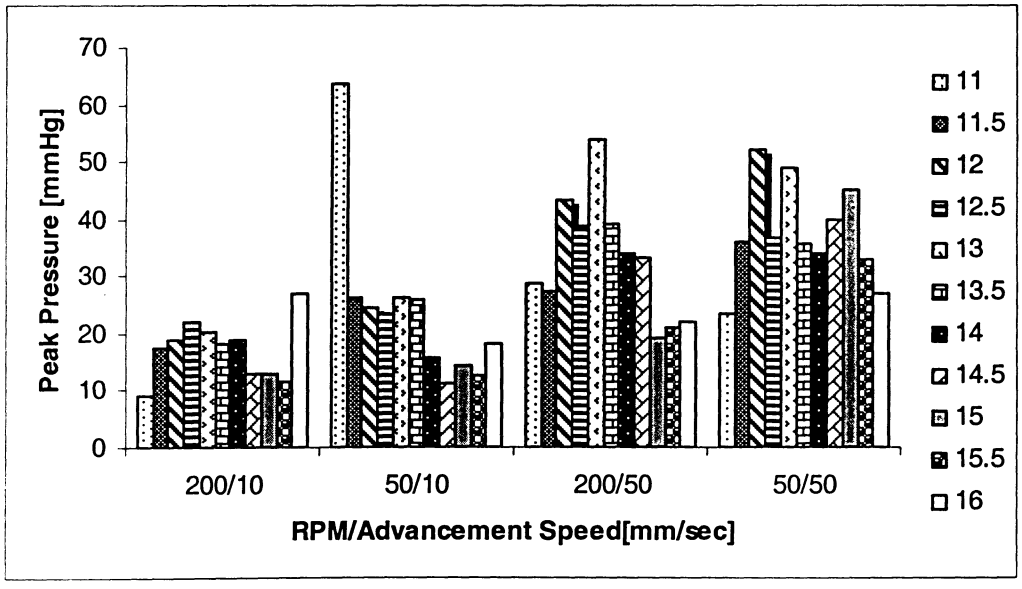

Figure 5-6-Bar graph representation of data from Table 5.3. Peak pressures observed from pressure transducer #1.

P_2 [mmHg]	Rotational Speed (B)			
	50 [RPM]		200 [RPM]	
Reamer Size (A) [mm]	Advancement Speed (C)		Advancement Speed (C)	
	$10\ [\frac{mm}{sec}]$	$50\ [\frac{mm}{sec}]$	$10\ [\frac{mm}{sec}]$	$50\ [\frac{mm}{sec}]$
11	28.3	17.8	14.0	34.3
11.5	49.1	81.8	14.5	39.5
12	36.1	57.2	18.2	54.3
12.5	31.0	51.5	23.2	55.8
13	27.9	73.3	21.7	66.7
13.5	31.1	51.3	18.4	47.4
14	18.2	60.2	17.7	47.4
14.5	18.0	64.5	11.7	63.0
15	24.3	62.0	16.0	35.6
15.5	28.7	70.1	17.3	41.1
16	26.0	57.7	22.3	38.9

Table 5.4- Parametric study #1-Peak pressures recorded by pressure transducer #2

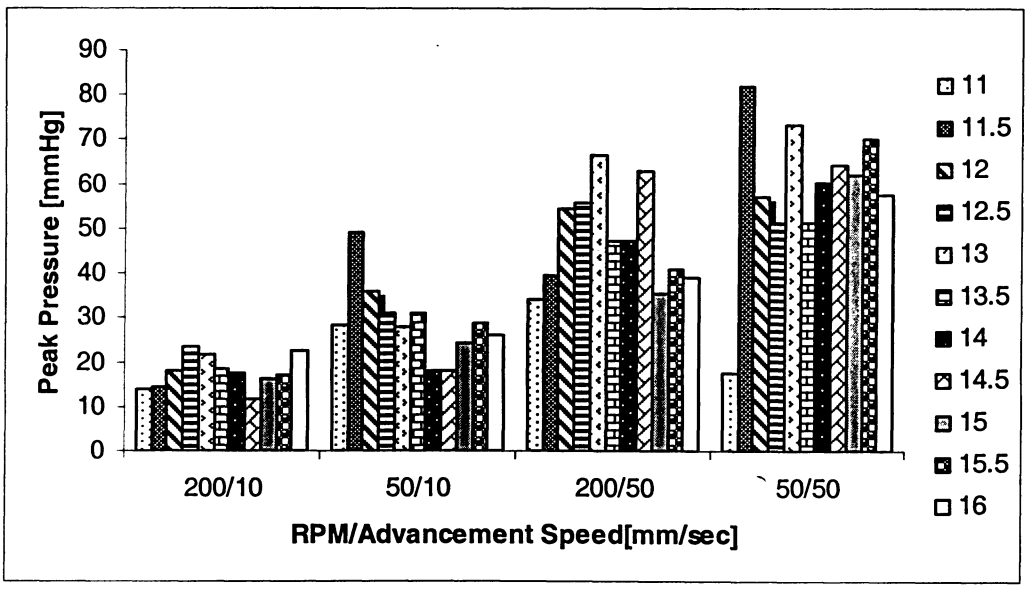

Figure 5-7- Bar graph representation of data from Table 5.4. Peak pressures observed from pressure transducer #2.

P_3 [mmHg]	Rotational Speed (B)			
	50 [RPM]		200 [RPM]	
Reamer Size (A) [mm]	Advancement Speed (C)		Advancement Speed (C)	
	10 [$\frac{mm}{sec}$]	50 [$\frac{mm}{sec}$]	10 [$\frac{mm}{sec}$]	50 [$\frac{mm}{sec}$]
11	42.6	13.5	12.9	41.4
11.5	40.4	112.1	17.0	100.5
12	48.5	132.0	14.8	51.4
12.5	20.2	56.6	11.3	43.5
13	25.4	54.2	11.9	62.2
13.5	24.0	48.4	10.9	39.8
14	16.3	49.8	8.3	40.2
14.5	15.7	93.7	8.8	41.6
15	20.7	46.0	11.5	35.3
15.5	21.4	46.3	11.6	31.2
16	27.9	28.4	13.9	28.7

Table 5.5- Parametric study #1-Peak pressures recorded by pressure transducer #3

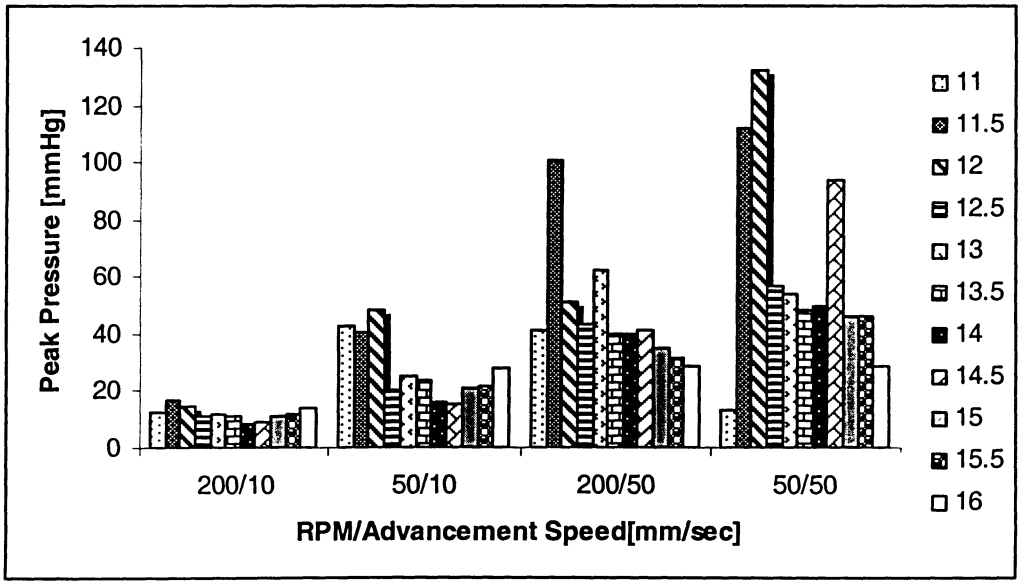

Figure 5-8- Bar graph representation of data from Table 5.5. Peak pressures observed from pressure transducer #3.

To determine the statistical significance of these observations, and thus show how changes in RPM and advancement speed influenced the simulated intramedullary pressure, the results from ANOVA, based on the comparison of *peak pressures* detected

during each run, are reported in Table 5.6, 5.7, and 5.8 for pressure transducers #1, 2 and 3, respectively.

Pressure Transducer #1 (P_1)					
Source of Variation	**Sum of Squares**	**Degree of Freedom**	**Variance**	***F*-value**	***p*-value**
Reamer Size(A)	1156.4	10	115.6	1.2	0.3558
RPM (B)	352.2	1	352.2	3.5	0.0701
Advancement Speed (C)	2345.9	1	2345.9	23.4	0
Error	3101.5	31	100.0		
Total	6956.1	43			

Table 5.6-Parametric study #1-Statistical analysis (ANOVA) for pressure transducer #1

Pressure Transducer #2 (P_2)					
Source of Variation	**Sum of Squares**	**Degree of Freedom**	**Variance**	***F*-value**	***p*-value**
Reamer Size(A)	1619.3	10	161.9	1.6	0.1584
RPM (B)	1383.7	1	1383.7	13.5	0.0009
Advancement Speed (C)	9832.3	1	9832.3	96.1	0
Error	3172.2	31	102.3		
Total	16007.5	43			

Table 5.7- Parametric study #1-Statistical analysis (ANOVA) for pressure transducer #2

Pressure Transducer #3 (P_3)					
Source of Variation	**Sum of Squares**	**Degree of Freedom**	**Variance**	***F*-value**	***p*-value**
Reamer Size(A)	8305.9	10	830.6	2.6	0.0196
RPM (B)	2559.3	1	2559.3	8.1	0.0079
Advancement Speed (C)	13158.1	1	13158.1	41.4	0.0000
Error	9841.0	31	317.5		
Total	33864.3	43			

Table 5.8- Parametric study #1-Statistical analysis (ANOVA) for pressure transducer #3

5.4.2.1 Effect of reamer diameter

Based on Figure 5-6, 5-7 and 5-8, no particular systematic variation of pressure with reamer diameter was observed. Results from ANOVA (Table 5.6 to 5.8) also show that the reamer diameter had no significant influence on the pressure at the open end or mid-shaft of the bone (transducers #1 and 2, $p = 0.36$ and 0.16 respectively). This result is in accordance with that of Peter et al.[19], who reported no links between the mid-shaft pressure elevations due to increasing reamer diameter, based on *in-vivo* measurements on nine patients undergoing orthopaedic reaming.

Nevertheless, in the case of the most distal pressure transducer (transducer #3,Figure 5-8), the smaller diameter reamers created higher peak pressures than the larger diameter reamers. This is probably because, when reaming with the smaller diameters (e.g., 11, 11.5, 12, 12.5 mm), more cancellous material was available in the bone, which makes it more difficult for the marrow fluid to escape through the open entrance, hence pushing the fluid towards the closed end of the bone where higher pressure peaks are observed during initial reaming. Starting from reamer size 13 mm and up, there was little cancellous material left in the bone. Therefore, the gap between the reamer and cortical layer (outer layer) was less blocked by cancellous material, which allowed the marrow to escape through the open entrance more easily, resulting in less pressure buildup at the closed end of the bone where pressure transducer #3 is located. This is in agreement with the results of Johnson et al.[8] and Heim et al.[21], who both found that typically the first few reamers inserted in the bone resulted in higher pressure peaks than the consecutive ones. They also reasoned this phenomenon was due to higher available cancellous bone in the first few reamer penetrations, stopping the marrow from traveling to the open entrance of

the bone and creating the high pressures at the closed end of the bone. Results from ANOVA in the present work confirm that changes in the reamer diameter significantly affected the pressure elevation at the distal end of the bone, at pressure transducer #3 ($\sim p<0.02$).

5.4.2.2 Effect of advancement speed

Results from ANOVA (Table 5.6 to 5.8) showed that advancement speed of the reamer had the most significant effect on the pressure, ($p \approx 0$). Higher pressure elevations were observed during reaming at a higher advancement speed, whereas lower pressures corresponded to lower advancement speed (see Figure 5-6 to 5-8). To see this trend more clearly, the *mean of the peak pressures* detected while reaming the cancellous layer with eleven reamers were compared at each pressure transducer in Figure 5-9. It was observed that the *peak pressures,* on average, were 2.1 times larger in magnitude using high advancement speed ($50\frac{mm}{\text{sec}}$) than low advancement speed ($10\frac{mm}{\text{sec}}$). This result is in accordance with those reported by Mousavi et al.[9] and Peter et al.[19]. Dobrjanski[11] also reported very high pressure increase in the proximal part of the bone, at faster advancement speeds, while hammering rubber tip implants into the cortical layer of the presently utilized synthetic bone analogue.

5.4.2.3 Effect of RPM

Comparison of the mean of the peak pressures (Figure 5-9) for the 50/10 and 200/10 (or 50/50 and 200/50) cases shows that higher peak pressures were detected at lower RPM. These results match with those reported by Mousavi et al.[9] based on reaming experiments using silicone cylindrical shells filled with a mixture of 1:2 ratio of paraffin

and petroleum jelly. Mousavi et al.[22]also reported similar intramedullary elevations while reaming at low RPM, when conducting animal studies with either fractured or intact femur.

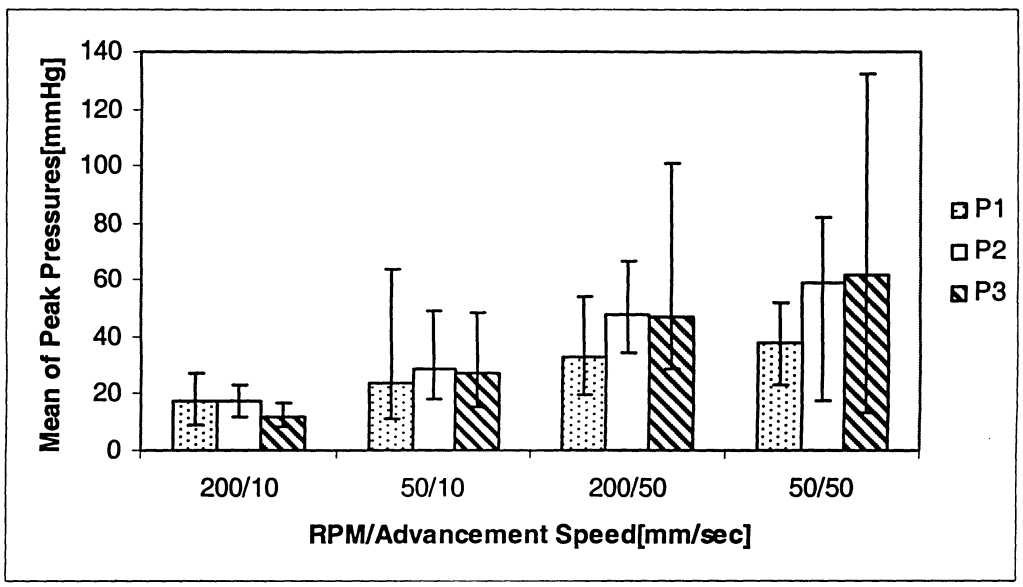

Figure 5-9 Effect of reaming rpm and advancement speed on mean of the peak pressures recorded using all eleven reamer sizes. Bars represent the mean of the peak pressures, and the vertical lines show the range of peak pressures.

Based on results from ANOVA (Table 5.6 to 5.8), the influence of the reamer RPM on the intramedullary pressure was statistically significant throughout the bone. However, the effect of variations in reamer RPM was more significant on the mid-shaft, transducer #2, and end of bone, transducer #3, ($\sim p < 0.001$) than at the reamer entrance, transducer #1, ($\sim p < 0.07$). This implies that, at the reamer entrance, the RPM has less effect on the pressure than the other factor (advancement speed). The reason can be speculated that, at any constant advancement speed, the amount of marrow escaping the reamer entrance is the same for high and low RPM, hence generating the same pressure elevations at the reamer entrance (transducer #1).

5.5 *Parametric Study 2: Effect of Reamer Diameter, Bone Marrow Viscosity and Clogged Reamer on Intramedullary Pressure Elevation*

5.5.1 Methodology

During orthopaedic reaming, clogging of the reamer is expected due to the destruction of a large volume of cancellous layer in the bone. As the bone debris mixes with the bone marrow, the mixture fills up the reamer flutes, which can behave like a piston and cylinder system (see Section 2.6.3), potentially causing intramedullary pressure elevation.[8] However, the synthetic cancellous material (carbon foam) did not appear to clog the reamer flutes as has been reported in the literature.[19,8,56] The reason was the tendency of the carbon foam to disintegrate into powder and mix with the bone marrow, creating a paste that covered the flutes, rather than clogging them. This was likely due to the carbon foam being more brittle than real cancellous bone. Even though the Young's modulus and strength of the synthetic cancellous layer matched those of real cancellous bone, the fracture mechanics properties of cancellous bone analogue were apparently not similar to that of the real bone. Therefore, to simulate the clogging of the reamer, the reamer flutes were carefully filled with silicon sealant (LePage all-purpose clear silicon sealant, North York, ON., Canada) to study the effect of a clogged reamer.

Bryant et al.[36], reported variations in the marrow viscosity between the distal and proximal region of the femur (50cP and 600cP respectively). In the subsequent experiments, to incorporate viscosity variation of bone marrow, the ratio of petroleum jelly/ paraffin was varied as previously discussed in Section 4.3.

The factorial design established to evaluate the effect of reamer diameter (factor A), bone marrow viscosity (factor B) and clogged reamer (factor C) on intramedullary

canal pressure is summarized in Table 5.9. Factor A had four levels and factors B and C had two levels each. Forty four experiments were conducted (originally considering eleven levels for factor A) using the same procedure described in Section 5.3.1, but with 200 RPM spindle speed and advancement speed of $20\frac{mm}{sec}$ However, these experiments were conducted prior to the introduction of the stainless steel adaptors (see Section 4.4.5.1and 5.2), and thus the pressure transducers were directly attached to the bone. Unfortunately due to insufficient supply of raw material, it was not possible to repeat these experiments after the modifications were made to the experimental set-up. Nevertheless, the unrealistically high pressure spikes, discussed in Section 5.2, and shown in Appendix B (Figures B.1 to B.44) were easily identified, and thus experiments in which any of the three pressure transducers experienced spikes were not considered for the statistical analysis of this study. Therefore, only data from reamer sizes 11, 11.5, 12 and 15 mm were used, in which no spikes were evident. This left only four levels for factor A (reamer size) to be considered for statistical analysis, thus a total of sixteen experiments were considered.

Bone #	Reamer Size [mm] (Factor A)	Rotational Speed [rpm] (Factor B)	Advancement Speed [$\frac{mm}{sec}$] (Factor C)	Bone Marrow Viscosity [cP]	Reamer Clogging Factor
1	11,11.5,12,15	200	20	82.6	Clogged
2				82.6	Unclogged
3				396	Clogged
4				396	Unclogged

Table 5.9-Parametric study#2-Summary of factors and levels.

As before, the maximum pressures recorded by the pressure transducers during each experiment were used for the purpose of statistical analysis for the selected reamer sizes (Table 5.9), and data from each pressure transducer was analyzed separately. Appendix B (Figures B.1 to B.44) shows the pressure profiles of the raw experimental data used in parametric study #2.

5.5.2 Results and Discussion

Table 5.10, 5.11 and 5.12 respectively show the *peak pressures* recorded by pressure transducers #1, 2 and 3 corresponding to each reamer size at different reaming conditions. To better observe the variation of pressure due to these factors, bar graph representations of the latter data are shown in Figure 5-10, 5-11 and 5-12.

P_1 [mmHg]	Bone Marrow Viscosity (B)			
	82.6 [cP]		396 [cP]	
Reamer Size (A) [mm]	Clogging Factor (C)		Clogging Factor (C)	
	CR	UR	CR	UR
11	77.3	14.2	208.4	146.7
11.5	127.7	12.6	289.6	125.5
12	112.1	32.1	409.1	115.0
15	112.3	21.9	99.4	44.3

Table 5.10-Parametric study #2-Peak pressures recorded by pressure transducer #1. CR: "Clogged Reamer" and UR:" Unclogged Reamer

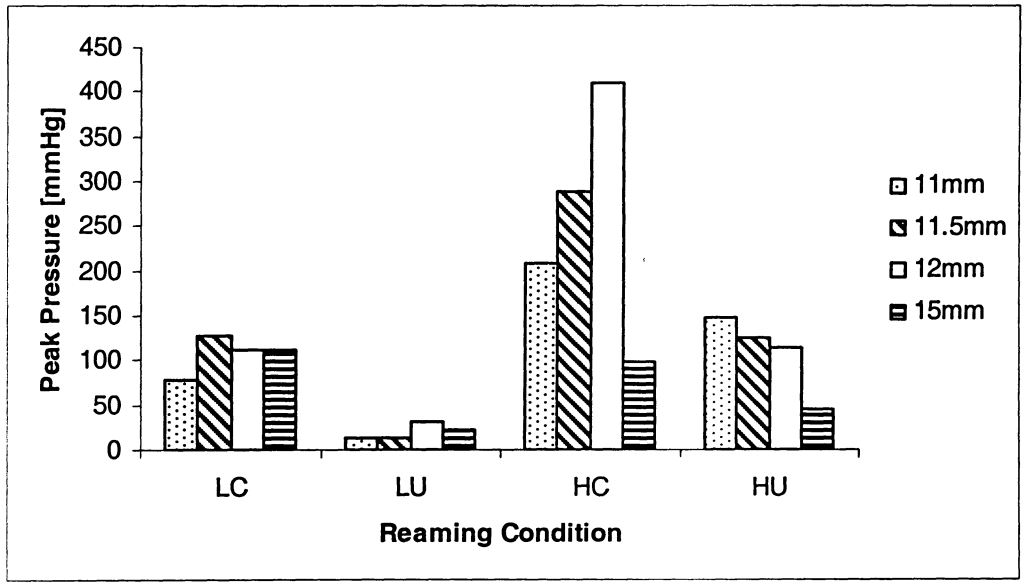

Figure 5-10-Reaming conditions versus peak pressures detected by transducer #1. Each column represents the maximum pressure detected by transducer #1 while reaming with the corresponding reamer size and reaming condition(LC:Low viscosity marrow/Clogged reamer, LU:Low viscosity marrow/Unclogged reamer, HC:High viscosity marrow/Clogged reamer, HU: High viscosity marrow/Unclogged reamer)

P_2 [mmHg]	Bone Marrow Viscosity (B)			
	82.6 [cP]		396 [cP]	
Reamer Size (A) [mm]	Clogging Factor (C)		Clogging Factor (C)	
	CR	UR	CR	UR
11	89.1	25.2	325.0	318.8
11.5	105.5	20.2	283.0	119.5
12	83.7	61.8	291.6	106.8
15	111.5	29.8	165.8	76.8

Table 5.11-Parametric study #2-Peak pressures recorded by pressure transducer #2. CR: "Clogged Reamer" and UR:" Unclogged Reamer

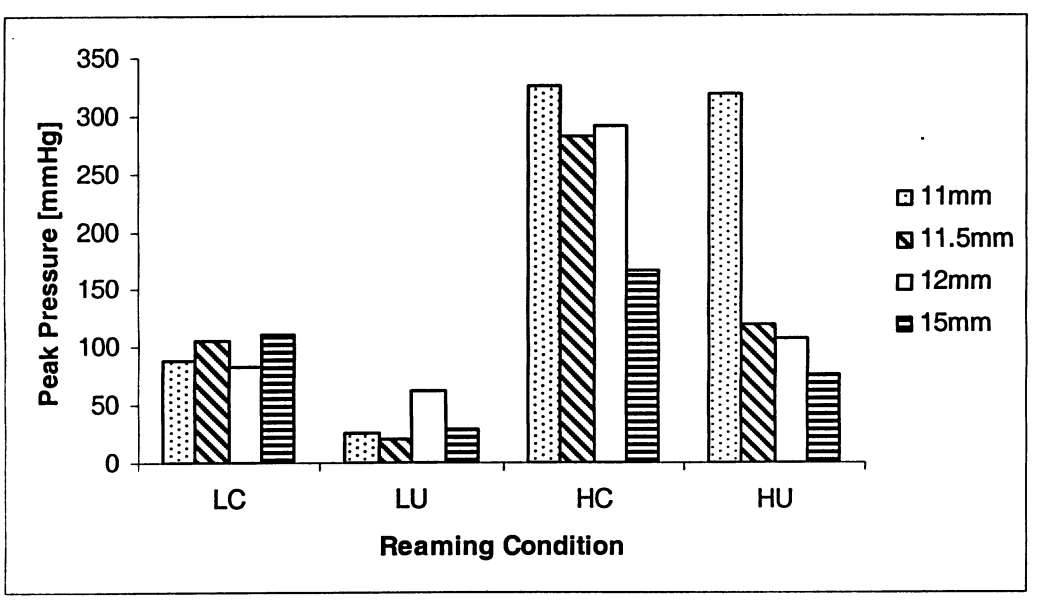

Figure 5-11- Reaming conditions versus peak pressures detected by transducer #2. Each column represents the maximum pressure detected by transducer #2 while reaming with the corresponding reamer size and reaming condition (LC: Low viscosity marrow/Clogged reamer, LU: Low viscosity marrow/Unclogged reamer, HC: High viscosity marrow/Clogged reamer, HU: High viscosity marrow/Unclogged reamer)

P_3 [mmHg]	Bone Marrow Viscosity (B)			
	82.6 [cP]		396 [cP]	
Reamer Size (A) [mm]	Clogging Factor (C)		Clogging Factor (C)	
	CR	UR	CR	UR
11	85.6	16.3	279.4	120.7
11.5	50.2	10.6	234.1	64.4
12	57.9	34.7	258.5	107.2
15	95.4	14.7	206.3	62.6

Table 5.12-Parametric study #2-Peak pressures recorded by pressure transducer #3. CR: "Clogged Reamer" and UR:" Unclogged Reamer

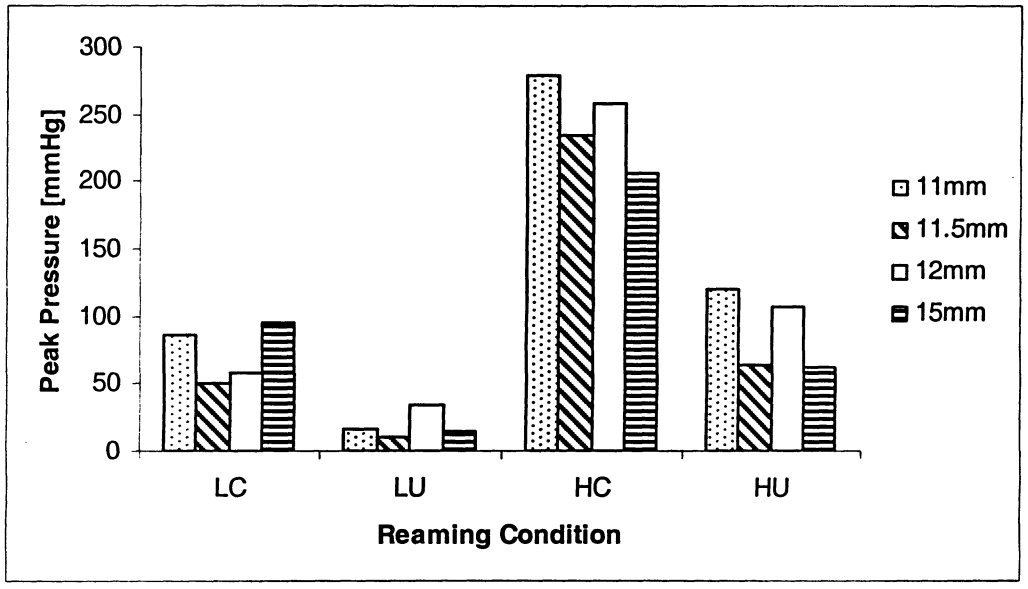

Figure 5-12- Reaming conditions versus peak pressures detected by transducer #3. Each column represents the maximum pressure detected by transducer #3 while reaming with the corresponding reamer size and reaming condition (LC: Low viscosity marrow/Clogged reamer, LU: Low viscosity marrow/Unclogged reamer, HC: High viscosity marrow/Clogged reamer, HU: High viscosity marrow/Unclogged reamer)

In general, the highest peak pressures at each transducer were observed while using high viscosity marrow and clogged reamer, and the lowest peak pressures were observed while using low viscosity marrow and unclogged reamer. To confirm these observations, the results of the ANOVA analysis are reported in Table 5.13, 5.14 and 5.15, respectively, for pressure transducers #1, 2 and 3.

Pressure Transducer #1 (P_1)					
Source of Variation	**Sum of Squares**	**Degree of Freedom**	**Variance**	***F*-value**	***p*-value**
Reamer Size(A)	20739.6	3.0	6913.2	1.7	0.2348
Viscosity (B)	53807.4	1.0	53807.4	13.0	0.0048
Clogging Factor(C)	53315.1	1.0	53315.1	12.9	0.0049
Error	41276.2	10.0	4127.6		
Total	169138.2	15.0			

Table 5.13-Parametric study #2-Results of statistical analysis (ANOVA) for pressure transducer #1

Pressure Transducer #2 (P_2)					
Source of Variation	**Sum of Squares**	**Degree of Freedom**	**Variance**	***F*-value**	***p*-value**
Reamer Size(A)	17851.5	3.0	5950.5	1.6	0.2490
Viscosity (B)	84162.8	1.0	84162.8	22.7	0.0008
Clogging Factor(C)	30309.6	1.0	30309.6	8.2	0.0169
Error	37015.5	10.0	3701.6		
Total	169339.4	15.0			

Table 5.14-Parametric study #2-Results of statistical analysis (ANOVA) for pressure transducer #2

Pressure Transducer #3 (P_3)					
Source of Variation	**Sum of Squares**	**Degree of Freedom**	**Variance**	***F*-value**	***p*-value**
Reamer Size(A)	3375.2	3.0	1125.1	0.8	0.5348
Viscosity (B)	58540.6	1.0	58540.6	40.3	0
Clogging Factor(C)	43709.8	1.0	43709.8	30.1	0.0003
Error	14541.4	10.0	1454.1		
Total	120167.0	15.0			

Table 5.15- Parametric study #2-Results of statistical analysis (ANOVA) for pressure transducer #3

5.5.2.1 Effect of reamer diameter

It was observed (Figure 5-10 to 5-12) that the reamer diameter had no significant effect on intramedullary pressure elevations in comparison to the effect of other two factors (viscosity and clogged bone). Also, based on results from ANOVA (Table 5.13-5.15), it was concluded that the reamer size did not significantly influence the intramedullary pressure elevation in any of the pressure transducers, with p-values of 0.235, 0.249 and 0.535 respectively.

5.5.2.2 Effect of marrow viscosity

In Figure 5-10 to 5-12, it can be seen that an increase in marrow viscosity resulted in a higher peak pressure for all transducers (an average 2.4 times increase). Other investigators[8,36] have also reported similar behaviour, which can be explained due to the fact that higher viscosity marrow flows with greater difficulty through the open entrance or the porous walls of the bone, resulting in higher pressures. The ANOVA results (Table 5.13-5.15) also confirm that variation in bone marrow viscosity had a significant effect on the pressure ($\sim p < 0.01$).

5.5.2.3 Effect of clogging of the reamer

Figure 5-10 to 5-11 show that, when using reamers fully covered with silicon (clogged), the peak pressures at all transducers were in average 2.3 times higher in magnitude than when using those that were unclogged. This could be explained based on the piston and cylinder theory, described in Section 2.6.3. As the reamer begins to clog with bone debris (in this case, covered by silicon), the reamer flutes are covered, hence

preventing fluid escape through the flute passage. The results from ANOVA (Table 5.13-5.15), confirm that the clogged reamer has a significant effect on pressure elevations ($\sim p<0.02$), as also reported by Johnson et al. [8]

5.6 Comparison to Literature

Maximum pressures observed during orthopaedic reaming differed from study to study depending on the nature of the bone specimen used in each study. For example, results from studies using intact bone (unbroken) differed from those using fracture bones. Typically, lower intramedullary pressures were reported from fractured bone. For example, Frolke et al.[56]reported peak pressures of 1005 mmHg and 493 mmHg for an intact, and fractured femur, respectively, when reaming human cadaveric femurs. They reasoned that the difference was due to a lack of decompression in an intact bone compared to that of a fractured bone, wherein fluid can escape via the fracture.

The bone analogue design used in this paper experienced a significant back flow of marrow escaping the bone from the open end of the cylinder, causing a similar decompression. In a real bone reaming procedure, depending on the reamer design, the back flow through the open end of the bone may become clogged with bone fragments, significantly raising the pressures from those seen in the present work.

In the current work, the pressures seen were in the range of 10 to 409 mmHg, with the higher pressures being seen when the reamer blades were fully clogged, at 200 rpm and 20 $\frac{mm}{sec}$ advancement speed. These values match well with those of Peter et al.[19], who reported a maximum intramedullary pressure ranging from 300 to 450 mmHg while reaming nine fractured human femur at 350 rpm with the smallest reamer diameter of 9

mm. This pressure is also relatively close to the peak pressure of 511mmHg reported by Heim et al.[21], based on experiments on intact (unfractured) human cadaveric femurs. Even though Heim et al. used intact bones, the maximum pressure they recorded was lower than many other studies[22,23] utilizing intact bone. The reason could be due to the fact that in their study, the pressure transducers were indirectly attached to the bones using connecting adaptors, as also employed in the current work. As described in 5.2, it was demonstrated that the connecting adaptors prevented the unrealistically high pressure spikes associated with transducer vibration. It is possible that some of the studies in the literature reporting the extremely high peak pressures could also have suffered from this phenomenon. Such studies include those of Mousavi et al.[22], who reported a maximum intramedullary pressure of 700mmHg while reaming of intact adult sheep femur, and Kropfl et al.[23], who reported maximum intramedullary pressure of 936±48 mmHg while reaming of intact femoral shaft of eight baboons. However, the reason for these high pressure reports could be also be due to the fact they were mainly based on animal studies rather than human or cadaveric bones.

6 Analysis of Imposed Forces and Torque during Reaming Procedures

The planar force components in x and y, F_x and F_y, as well as the axial force in z-direction, F_z (Figure 6-1 and 6-2), were monitored using a dynamometer during the reaming experiments, as explained in Section 4.4.6. Measurements of force components were required to assess the correlation between the simulated intramedullary pressure and applied forces to the bone. The measured force components were also used by another Ryerson graduate student to study the radial variations in the diameter of the reamed intramedullary canal due to system vibrations, as mentioned in Section 3.3.[46,47]

Data corresponding to the three forces were collected in separate channels using the DAQ system with the rate of 20000 samples per second (20 kHz). A schematic of forces and their corresponding directions on the load cell (dynamometer) is shown in Figure 6-1. The orientation of forces applied on the bone attached to the set-up is shown in Figure 6-2.

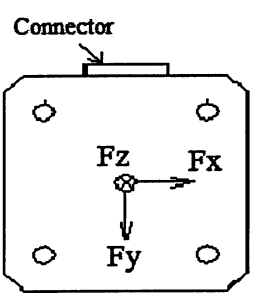

Figure 6-1- Schematic of forces as they appear on the dynamometer. Bone analogue is attached to the dynamometer perpendicular to the x-y plane, with gravity in the y direction.

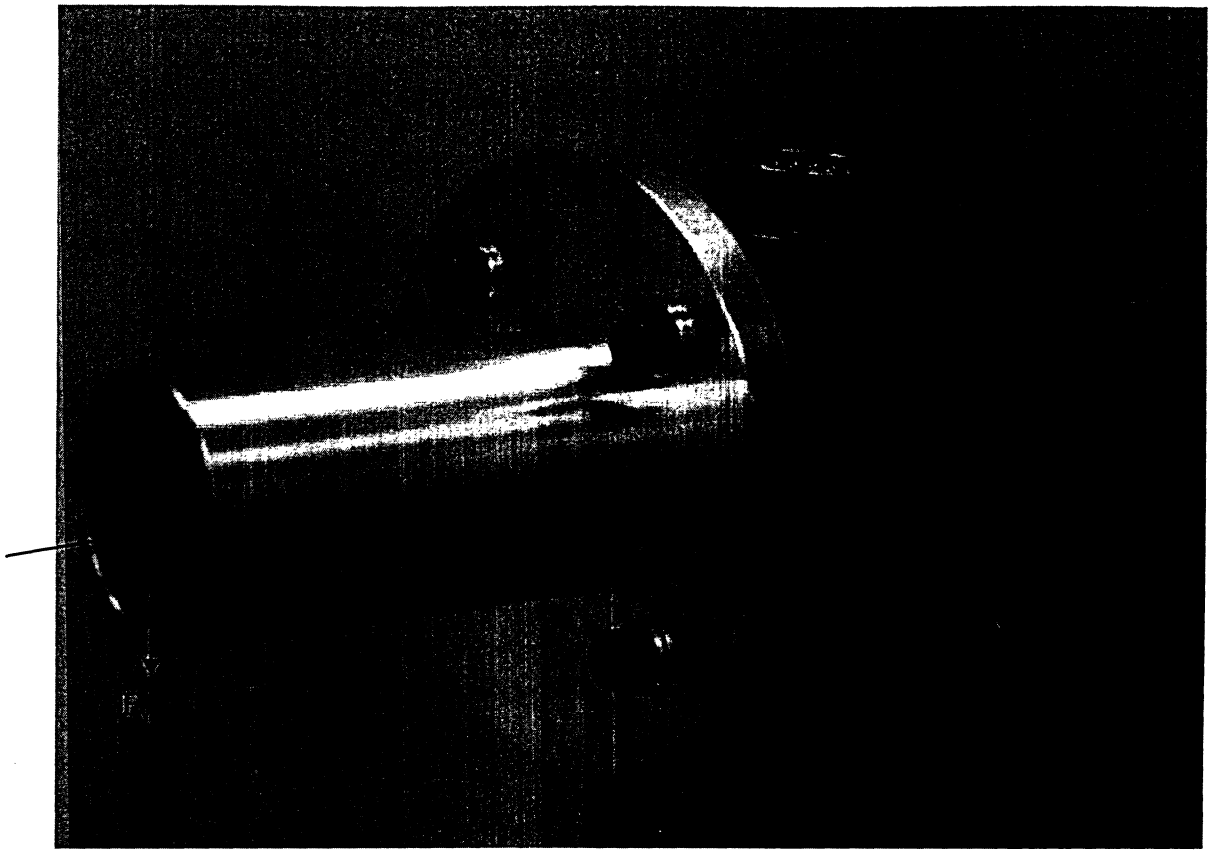

Figure 6-2-Orientation of forces applied to the bone on the apparatus

6.1 Typical Force Data

A typical force versus time curve generated during a reaming experiment is shown in Figure 6-3 . Similar to the pressure signals discussed in Chapter 5, it can be seen that this curve follows a periodically repeating pattern as the reamer rotates. The pattern was repeated with the same frequency as that of one reamer revolution (see Section 5.1 for further detail on the observed dominant frequency). During each revolution of the reamer, the force from each channel reached a maximum and a minimum peak.

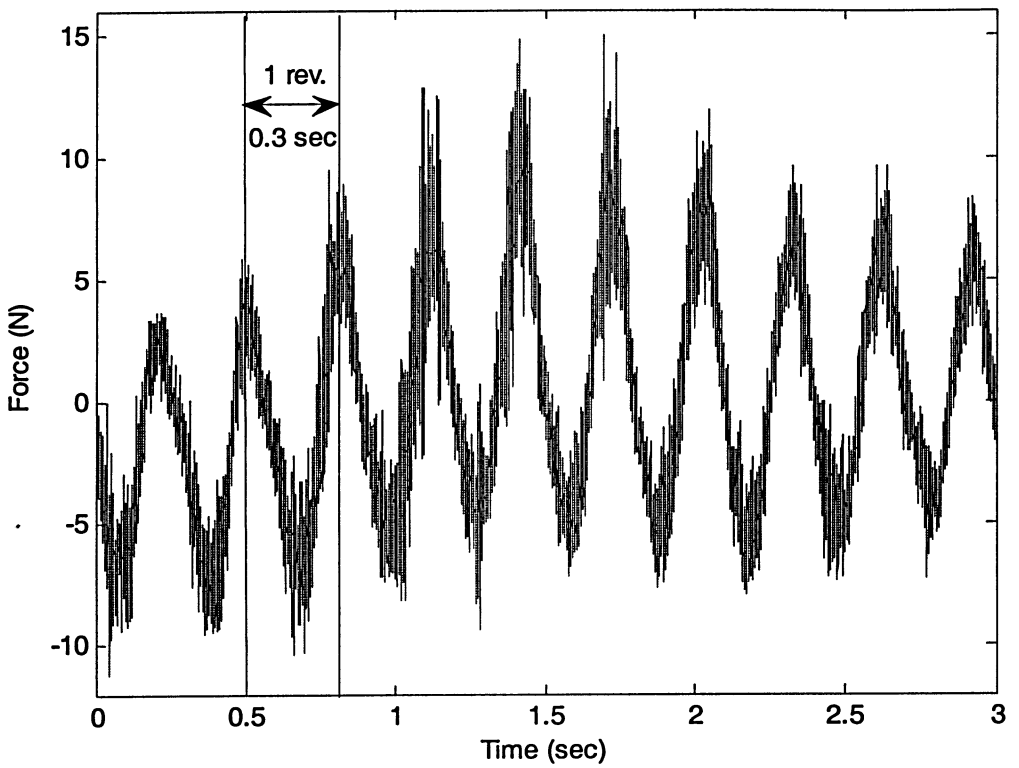

Figure 6-3-Typical force data versus time. A three-second time frame is depicted in this figure from the force component in y-direction, Fy. This sample is taken from an experiment with rotational speed of 200RPM and advancement speed of 20 mm/sec using bone marrow viscosity of 82.6 cP. Period of 0.3 second for one revolution of reamer is calculated based on rotational speed of 200 RPM.

The planar force components (F_x and F_y) measured by load cell were the equivalent sum of all the forces applied to the blades during reaming. This is shown in Figure 6-4.

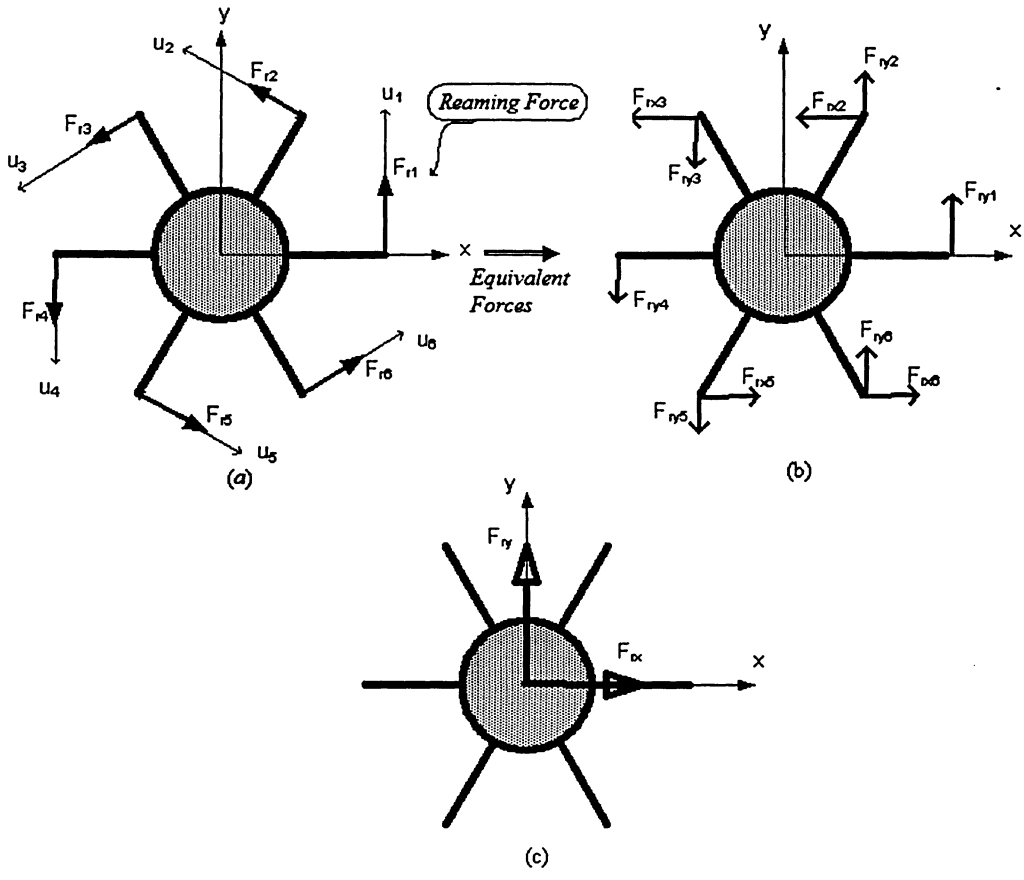

Figure 6-4-A cross-sectional view of a simplified geometry six-blade reamer with the applied forces; (a) shows a rough approximation of the forces applied to the reamer on each blade, in their original direction. (b) shows the reaming force components applied to each blade, in x and y direction. (c) shows the resultant force components in x and y direction

A comparison of the three force components during reaming is shown in Figure 6-5. It is evident that there was a time delay between maximum peaks of F_x and F_y. Further investigations showed that this time delay was equivalent to that of a quarter of one revolution. The reason is that the reamers were likely slightly warped, and as the blade passed the positive direction of the y-axis there was a time lag of ¼ of a revolution before it passed the positive direction of the x-axis. There was no time lag between the peaks of F_x and the axial force, F_z.

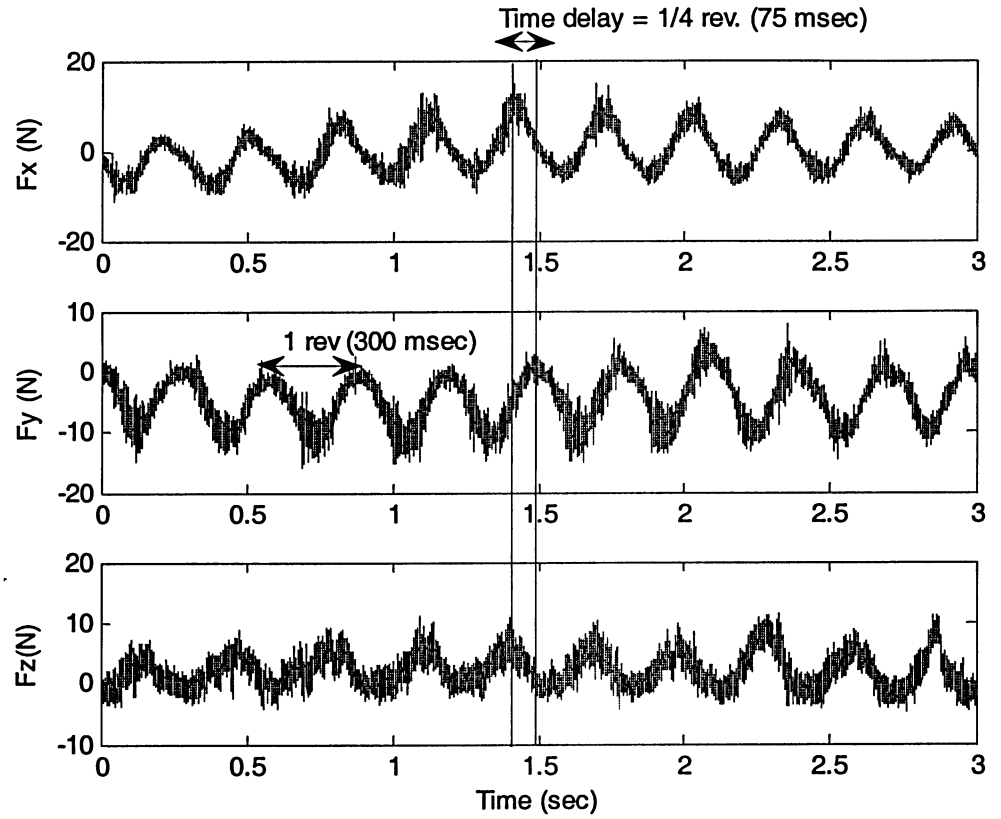

Figure 6-5-Time delay between the force components. Data was taken while reaming with an unclogged 12.5mm reamer at 200 rpm and 20 mm/sec advancement speed using low viscosity marrow (82.6 cP).

6.2 Correlation Analysis

6.2.1 Definitions

Correlation analysis attempts to measure the correlation between two or more variables. *Correlation* is a measure of the relationship between two or more variables. The *correlation coefficient*, *R*, is a single number that describes the degree of strength of such relationships between two variables, *X* and *Y*. Correlation coefficients can range from -1 to +1, where a value of -1 represents a perfect negative correlation, +1 represents a perfect positive correlation and a value of 0 represents a lack of correlation. The

coefficient of determination, R^2, represents the proportion of common variation between two variables. In other words, $\%R^2$ is the percentage of variations in variable Y, which is accounted for by a linear relationship with X[57]. The formula to calculate the correlation coefficient is given by Equation (6.1):

$$R = \frac{N\sum XY - \left(\sum X\right)\left(\sum Y\right)}{\sqrt{\left[N\sum X^2 - \left(\sum X\right)^2\right]\left[N\sum Y^2 - \left(\sum Y\right)^2\right]}} \qquad (6.1)$$

where,

N : Number of pairs in the measurement sample

$\sum X$ and $\sum Y$: Sum of values of X and Y, respectively

$\sum X^2$ and $\sum Y^2$: Sum of squared values of X and Y, respectively

$\sum XY$: Sum of product of paired values, X and Y

6.2.2 *Testing the Significance of a Correlation*

The significance level of the coefficient of correlation shows the level of reliability of this factor. A test of significance can be established based on analysis of a *t*-distribution with N-2 degrees of freedom, where N is the number of pairs in the measurement sample. The *t*-value can be calculated using Equation (6.2)[57]:

$$t = \frac{R\sqrt{N-2}}{\sqrt{1-R^2}} \qquad (6.2)$$

The *p*-value reported with the *t*-test is representative of the significance of the corresponding correlation coefficient, *R*. Precisely, the *p*-value is the probability of error involved with accepting/rejecting the Null Hypothesis, H_o. In this regard, acceptance or rejection of Null Hypothesis, H_o, is essential to establish the significance and reliability of the correlation.[58]

Null Hypothesis, H_o: There is *no* correlation between two variables.

The *p*-level reported with a *t*-test represents the probability of error involved in rejecting H_o.

$$\left\{\begin{array}{l} \text{If the p - value is small} \Rightarrow \text{Reject } H_o \Rightarrow \left\{\begin{array}{c}\text{There is a correlation}\\ \text{with the strength of the calculted R - value}\end{array}\right. \\ \text{If the p - value is large} \Rightarrow \text{Accept } H_o \Rightarrow \left\{\begin{array}{l}\text{There is NO correlation}\\ \text{The true R - value is zero}\end{array}\right. \\ \text{If the p - value is neither small nor large} \Rightarrow \text{No decision should be made in general} \end{array}\right\}$$

6.3 Correlation between Axial Force and Intramedullary Pressure

6.3.1 Methodology

Data from the forty four experiments conducted for parametric study #1 (see Section 5.4.1) were used in this analysis. Paired statistical comparison between the *average intramedullary pressure* and the corresponding *axial force* was conducted to assess the correlation between the two variables. In this study, the mean of concurrent pressures recorded by each pressures transducer #1, 2 and 3 was used to represent the *average intramedullary pressure* within the bone (i.e., $P_{avg} = P_1 + P_2 + P_3$ for each sample collected during each run). The *axial force* corresponding to each P_{avg} was paired

to create paired samples. Refer to Appendix D (Table D.1 to D.44) for graphs presenting the axial forces used in this study.

Since a large number of data points was recorded during each run (20000 samples per second), it was required to reduce the number of sampled pairs (P_{avg} and corresponding axial force) used for the correlation analysis. For this reason, the paired sample corresponding to every 10 blocks of data (5120 data points) were collected from each run. The reason data were collected from every 10 blocks, as opposed to any other number (e.g., every 5 blocks) was simply because it was more manageable to fit the data on an Excel sheet in order to run a correlation analysis. Taking RPM and advancement speed as constant factors, all the experiments (including reamer size 11-16mm) were grouped together for the purpose of analysis, thus creating 900-2500 pairs of data depending on the advancement speed of the reamer (Table 6.1).

6.3.2 Results and Discussion

Results from correlation analysis among all variables (P_{avg}, P_1, P_2, P_3, F_x, F_y, F_z and torque) are presented in Appendix C (Table C.1 to C.12). Results from correlation analysis between P_{avg} and axial force are summarized in Table 6.1.

Based on Table 6.1, no correlation was observed between P_{avg} and the axial force while reaming at 50 rpm and 50 $\frac{mm}{\text{sec}}$ advancement speed (H_o can be accepted with $p\approx80\%$, hence $R\approx0$). However, a very small correlation (R^2=1.17%, 11% and 0.6%) was observed between P_{avg} and the axial force at other RPM and speeds (respectively for 200/10, 200/50, 50/10) by rejecting H_o with $p<0.004$. These results showed that, even though there was a statistically significant correlation between P_{avg} and the axial force, it is quite

small. This is consistent with the results in the literature by Johnson et al.[8], in 1995, who reported a statistically small correlation between the distal canal pressure and applied axial force (R^2=19.1%, p-value<0.048).

Bone #	RPM, Speed $[\frac{mm}{\text{sec}}]$	Feed $[\frac{mm}{rev}]$	# of Sampled Pairs	R	R^2 (%)	p-value
1	200,10	3	728	0.1084	1.17	0.0034
2	50,10	12	818	0.3320	11.02	0
3	200,50	15	1367	-0.0775	0.60	0.0042
4	50,50	60	2464	-0.0049	0.0024	0.8092

Table 6.1- Summary of results from correlation analysis between the average intramedullary pressure and axial force at different reaming parameters

Figure 6-6 shows the *average axial forces* detected at different reaming conditions. *Average axial force* represents the mean of all the axial forces detected by dynamometer while reaming the bone using eleven reamers at constant RPM and advancement speed. It was observed that the average axial force was higher in the case with lower RPM (50 rpm) compared to the cases with higher RPM (200 rpm). This could be explained by higher fluid compression (due to less marrow escape through the walls of the bone) towards the end of the bone at lower RPM, which created more compression force in the z-direction. At higher RPM, more marrow could escape through the porous walls and open end hence causing less fluid compression at the end of the bone, creating lower axial force.

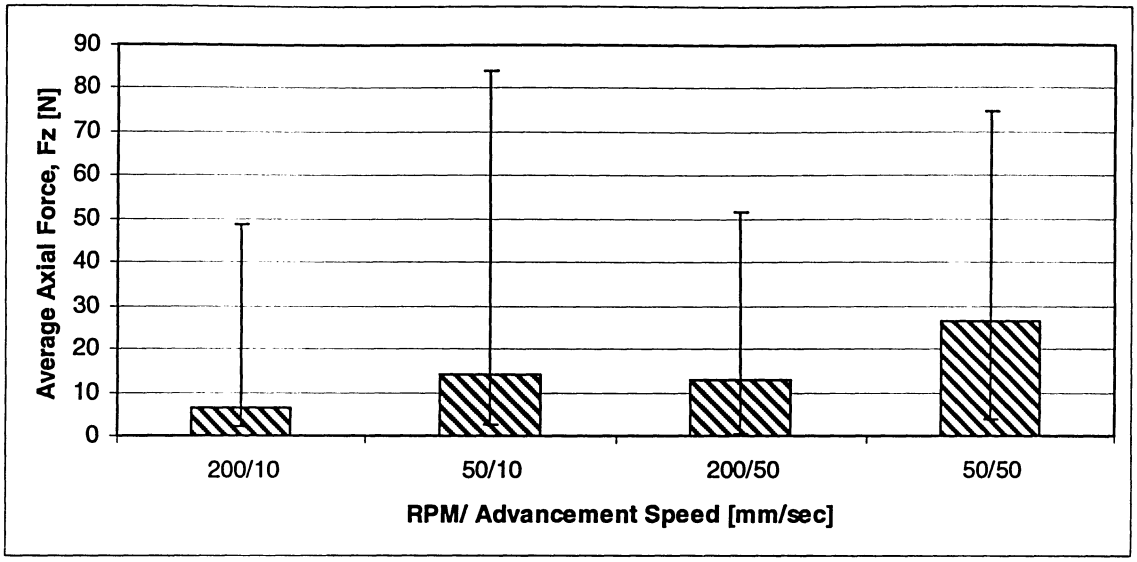

Figure 6-6-Average axial force at different reaming conditions. Each column represents the average axial force, which is the mean of axial forces detected while reaming the synthetic cylinder using eleven reamers. The vertical lines represent the range of axial forces detected during each reaming condition.

The horizontal bars in Figure 6-6 represent the maximum and minimum axial forces. Based on this figure, it was observed that the maximum axial forces ranged between 48 to 83 N while reaming the synthetic bone analogue. These results match well with the range of 59 to 107 N, reported by Muller et al.[20], who studied the variation of compression forces (axial forces) during reaming of five cadaveric human femurs.

6.4 Correlation between the Torque and Intramedullary Pressure

6.4.1 Methodology

The torque applied to the reamer was measured using a torque transducer, as explained in Section 4.4.7. Paired statistical analysis was employed to establish possible correlation between the torque and intramedullary pressure. The same methodology

described in Section 6.3.1 was applied to make paired samples between the torque and P_{avg}.

6.4.2 Results and Discussion

Table 6.2, shows the summary of correlation analysis between the torque and P_{avg} at the different reaming parameters.

Bone #	RPM, Speed $[\frac{mm}{\text{sec}}]$	Feed Rate $[\frac{mm}{rev}]$	R	R^2 (%)	p-value
1	200,10	3	-0.095	0.90	0.01
2	50,10	12	0.4813	23.16	0
3	200,50	15	-0.1253	1.57	0
4	50,50	60	-0.2119	4.49	0

Table 6.2- Summary of results from correlation analysis between the reaming torque and P_{avg}, at different reaming conditions

Based on Table 6.2, it was evident that no large correlation could be established. The highest correlation between the torque and P_{avg} was observed to be R^2=23.16% with p-value□0 at 50 rpm and $10\frac{mm}{\text{sec}}$ advancement speed.

Figure 6-7 shows the *average reaming torque* applied to the reamer at different reaming conditions. The *average torque* represents the mean of torques detected while reaming the bone using eleven reamers at the corresponding reaming RPM and advancement speed. The maximum torque applied to the reamer during reaming of the synthetic cylinder ranged from 560 to 1264 N mm. To the knowledge of author, there is no literature reporting the torque measurements during orthopaedic reaming.

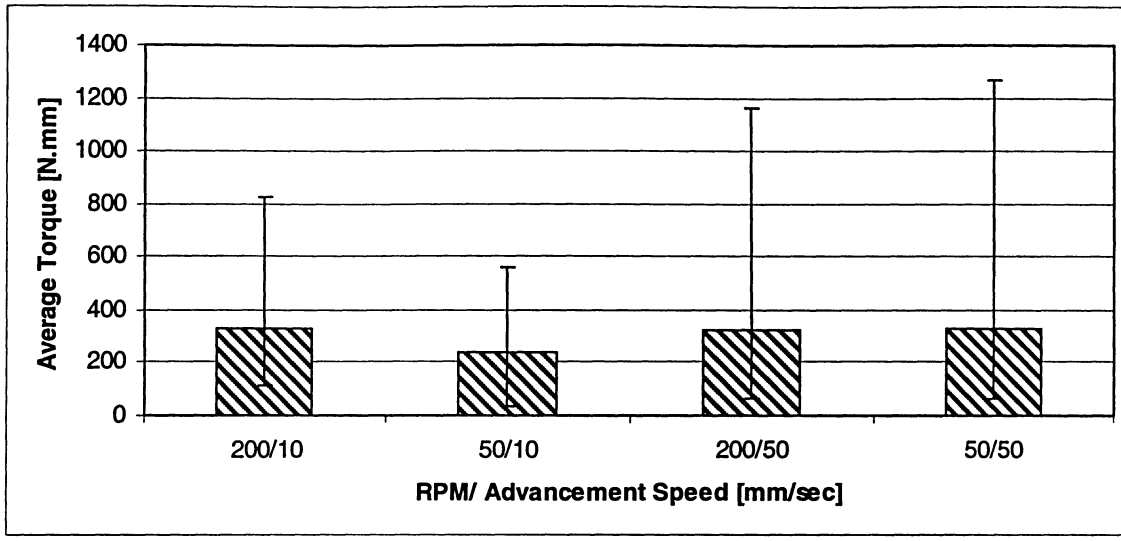

Figure 6-7- Average torque at different reaming conditions. Each column shows the average torque at the corresponding reaming parameters. The vertical lines represent the range of measured torques.

It is evident from Figure 6-7 that the *average torque* remained relatively constant, irrespective of reaming conditions. In this figure, the horizontal bars at the end of the vertical lines represent the maximum and minimum reaming torques. Comparing reaming conditions 50/10 and 50/50 (or 200/10 and 200/50), it is evident that the *maximum torque* was higher at the higher advancement speed ($10\frac{mm}{\text{sec}}$). This could be due to the fact that at higher advancement speed, the reamers encounter more resistance due to more rapid removal of cancellous material, which may cause higher torque on the reamer.

7 Conclusions

7.1 Summary

The development of intramedullary reaming techniques in 1942 gave rise to various studies of the reaming process which led to investigation of problems associated with fat embolism during intramedullary reaming.[14] In this thesis, an experimental procedure for the analysis of factors leading to intramedullary pressure elevations, and thus .potential development of fat embolism syndrome during reaming of femoral intramedullary canal, was proposed. The experimental model employed a controlled reaming system to assess the effect of these factors while reaming a synthetic bone analogue model. In contrast to previously used bone analogues, this is the first work employing a two layer open cell structure, simulating both the cortical and cancellous structures of the bone. The outer layer, a porous open cell plastic tube, had similar porous properties to human cortical bone. The inner layer, an open cell porous carbon foam tube, had similar porous and mechanical properties to human cancellous bone. To reproduce the bone marrow within the medullary canal, a petroleum jelly/paraffin mixture was used. This bone analogue was used in an experimental set up to conduct parametric studies to examine the effect of parameters such as reamer RPM, reamer advancement speed, reamer diameter, bone marrow viscosity and clogging of the reamers on simulated intramedullary pressure.

The most important conclusions from this thesis are summarized below:

I. A two layer open cell porous structure synthetic bone analogue was used to simulate the femoral behavior during reaming experiments. Simulated intramedullary pressure elevations were within the reported range in the literature for cadaver bones..

II. In cases where there were no complications such as a high viscosity marrow or a clogged reamer, the maximum intramedullary pressure was 132 mmHg. However, introduction of these complications resulted in a higher maximum pressure of 409 mmHg. This is more than 8 times the critical pressure to allow passage of bone marrow into the capillaries, and twice as much as the pressure that can cause configured emboli.

III. Changes in the reamer size displayed no significant effect on intramedullary pressure compared to the effect of marrow viscosity and clogged reamer. However, compared to the effect of RPM and advancement speed, the reamer diameter significantly influenced the medullary pressure at the closed end of the bone ($\sim p<0.02$), but no significant effect was observed in any other locations.

IV. Reamer RPM had a statistically significant influence on the pressure increase within the bone, particularly in the mid-shaft and end of the bone ($\sim p <0.001$).

V. The advancement speed of the reamer was found to be the most significant factor affecting the intramedullary pressure ($p \approx 0$).

VI. Variation in bone marrow viscosity was found to have a significant effect on pressure elevations within the bone cavity ($\sim p < 0.01$).

VII. Clogging of the reamer had a significant effect on intramedullary pressure elevations ($\sim p<0.02$).

VIII. A very small statistically significant correlation could be established between the intramedullary pressure and axial force (with the highest correlation found as R^2=11% with $p\approx0$).

IX. A small statistically significant correlation was found between the intramedullary and torque (with the highest correlation of R^2=23.16% with $p\approx0$)

X. It was observed that in the vicinity of the reamer entrance (transducer#1), the pressure elevation is mainly and significantly created by the effect of reamer advancement speed ($p\approx0$), but not by the reamer size or RPM (p = 0.0196 and p = 0.0079 respectively).

7.2 Use of a Synthetic Bone Analogue

The advantage of using a synthetic bone analogue to examine the effect of reaming parameters on the intramedullary pressure instead of those based on human or animal studies is evident:

I. Use of the proposed synthetic model eliminates the need for cadaver bone storage.

II. The porosity and pore size of the proposed bone structure is constant throughout the bone, which can greatly reduce the specimen to specimen variability associated with cadaveric bones and allow more controlled repeatable results.

III. The analogue, because it is of a regular geometry and constant properties, allows for verification of numerical models aimed at comparative assessment of the effect of changes in operative procedure.

IV. The analogue can fairly easily be modified to accommodate changes in geometry, porosity, pore size and mechanical properties, as the manufacturer can change

these parameters on demand. This would allow for parametric studies which aim to establish, for example, the effect of aging on the resulting pressures generated in the intramedullary canal during reaming

There are three advantages to the bone analogue model proposed in this thesis compared to those previously proposed in the literature:

I. The model has a two layer structure representing both cortical bone and cancellous bone as opposed to most other models that only incorporate the cortical layer. This provided a more realistic response to cancellous bone reaming.

II. The current model has an open cell porous structure unlike those proposed in the literature, which have a closed structure. The present model thus is the first to allow fluid flow through the simulated bone walls.

III. Compared to closed cell structured bone analogues, this model gave more comparable results to those reported in the literature using cadaveric bones.

7.3 Limitations of Approach

The experimental approach employed in this thesis was based on the following assumptions:

I. The proposed axi-symmetric synthetic bone analogue, designed based on a constant porosity and pore size throughout the bone, did not incorporate the variation of porosity and pore size observed in cadaveric bone (depending on age, bone composition and health).

II. A constant viscosity bone marrow was used throughout the bone which did not incorporate the variation of marrow viscosity between the distal and proximal regions of real femur.

III. A constant RPM and advancement speed was used during the experiments, using a controlled reaming system, to allow interpretation of the effect of reaming parameters. In fact, during orthopaedic reaming, surgeons actually apply a variety of RPM and penetration speeds, depending on a number of factors including the fact that different surgeons use different procedures.

IV. In the current set-up, the bone analogue cavity was refilled before every experiment to simulate the lack of backflow of the blood stream. However, in the actual surgeries, the blood fills up the bone cavity as the reamer advances through the bone, which could not be incorporated into this design.

V. The diastolic blood pressure of 30-50 mmHg, a typical intramedullary pressure range prior to orthopaedic complications, was not considered in this study while reaming the synthetic bone analogue.

VI. The simplified cylindrical geometry of the proposed bone analogue did not consider the diameter variation in the distal cavity of the real bone. This may have affected the results in terms of not considering the reamer contact with the cortical bone in the areas with smaller distal canal, which could have slowed down the advancement speed and resulted in elevation of intramedullary pressure.

VII. Debris from the cancellous analogue (carbon foam debris) did not properly clog the reamers, as seen in the real surgeries. The reason was speculated to be due to the fact that fracture mechanics properties of the synthetic cancellous material did not match that of real bone even though the modulus of elasticity and strength of this material were closely matched with real bone. Instead, to simulate clogging of the reamers by bone debris, the reamer flutes were fully covered by silicon sealant. This could have resulted in

higher pressure elevations as the reamers were fully clogged, whereas in real surgeries the reamer may be partially clogged.

VIII. The reamers used in this study were long shaft solid straight fluted reamers. These reamers, while commonly used, occupy a higher volume compared to the more recently designed reamers with hollow flexible thin drives, and thus potentially created more pressure elevations in the synthetic bone cavity.

Nevertheless, the results of the parametric studies conducted in this thesis were useful for the comparative studies to assess the effect of reaming parameters.

7.4 Recommendations for Surgeons

Based on the present studies, a number of techniques to minimize the intramedullary pressure during orthopaedic procedures can be suggested:

I. The RPM should be kept as high as possible, but not exceeding 500 rpm, which may cause chatter.

II. A low advancement speed should be used during reaming. It should be noted that in the cases where the advancement speed is too low, the operation time is increased, which is not recommended by surgeons.

III. The surgeon should be conscious of the possibility of the reamer clogging, as this can lead to significantly higher intramedullary pressures. Therefore, it is recommended that the reamer flutes be cleaned as many times as possible during orthopaedic surgeries.

IV. Based on comparison to the literature, it was found that reamers with thin flexible drives, in which the flexible drive is not fluted, are less likely to become clogged than the solid straight fluted reamers used in this study.

V. It is highly recommended to evacuate the high viscosity marrow from the proximal regions of the femur by diluting the marrow with injecting physiological serums into the intramedullary canal or by using suction techniques. This is important as the higher viscosity marrow can create higher pressure elevations within the bone.

7.5 Recommendations for Future Work

A possible enhanced model for the reaming experiments would involve a combination of aluminum and RVC foam for cortical and cancellous bone replacement, respectively. The advantage is a much higher friction between the two layers, which lowers the chance of slippage during simulated reaming. In this case, the manufacture of the inner and outer cylinder could be done simultaneously, making the final product more rigid and precise. A further improvement would be to mould synthetic bones of more realistic shape, allowing for study of the effects of bone size and shape on the pressures generated during orthopaedic procedures. To simulate a more realistic clogging behavior, it is recommended to also match the fracture mechanics properties of the synthetic cancellous material to those of real bone (in additional to Young's modulus and strength). Future bone analogue designs could also incorporate a better seal between reamer and bone for simulation of this higher pressure case.

As a continuation of this work, it is also highly recommended to conduct a parametric study on the effect of variation in structural properties of the bone (porosity and pore size) to establish the significance of patient age, activity, etc., on the likelihood of developing FES.

References

[1] Shergill, G., Parmar, H. *Fat embolism and the fat embolism syndrome,* http://www.orthopaedics.com/institute/teaching/talks/fat%20embolism.htm.

[2] Meller, A., Soni, N., *Fat embolism*, review article Anaesthesia, 2001, 56, pp. 145-154.

[3] An Y.H., Draughn R.A. *Mechanical testing of bone and the bone-implant interface*, CRC Press LLC, 2000, p.7.

[4] Bulger, E.M. , Smith, D.G., Maier, R.V., Jurkovic, G.J., *Fat Embolism Syndrome,* Archives of Surgery, 1997;132:pp. 435-439.

[5] Limbird, T.J., Ruderman, R.J., *Fat embolism in children,* Clin. Orthop. 1978; 136:pp. 267-269.

[6] Kirkland, L. , *Fat embolism*, eMedicine, http://www.emedicine.com/med/topic652.htm

[7] Wenda, K., Runkel, M., Degreif, J., Ritter, G., *Bone marrow remobilization in reaming*, Injury, 1993; 3: pp 73-81.

[8] Johnson, J.A., Berkshire, A., Leighton, R.K., Gross, M., Chess, D.G., Petrie, D., *Some basic biomechanical characteristics of intramedullary pressure generation during reaming of the femur*, Injury, Vol. 26, No. 7, 1995, pp. 451-454.

[9] Mousavi M, David R, Ehteshami J, Pajenda G, Vecsei V. *Pressure changes during reaming with different parameters and reamer designs.* Clinical Orthopaedics and Related Research, 1999; 373: 295-303.

[10] Muller Chr.,Mc Iff T., Pfister U., Perren S.M., Weller S., *Influence of the compression force on the intramedullary pressure development in reaming of the femoral medullary cavity,* AO research institute, 7270 Davos, Switzer land, Injury 1993, Supplement 3.

[11] Dobranski, D, *Experimental Parametric Study of the Factors Leading to Elevated Femoral Intramedullary Pressure and Fat Embolus Syndrome in Orthopaedic Procedures*, MASc Thesis, Ryerson University, 2005.

[12] Fat embolism, The encyclopedia of medical imaging, vol. 1, Medcyclopaedia, http://www.medcyclopaedia.com.

[13] Schult, M., Frerichmann, U., Schiedel, F., Brug, E., Joist, A., *Pathophysiology of fat embolism after intramedullary reaming,* Euoropean Journal of Trauma, 2003; 29:pp.68-73.

[14] Knothe U., Tate M. L. K., Perren S. M., *300 Years of Intramedullary Fixation – from Aztec Practice to Standard Treatment Modality,* Review article, European Journal of Trauma 2000;26:pp.217–25.

[15] Fahmy, N.R., Chandler, H.P., Danylchuk, K., Matta, E.B., Sunder, N., Siliski, J.M., *Blood-gas and circulatory changes during Total Knee Replacements,* Journal of Bone and Joint Surgery, 1990; 72-A-1:pp.19-26.

[16] Herndon, J.H., Bechtol, C.O., Crickenberger, D.P., *Fat embolism during Total Hip Replacemen,* , Journal of Bone and Joint Surgery, 1974; 56-A-7: pp.1350-1362.

[17] Hofmann, S., Hopf, R., Mayr, G., Schlag, G., Salzer, M. *In vivo femoral intramedullary pressure during uncemented hip arthroplasty,* Clin. Orthop. 1999, 360, pp. 136-146.
[18] Parvisi, J., Holiday, A.D., Ereth, M.H., Lewallen, D.G., *Sudden death during primary hip arthroplasty.* Clin. Orthop. 1999, 369, pp. 39-48.
[19] Peter R.E., Selz T., Koestli A., *Influence of the reamer shape in intraosseus pressure during closed intramedullary nailing of the unbroken femur: A preliminary report.* Injury 1993, Supplement 3.
[20] Muller Chr.,Mc Iff T., Pfister U., Perren S.M., Weller S., *Influence of the compression force on the intramedullary pressure development in reaming of the femoral medullary cavity,* AO research institute, 7270 Davos, Switzer land, Injury 1993, Supplement 3.
[21] Heim D, Schlegel U, Perren SM. *Intramedullary Pressure in Reamed and Unreamed Nailing of the Femur and Tibia-an invitro study in intact, human bones.* Injury. 1993; 24(3): pp.S56-63.
[22] Mousavi, M., Kolonja, A., Schaden, E., Gabler, C., Ehteshami, J.R., Vecsei, V. *Intracranial pressure-alterations during controlled intramedullary reaming of femoral fractures: an animal study,* Injury, Int. J. Care Injured 32, 2001, pp.679-682.
[23] Kropfl, A., Davies, J., Berger, U., Hertz, H., and Schlag, G., *Intramedullary pressure and bone marrow fat extravasation in reamed and undreamed femoral nailing,* Journal of Orthopaedic Research, Vol. 17, No. 2, 1999, pp.261-268.
[24] Sturmer K.M., *Measurement of intramedullary pressure in an animal experiment and propositions to reduce the pressure increase.* Injury, Supplement 3, 1993, pp.S7-21.
[25] Weiner, S. and Traub, W. *Bone structure: from angstroms to microns,* The FASEB journal, 1992, 6: pp.879-885.
[26] Smith, E.L., R.L. Hill, I.R. Lehman, R.J. Lefkowitz, P. Handler, and A. White, *Principles of Biochemistry: Mammalian Biochemistry.* 1983, Seventh edition. New York: McGraw-Hill Book Company.
[27] Hare, P.E., *Organic geochemistry of bone and its relation to the survival of bone in the natural environment.* In Behrensmeye, A.K., and A.P. Hill (eds), Fossils in the Making: Vertebrate Taphonomy and Paleoecology, Chicago: The University of Chicago Press, 1980, pp.208-219.
[28] Ascenzi, A. and Benvenuti, A. *Orientation of collagen fibers at the boundary between two successive osteonic lamellae and its mechanical interpretation,* Journal of Biomechanics, 1986, 19:pp.455-463.
[29] Cowin, S.C., Van Buskirk, W.C., and Ashman, R.B. Properties of Bone. Chapter 2 in *Handbook of Engineering*. Edited by Skalak, R. and Chien, S. McGraw-Hill book Company, New York.
[30] Wang X, Qingwen N. *Determination of cortical bone porosity and pore size distribution using a low field pulsed NMR approach.* Journal of Orthopaedic Research. 2003; 21: pp. 312-319.
[31] An Y.H., Draughn R.A. *Mechanical testing of bone and the bone-implant interface,* CRC Press LLC, 2000, pp.42-44.
[32] Carter D. R. and Spengler D. M., *Mechanical properties and composition of cortical bone*, Clin. Orthop., pp.135-192, 1978.

[33] Schaffler, M.B. and Burr, D.B. *Stiffness of compact bone: Effects of porosity and density*, 1988, J. Biomechanics, 21:pp.13-16.
[34] Bruyn P.P.H.de, Breen P.C., Thomas T.B. *The microcirculation of the bone marrow.* Anat. Rec.1970, 168:pp. 55-68.
[35] Draenert K, Draenert Y. *The Vascular System of Bone Marrow.* Scanning Electron Microscopy. 1980, 113-121.
[36] Bryant JD, David T, Gaskell PH, King S, Lond G. *Rheology of bovine bone marrow. Proceedings of the Institution of Mechanical Engineers.* 1989, 203: pp.71-75.
[37] Dobrjanski D, Gaber O, Saghir Z, Behdinan K, Zalzal P, de Beer J, Papini M. *The pressure generated during the insertion of an intramedullary device: experiments and numerical modeling.* Biomedicine 2005 Conference, Bologna, Italy. 2005.
[38] Gaber O , *Numerical modeling of fat embolism syndrome for knee replacement operation,* MASc Thesis, Ryerson University, 2005.
[39] Saadetian P, Dobrjanski D, Behdinan K, Saghir Z, Zalzal P, de Beer J, Papini M. A *Finite Element simulation of the insertion of an intramedullary implant.* 2005 (under review).
[40] Bahen J., *Numerical modeling of the effect of reaming on pressure and temperature in orthopaedic procedures of long bones.* MASc Thesis, Ryerson University, 2006.
[41] Bahen J., Gaber O., Behdinan K., De Beer J., Zalzal P., Papini M., and Saghir M. Z., *Computacional fluid dynamics modeling of the effect of rotating during reaming of the intramedullary canal of the long bone.* FDMP, Vol. 1, No. 4, pp. 343-352.
[42] Chapter 11 Cutting tool applications: *Reaming and Tapping, George Schneider, Tooling and Production;* Nov. 2001; 67,8; Wilson Applied Science and Technology Abstracts.
[43] Kiyota H., Sakuma, K., *Hole accuracy with carbide-tipped reamers (1st Report),* Bull. Japan Soc. of Prec. Engg., Vol. 20, No. 2, 1986.
[44] Friedman, M.Y., Kitamura, I., Wu, S.M., *Rounding Mechanism of Reaming,* Dept. of Mechanical Engineering, University of Wisconsin, Madison, USA.
[45] Bayly, P.V., Young, K.A., Calvert, S. G., Halley, J.E., *Analysis of tool oscillation and hole roundness in a Quasi-Static model of reaming.* Journal of Manufacturing Science and Engineering, ASME, Vol. 123, 2001, pp.387-396.
[46] Towfighian S., *Finite element modeling of low speed reaming process in application to orthopedic surgeries*, MASc Thesis, Ryerson University, 2006.
[47] Towfighian S., Behdinan K., Papini M., Saghir Z., Zalzal P. & de Beer J., *Finite element modeling of low speed reaming vibrations with reamer geometry modifications*, Journal of Intelligent Manufacturing (under review).
[48] http://www.ergaerospace.com/duocel_foam.htm
[49] ERG Materials and Aerospace Corp. in Oakland, California, USA. Personal communication, Chris Ward.
[50] ERG Materials and Aerospace Corp. in Oakland, California, USA.
http://www.ergaerospace.com/literature/erg_rvc.pdf.
[51] Product data sheet:CFOAM carbon foam,
http://www.cfoam.com/pdf/CFOAMProductDataSheet.pdf.

[52] Sakuma, K., Kiyota, H., *Hole accuracy with carbide-tipped reamers(1st report),* Japan Soc. Of Prec. Engg, Vol. 19, No. 2, 1985, pp.89-108.
[53] Rutherford, A., *Introducing ANOVA and ANCOVA,* SAGE Publications, 2001.
[54] Turner, J.R., Thayer, J.F., *Introduction to Analysis of Variance,* SAGE Publications, 2001.
[55] Kawall, J.G, Class notes, ME8139: *Probability, statistics and stochastic processes,* Ryerson University.
[56] Frolke JM, Bakker FC, Patka P, Haarman HJ. *Intramedullary Pressure in Reamed Femoral Nailing with Two Different Reamer Designs.* European Journal of Trauma. 2001; 27 (5): pp.235-240.
[57] Walpole, R.E., Myers, R.H., Myers, S.L., *Probability and Statistics for Engineers and Scientists,* Prentice Hall, Sixth edition, pp. 394-440.
[58] StatSoft Inc., Tulsa, OK, USA, http://www.statsoft.com/textbook/stbasic.html#Correlationsp.

Appendix A

Pressure Profiles
Parametric Study #1

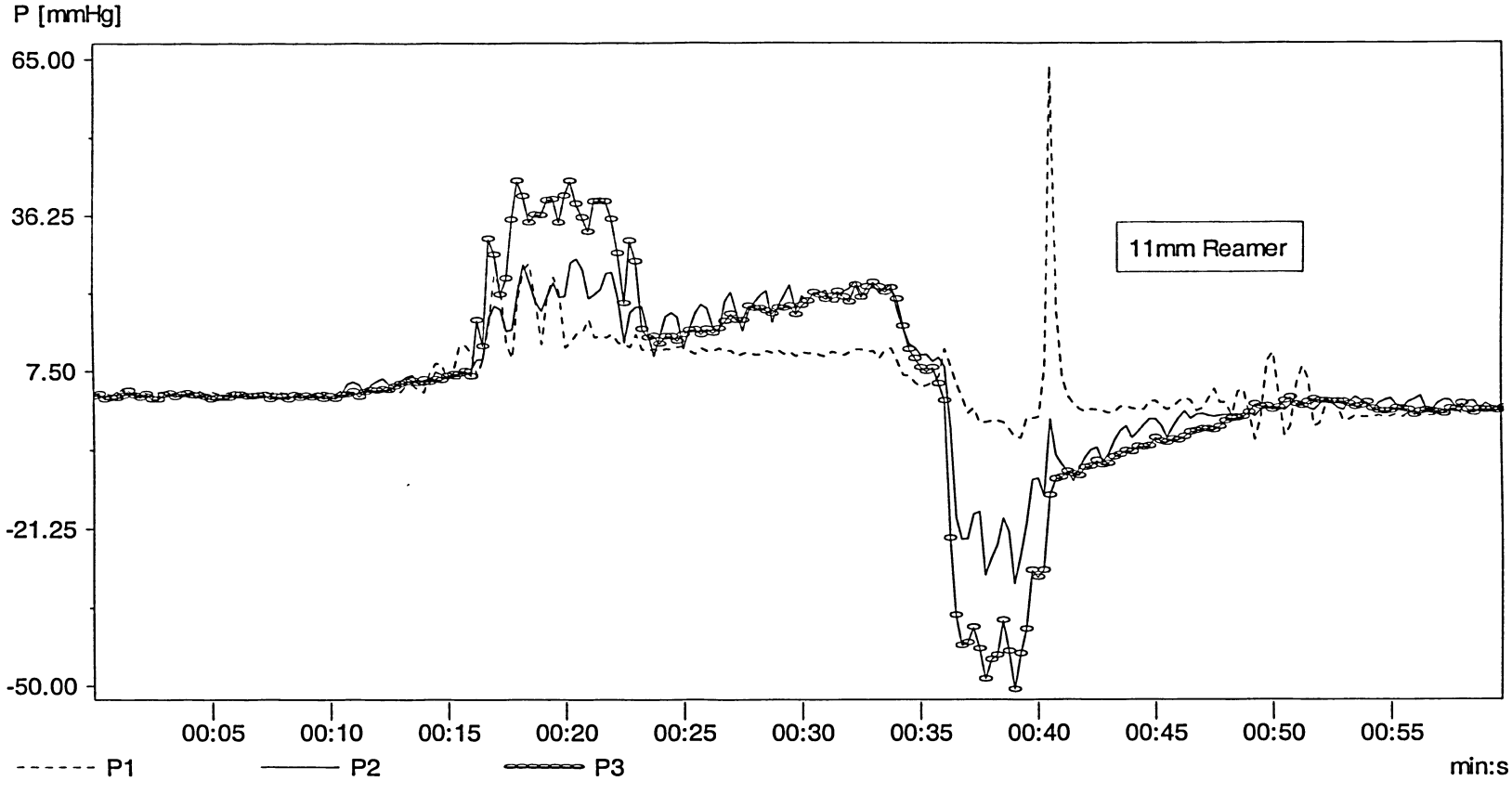

Figure A.1. Pressure variation using 11mm reamer, 50 RPM, 10 $\frac{mm}{sec}$ and 82.6 cP synthetic marrow viscosity. P_1, P_2 and P_3 are respectively corresponded to pressure transducer #1, 2 and 3.

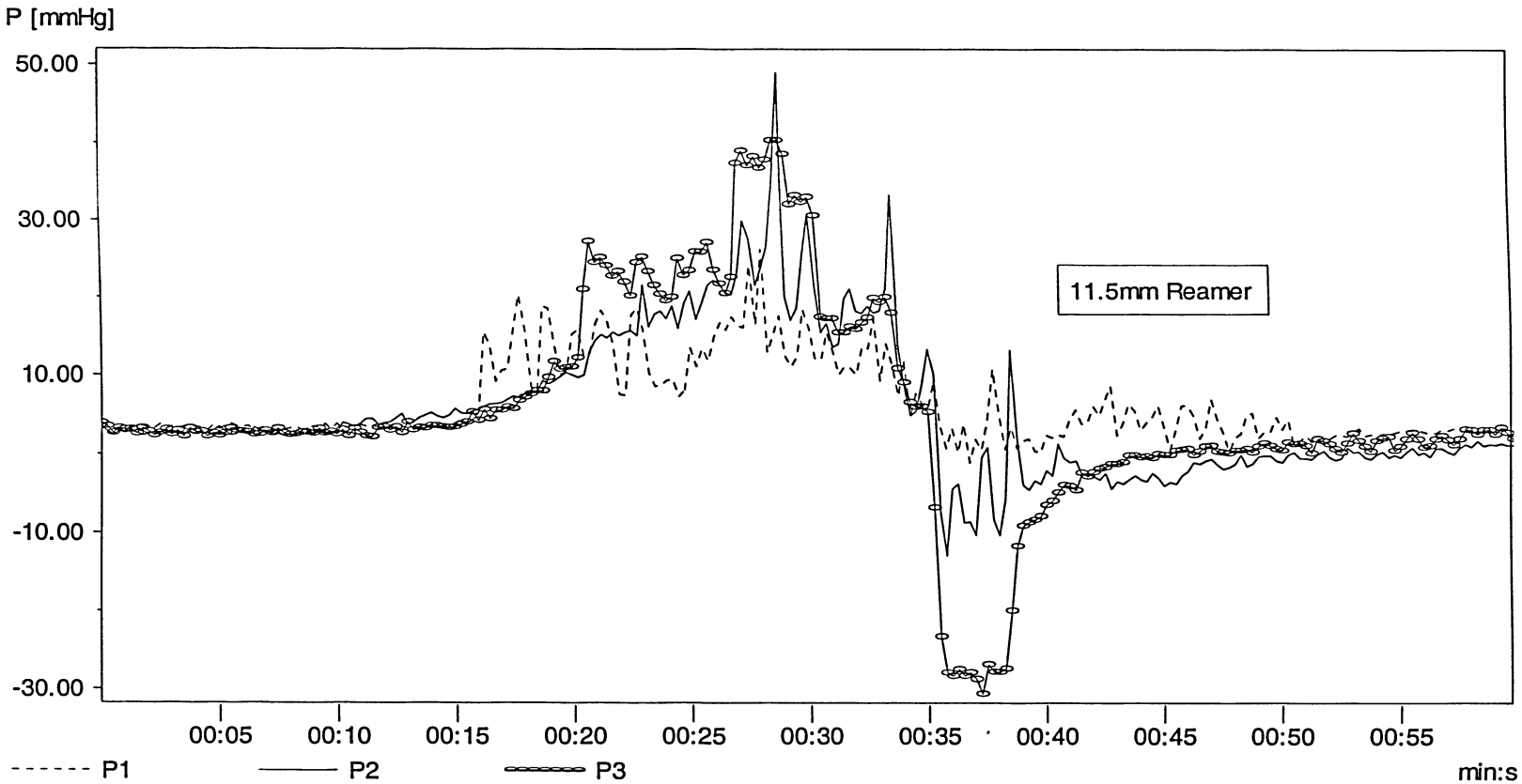

Figure A.2. Pressure variation using 11.5 mm reamer, 50 RPM, 10 $\frac{mm}{sec}$ and 82.6 cP synthetic marrow viscosity. P_1, P_2 and P_3 are respectively corresponded to pressure transducer #1, 2 and 3.

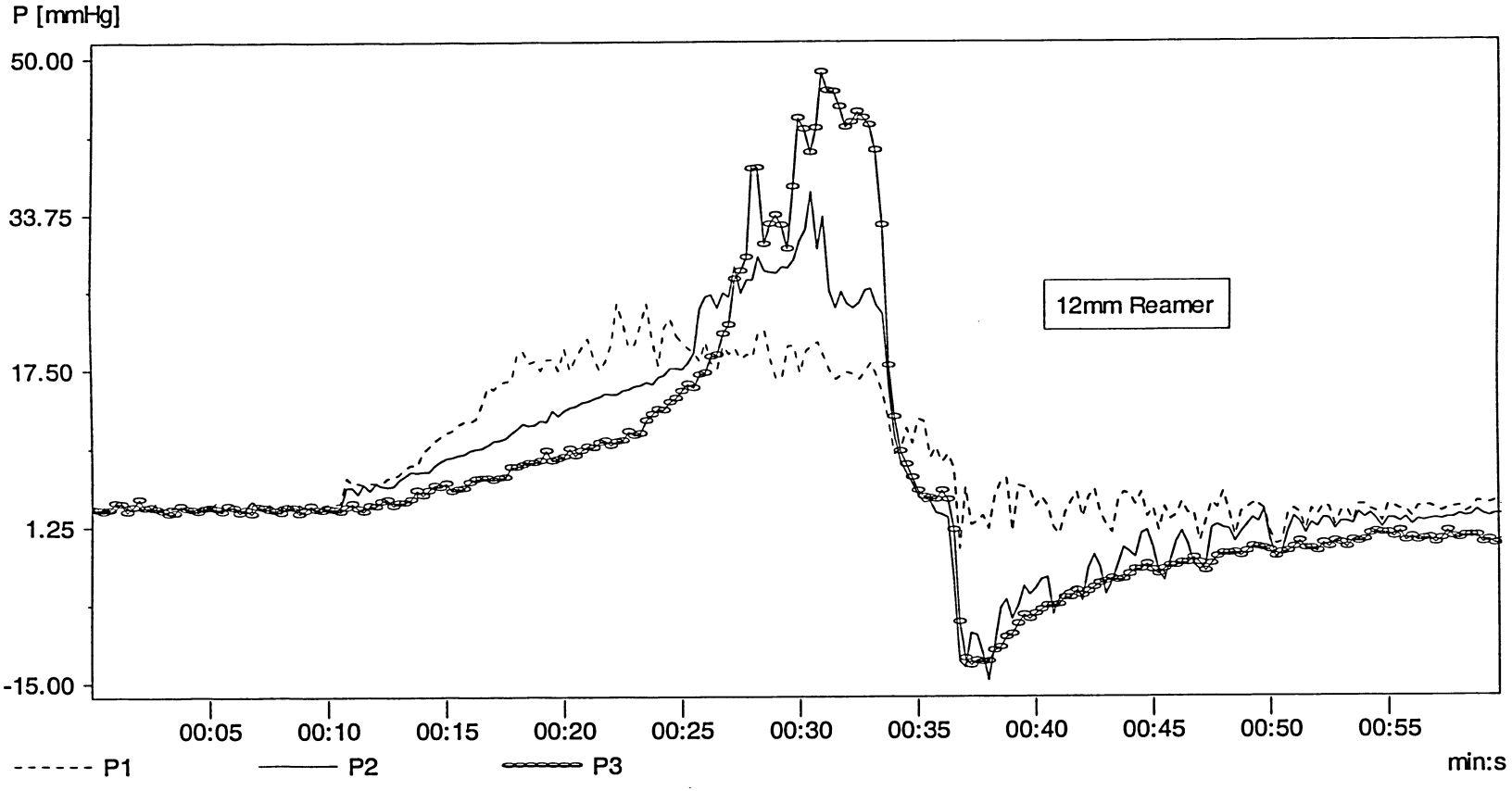

Figure A.3. Pressure variation using 12mm reamer, 50 RPM, 10 $\frac{mm}{sec}$ and 82.6 cP synthetic marrow viscosity. P_1, P_2 and P_3 are respectively corresponded to pressure transducer #1, 2 and 3.

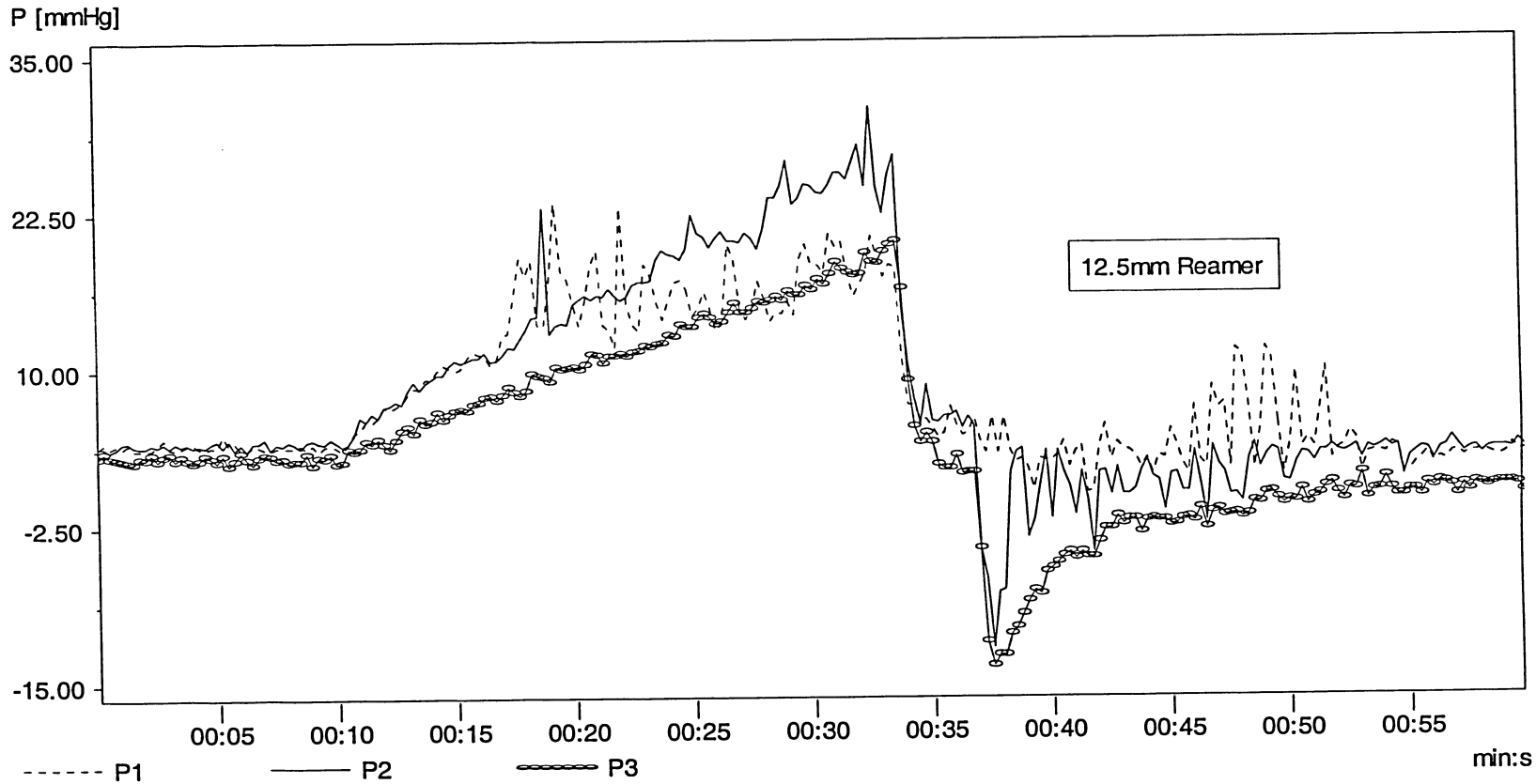

Figure A.4. Pressure variation using 12.5 mm reamer, 50 RPM, 10 and 82.6 cP synthetic marrow viscosity. P_1, P_2 and P_3 are respectively corresponded to pressure transducer #1, 2 and 3.

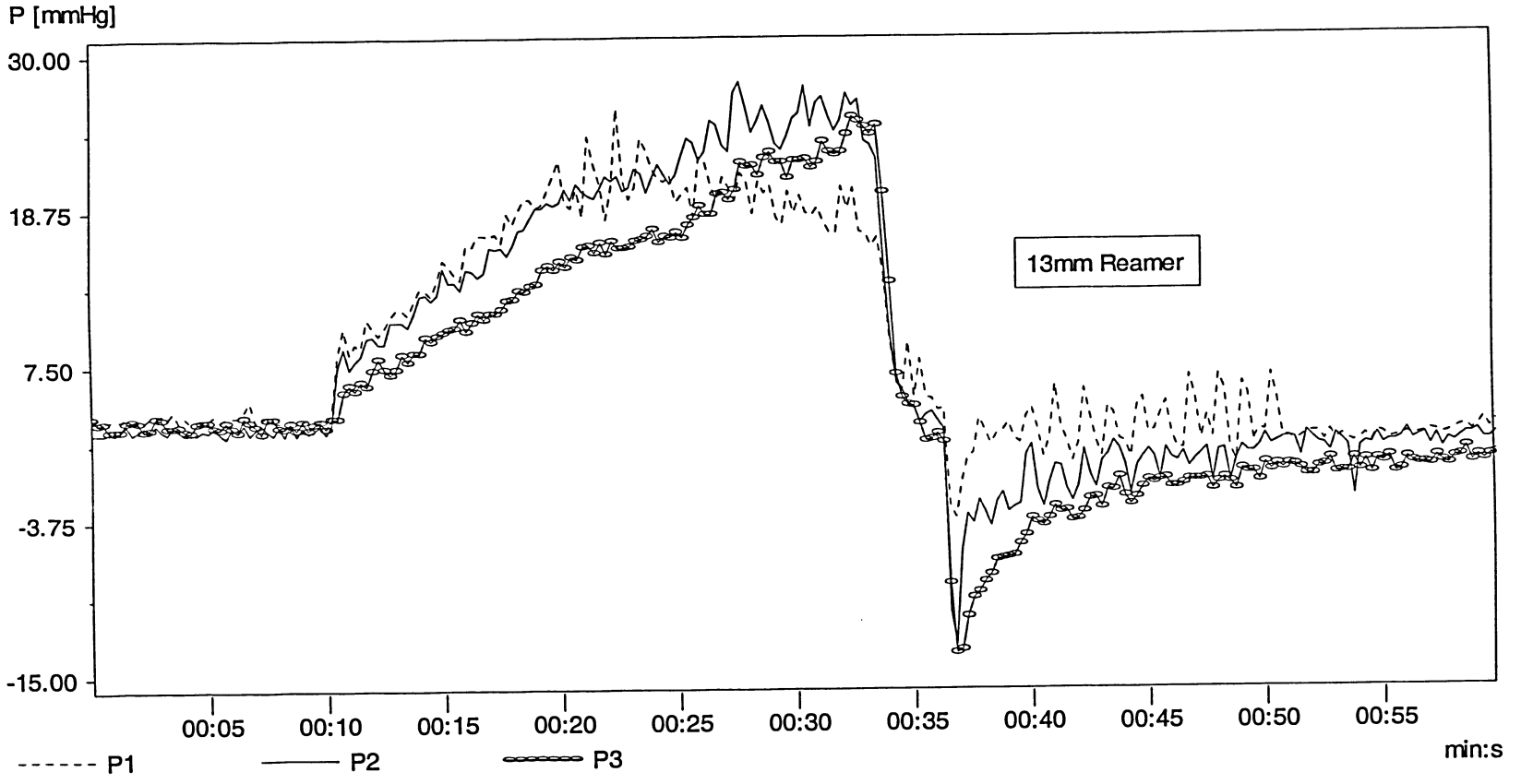

Figure A.5. Pressure variation using 13 mm reamer, 50 RPM, 10 $\frac{mm}{sec}$ and 82.6 cP synthetic marrow viscosity. P_1, P_2 and P_3 are respectively corresponded to pressure transducer #1, 2 and 3.

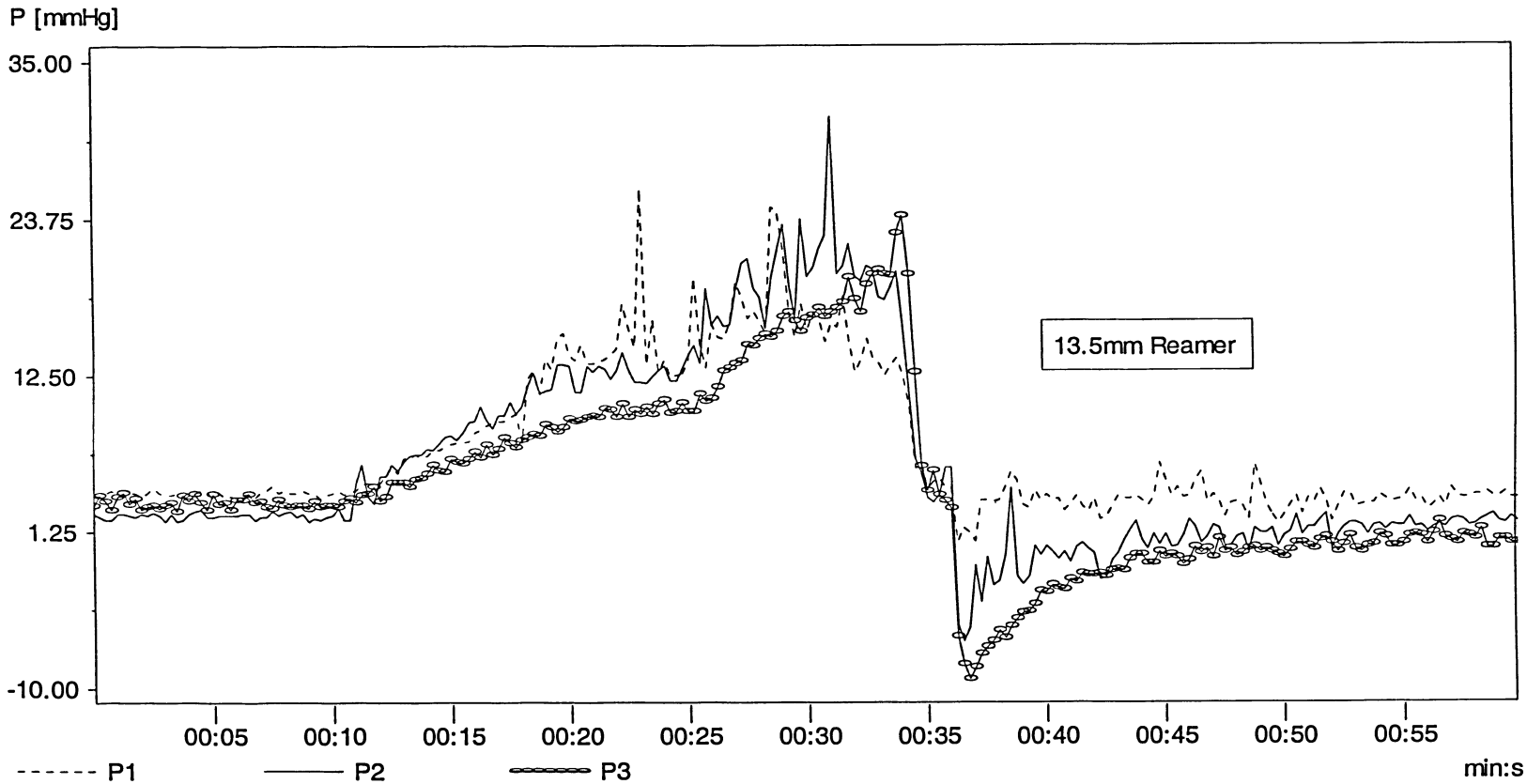

Figure A.6. Pressure variation using 13.5 mm reamer, 50 RPM, 10 and 82.6 cP synthetic marrow viscosity. P_1, P_2 and P_3 are respectively corresponded to pressure transducer #1, 2 and 3.

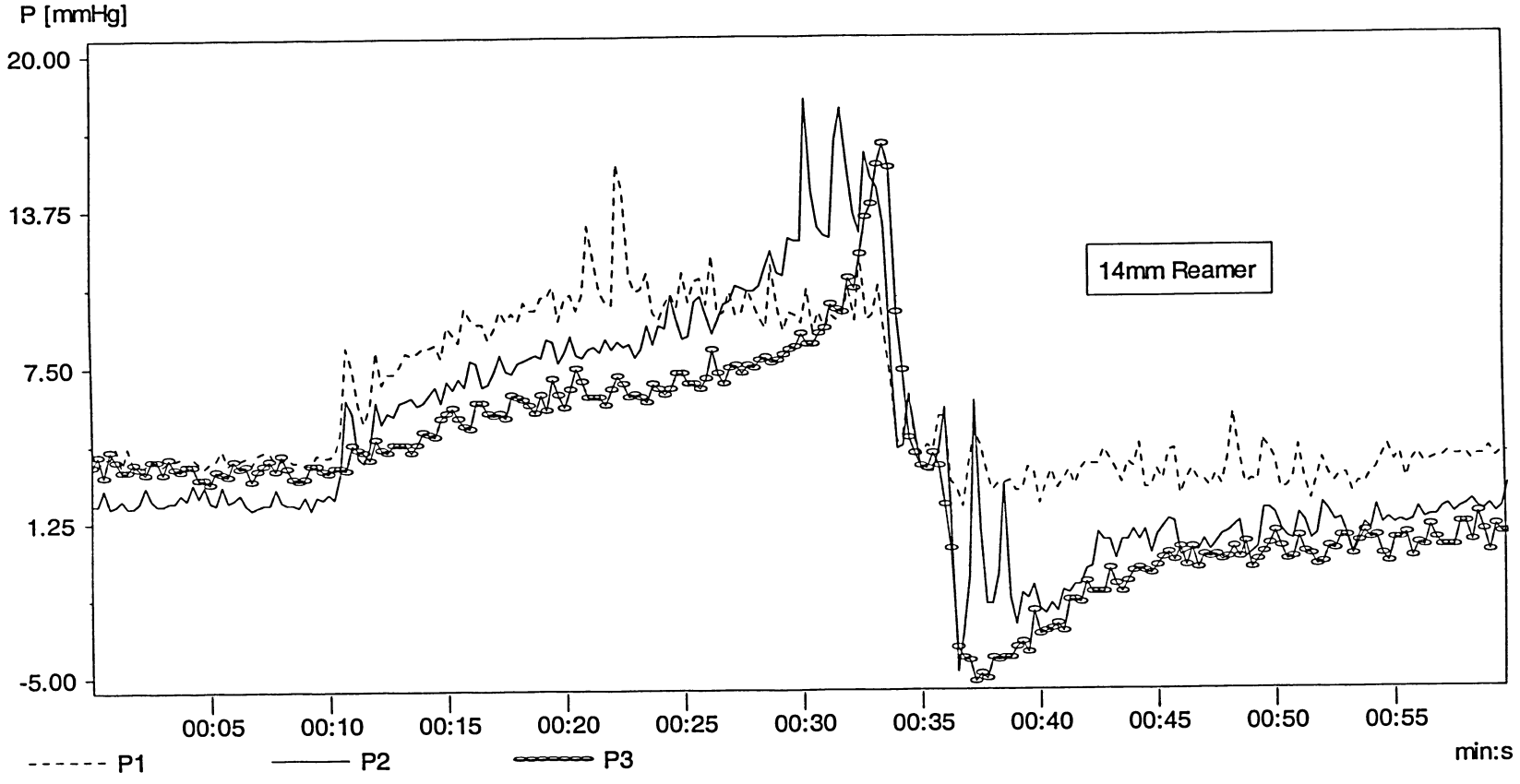

Figure A.7. Pressure variation using 14 mm reamer, 50 RPM, 10 $\frac{mm}{sec}$ and 82.6 cP synthetic marrow viscosity. P_1, P_2 and P_3 are respectively corresponded to pressure transducer #1, 2 and 3.

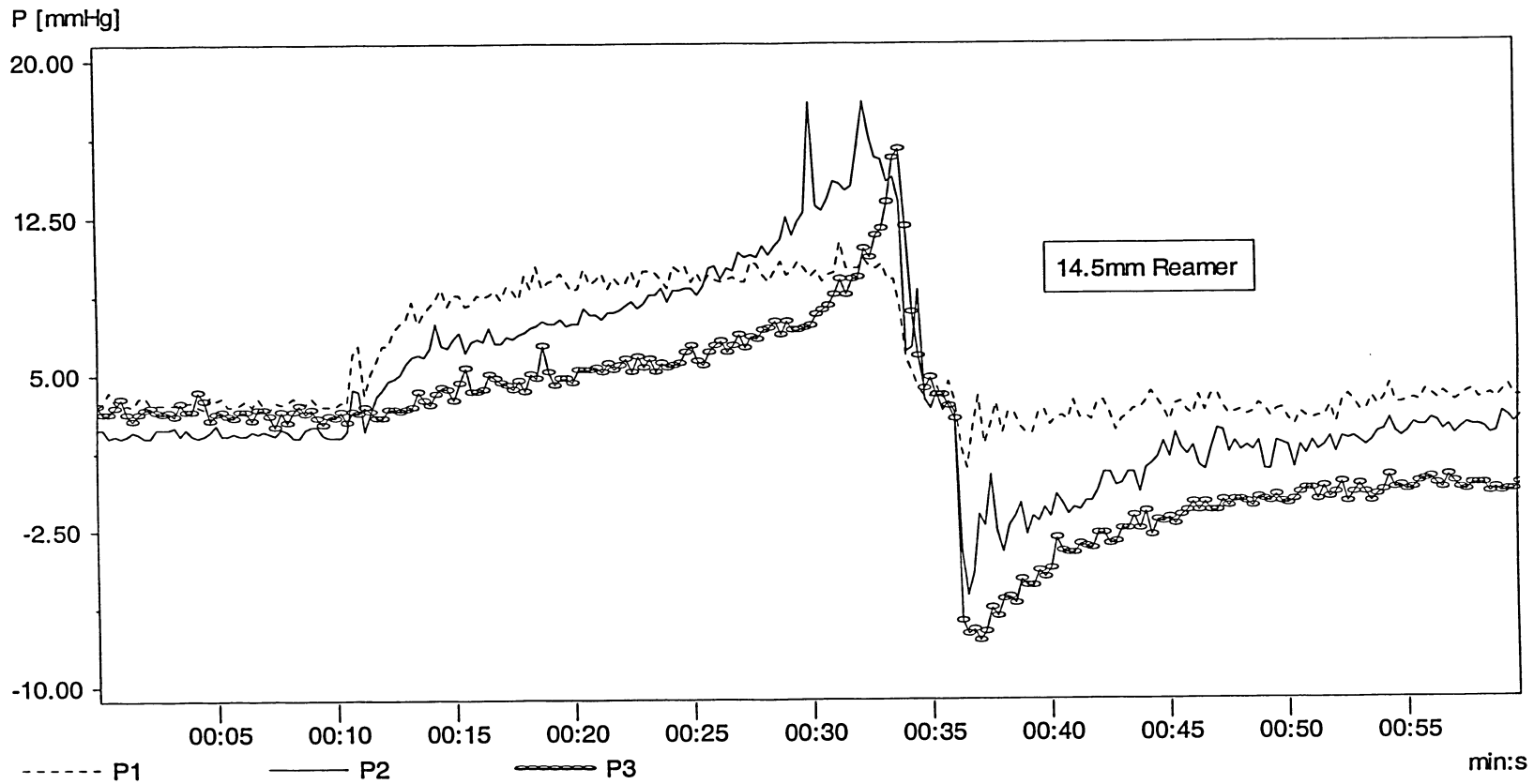

Figure A.8. Pressure variation using 14.5 mm reamer, 50 RPM, 10 $\frac{mm}{sec}$ and 82.6 cP synthetic marrow viscosity. P_1, P_2 and P_3 are respectively corresponded to pressure transducer #1, 2 and 3.

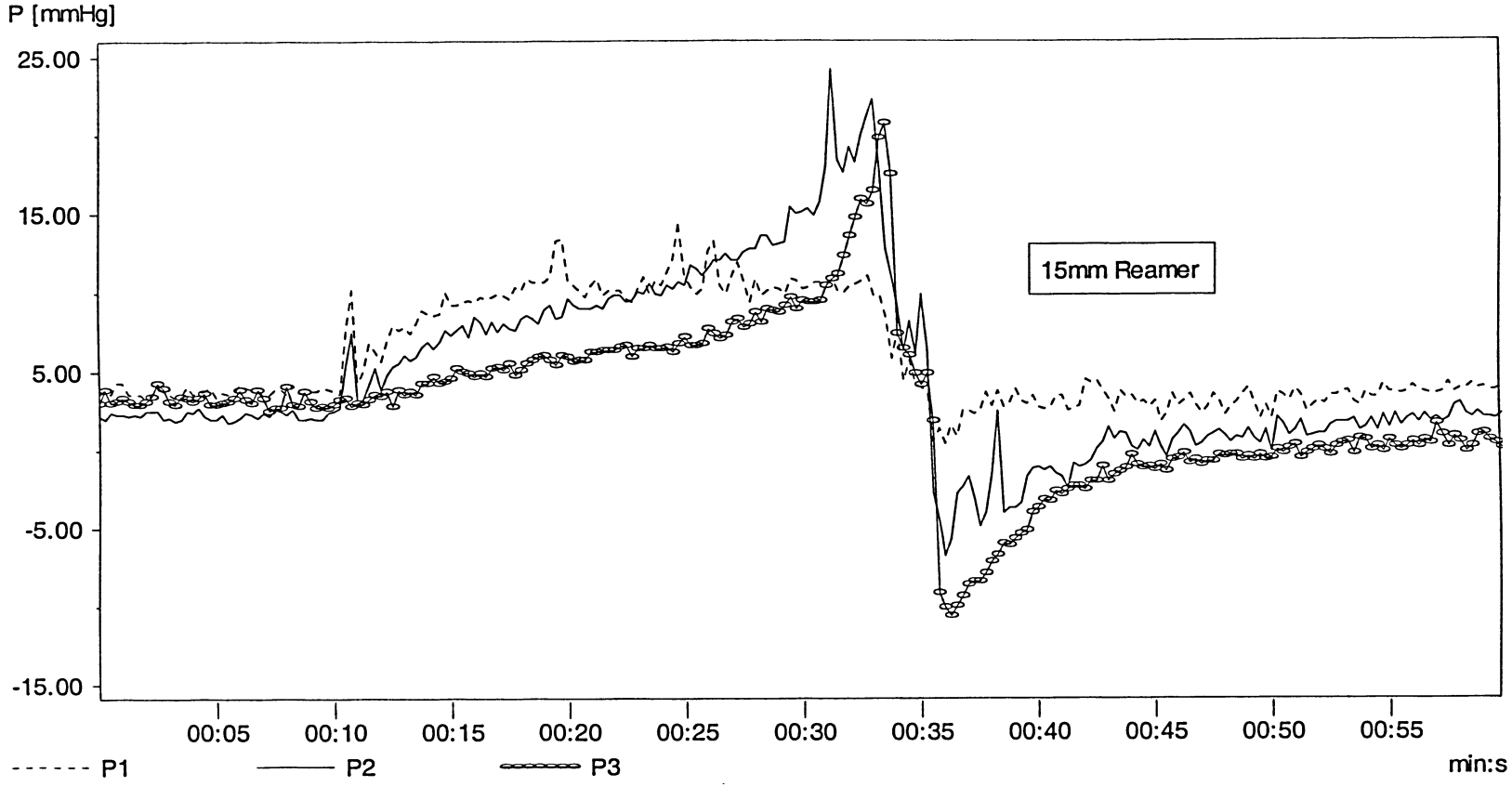

Figure A.9. Pressure variation using 15 mm reamer, 50 RPM, 10 $\frac{mm}{sec}$ and 82.6 cP synthetic marrow viscosity. P_1, P_2 and P_3 are respectively corresponded to pressure transducer #1, 2 and 3.

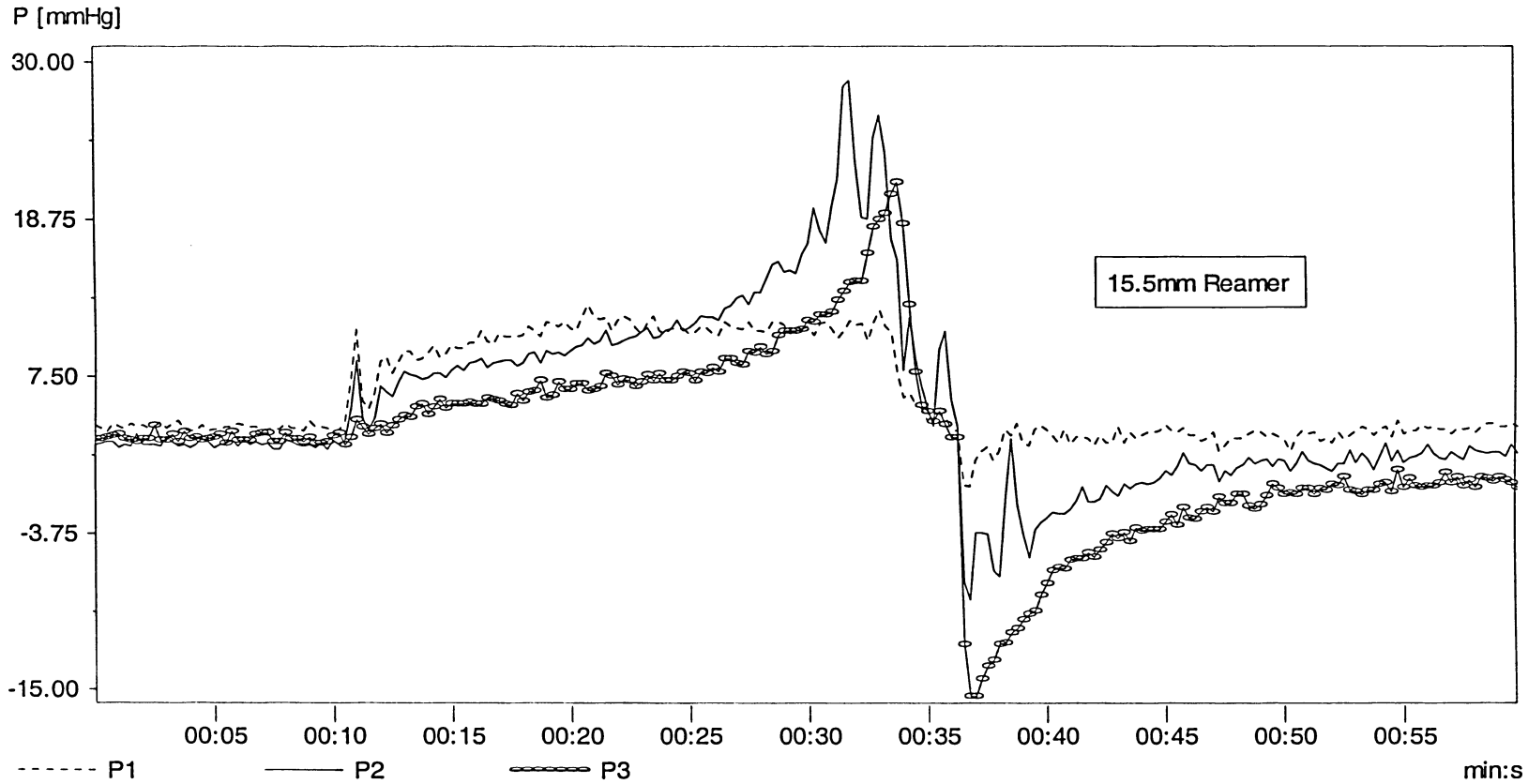

Figure A.10. Pressure variation using 15.5 mm reamer, 50 RPM, 10 $\frac{mm}{sec}$ and 82.6 cP synthetic marrow viscosity. P_1, P_2 and P_3 are respectively corresponded to pressure transducer #1, 2 and 3.

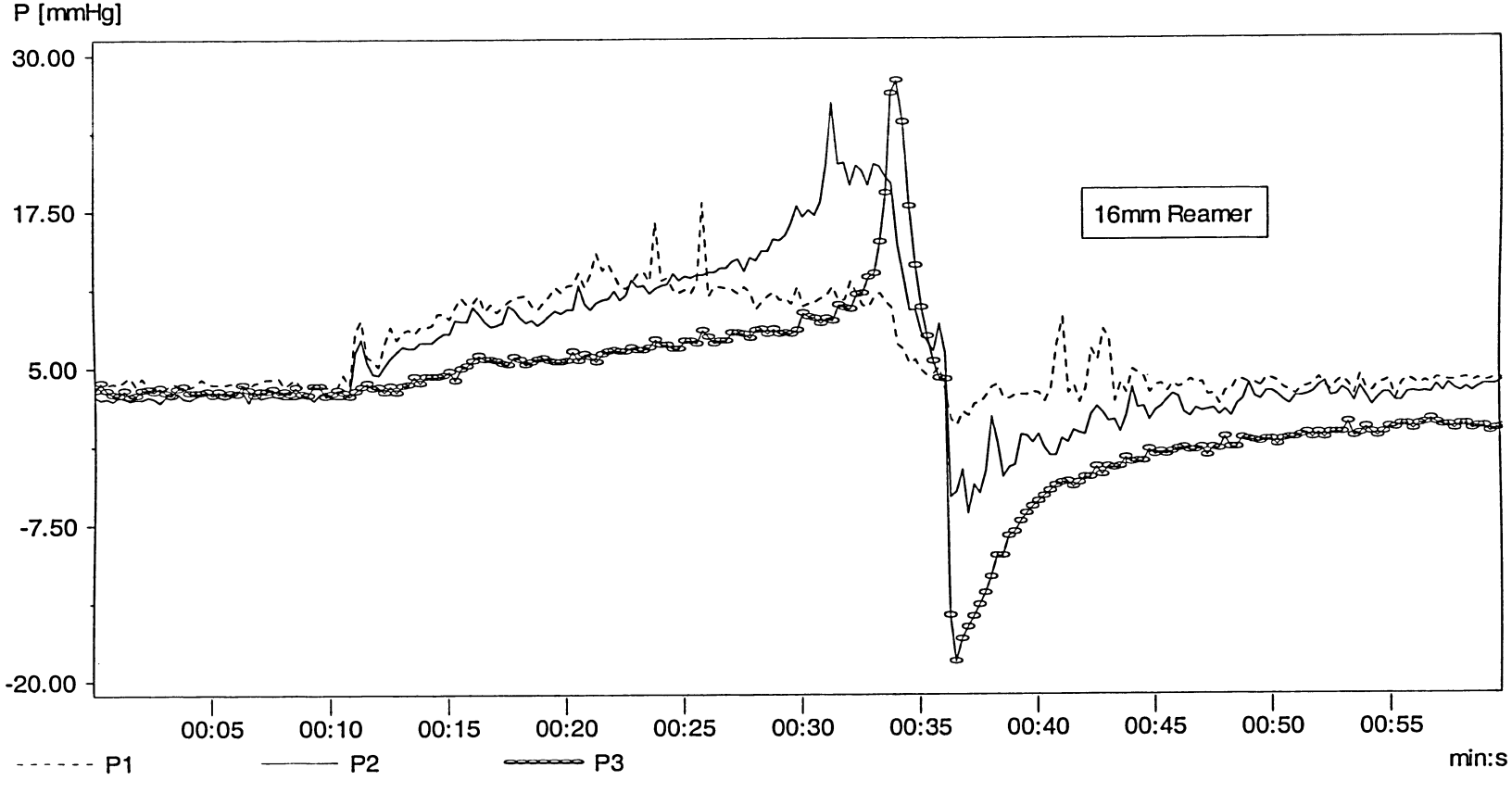

Figure A.11. Pressure variation using 16 mm reamer, 50 RPM, 10 $\frac{mm}{sec}$ and 82.6 cP synthetic marrow viscosity. P_1, P_2 and P_3 are respectively corresponded to pressure transducer #1, 2 and 3.

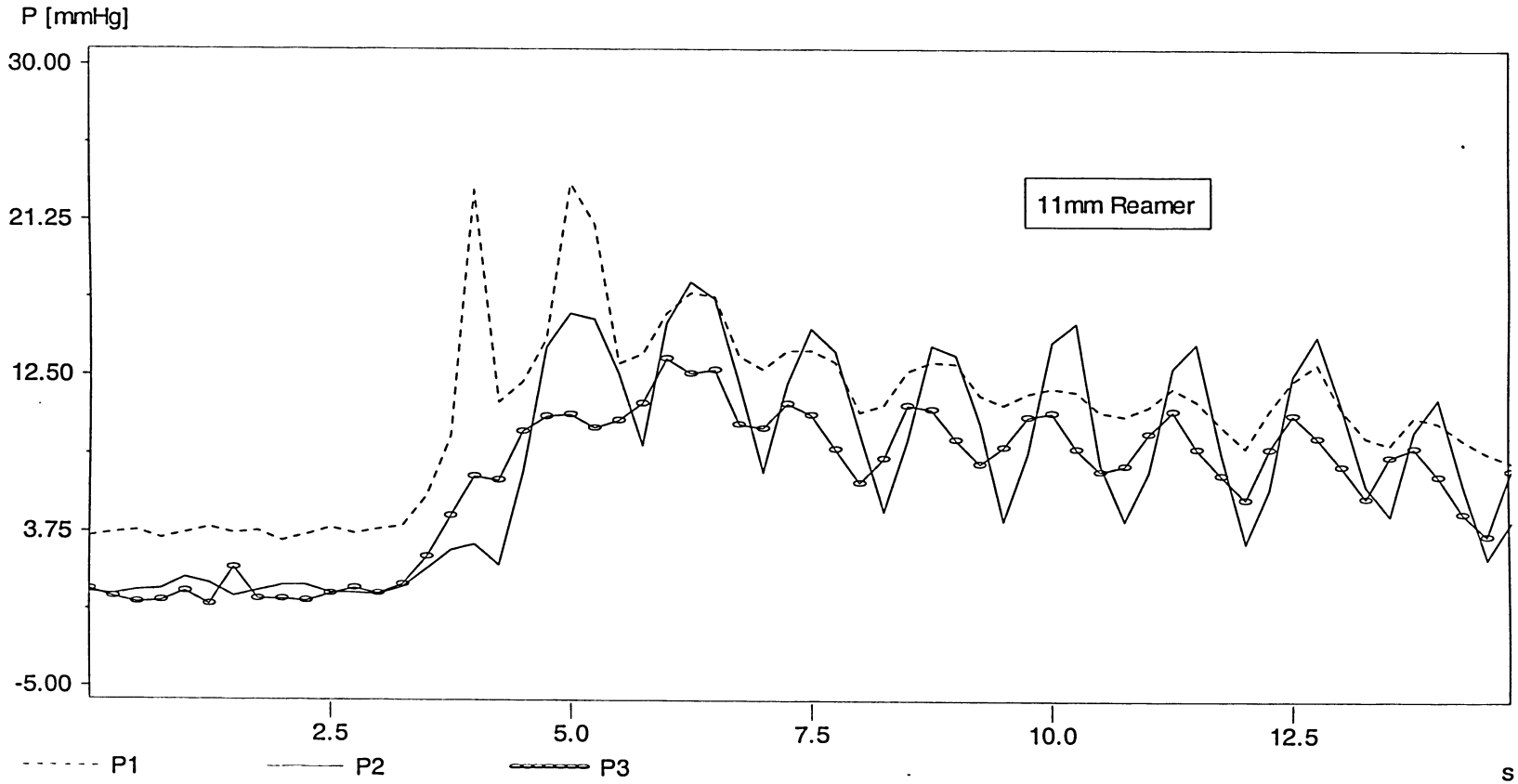

Figure A.12. Pressure variation using 11 mm reamer, 50 RPM, 50 $\frac{mm}{sec}$ and 82.6 cP synthetic marrow viscosity. P_1, P_2 and P_3 are respectively corresponded to pressure transducer #1, 2 and 3.

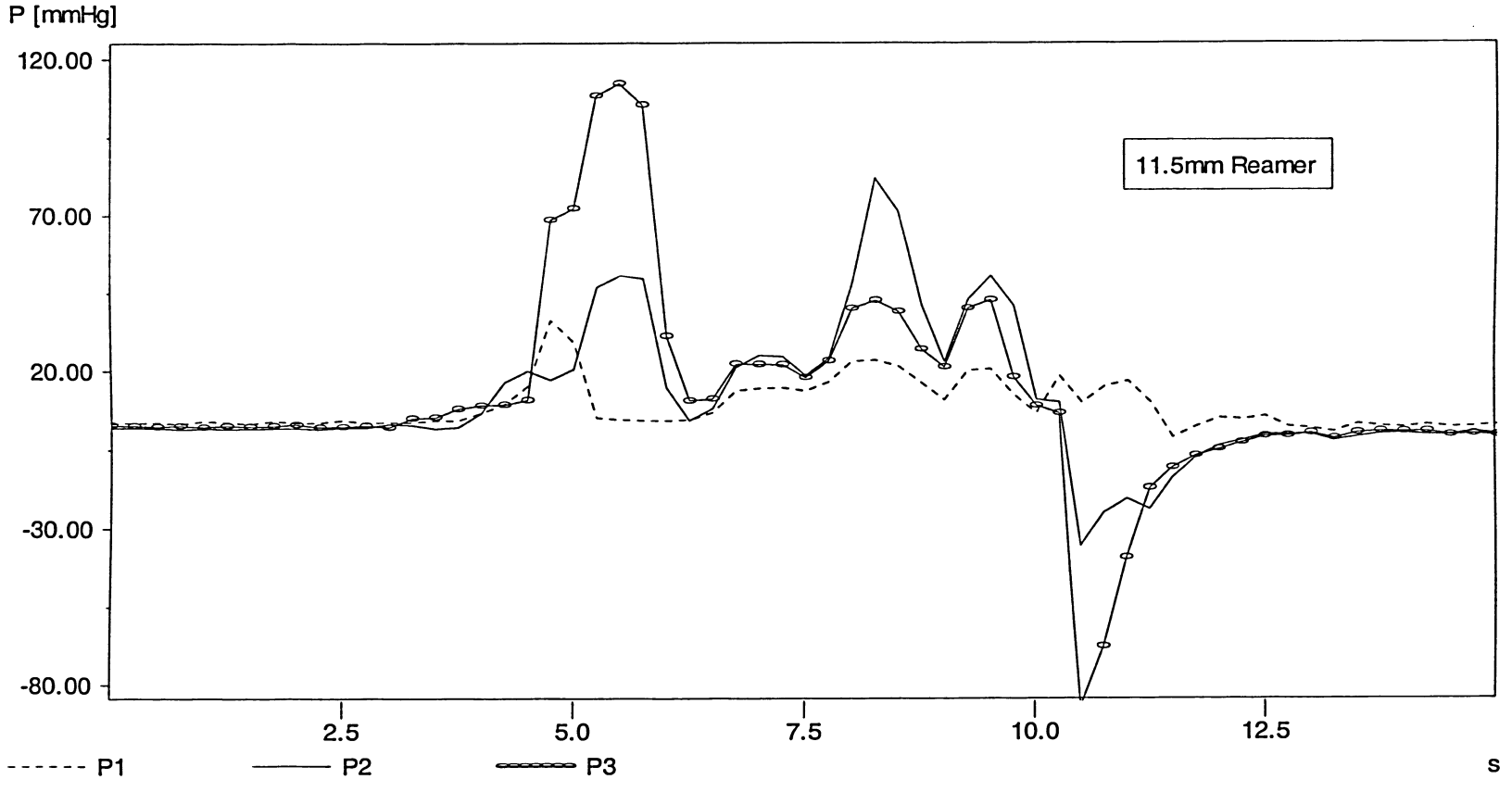

Figure A.13. Pressure variation using 11.5 mm reamer, 50 RPM, 50 $\frac{mm}{sec}$ and 82.6 cP synthetic marrow viscosity. P_1, P_2 and P_3 are respectively corresponded to pressure transducer #1, 2 and 3.

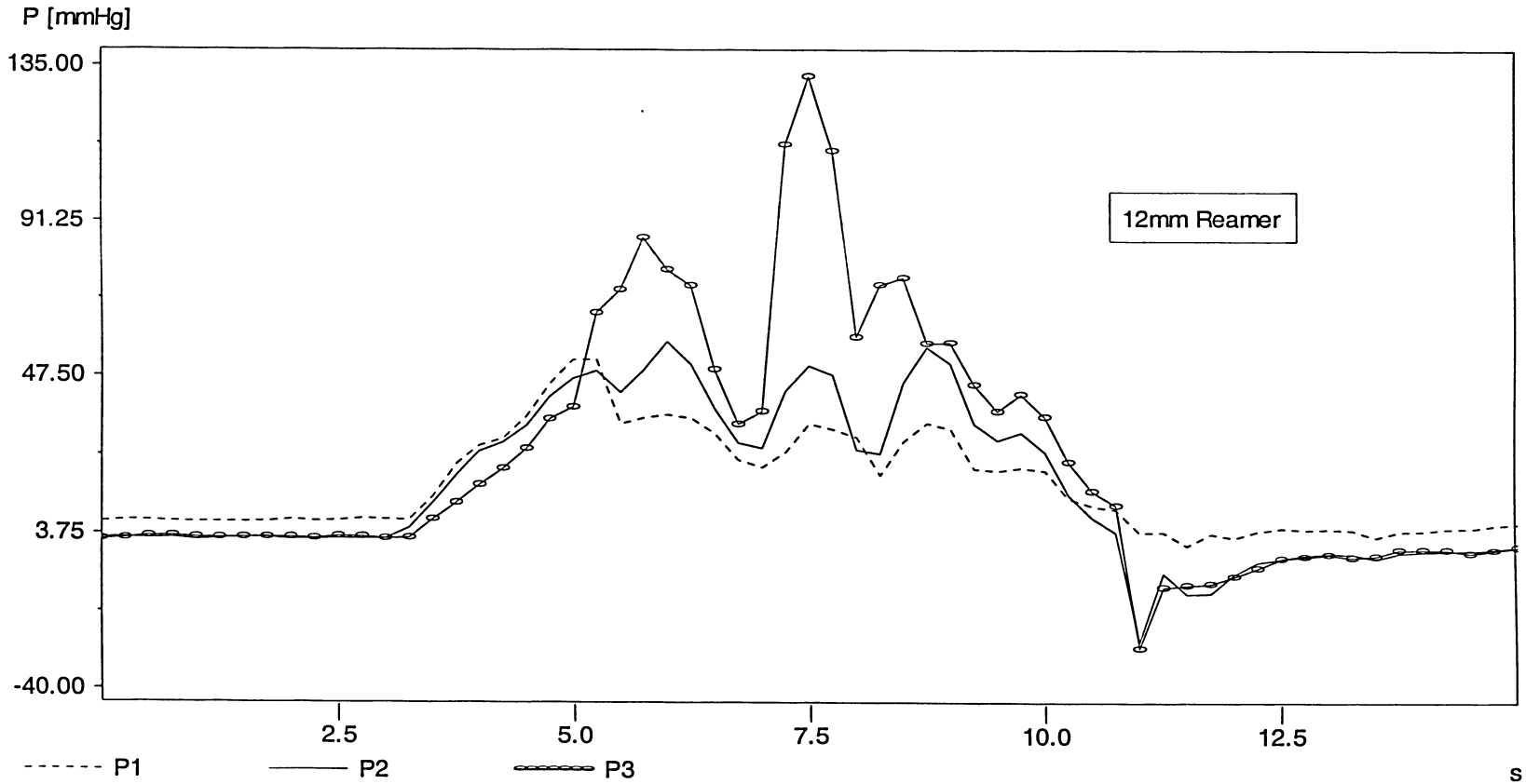

Figure A.14. Pressure variation using 12 mm reamer, 50 RPM, 50 $\frac{mm}{sec}$ and 82.6 cP synthetic marrow viscosity. P_1, P_2 and P_3 are respectively corresponded to pressure transducer #1, 2 and 3.

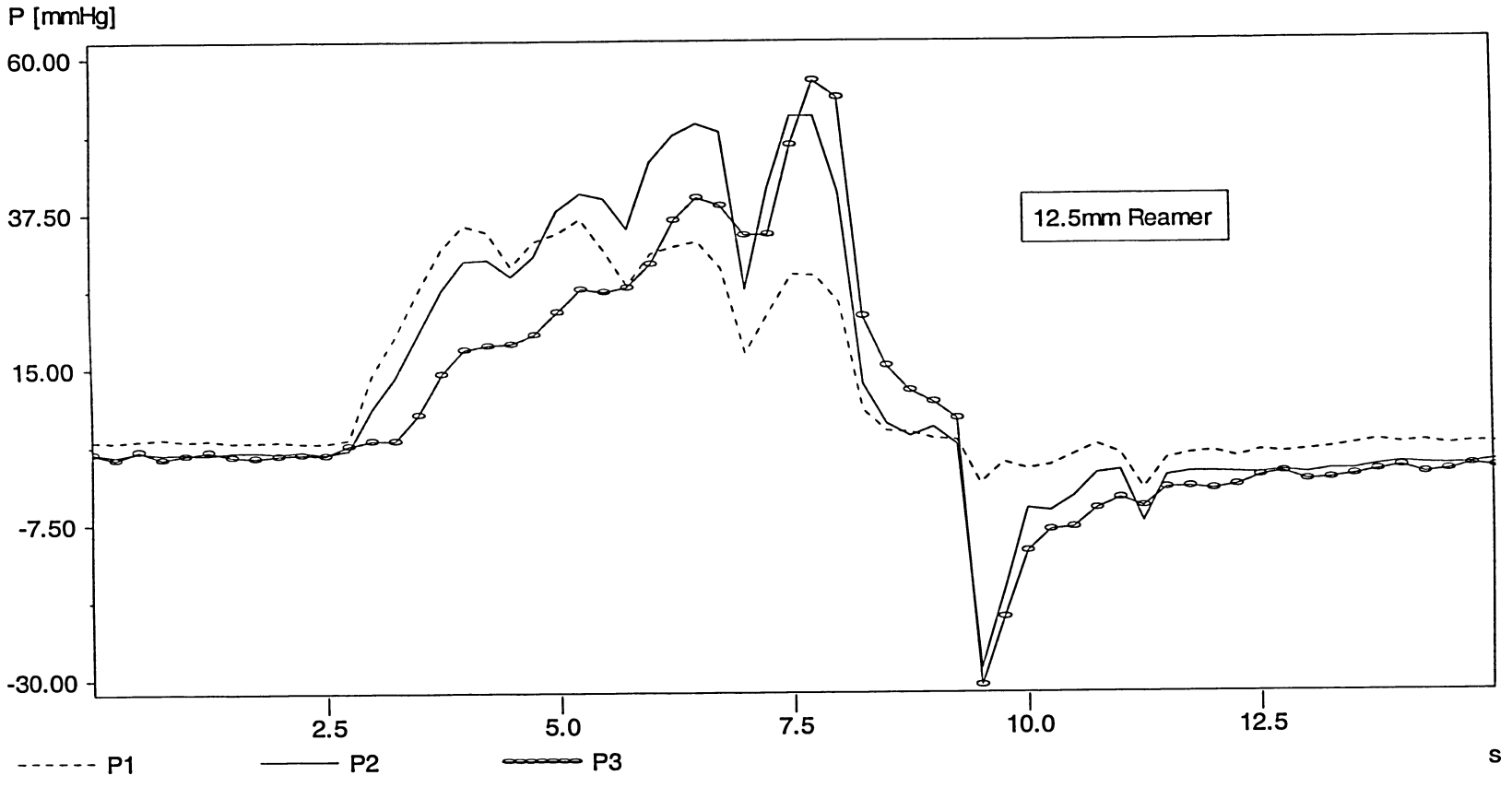

Figure A.15. Pressure variation using 12.5 mm reamer, 50 RPM, 50 $\frac{mm}{sec}$ and 82.6 cP synthetic marrow viscosity. P_1, P_2 and P_3 are respectively corresponded to pressure transducer #1, 2 and 3.

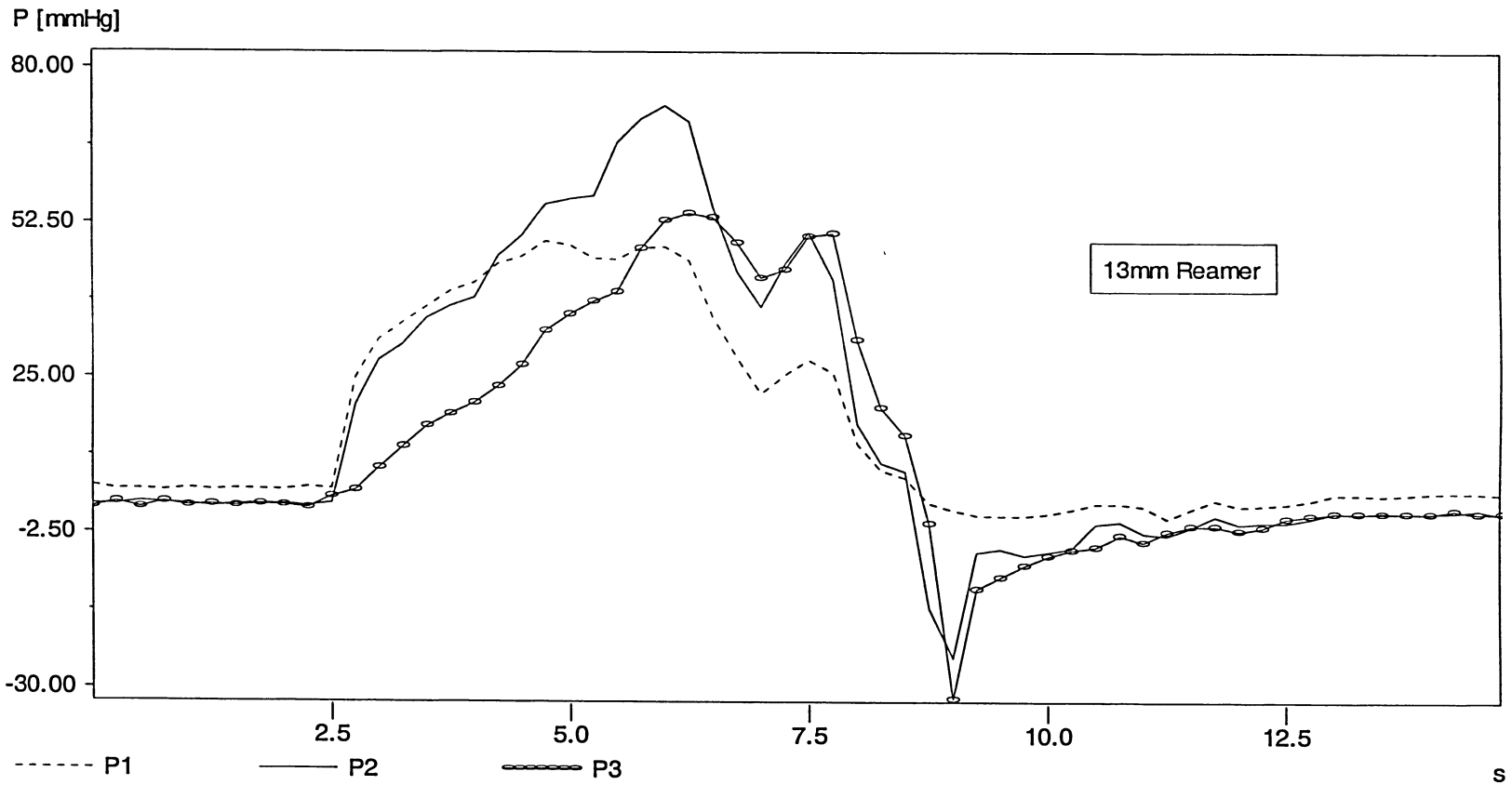

Figure A.16. Pressure variation using 13 mm reamer, 50 RPM, 50 $\frac{mm}{sec}$ and 82.6 cP synthetic marrow viscosity. P_1, P_2 and P_3 are respectively corresponded to pressure transducer #1, 2 and 3.

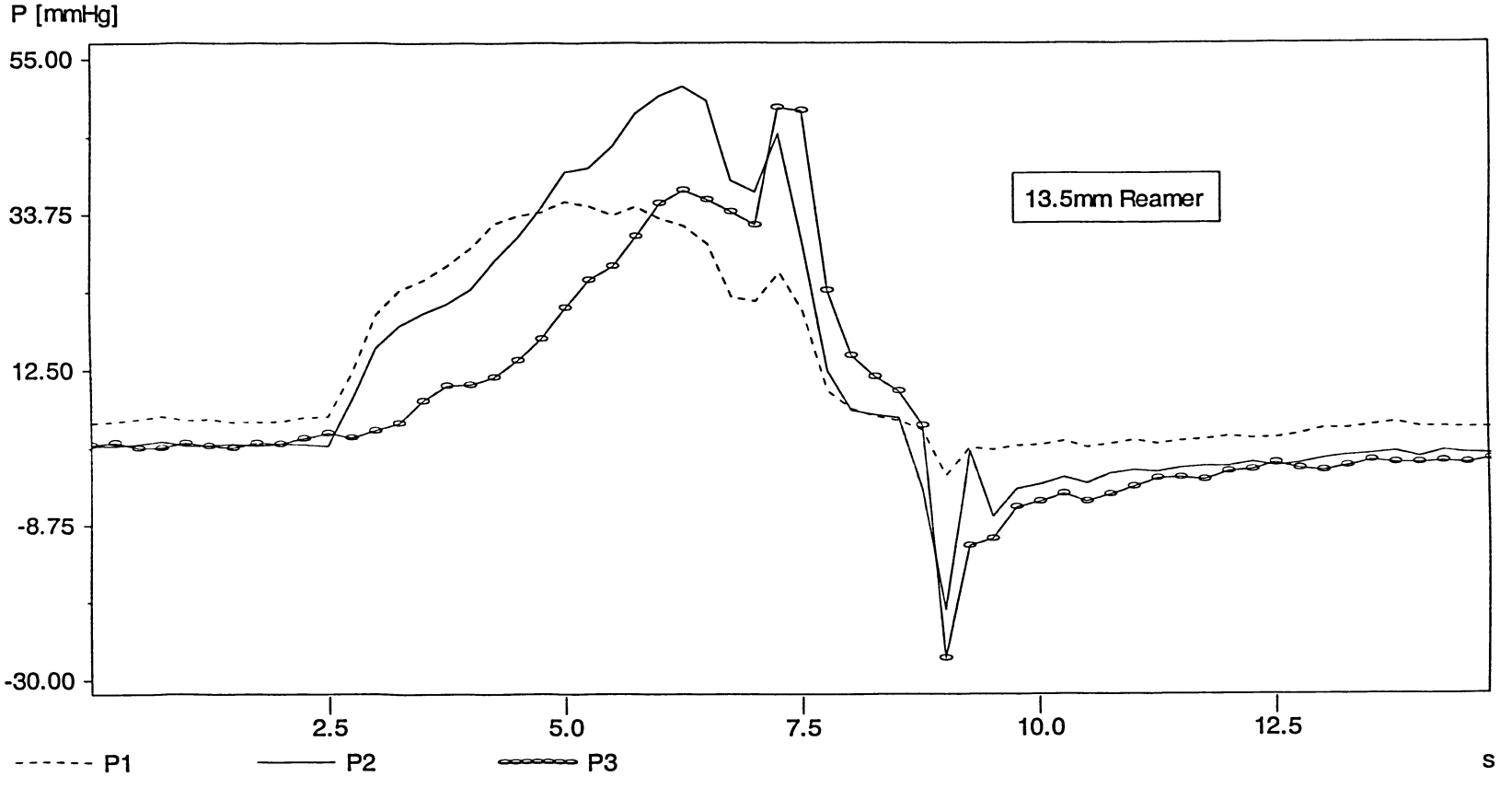

Figure A.17. Pressure variation using 13.5 mm reamer, 50 RPM, 50 $\frac{mm}{sec}$ and 82.6 cP synthetic marrow viscosity. P_1, P_2 and P_3 are respectively corresponded to pressure transducer #1, 2 and 3.

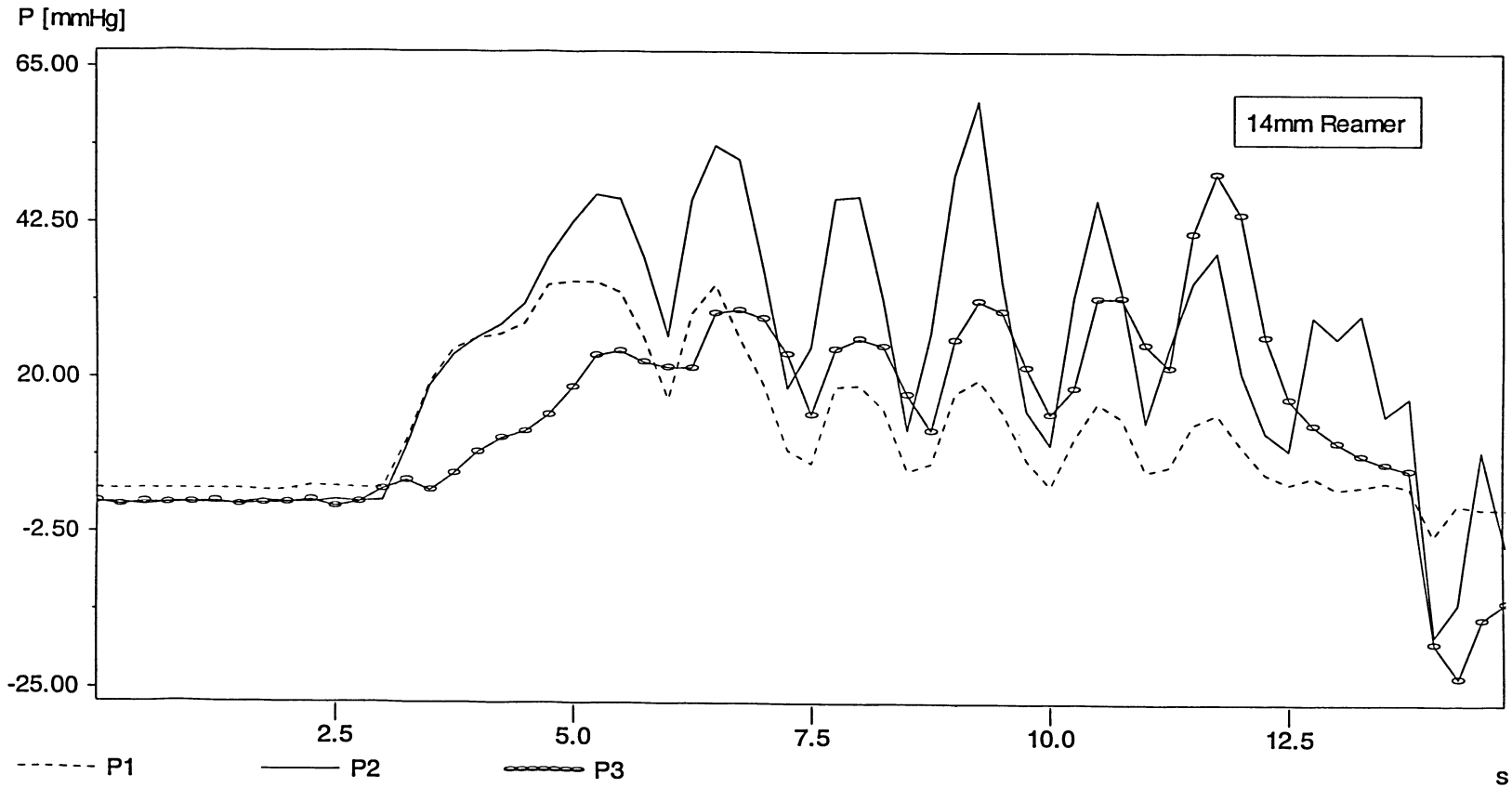

Figure A.18. Pressure variation using 14 mm reamer, 50 RPM, 50 $\frac{mm}{sec}$ and 82.6 cP synthetic marrow viscosity. P_1, P_2 and P_3 are respectively corresponded to pressure transducer #1, 2 and 3.

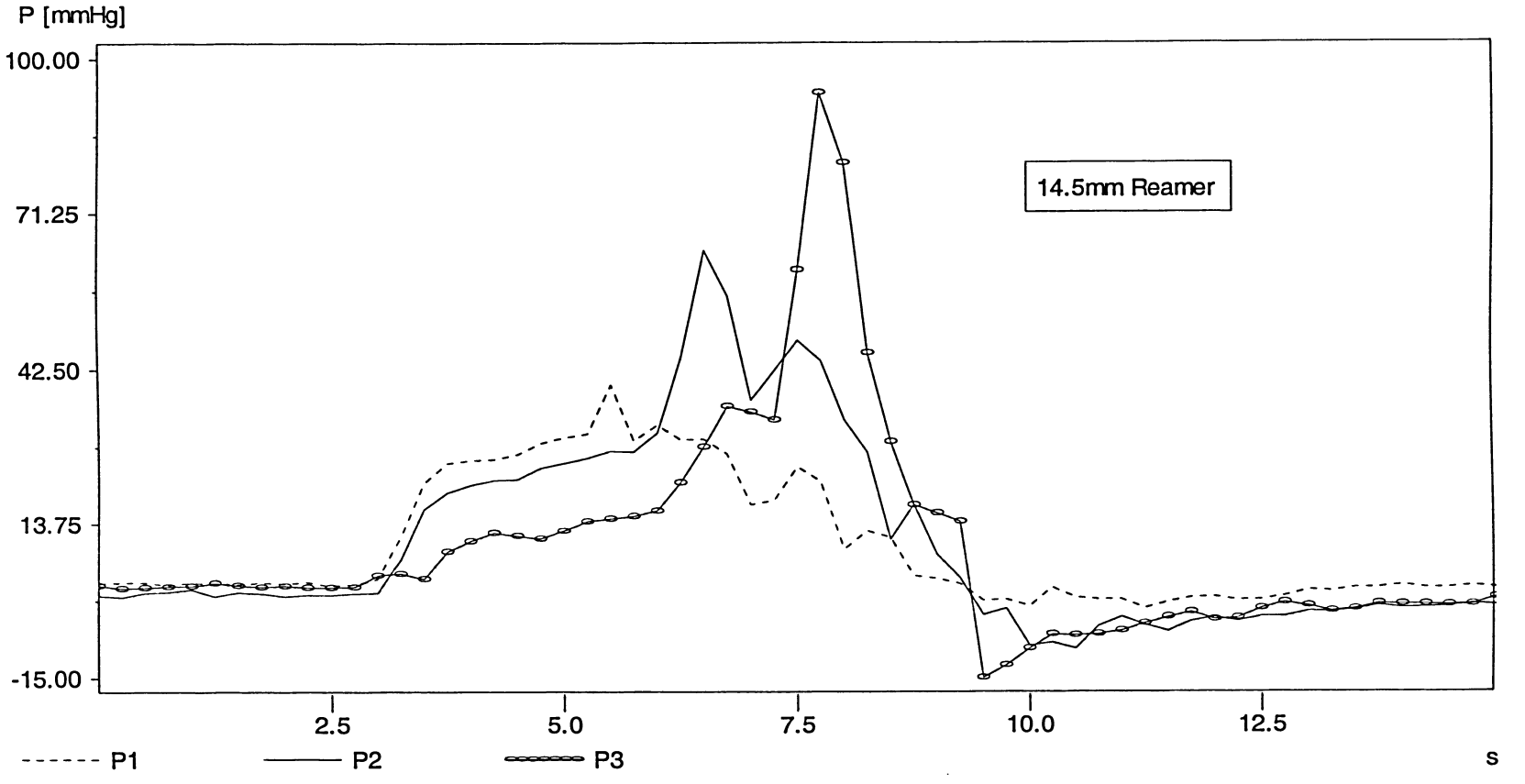

Figure A.19. Pressure variation using 14.5 mm reamer, 50 RPM, 50 $\frac{mm}{sec}$ and 82.6 cP synthetic marrow viscosity. P_1, P_2 and P_3 are respectively corresponded to pressure transducer #1, 2 and 3.

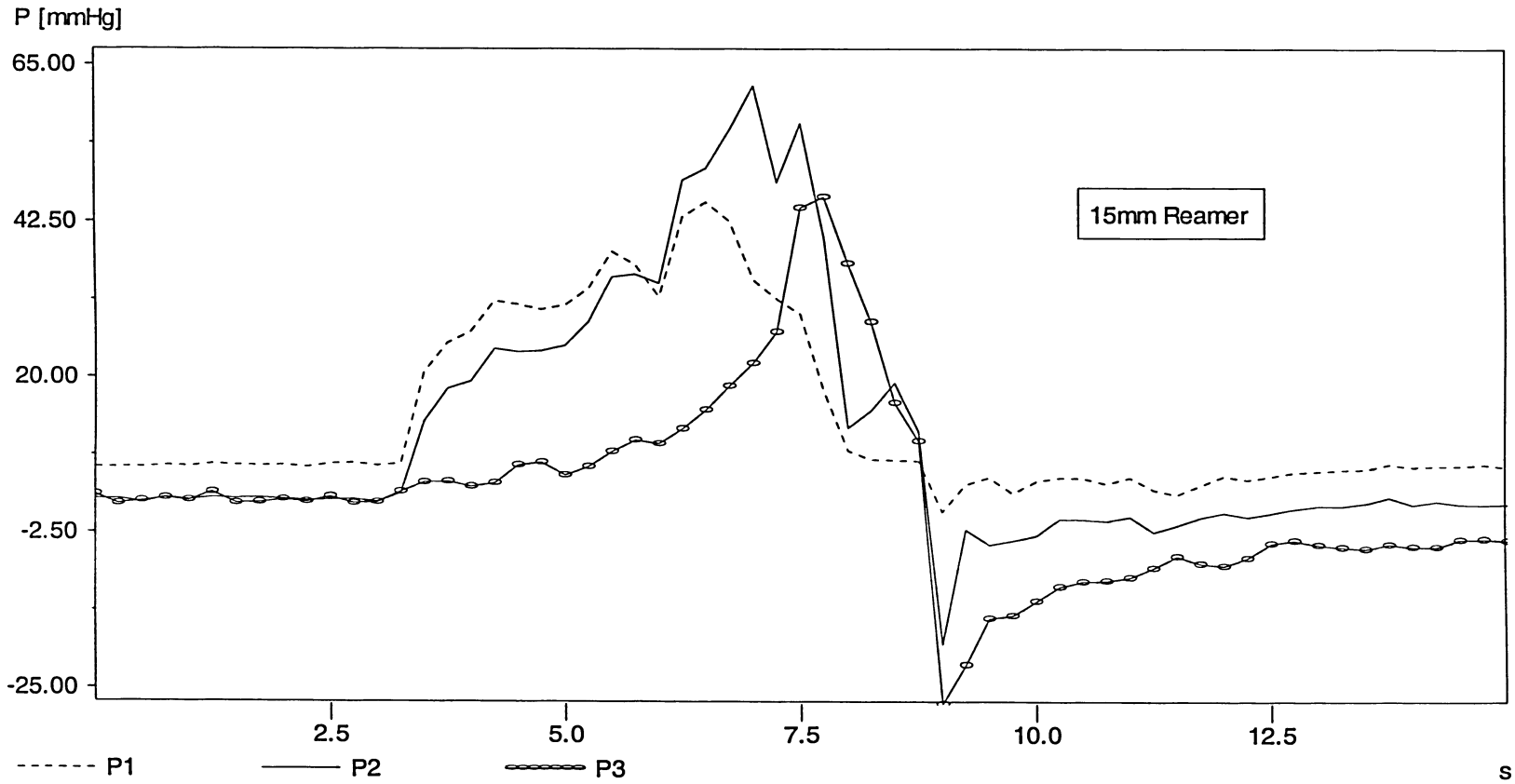

Figure A.20. Pressure variation using 15 mm reamer, 50 RPM, 50 $\frac{mm}{sec}$ and 82.6 cP synthetic marrow viscosity. P_1, P_2 and P_3 are respectively corresponded to pressure transducer #1, 2 and 3.

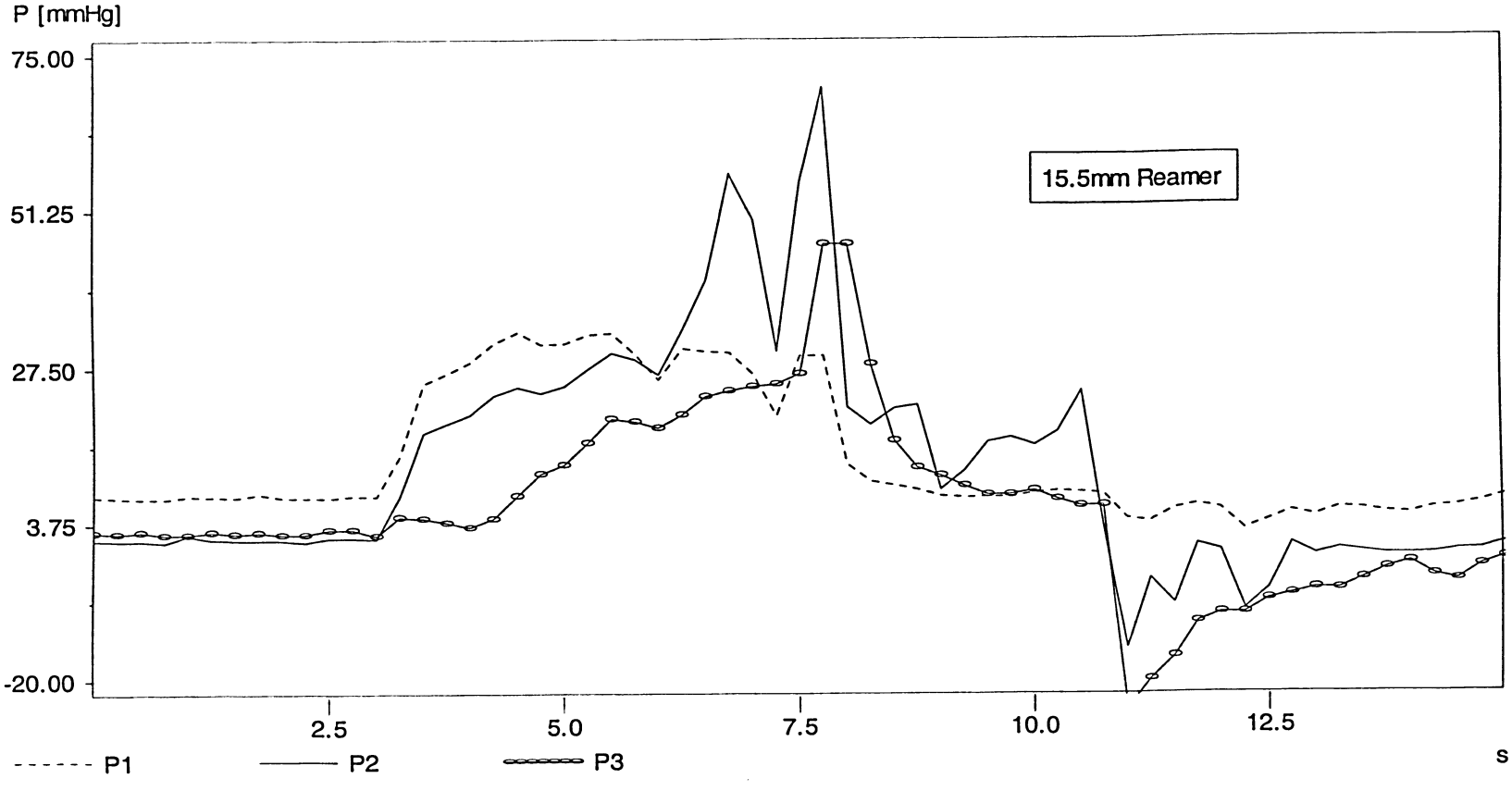

Figure A.21. Pressure variation using 15.5 mm reamer, 50 RPM, 50 $\frac{mm}{sec}$ and 82.6 cP synthetic marrow viscosity. P_1, P_2 and P_3 are respectively corresponded to pressure transducer #1, 2 and 3.

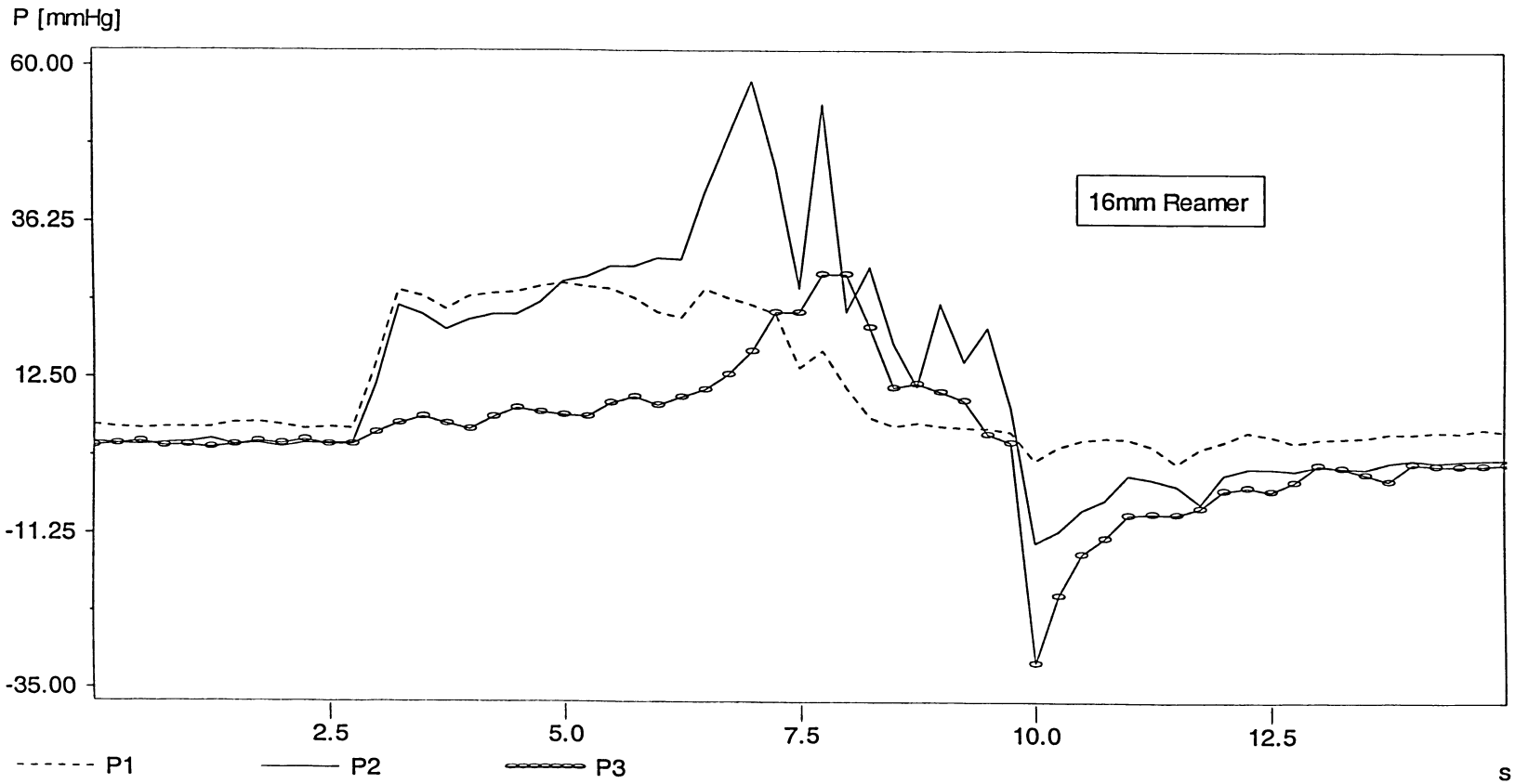

Figure A.22. Pressure variation using 16 mm reamer, 50 RPM, 50 $\frac{mm}{sec}$ and 82.6 cP synthetic marrow viscosity. P_1, P_2 and P_3 are respectively corresponded to pressure transducer #1, 2 and 3.

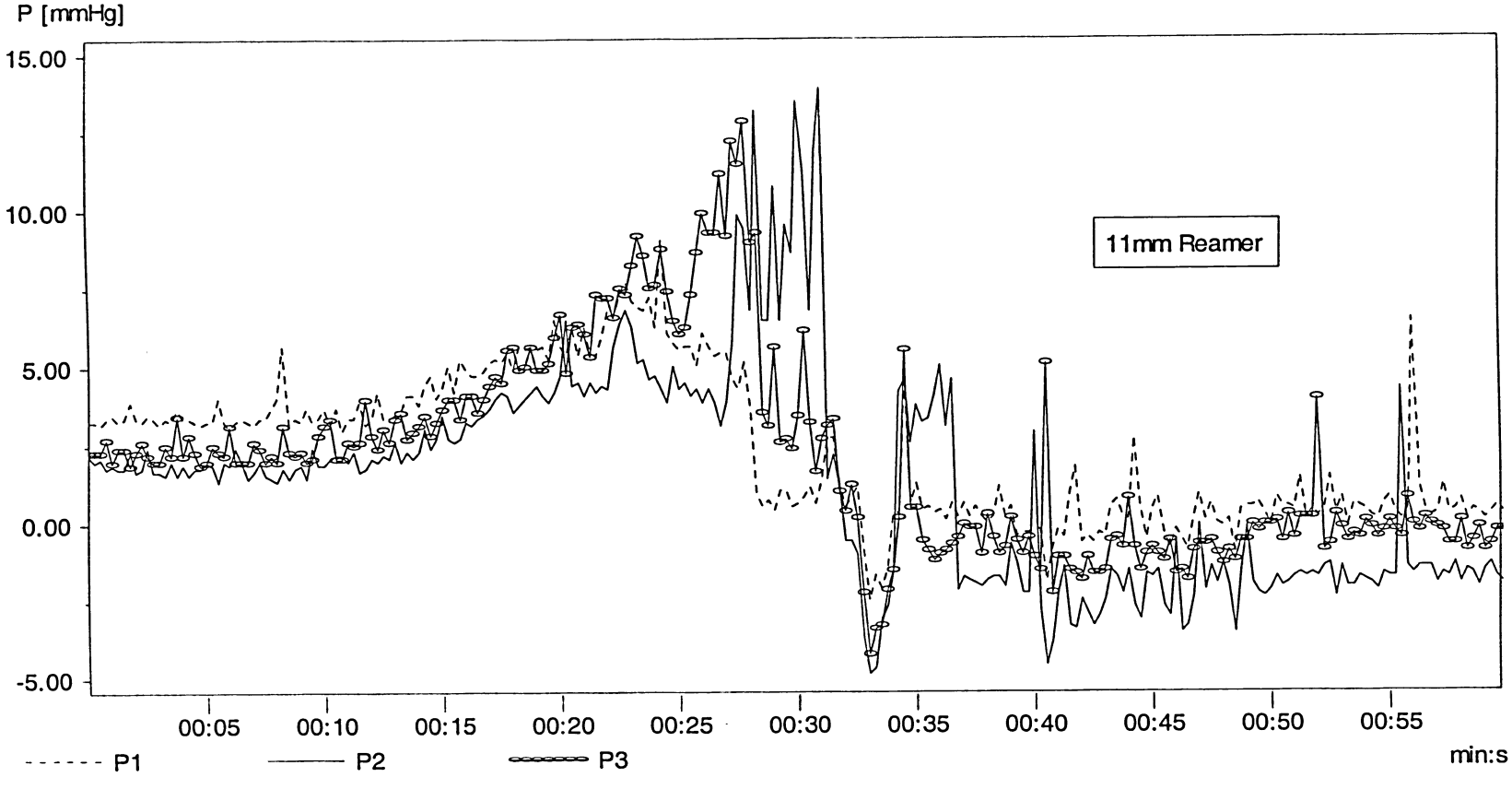

Figure A.23. Pressure variation using 11 mm reamer, 200 RPM, 10 $\frac{mm}{sec}$ and 82.6 cP synthetic marrow viscosity. P_1, P_2 and P_3 are respectively corresponded to pressure transducer #1, 2 and 3.

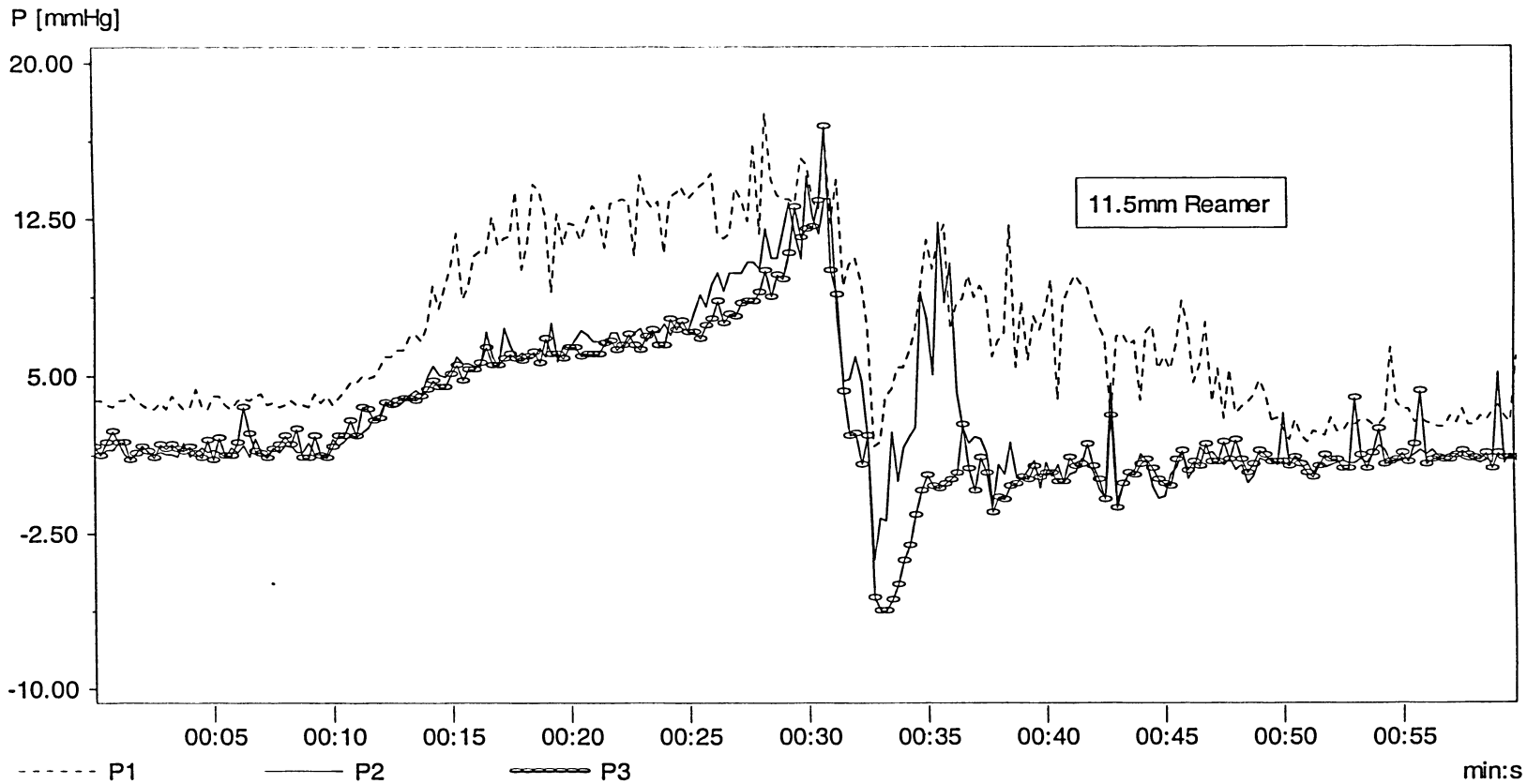

Figure A.24. Pressure variation using 11.5 mm reamer, 200 RPM, 10 $\frac{mm}{sec}$ and 82.6 cP synthetic marrow viscosity. P_1, P_2 and P_3 are respectively corresponded to pressure transducer #1, 2 and 3.

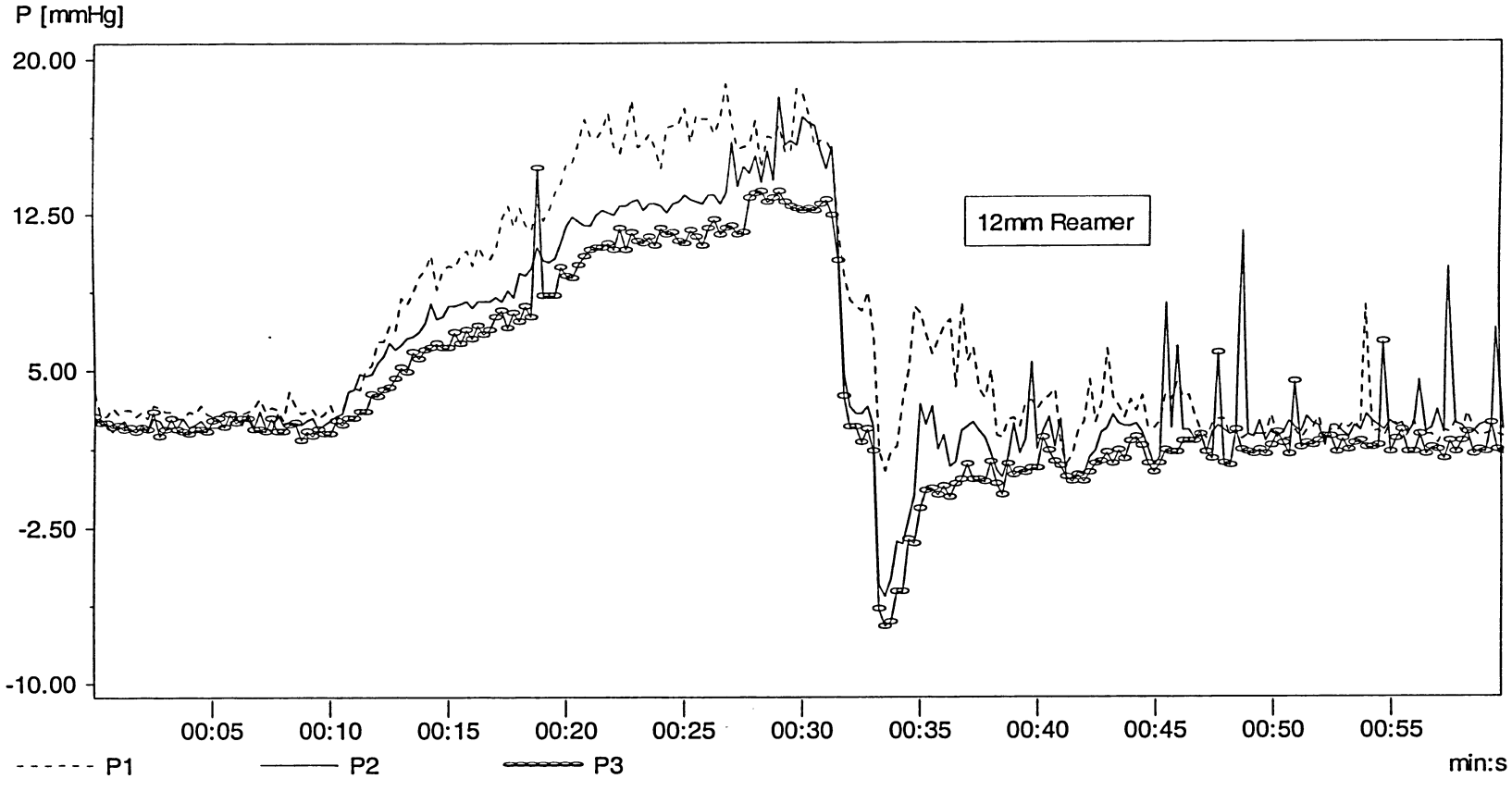

Figure A.25. Pressure variation using 12 mm reamer, 200 RPM, 10 $\frac{mm}{sec}$ and 82.6 cP synthetic marrow viscosity. P_1, P_2 and P_3 are respectively corresponded to pressure transducer #1, 2 and 3.

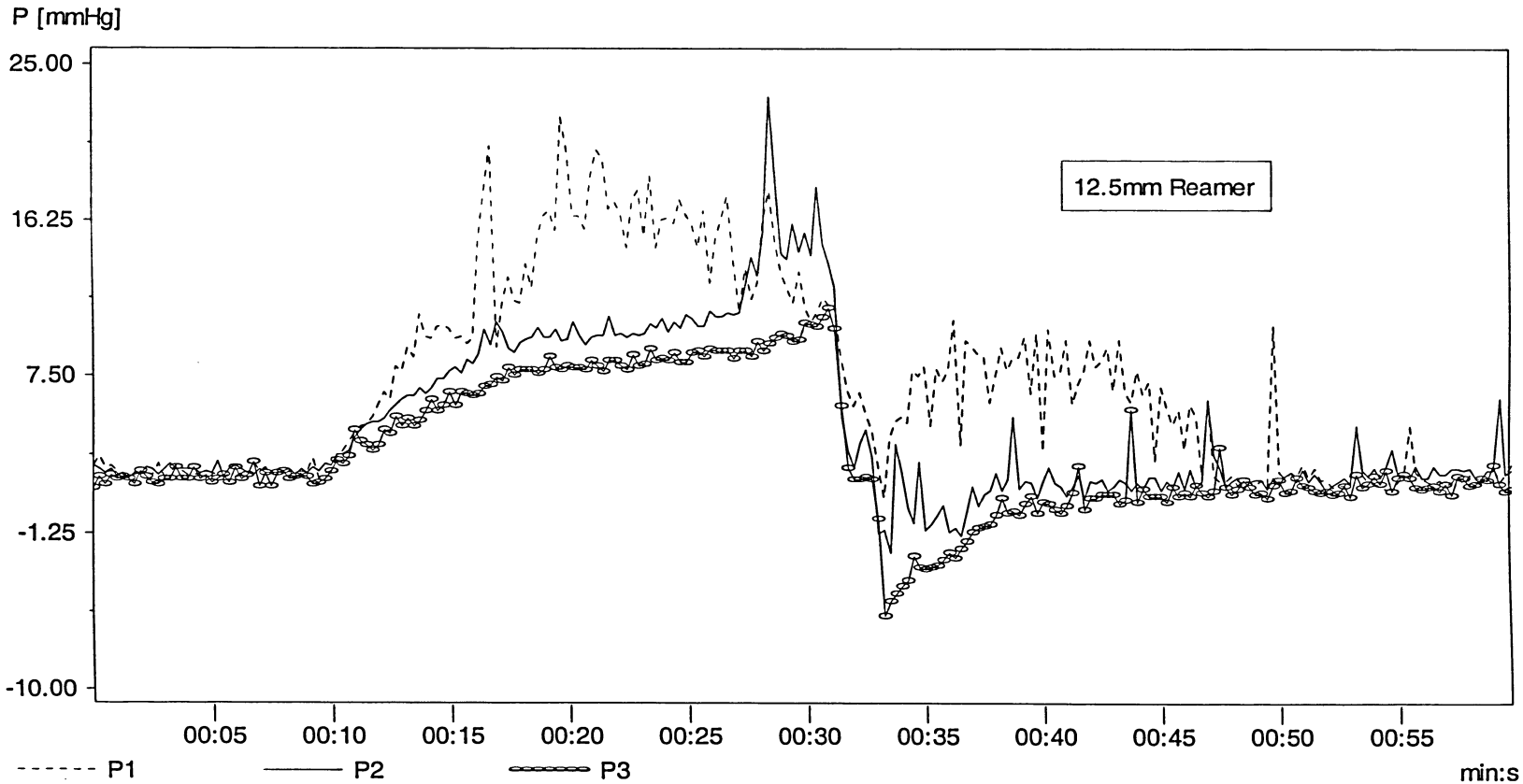

Figure A.26. Pressure variation using 12.5 mm reamer, 200 RPM, 10 $\frac{mm}{sec}$ and 82.6 cP synthetic marrow viscosity. P_1, P_2 and P_3 are respectively corresponded to pressure transducer #1, 2 and 3.

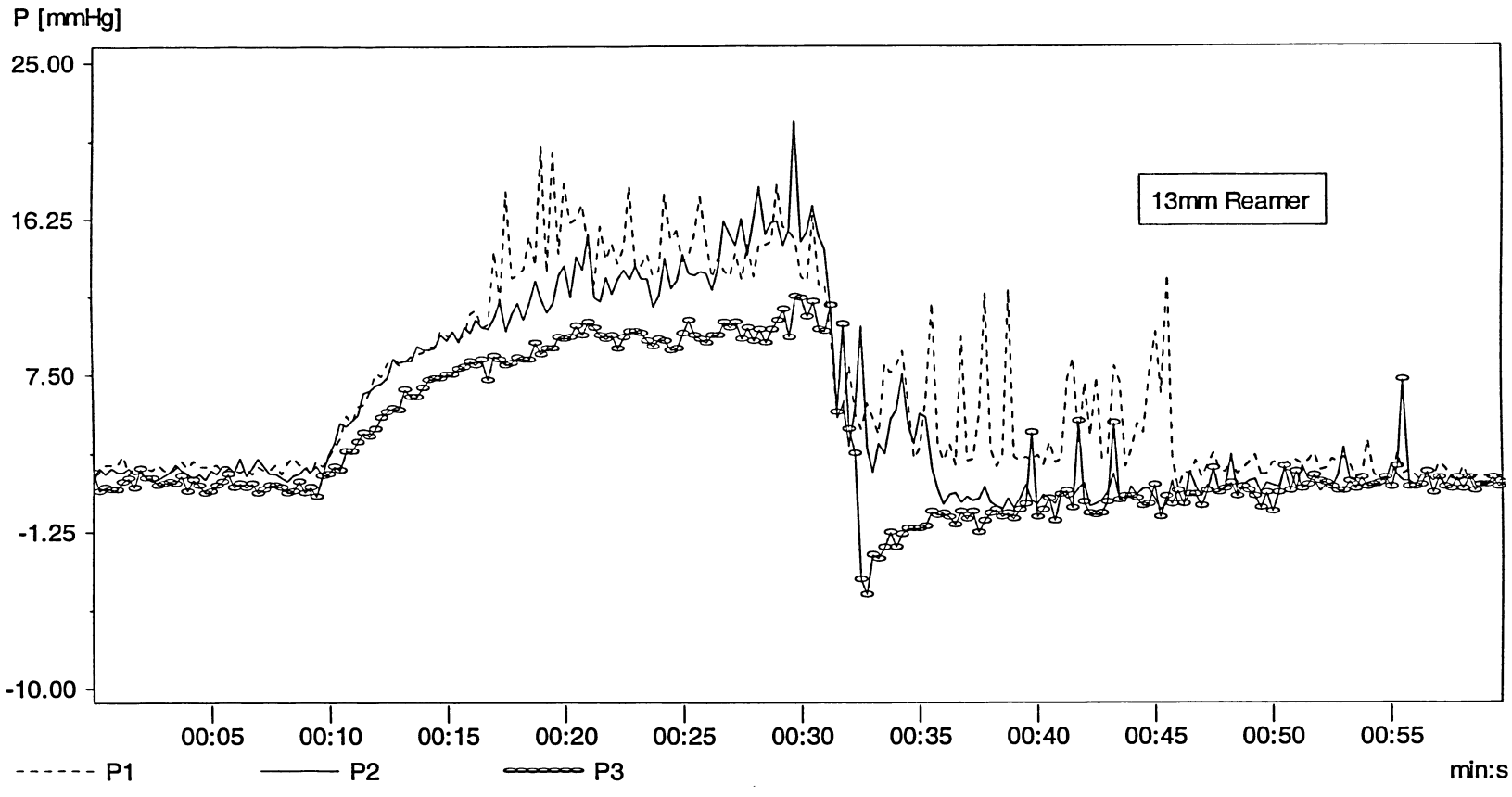

Figure A.27. Pressure variation using 13 mm reamer, 200 RPM, 10 $\frac{mm}{sec}$ and 82.6 cP synthetic marrow viscosity. P_1, P_2 and P_3 are respectively corresponded to pressure transducer #1, 2 and 3.

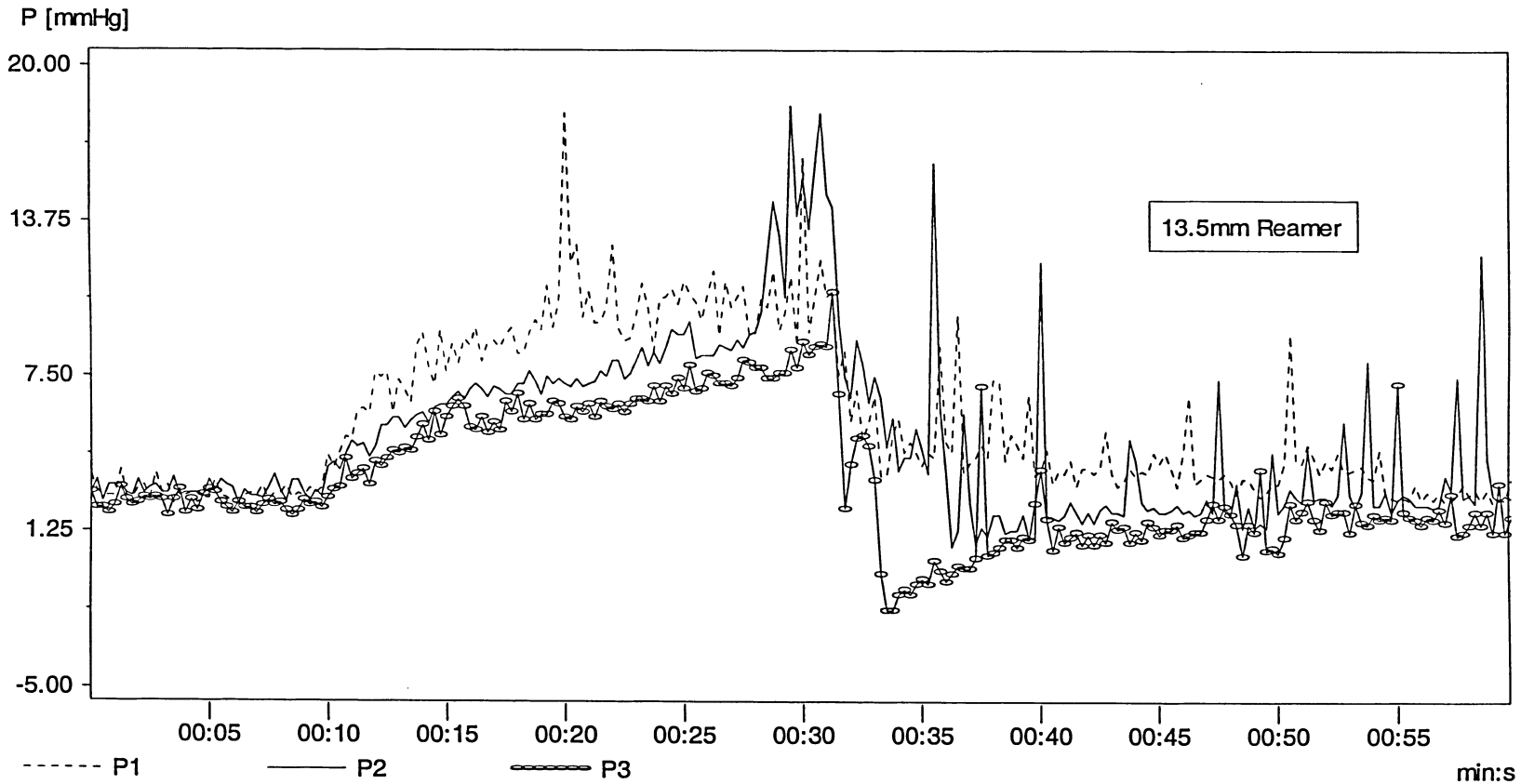

Figure A.28. Pressure variation using 13.5 mm reamer, 200 RPM, 10 $\frac{mm}{sec}$ and 82.6 cP synthetic marrow viscosity. P_1, P_2 and P_3 are respectively corresponded to pressure transducer #1, 2 and 3.

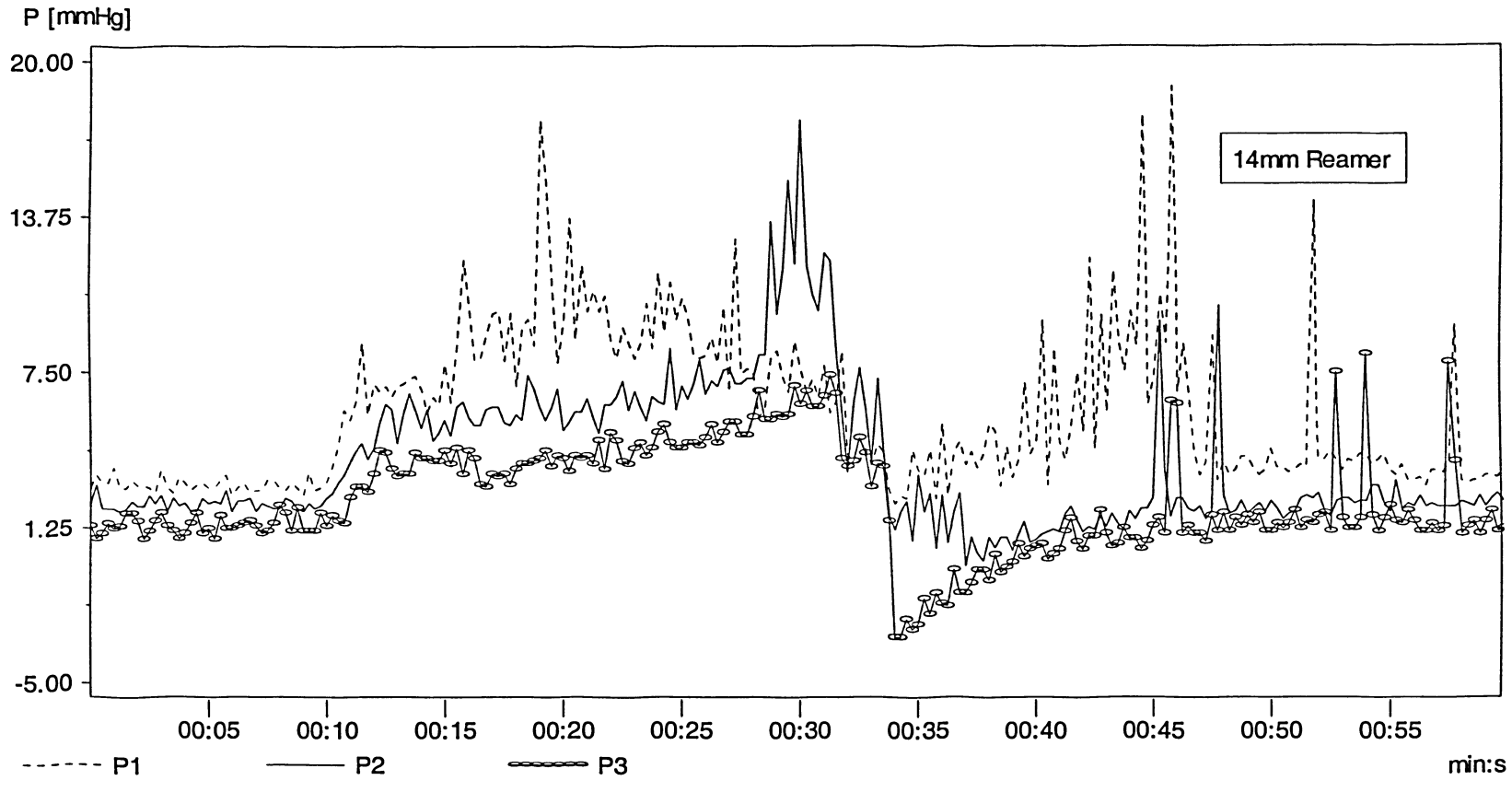

Figure A.29. Pressure variation using 14 mm reamer, 200 RPM, 10 $\frac{mm}{sec}$ and 82.6 cP synthetic marrow viscosity. P_1, P_2 and P_3 are respectively corresponded to pressure transducer #1, 2 and 3.

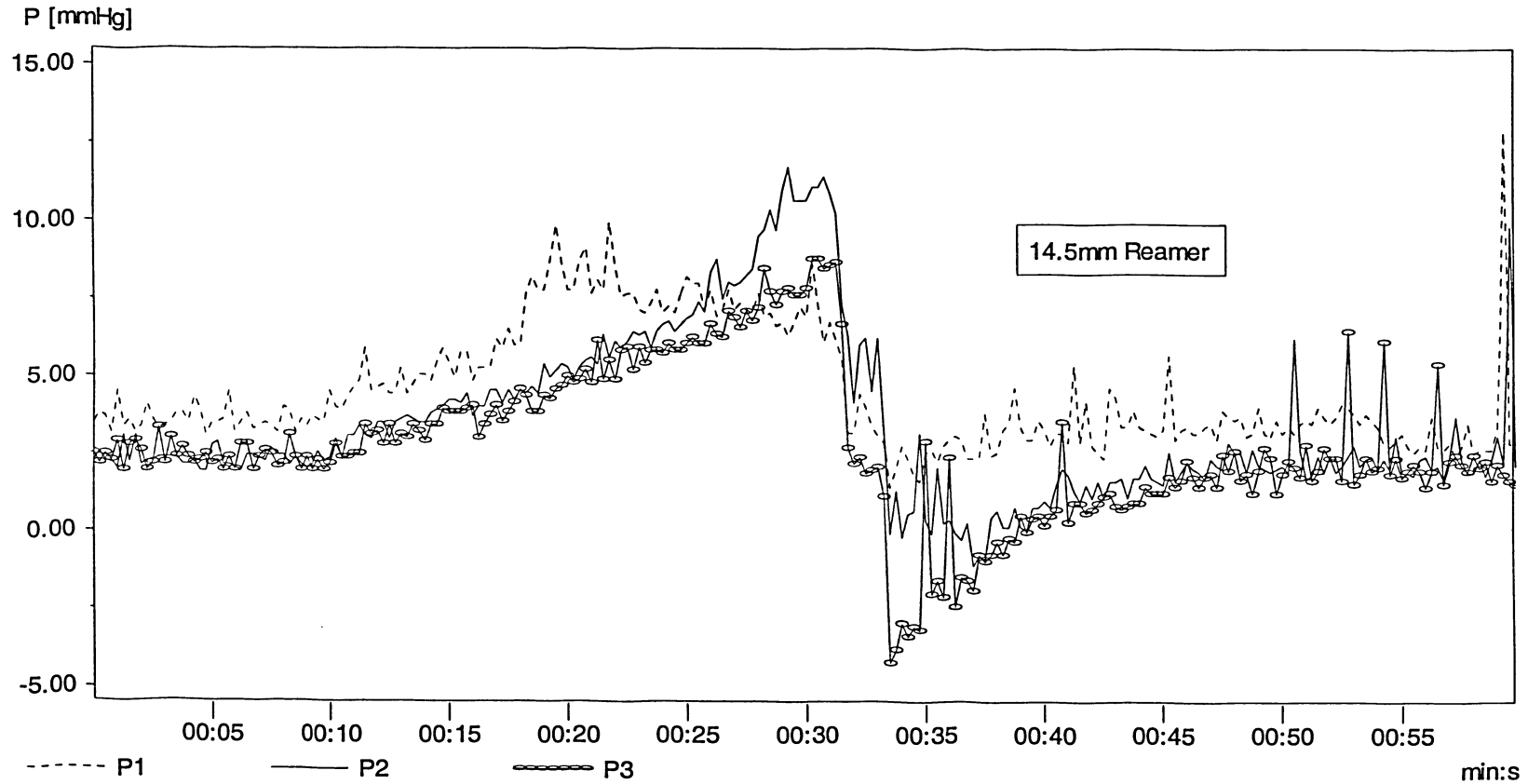

Figure A.30. Pressure variation using 14.5 mm reamer, 200 RPM, 10 $\frac{mm}{sec}$ and 82.6 cP synthetic marrow viscosity. P_1, P_2 and P_3 are respectively corresponded to pressure transducer #1, 2 and 3.

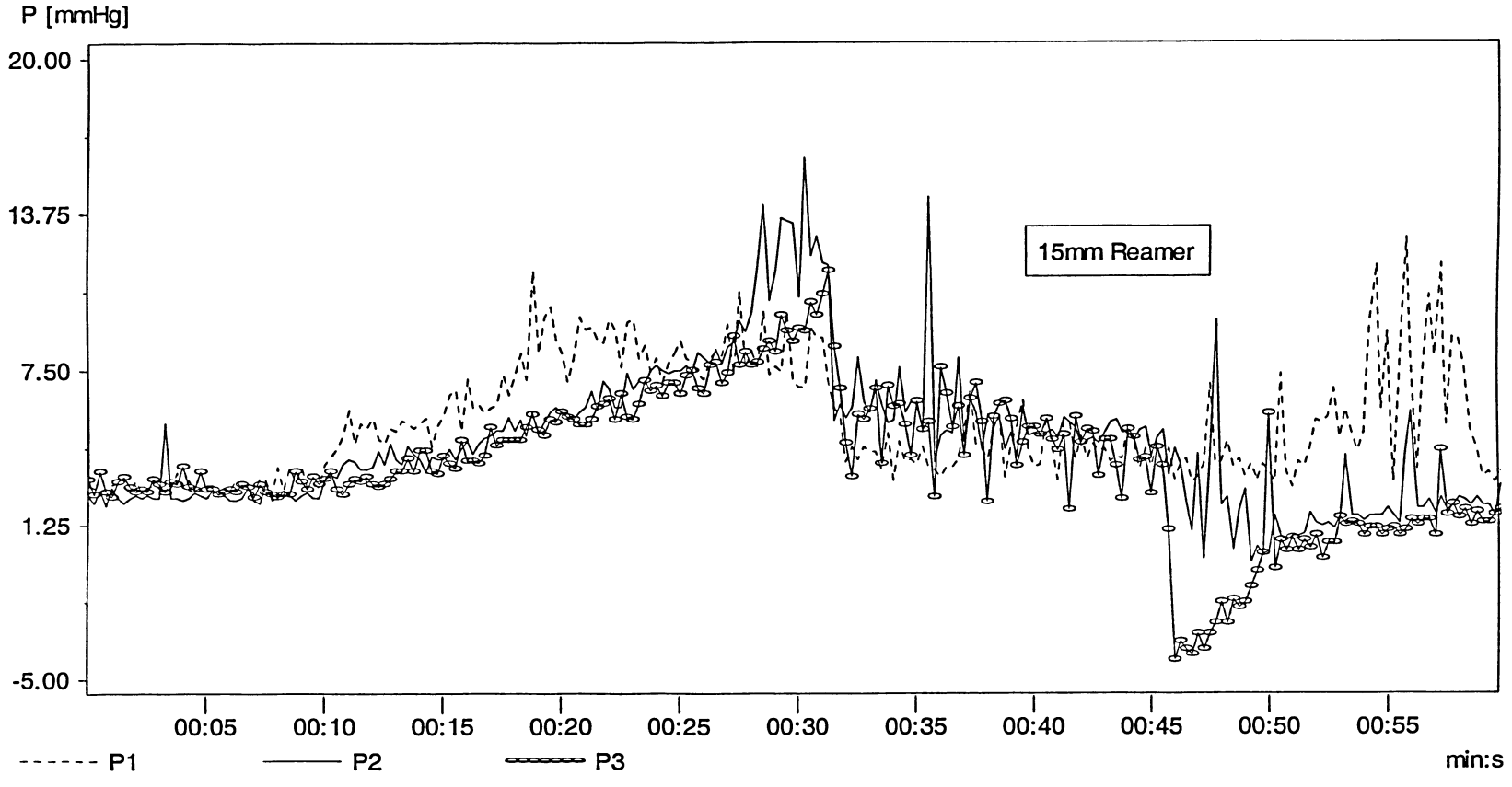

Figure A.31. Pressure variation using 15 mm reamer, 200 RPM, 10 $\frac{mm}{sec}$ and 82.6 cP synthetic marrow viscosity. P_1, P_2 and P_3 are respectively corresponded to pressure transducer #1, 2 and 3.

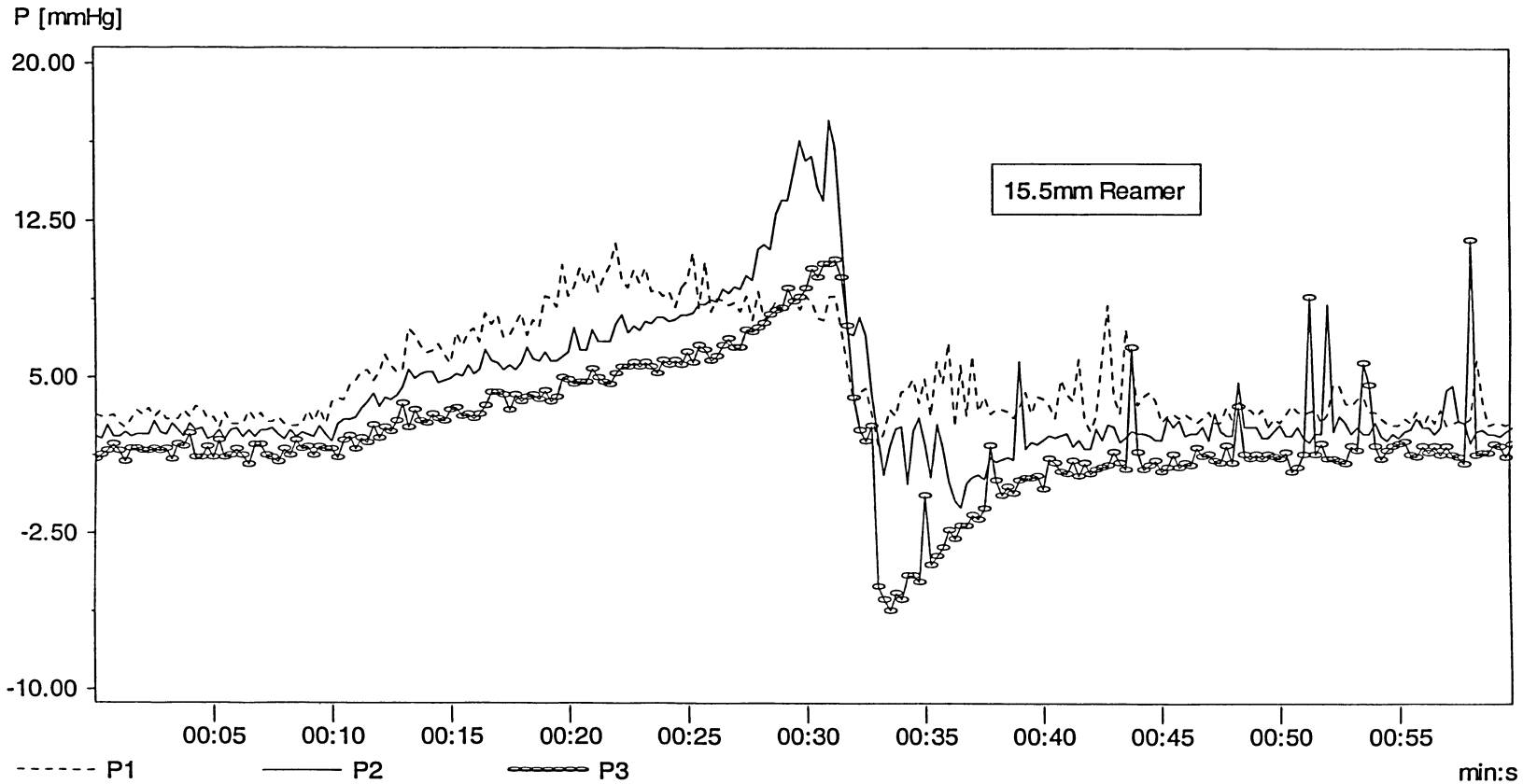

Figure A.32. Pressure variation using 15.5 mm reamer, 200 RPM, 10 $\frac{mm}{sec}$ and 82.6 cP synthetic marrow viscosity. P_1, P_2 and P_3 are respectively corresponded to pressure transducer #1, 2 and 3.

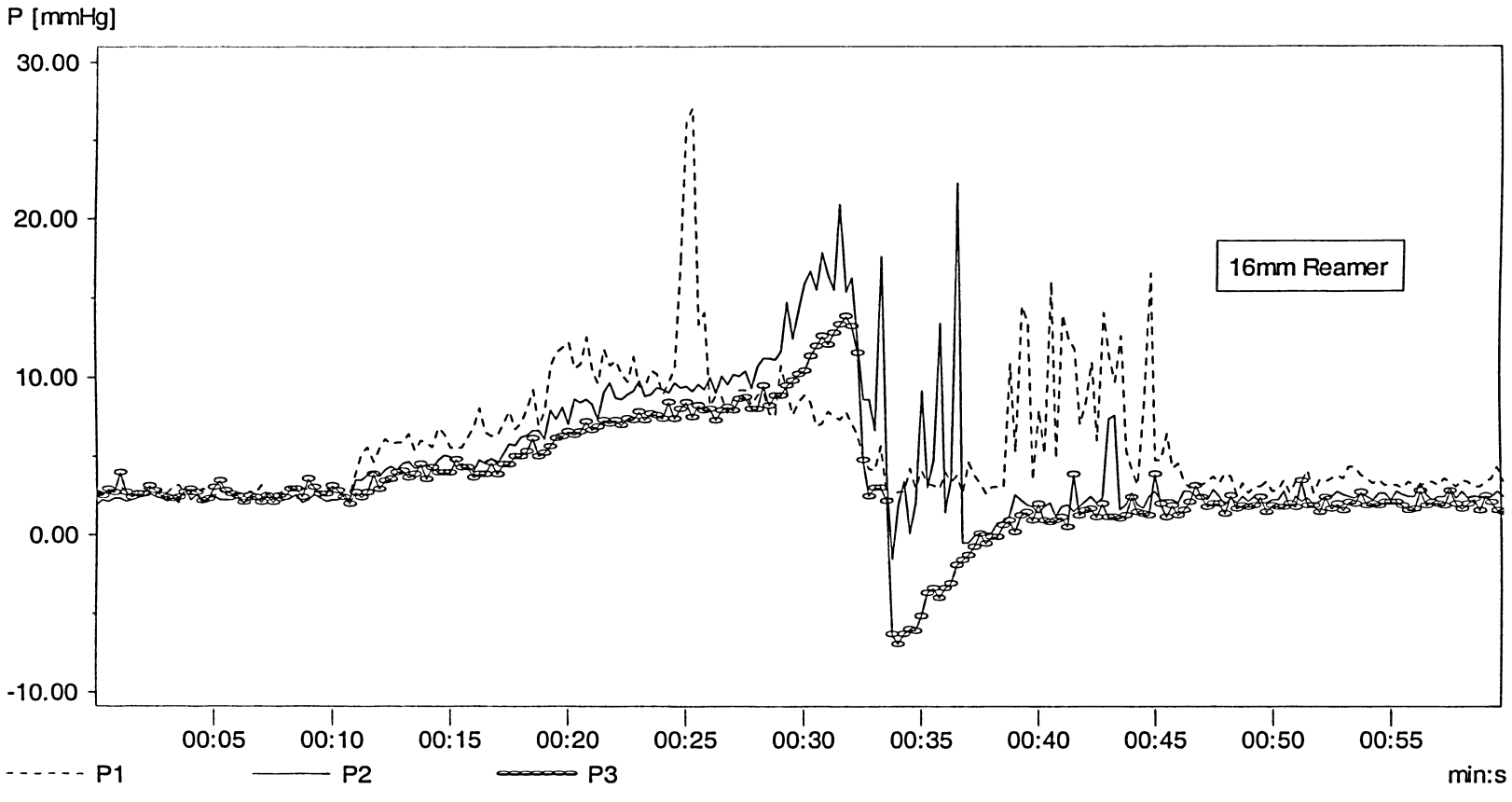

Figure A.33. Pressure variation using 16 mm reamer, 200 RPM, 10 $\frac{mm}{sec}$ and 82.6 cP synthetic marrow viscosity. P_1, P_2 and P_3 are respectively corresponded to pressure transducer #1, 2 and 3.

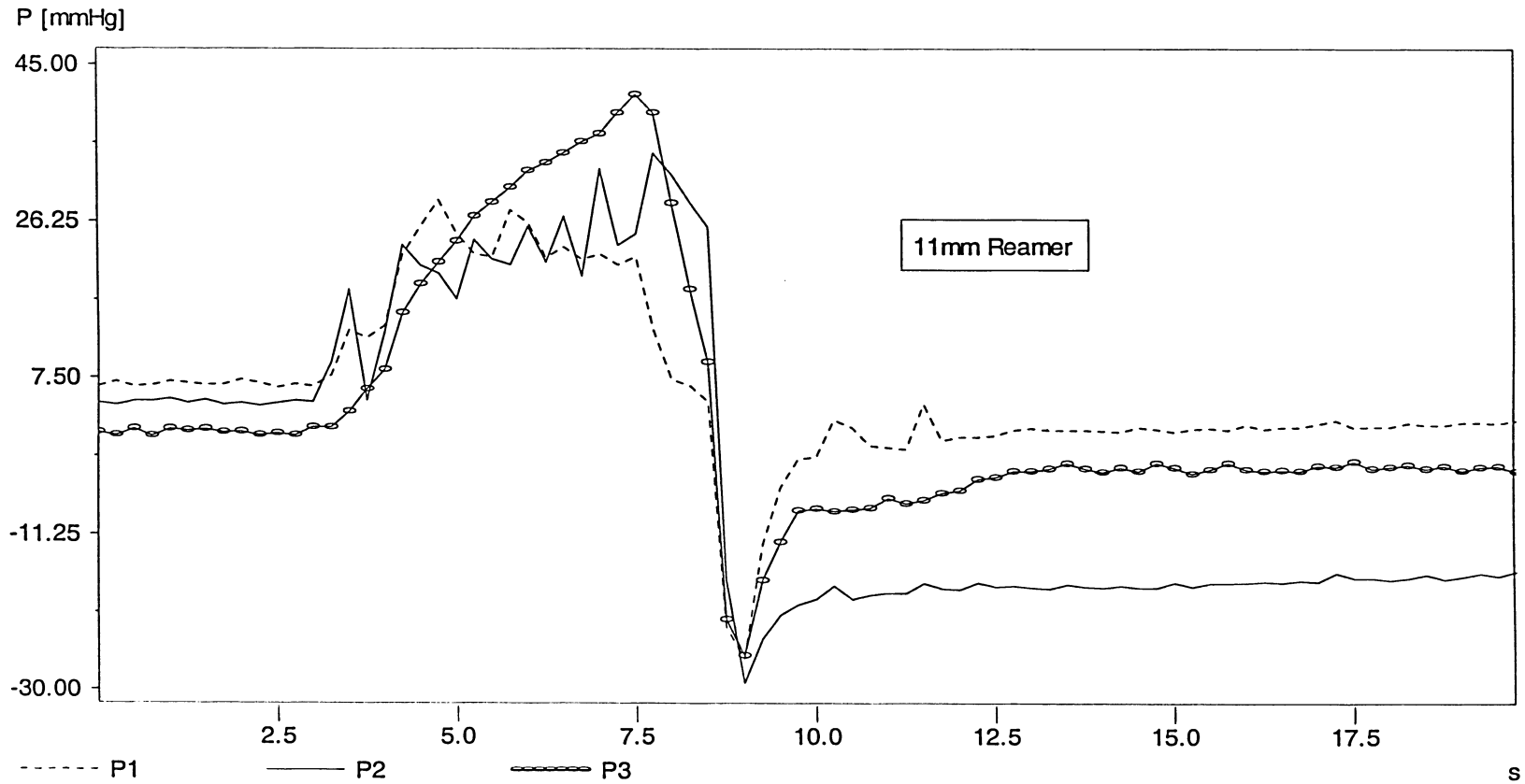

Figure A.34. Pressure variation using 11 mm reamer, 200 RPM, 50 $\frac{mm}{sec}$ and 82.6 cP synthetic marrow viscosity. P_1, P_2 and P_3 are respectively corresponded to pressure transducer #1, 2 and 3.

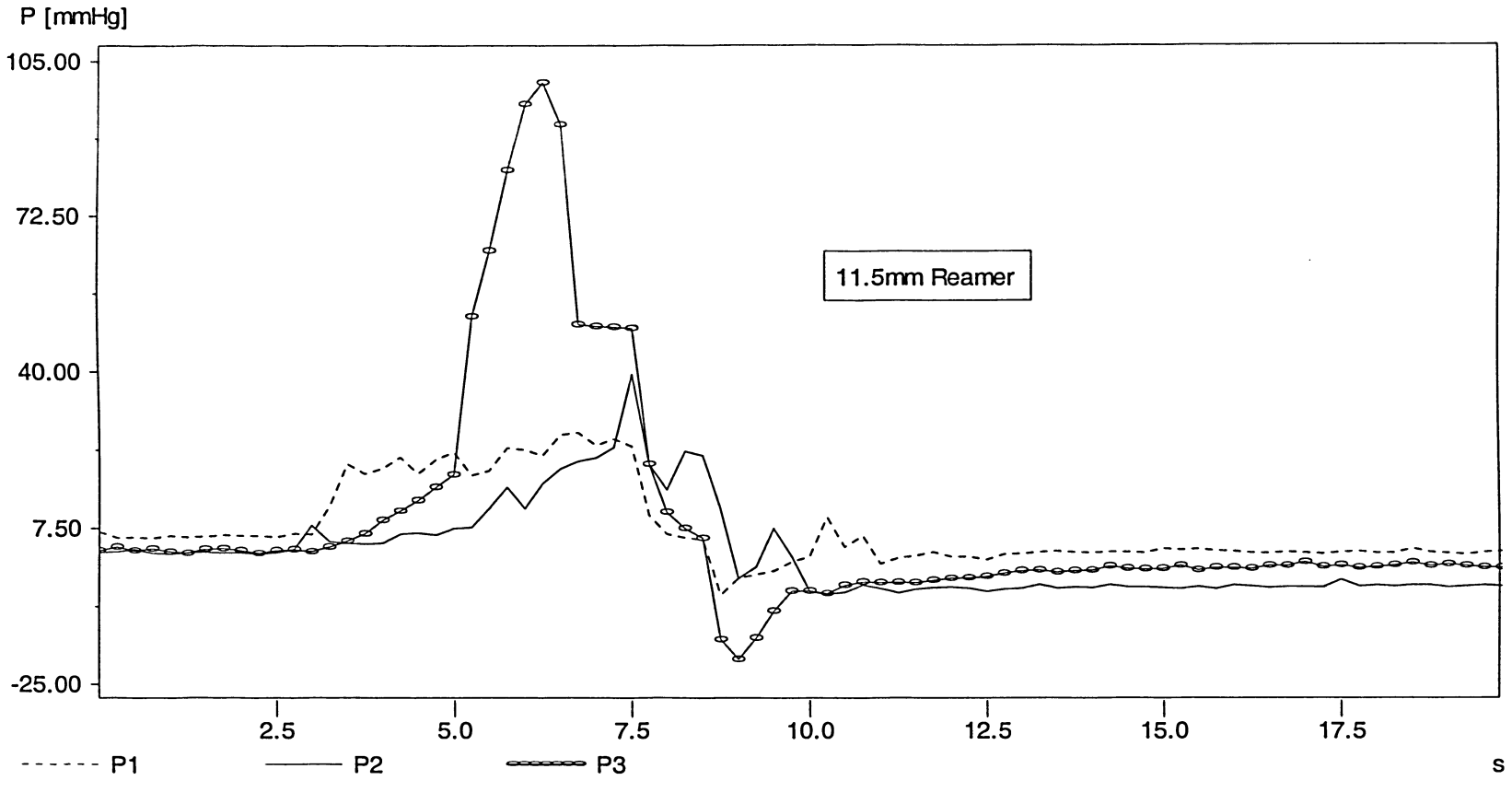

Figure A.35. Pressure variation using 11.5 mm reamer, 200 RPM, 50 $\frac{mm}{sec}$ and 82.6 cP synthetic marrow viscosity. P_1, P_2 and P_3 are respectively corresponded to pressure transducer #1, 2 and 3.

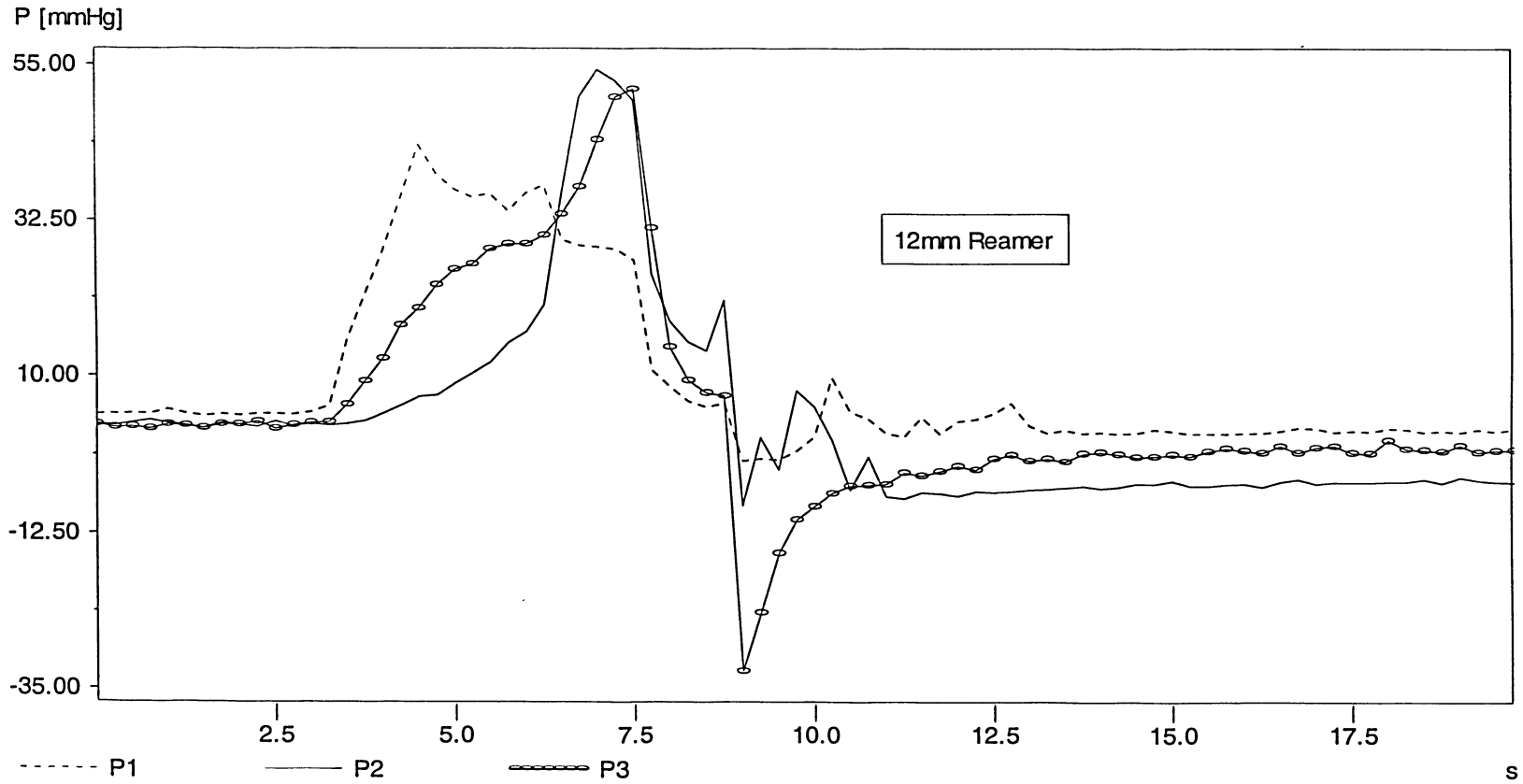

Figure A.36. Pressure variation using 12 mm reamer, 200 RPM, 50 $\frac{mm}{sec}$ and 82.6 cP synthetic marrow viscosity. P_1, P_2 and P_3 are respectively corresponded to pressure transducer #1, 2 and 3.

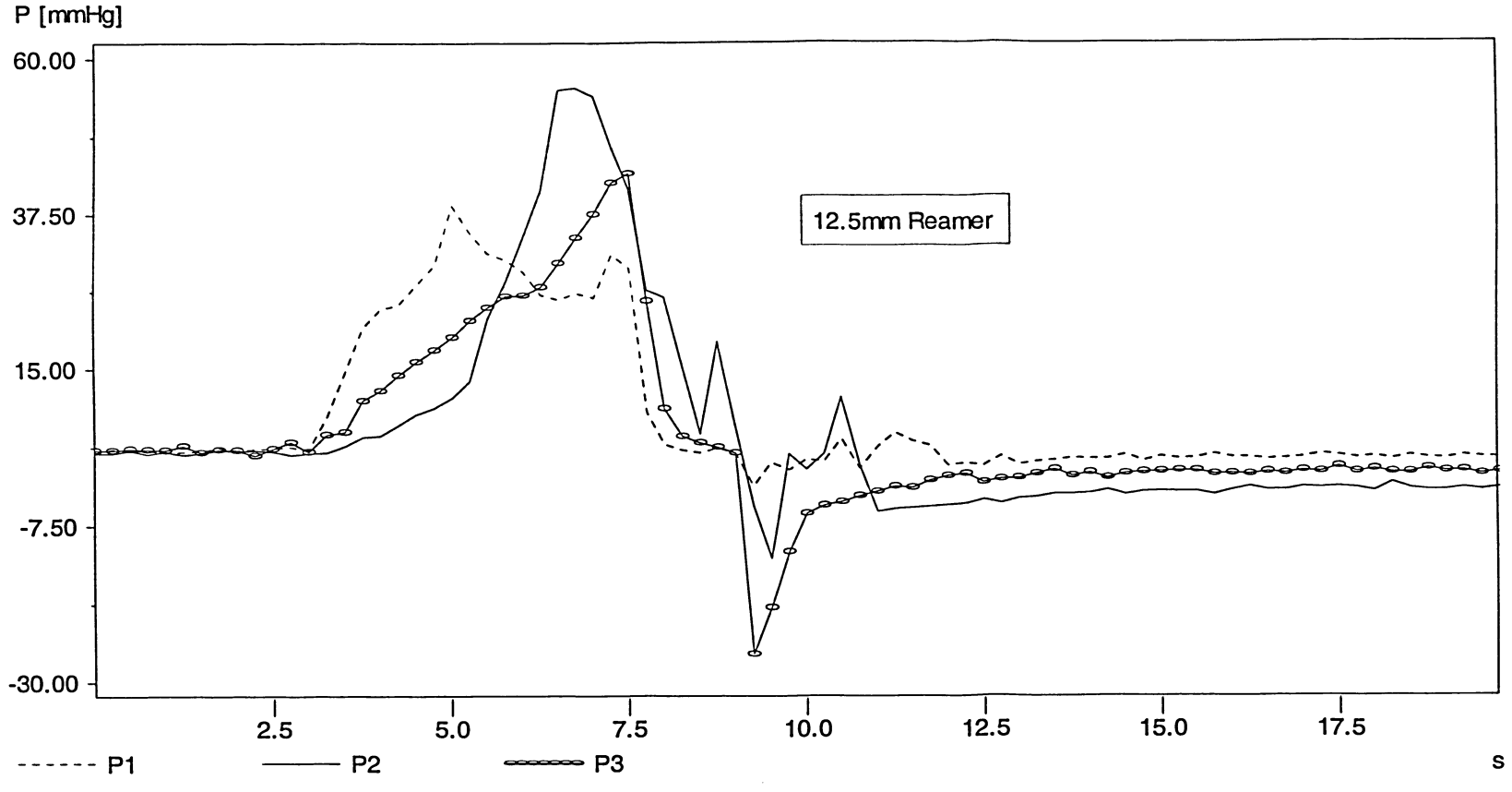

Figure A.37. Pressure variation using 12.5 mm reamer, 200 RPM, 50 $\frac{mm}{sec}$ and 82.6 cP synthetic marrow viscosity. P_1, P_2 and P_3 are respectively corresponded to pressure transducer #1, 2 and 3.

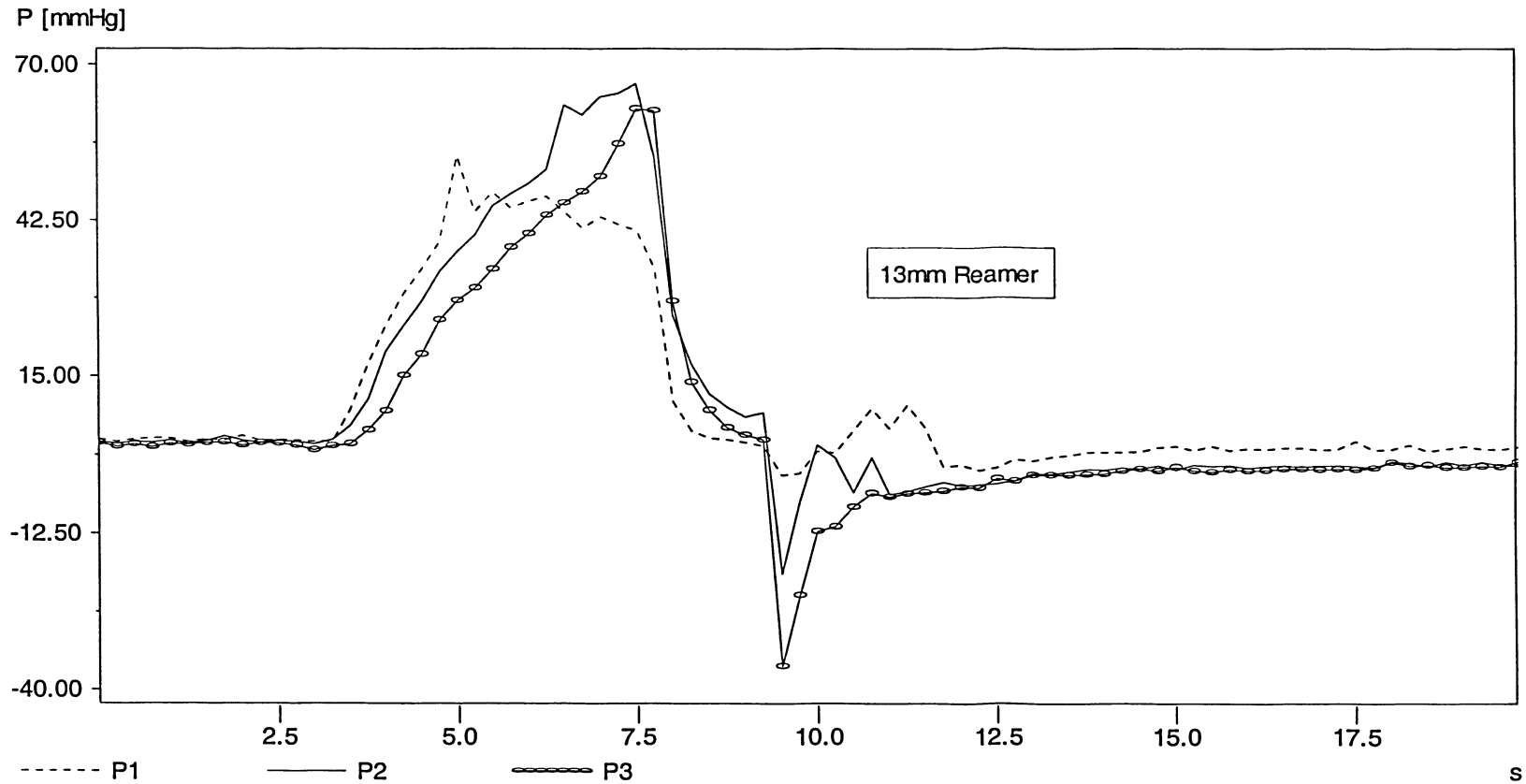

Figure A.38. Pressure variation using 13 mm reamer, 200 RPM, 50 $\frac{mm}{sec}$ and 82.6 cP synthetic marrow viscosity. P_1, P_2 and P_3 are respectively corresponded to pressure transducer #1, 2 and 3.

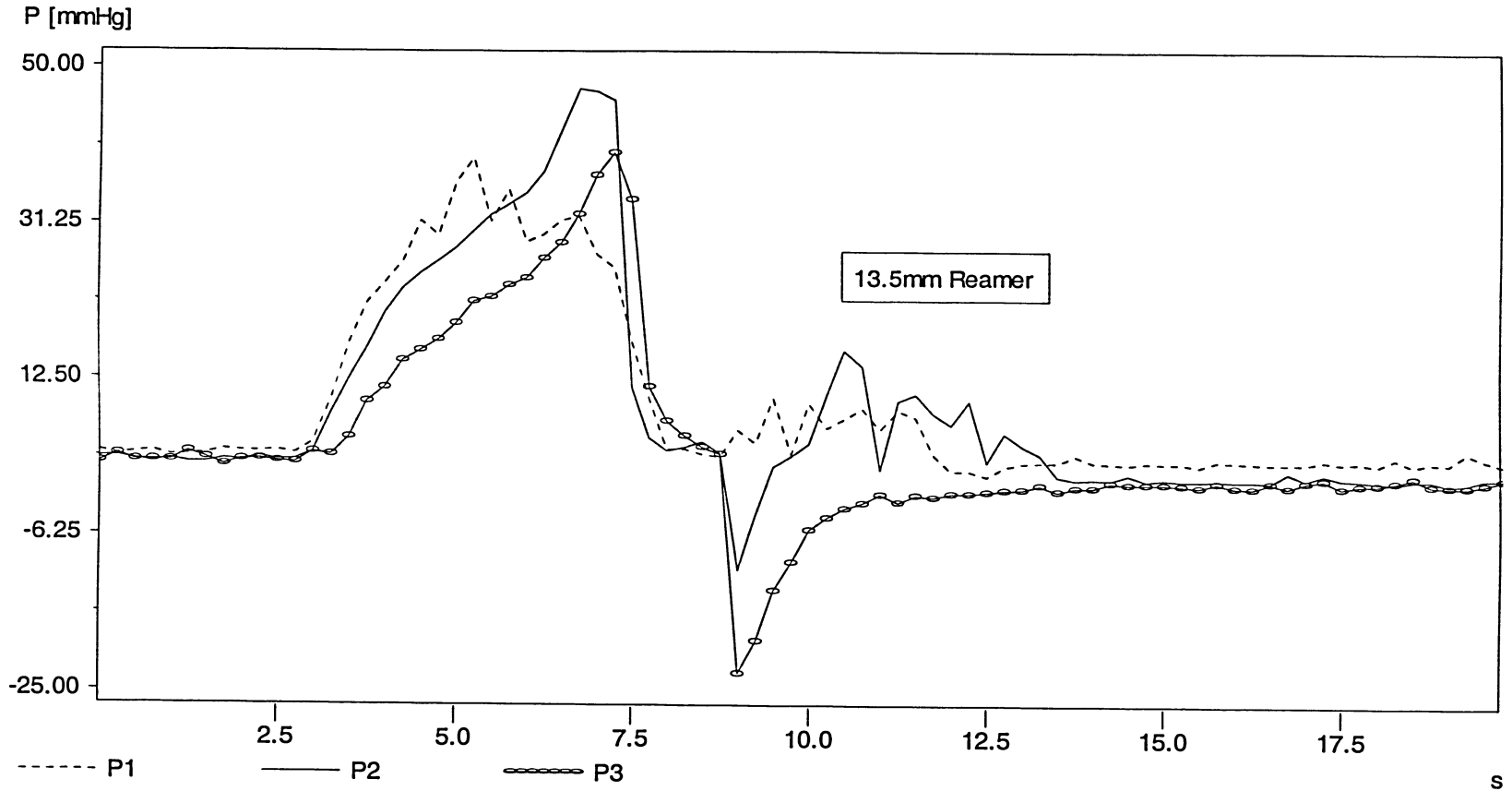

Figure A.39. Pressure variation using 13.5 mm reamer, 200 RPM, 50 $\frac{mm}{sec}$ and 82.6 cP synthetic marrow viscosity. P_1, P_2 and P_3 are respectively corresponded to pressure transducer #1, 2 and 3.

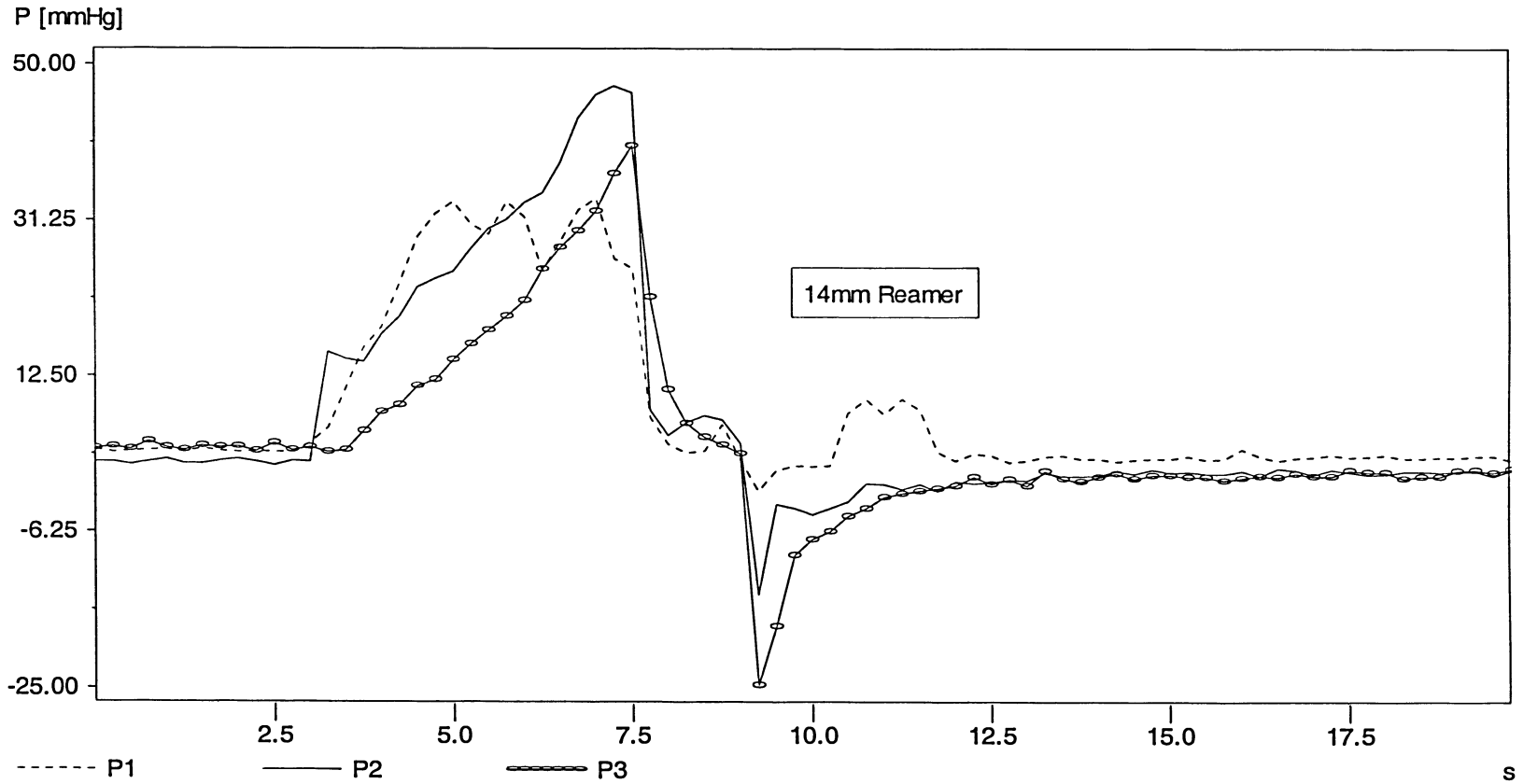

Figure A.40. Pressure variation using 14 mm reamer, 200 RPM, 50 $\frac{mm}{sec}$ and 82.6 cP synthetic marrow viscosity. P_1, P_2 and P_3 are respectively corresponded to pressure transducer #1, 2 and 3.

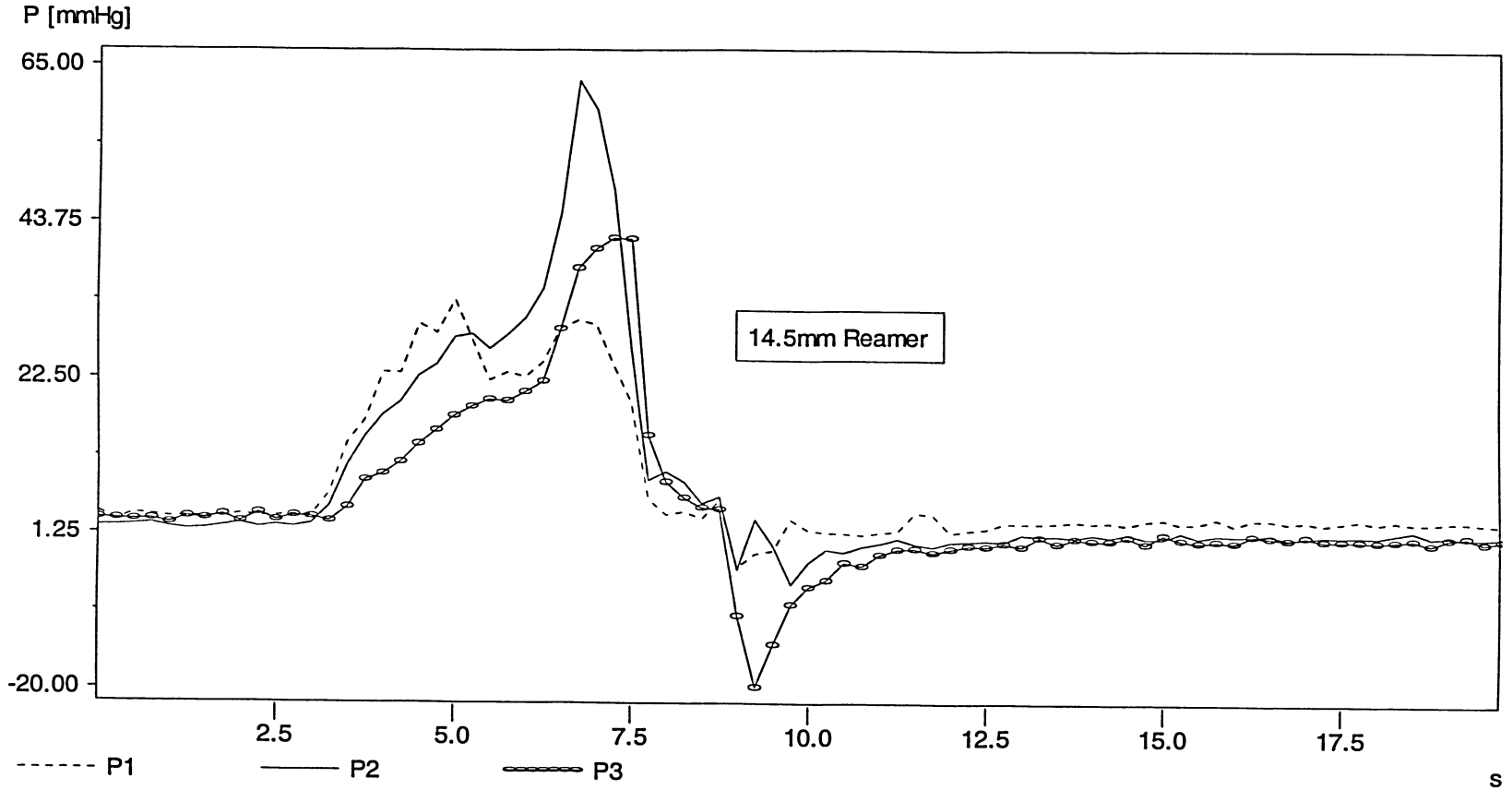

Figure A.41. Pressure variation using 14.5 mm reamer, 200 RPM, 50 $\frac{mm}{sec}$ and 82.6 cP synthetic marrow viscosity. P_1, P_2 and P_3 are respectively corresponded to pressure transducer #1, 2 and 3.

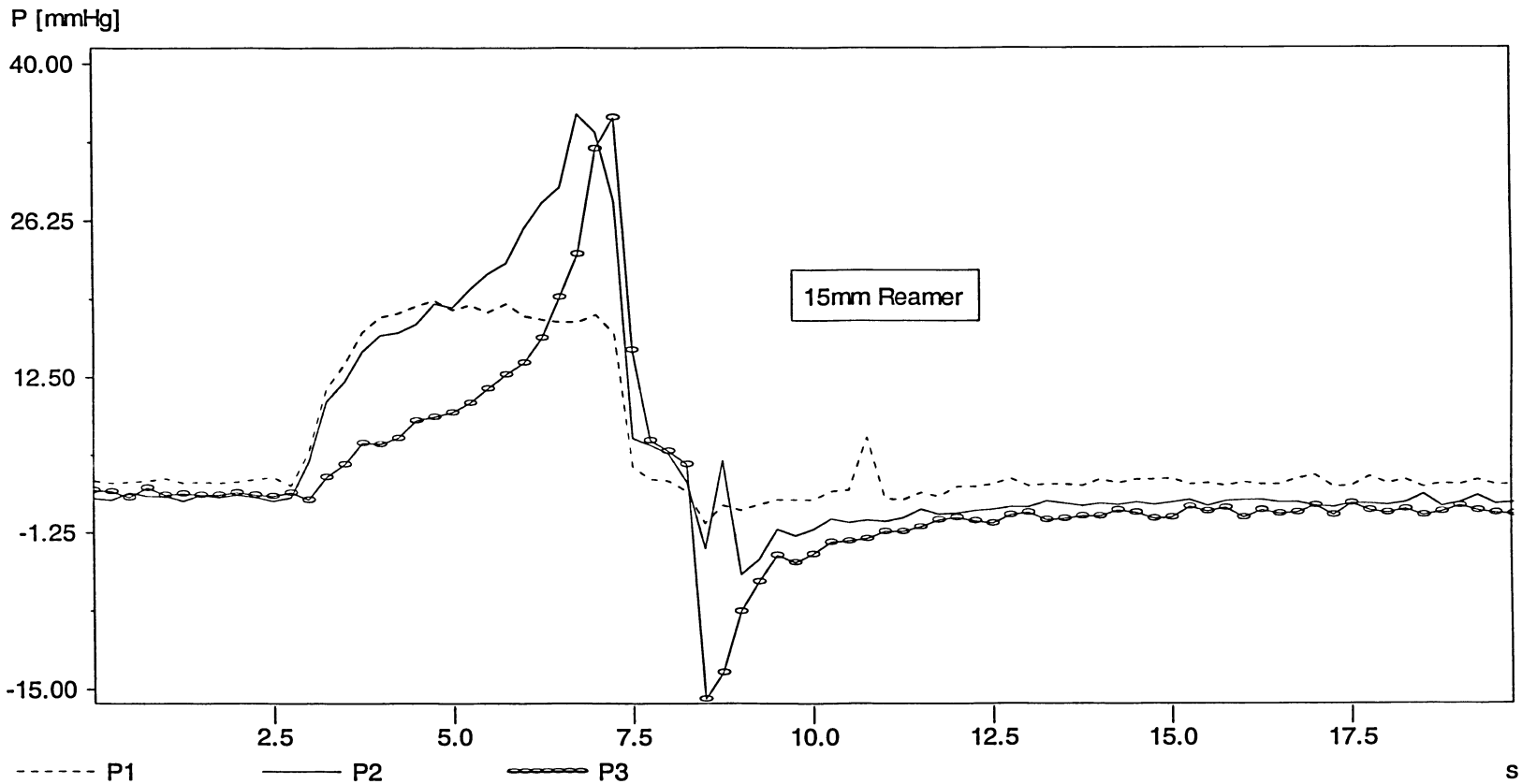

Figure A.42. Pressure variation using 15 mm reamer, 200 RPM, 50 $\frac{mm}{sec}$ and 82.6 cP synthetic marrow viscosity. P_1, P_2 and P_3 are respectively corresponded to pressure transducer #1, 2 and 3.

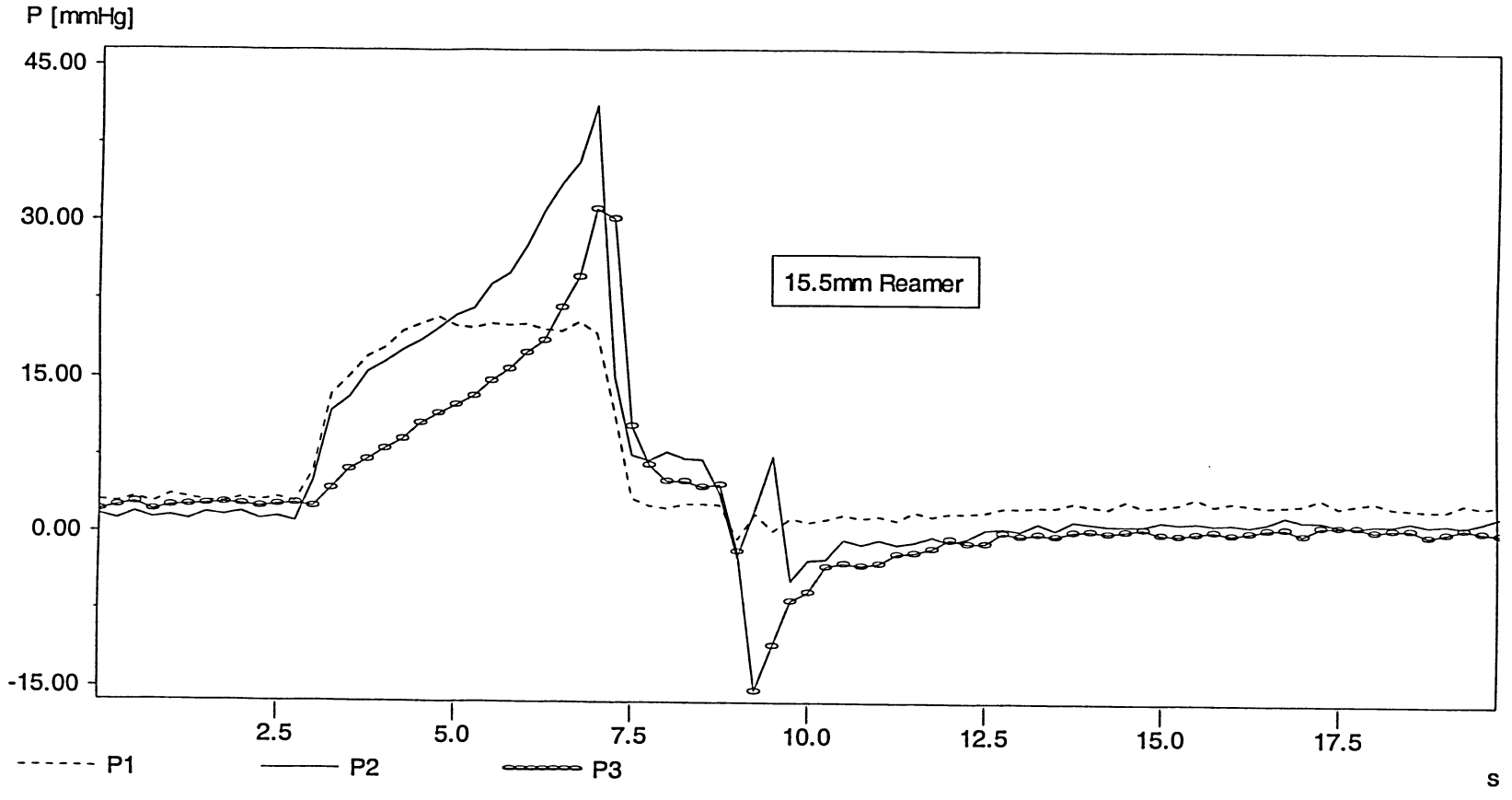

Figure A.43. Pressure variation using 15.5 mm reamer, 200 RPM, 50 $\frac{mm}{sec}$ and 82.6 cP synthetic marrow viscosity. P_1, P_2 and P_3 are respectively corresponded to pressure transducer #1, 2 and 3.

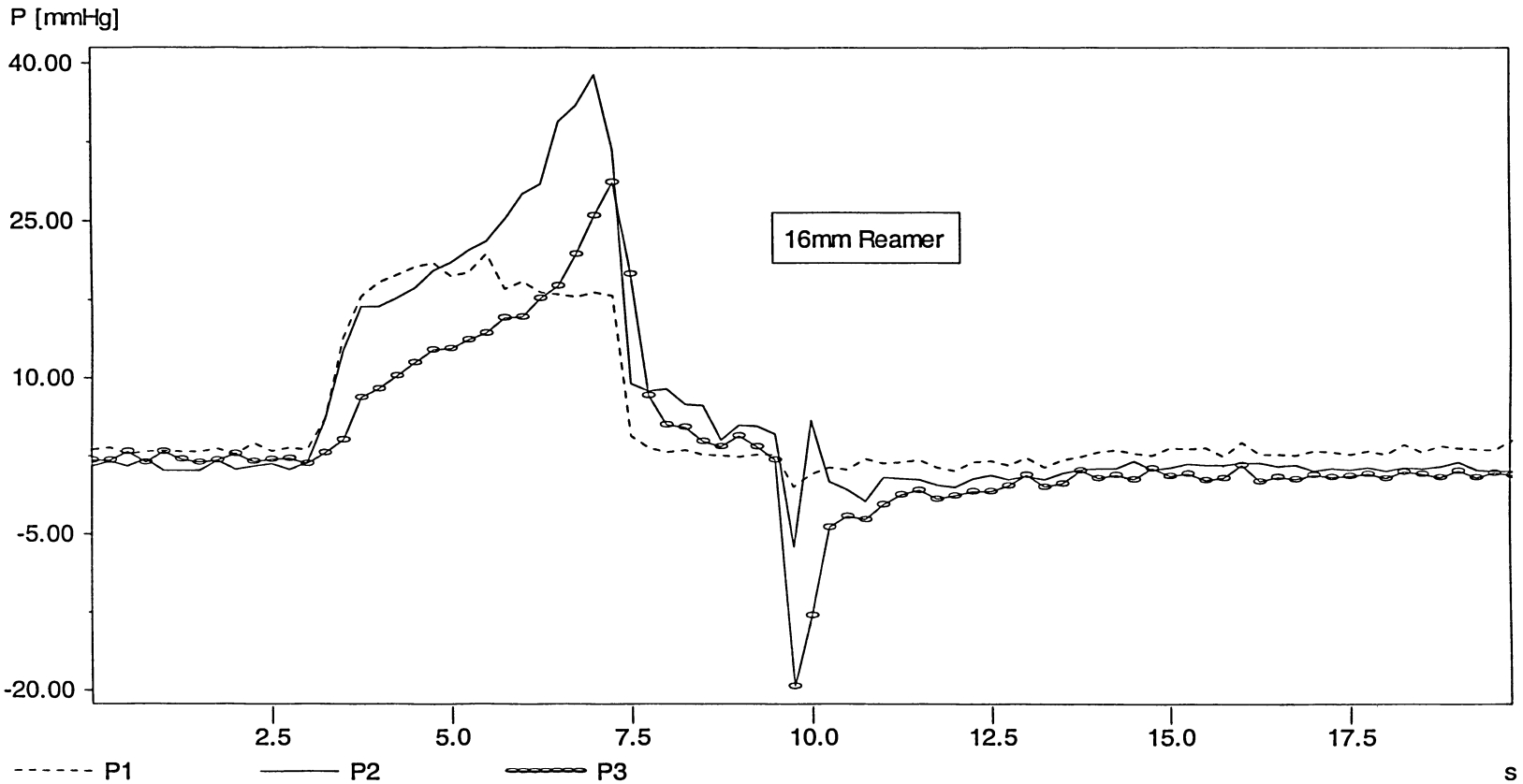

Figure A.44. Pressure variation using 16 mm reamer, 200 RPM, 50 $\frac{mm}{sec}$ and 82.6 cP synthetic marrow viscosity. P_1, P_2 and P_3 are respectively corresponded to pressure transducer #1, 2 and 3.

Appendix B

Pressure Profiles
Parametric Study #2

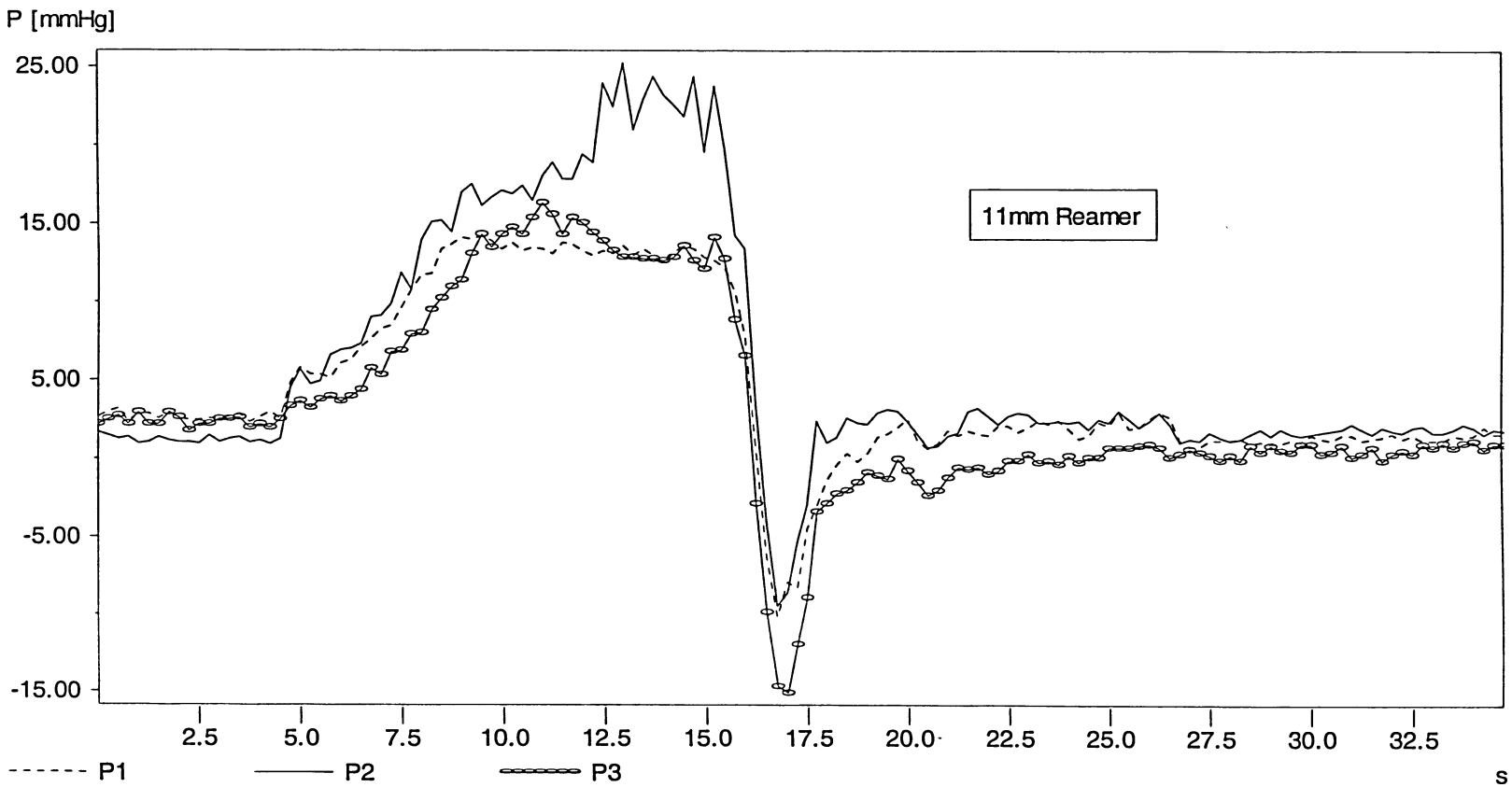

Figure B.1. Pressure variation using 11mm unclogged reamer, 200 RPM, 20 $\frac{mm}{sec}$ and low viscosity synthetic marrow (82.6 cP). P1, P2 and P3 are respectively corresponded to pressure transducer #1, 2 and 3.

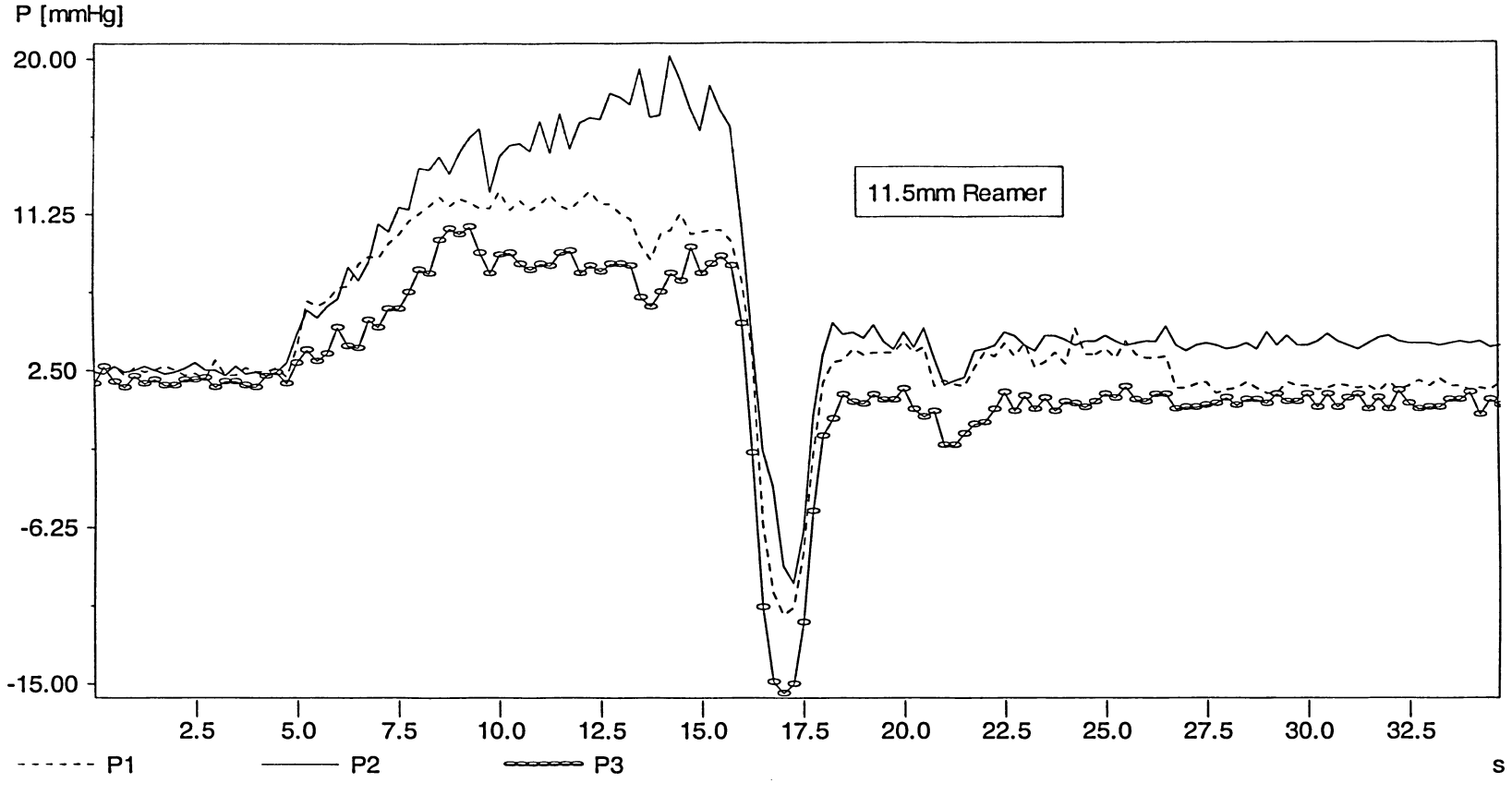

Figure B.2. Pressure variation using 11.5 mm unclogged reamer, 200 RPM, 20 $\frac{mm}{sec}$ and low viscosity synthetic marrow (82.6 cP).
P1, P2 and P3 are respectively corresponded to pressure transducer #1, 2 and 3.

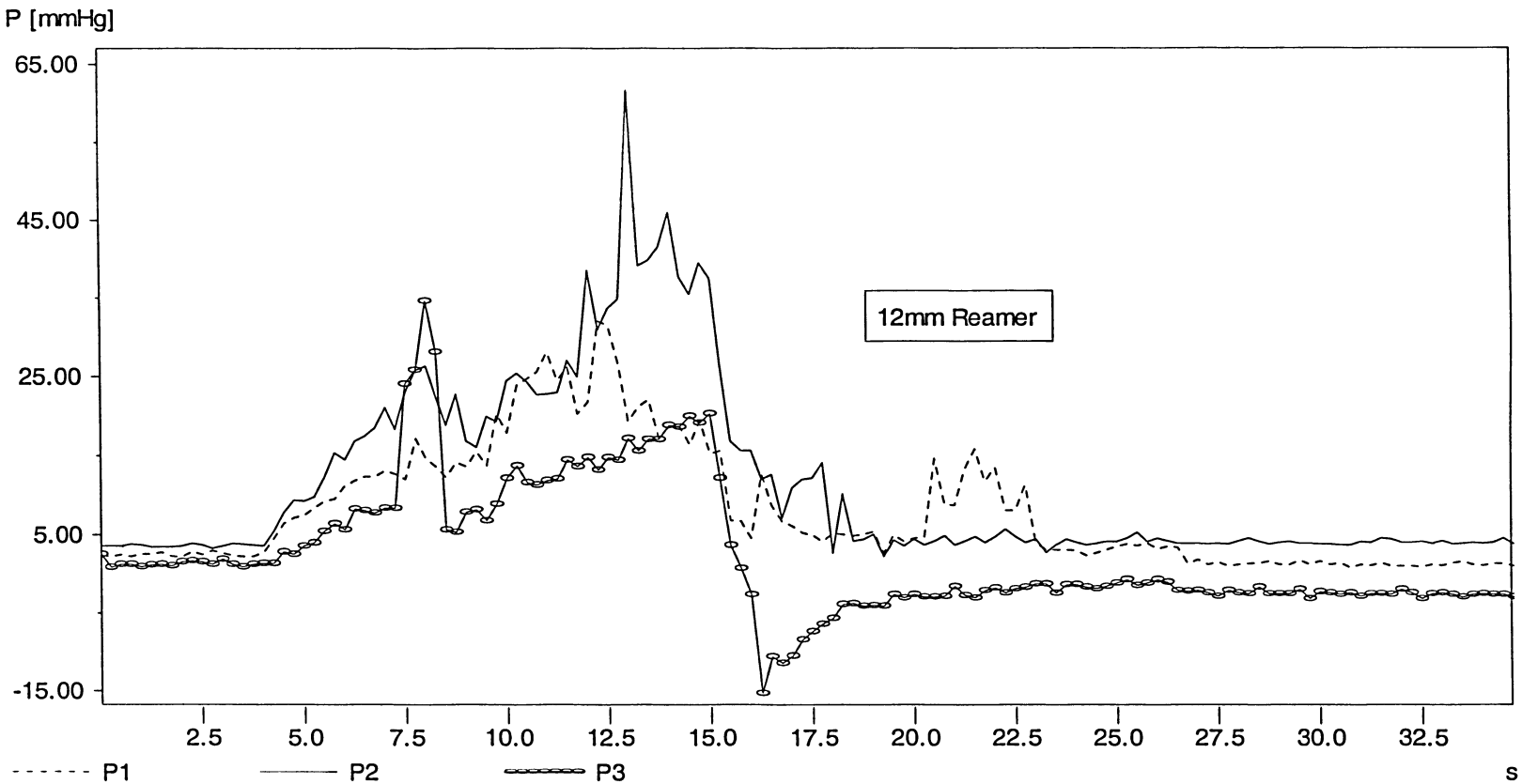

Figure B.3. Pressure variation using 12 mm unclogged reamer, 200 RPM, 20 $\frac{mm}{sec}$ and low viscosity synthetic marrow (82.6 cP). P1, P2 and P3 are respectively corresponded to pressure transducer #1, 2 and 3.

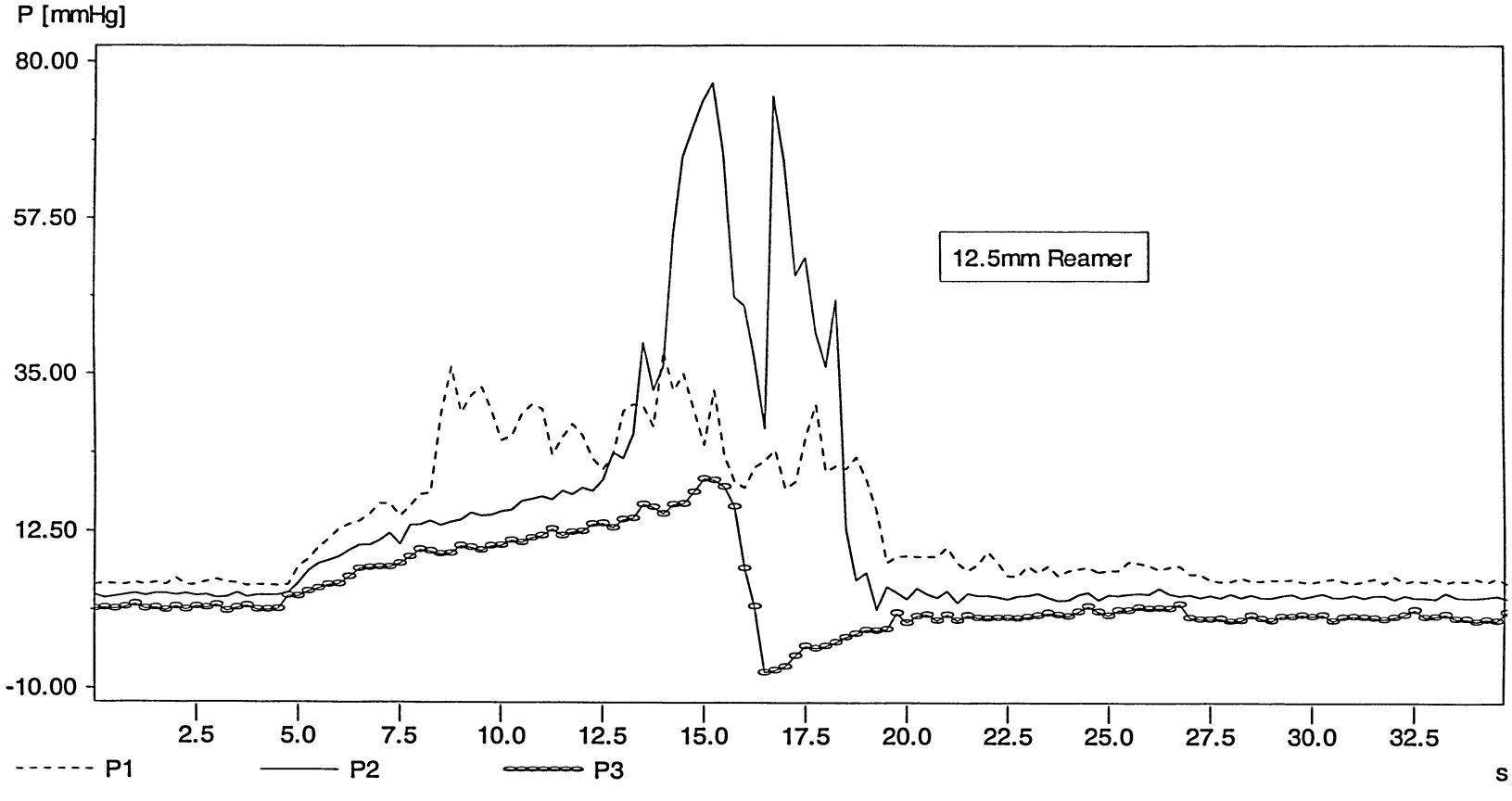

Figure B.4. Pressure variation using 12.5 mm unclogged reamer, 200 RPM, 20 $\frac{mm}{sec}$ and low viscosity synthetic marrow (82.6 cP). P1, P2 and P3 are respectively corresponded to pressure transducer #1, 2 and 3.

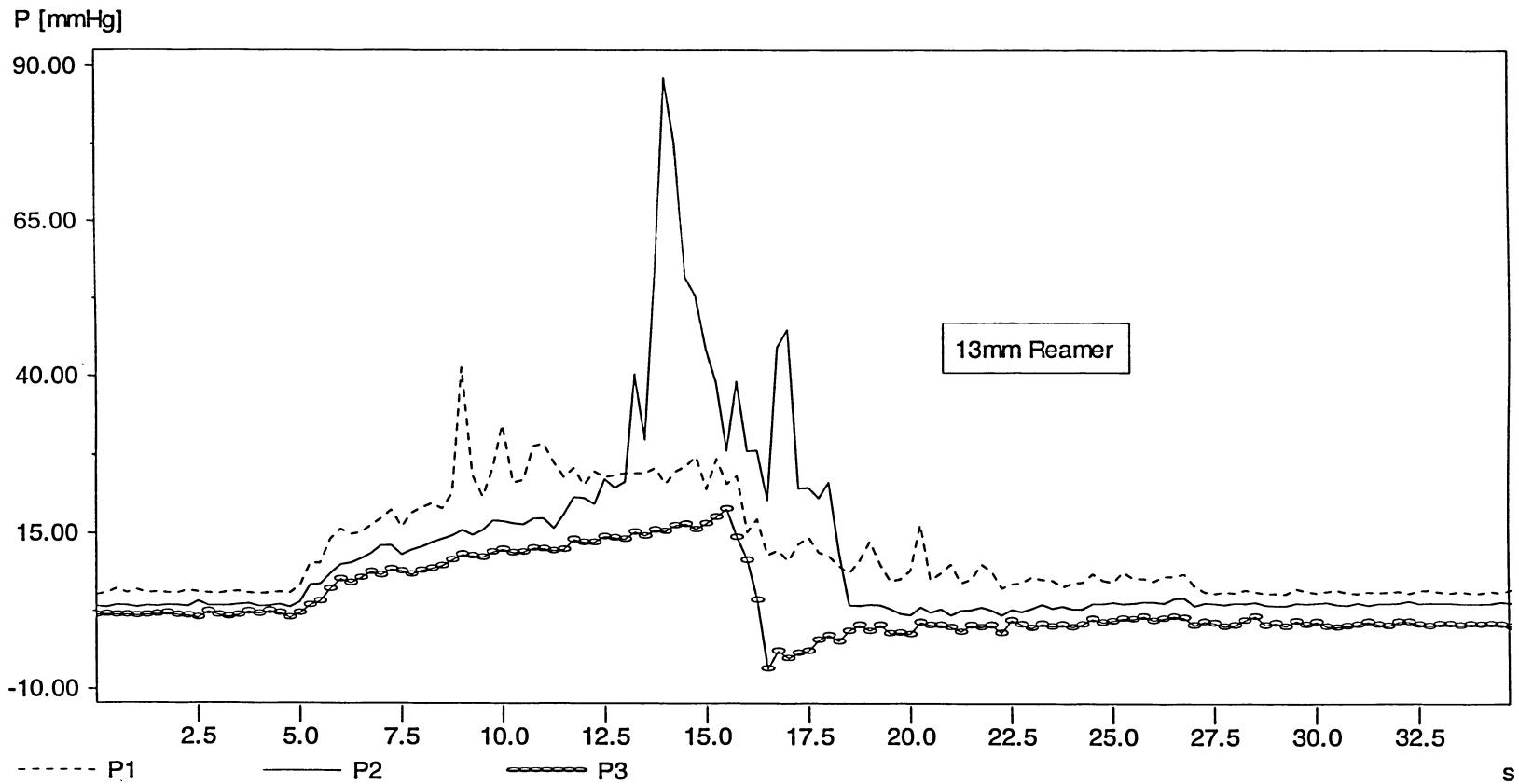

Figure B.5. Pressure variation using 13 mm unclogged reamer, 200 RPM, 20 $\frac{mm}{sec}$ and low viscosity synthetic marrow (82.6 cP). P1, P2 and P3 are respectively corresponded to pressure transducer #1, 2 and 3.

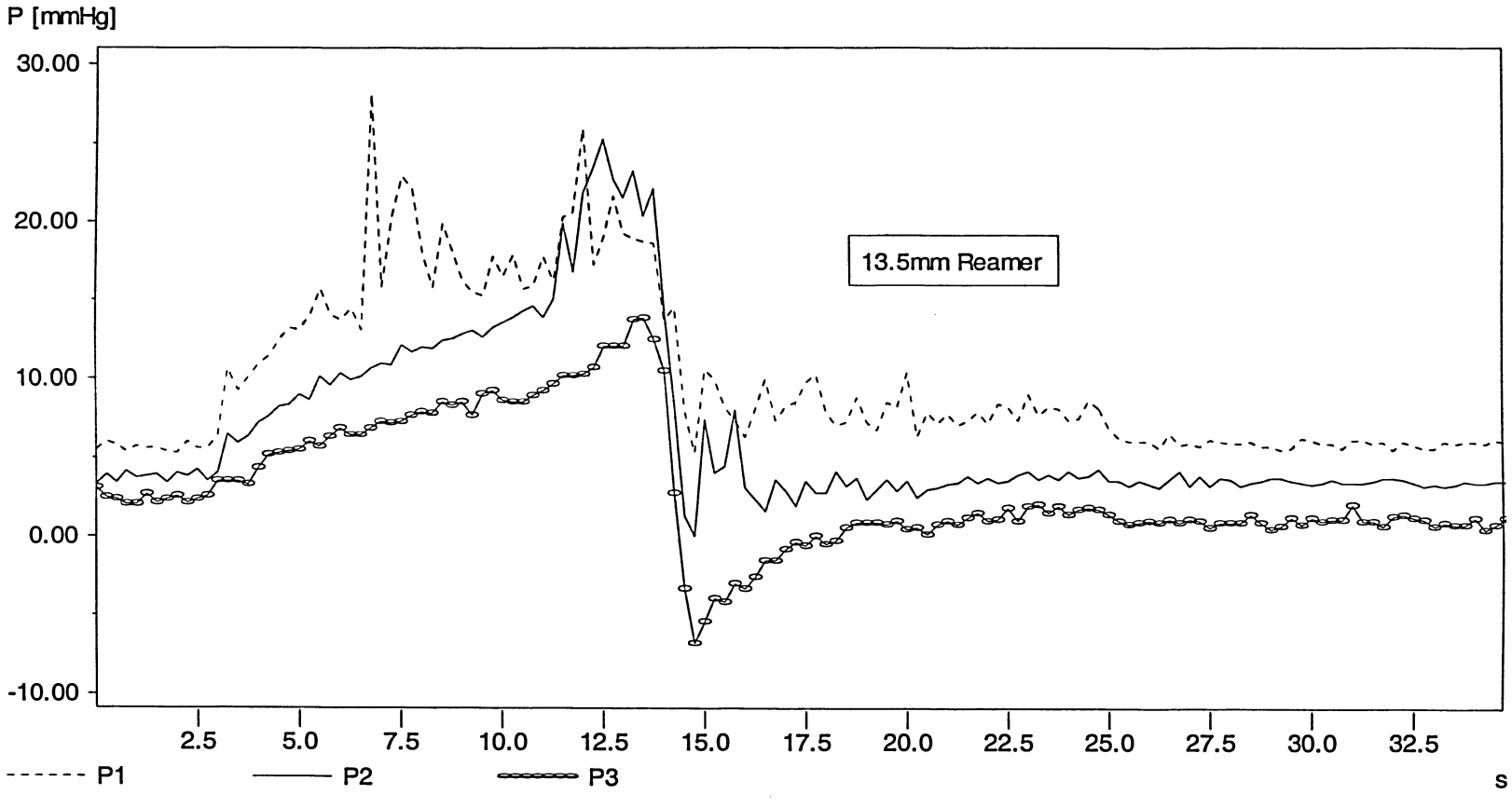

Figure B.6. Pressure variation using 13.5 mm unclogged reamer, 200 RPM, 20 $\frac{mm}{sec}$ and low viscosity synthetic marrow (82.6 cP). P1, P2 and P3 are respectively corresponded to pressure transducer #1, 2 and 3.

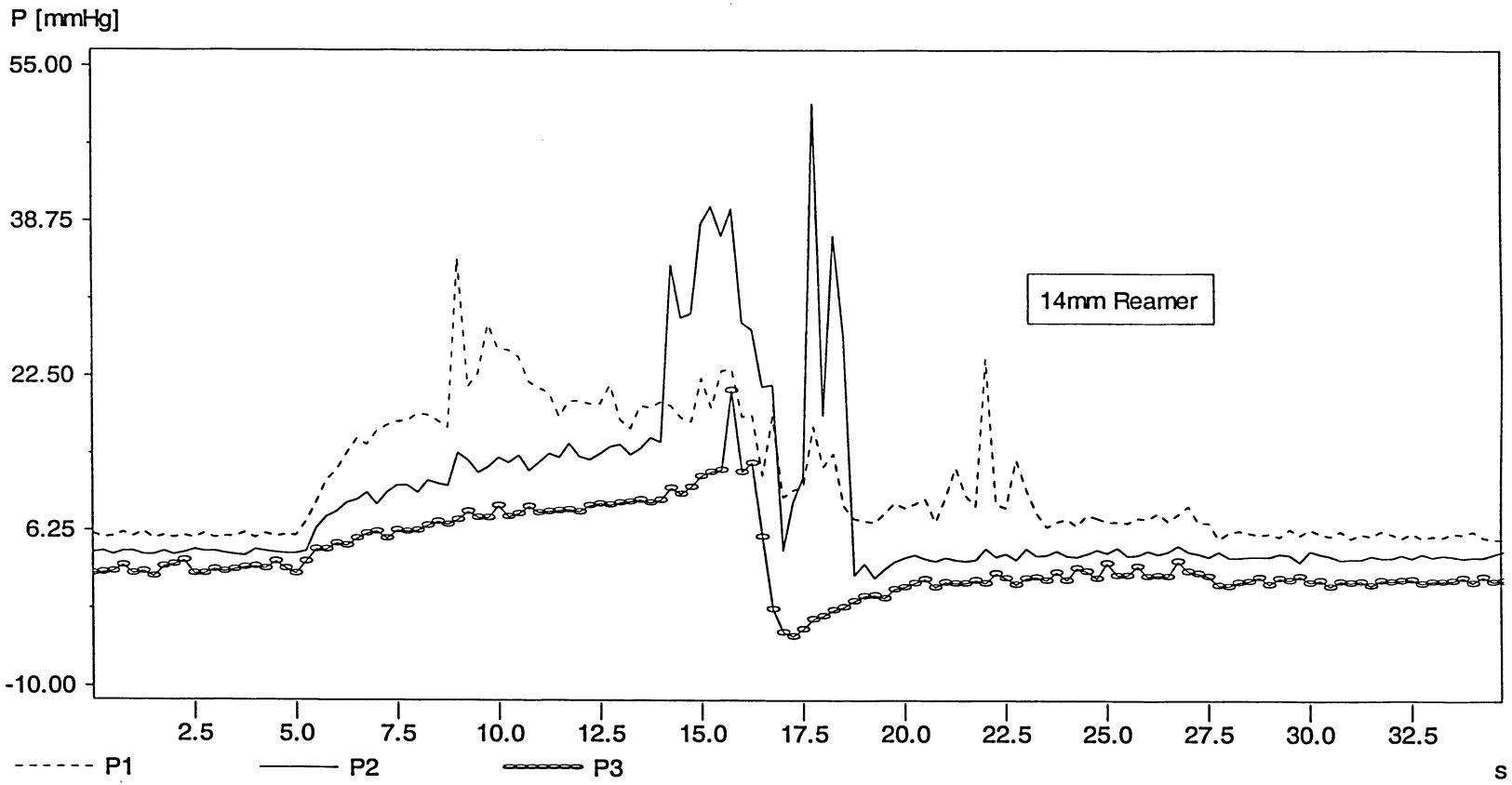

Figure B.7. Pressure variation using 14 mm unclogged reamer, 200 RPM, 20 $\frac{mm}{sec}$ and low viscosity synthetic marrow (82.6 cP). P1, P2 and P3 are respectively corresponded to pressure transducer #1, 2 and 3.

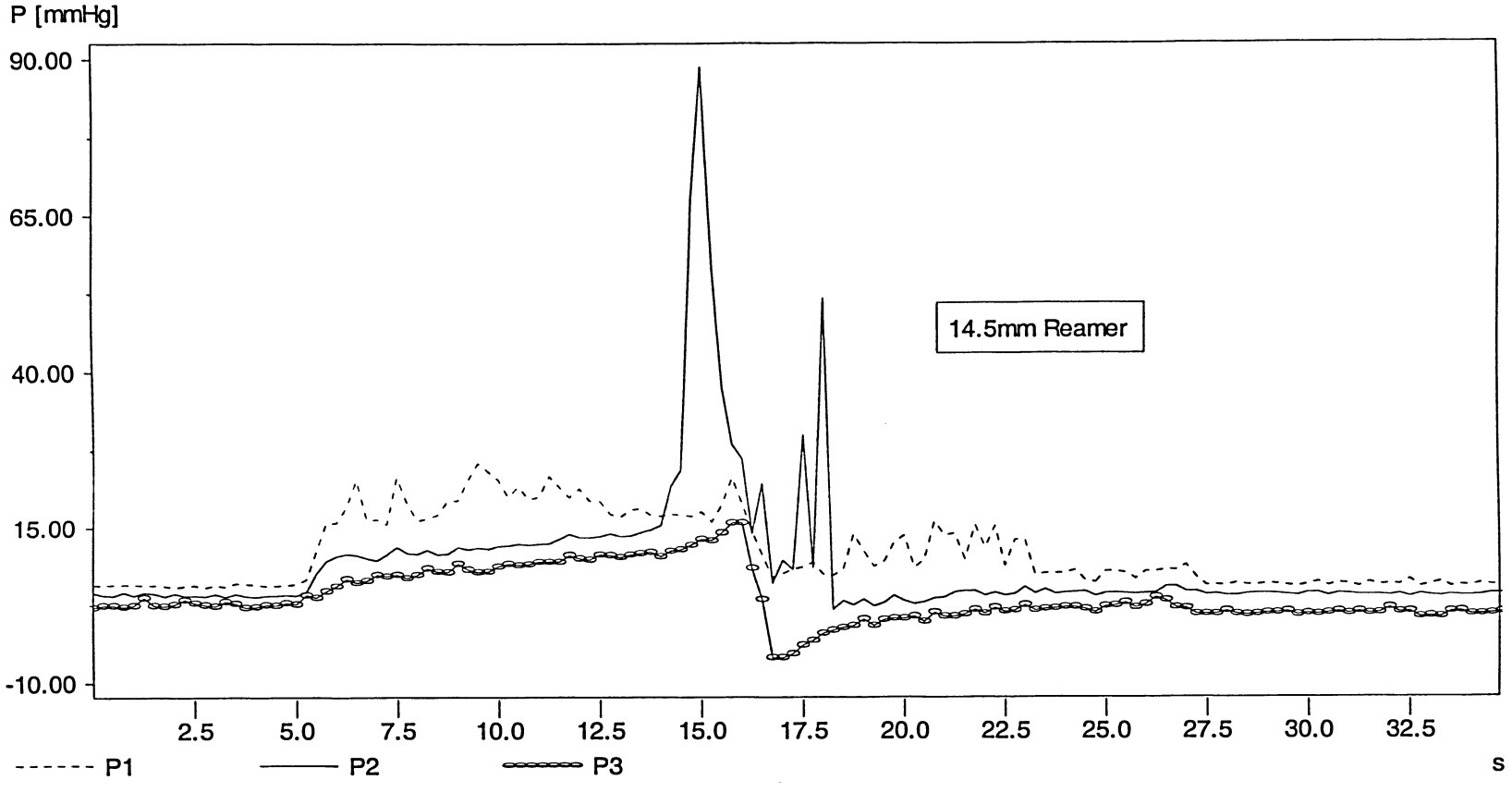

Figure B.8. Pressure variation using 14.5 mm unclogged reamer, 200 RPM, 20 $\frac{mm}{sec}$ and low viscosity synthetic marrow (82.6 cP).
P1, P2 and P3 are respectively corresponded to pressure transducer #1, 2 and 3.

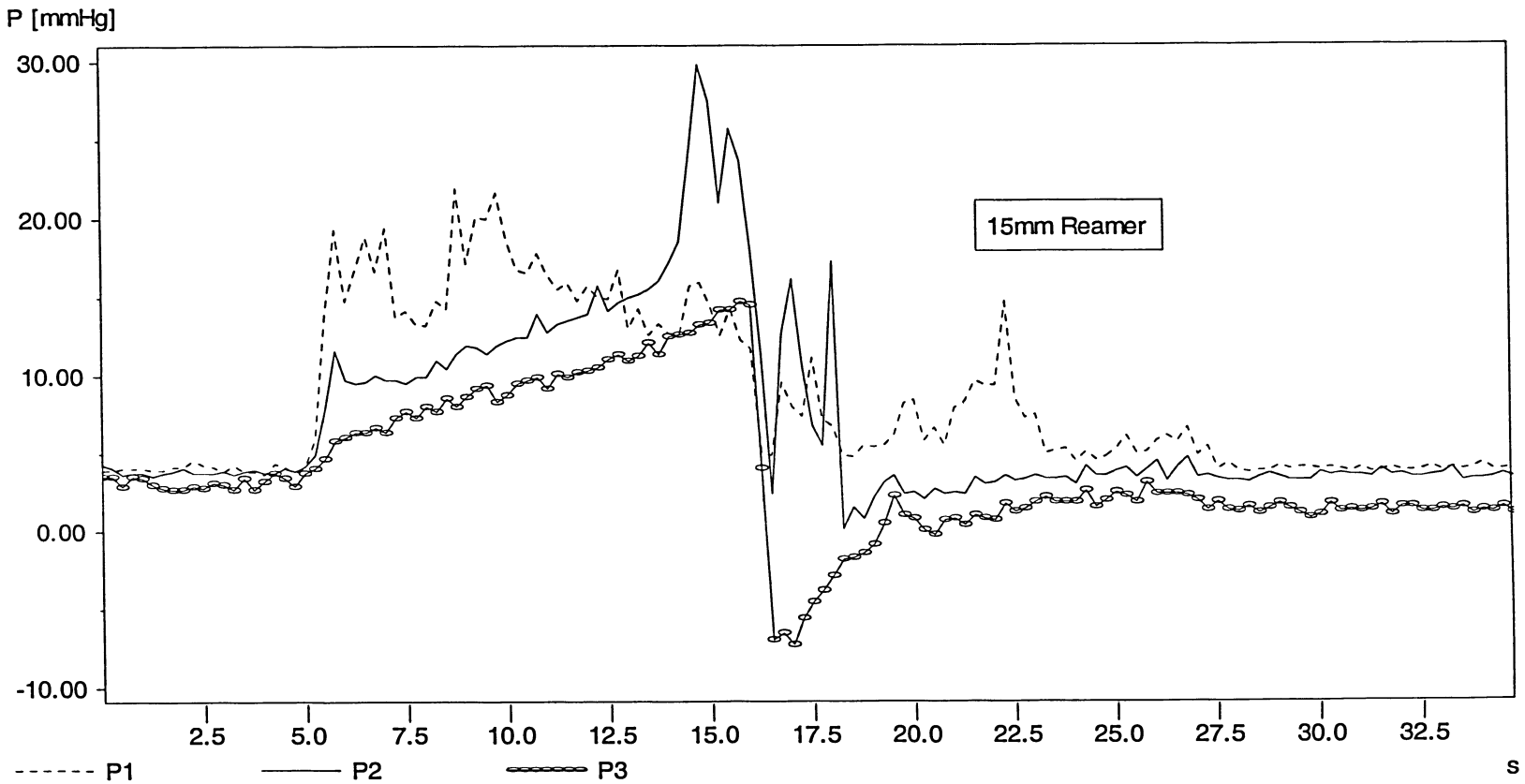

Figure B.9. Pressure variation using 15 mm unclogged reamer, 200 RPM, 20 $\frac{mm}{sec}$ and low viscosity synthetic marrow (82.6 cP). P1, P2 and P3 are respectively corresponded to pressure transducer #1, 2 and 3.

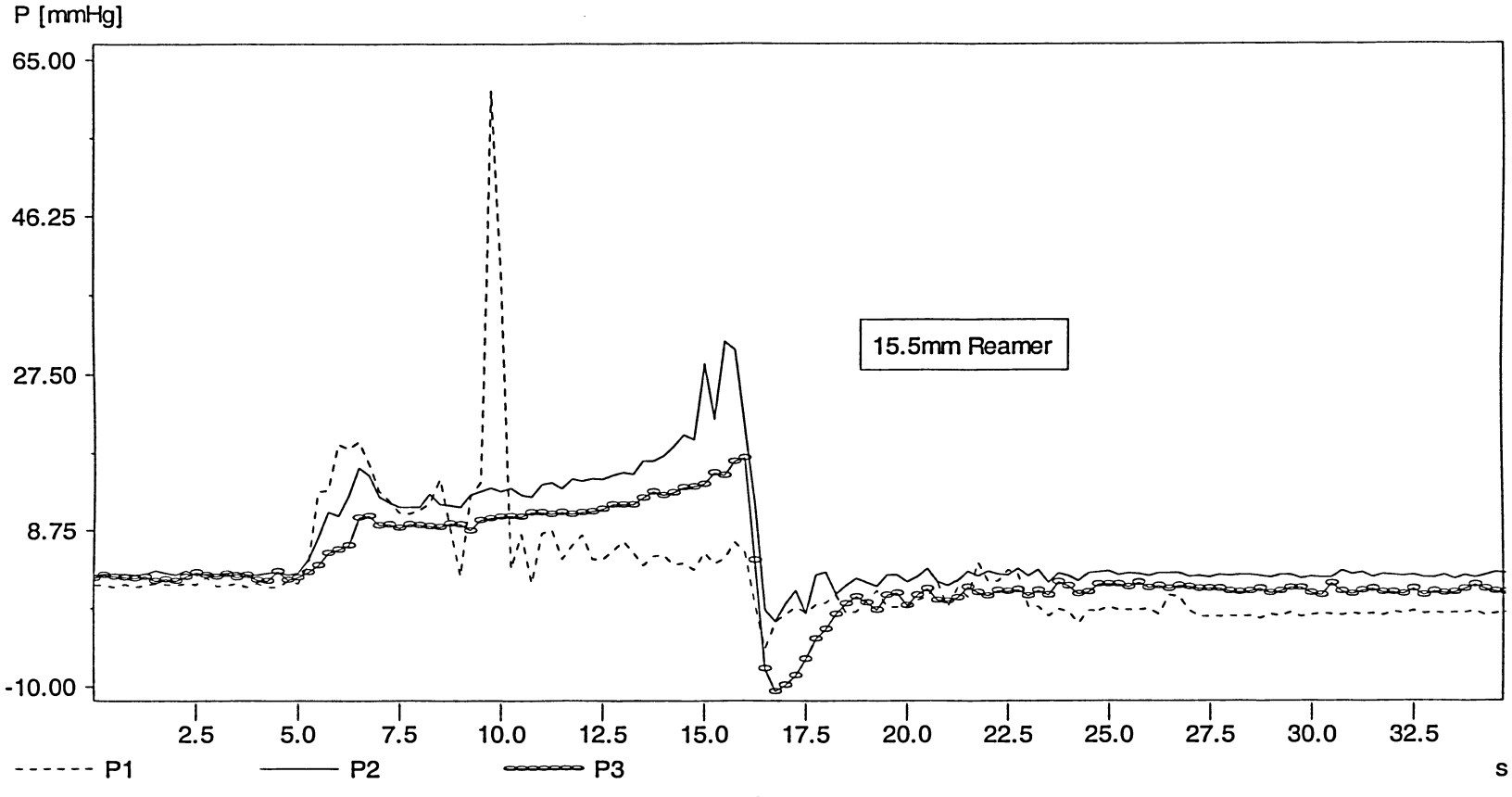

Figure B.10. Pressure variation using 15.5 mm unclogged reamer, 200 RPM, 20 $\frac{mm}{sec}$ and low viscosity synthetic marrow (82.6 cP). P1, P2 and P3 are respectively corresponded to pressure transducer #1, 2 and 3.

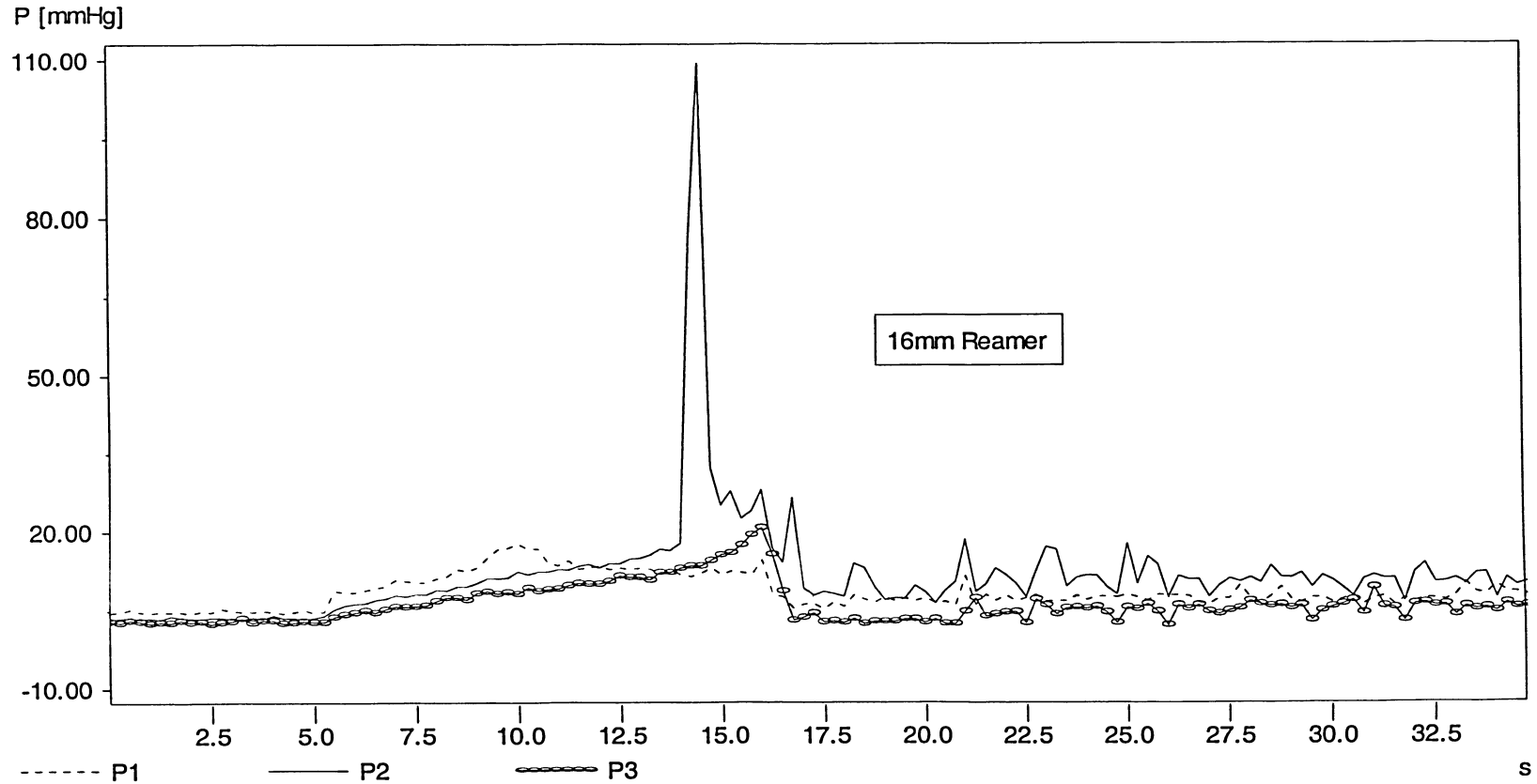

Figure B.11. Pressure variation using 16 mm unclogged reamer, 200 RPM, 20 $\frac{mm}{sec}$ and low viscosity synthetic marrow (82.6 cP). P1, P2 and P3 are respectively corresponded to pressure transducer #1, 2 and 3.

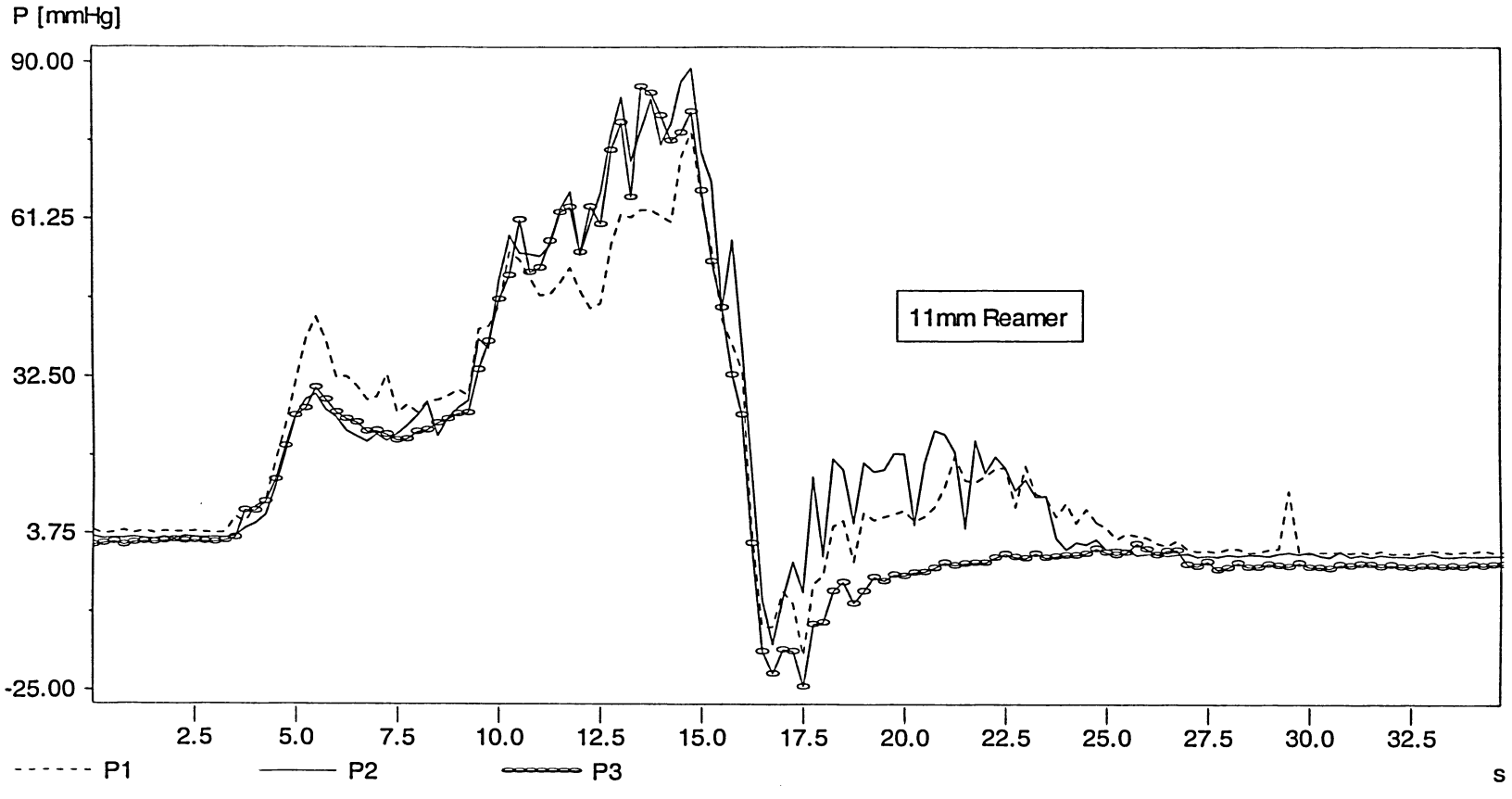

Figure B.12. Pressure variation using 11 mm clogged reamer, 200 RPM, 20 $\frac{mm}{sec}$ and low viscosity synthetic marrow (82.6 cP). P1, P2 and P3 are respectively corresponded to pressure transducer #1, 2 and 3. The reamer was clogged by fully covering the reamer flutes with silicon sealant.

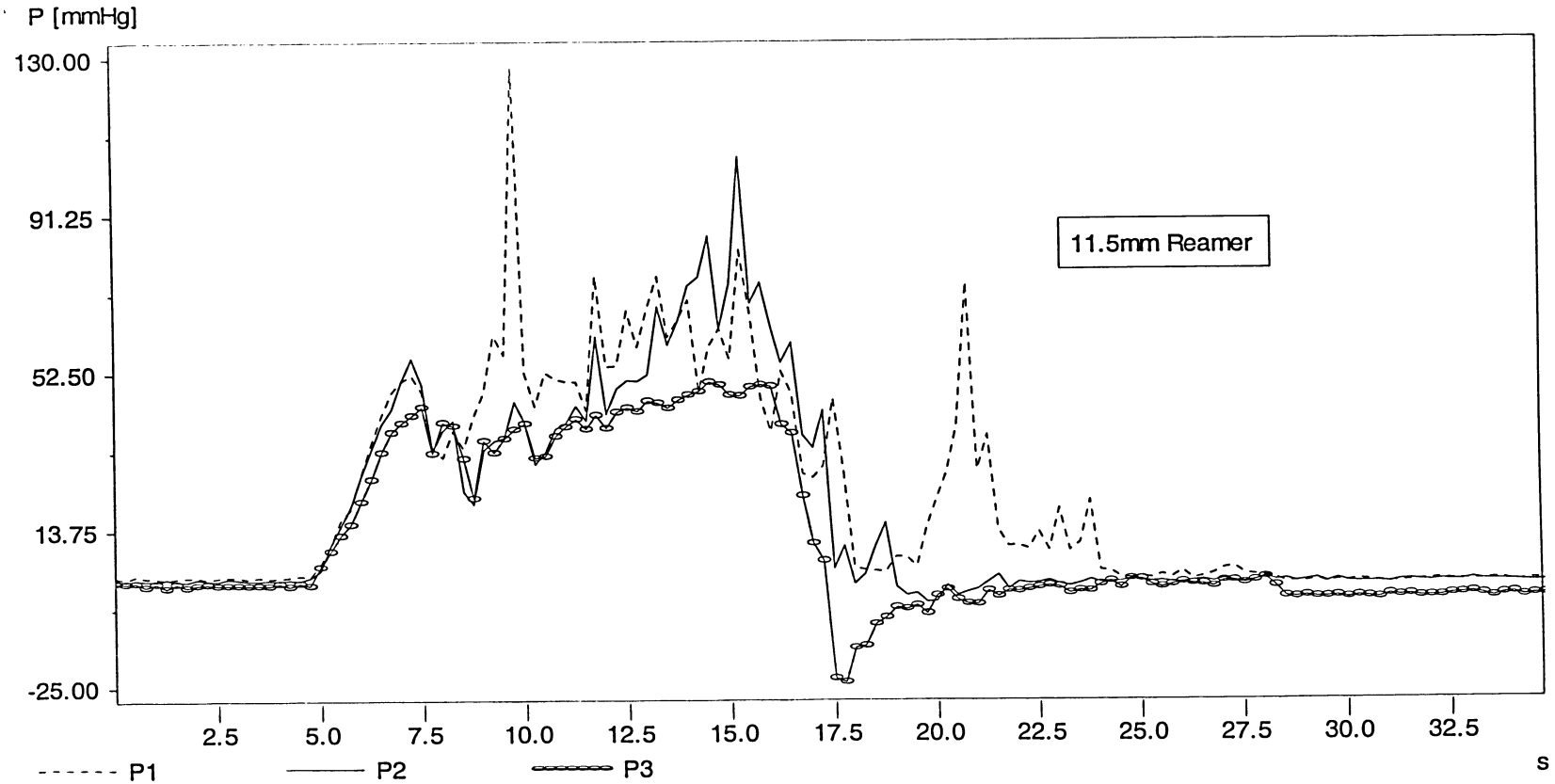

Figure B.13. Pressure variation using 11.5 mm clogged reamer, 200 RPM, 20 $\frac{mm}{sec}$ and low viscosity synthetic marrow (82.6 cP). P1, P2 and P3 are respectively corresponded to pressure transducer #1, 2 and 3. The reamer was clogged by fully covering the reamer flutes with silicon sealant.

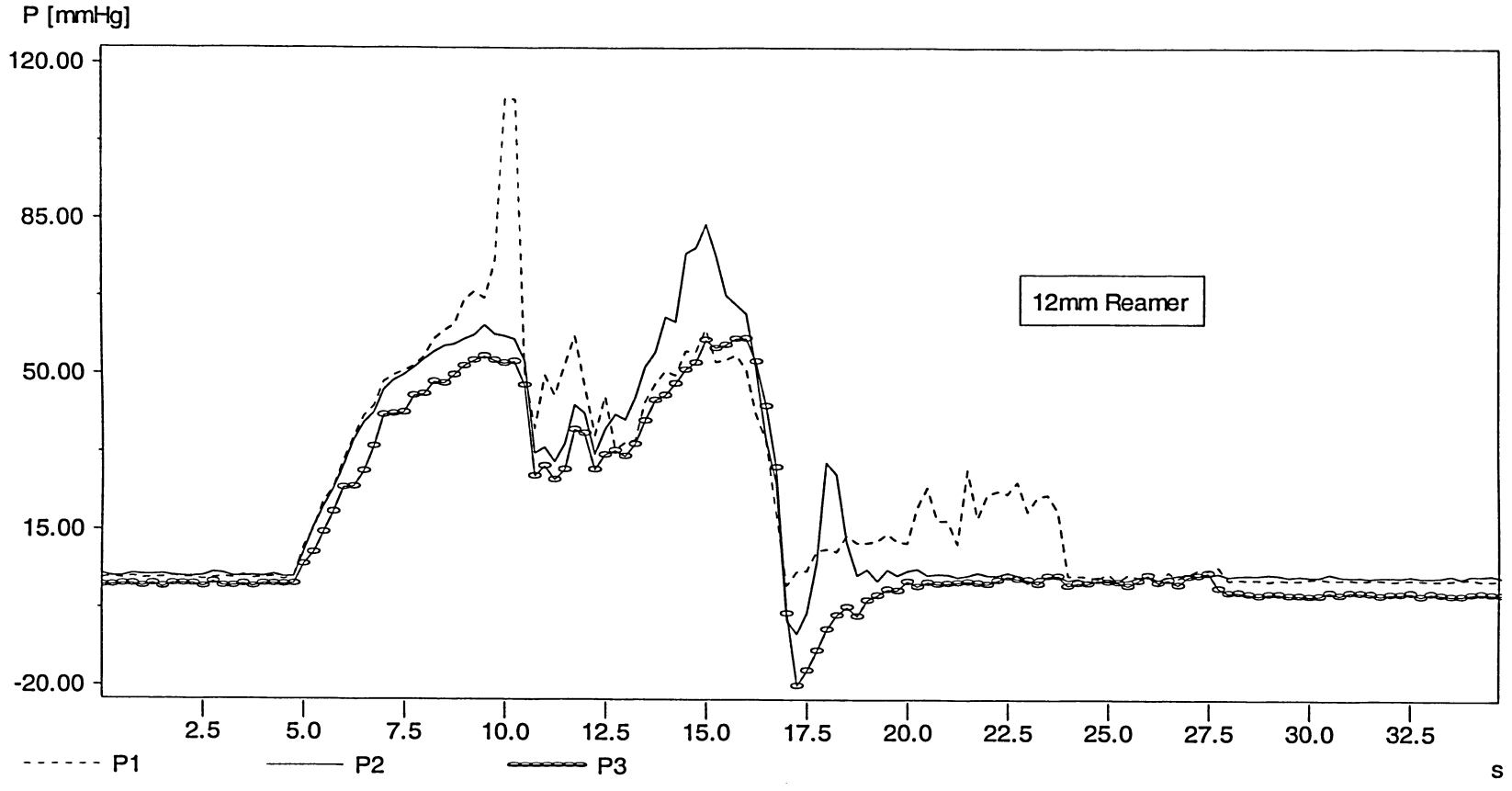

Figure B.14. Pressure variation using 12 mm clogged reamer, 200 RPM, 20 $\frac{mm}{sec}$ and low viscosity synthetic marrow (82.6 cP). P1, P2 and P3 are respectively corresponded to pressure transducer #1, 2 and 3. The reamer was clogged by fully covering the reamer flutes with silicon sealant.

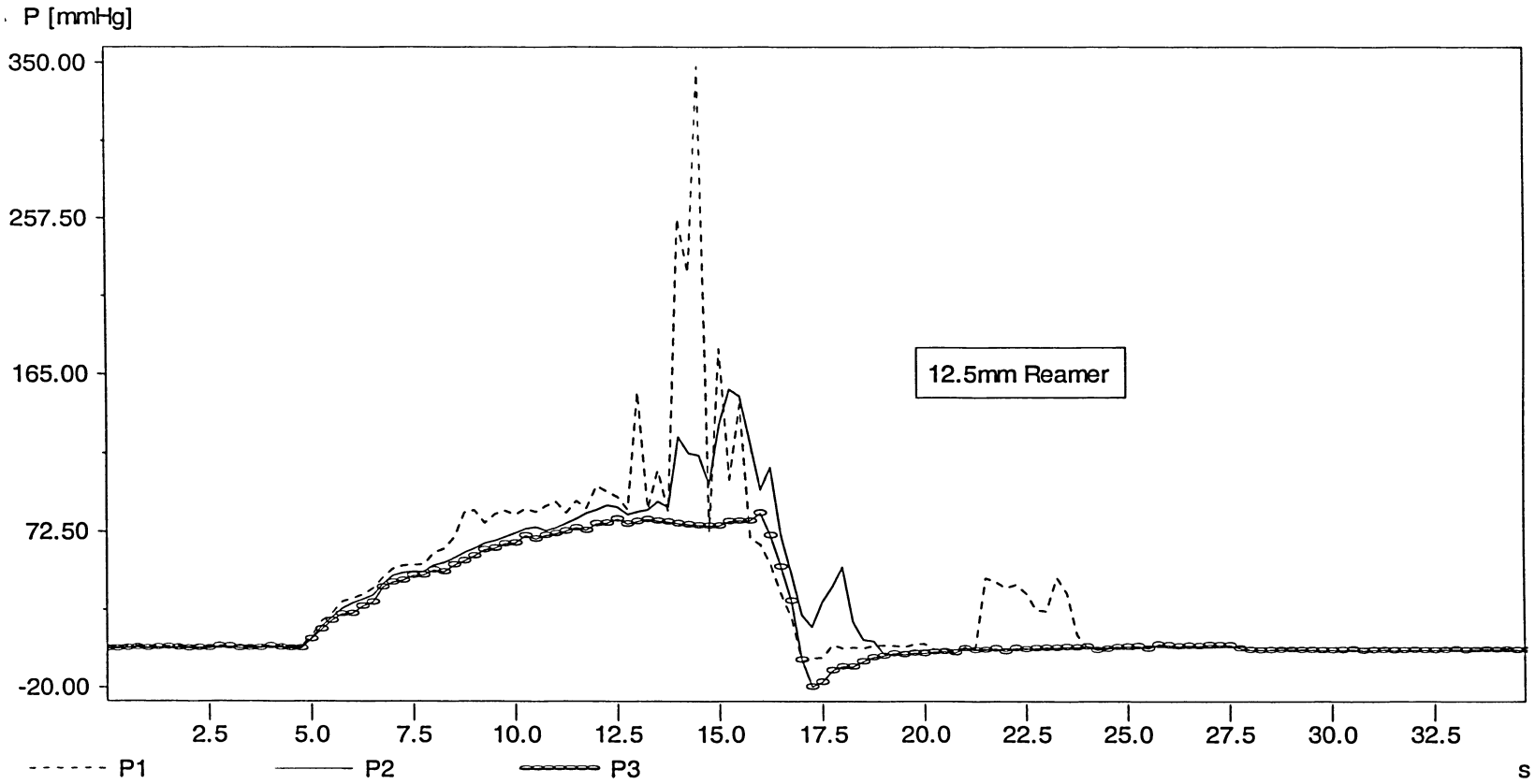

Figure B.15. Pressure variation using 12.5 mm clogged reamer, 200 RPM, 20 $\frac{mm}{sec}$ and low viscosity synthetic marrow (82.6 cP). P1, P2 and P3 are respectively corresponded to pressure transducer #1, 2 and 3. The reamer was clogged by fully covering the reamer flutes with silicon sealant.

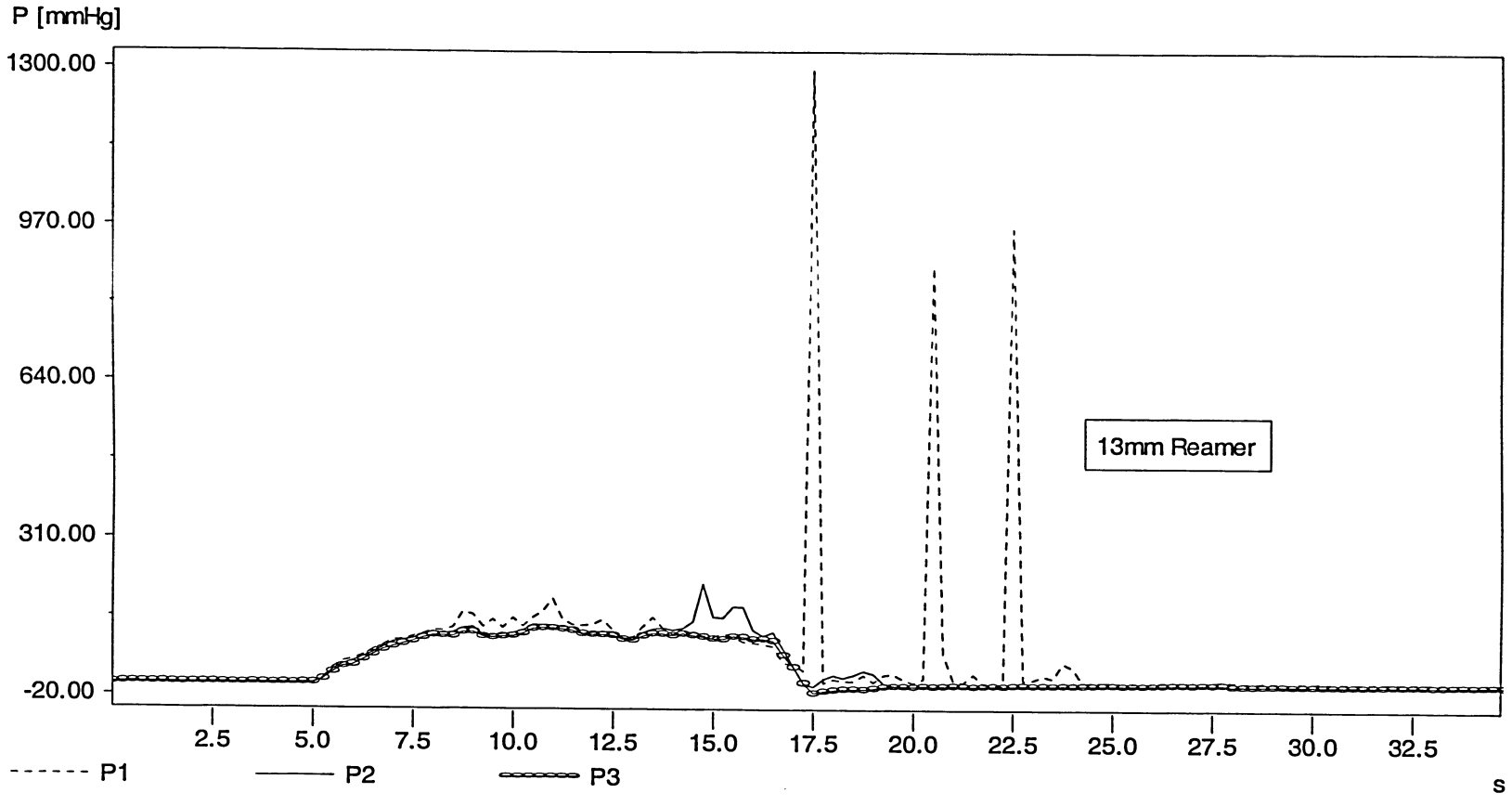

Figure B.16. Pressure variation using 13 mm clogged reamer, 200 RPM, 20 $\frac{mm}{sec}$ and low viscosity synthetic marrow (82.6 cP). P1, P2 and P3 are respectively corresponded to pressure transducer #1, 2 and 3. The reamer was clogged by fully covering the reamer flutes with silicon sealant.

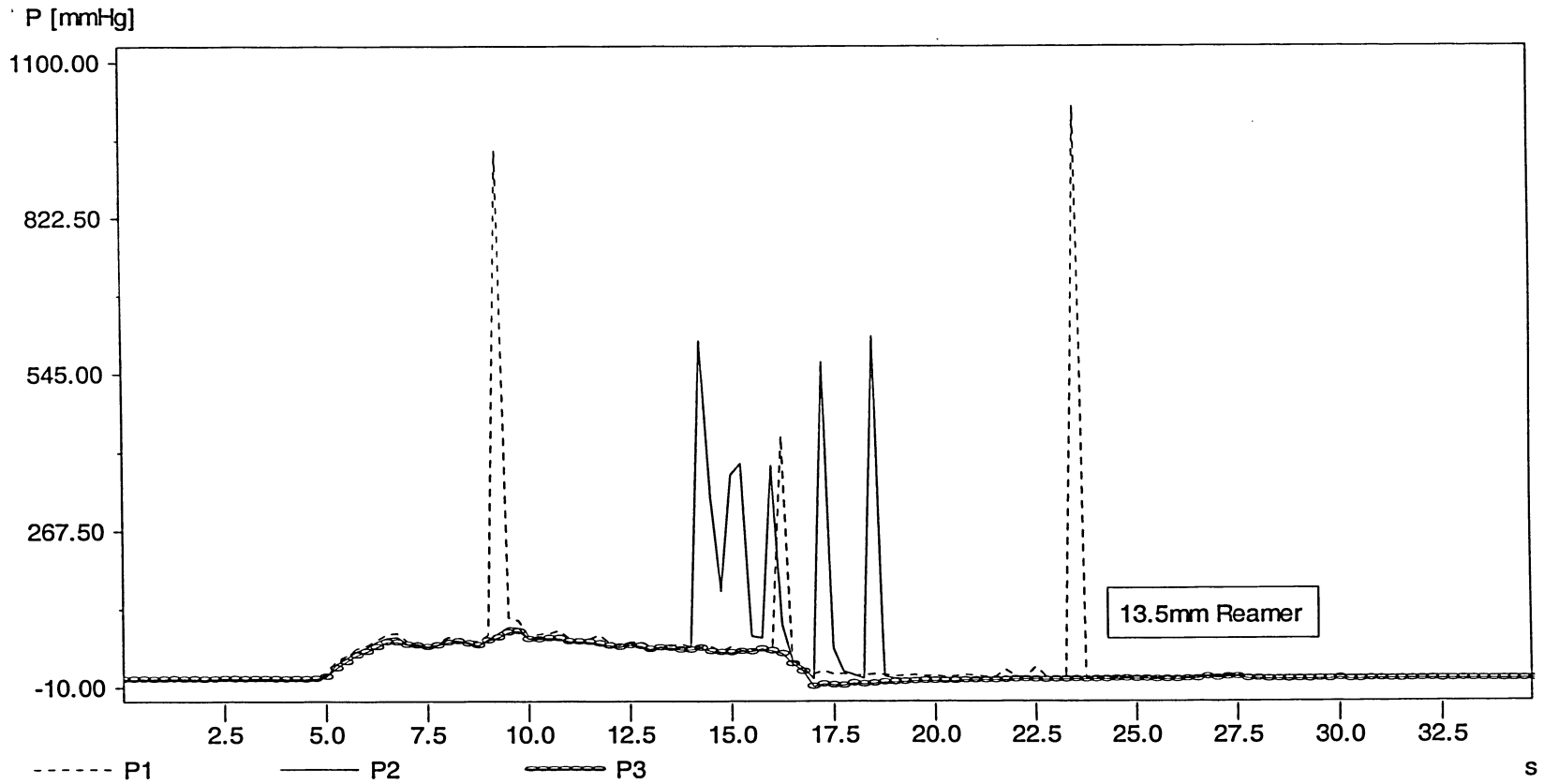

Figure B.17. Pressure variation using 13.5 mm clogged reamer, 200 RPM, 20 $\frac{mm}{sec}$ and low viscosity synthetic marrow (82.6 cP). P1, P2 and P3 are respectively corresponded to pressure transducer #1, 2 and 3. The reamer was clogged by fully covering the reamer flutes with silicon sealant.

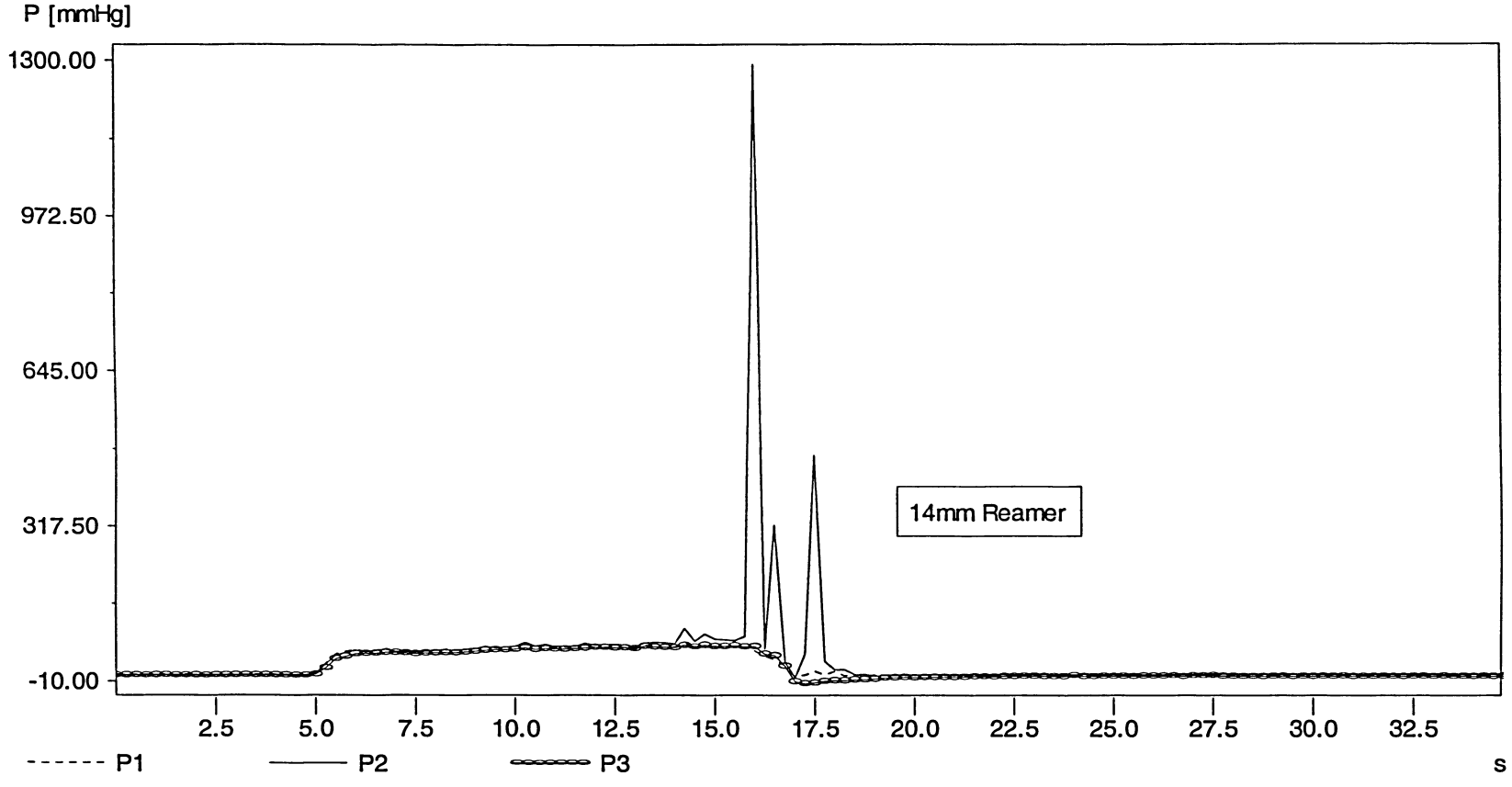

Figure B.18. Pressure variation using 14 mm clogged reamer, 200 RPM, 20 $\frac{mm}{sec}$ and low viscosity synthetic marrow (82.6 cP). P1, P2 and P3 are respectively corresponded to pressure transducer #1, 2 and 3. The reamer was clogged by fully covering the reamer flutes with silicon sealant.

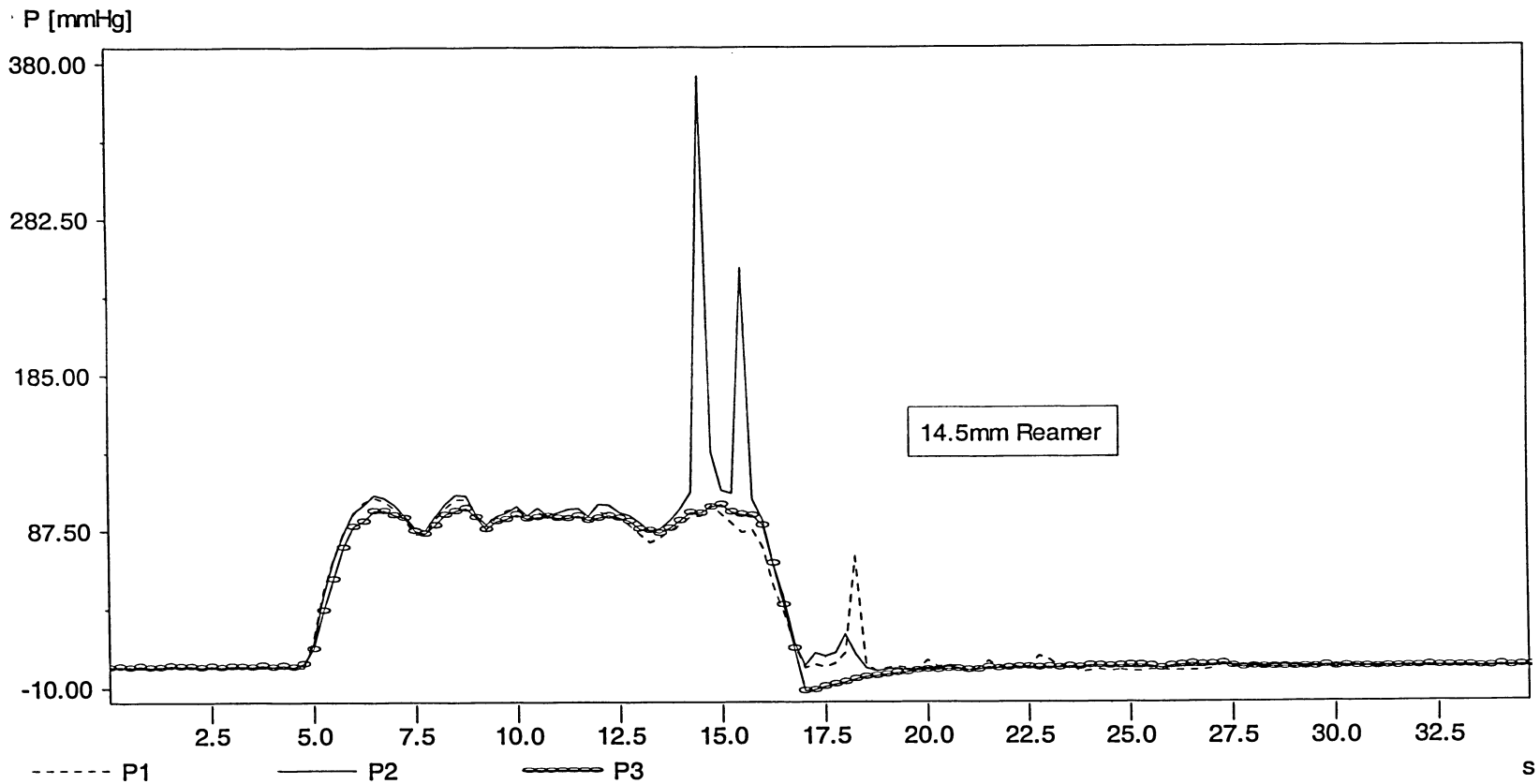

Figure B.19. Pressure variation using 14.5 mm clogged reamer, 200 RPM, 20 $\frac{mm}{sec}$ and low viscosity synthetic marrow (82.6 cP). P1, P2 and P3 are respectively corresponded to pressure transducer #1, 2 and 3. The reamer was clogged by fully covering the reamer flutes with silicon sealant.

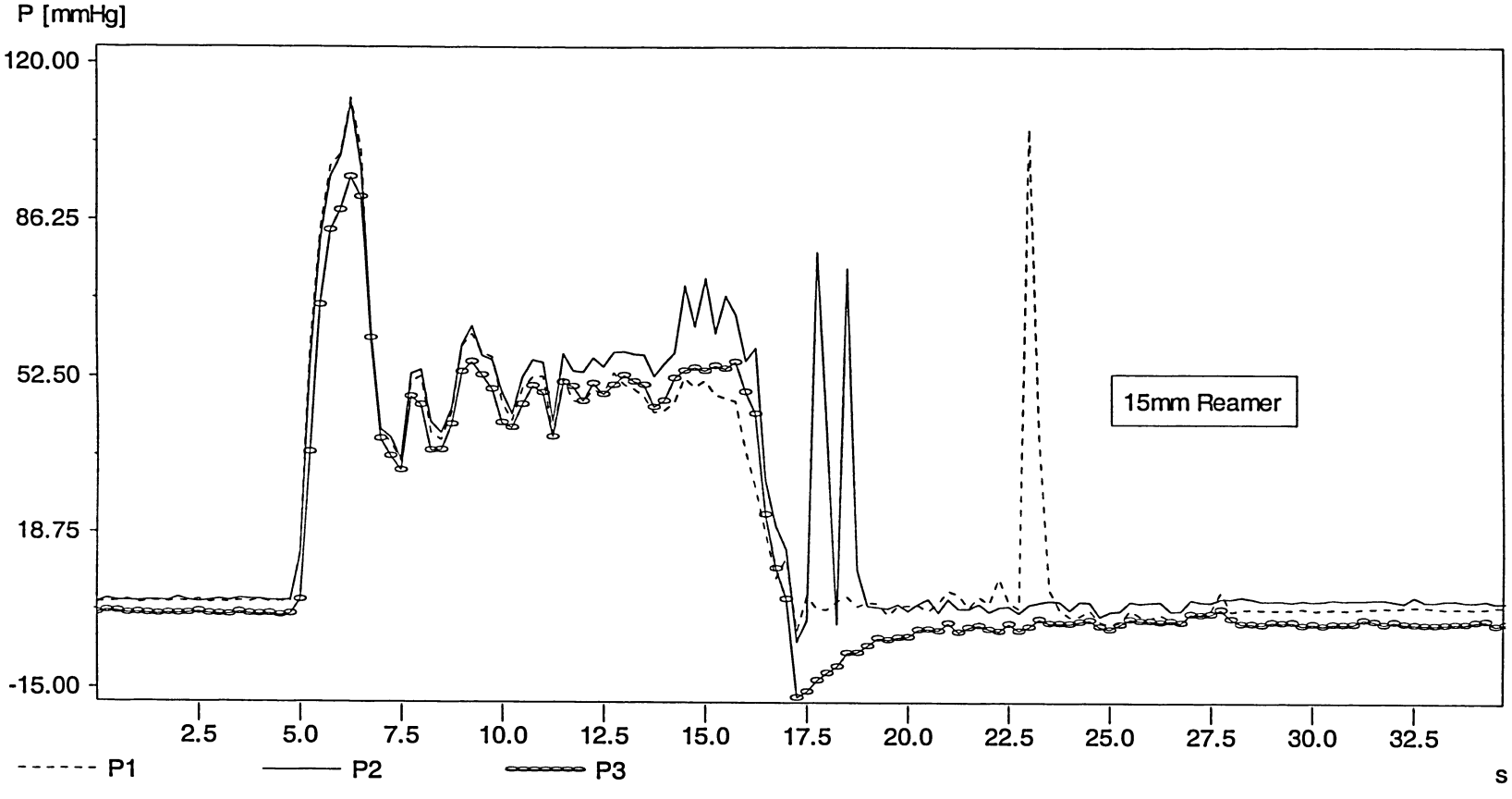

Figure B.20. Pressure variation using 15 mm clogged reamer, 200 RPM, 20 $\frac{mm}{sec}$ and low viscosity synthetic marrow (82.6 cP). P1, P2 and P3 are respectively corresponded to pressure transducer #1, 2 and 3. The reamer was clogged by fully covering the reamer flutes with silicon sealant.

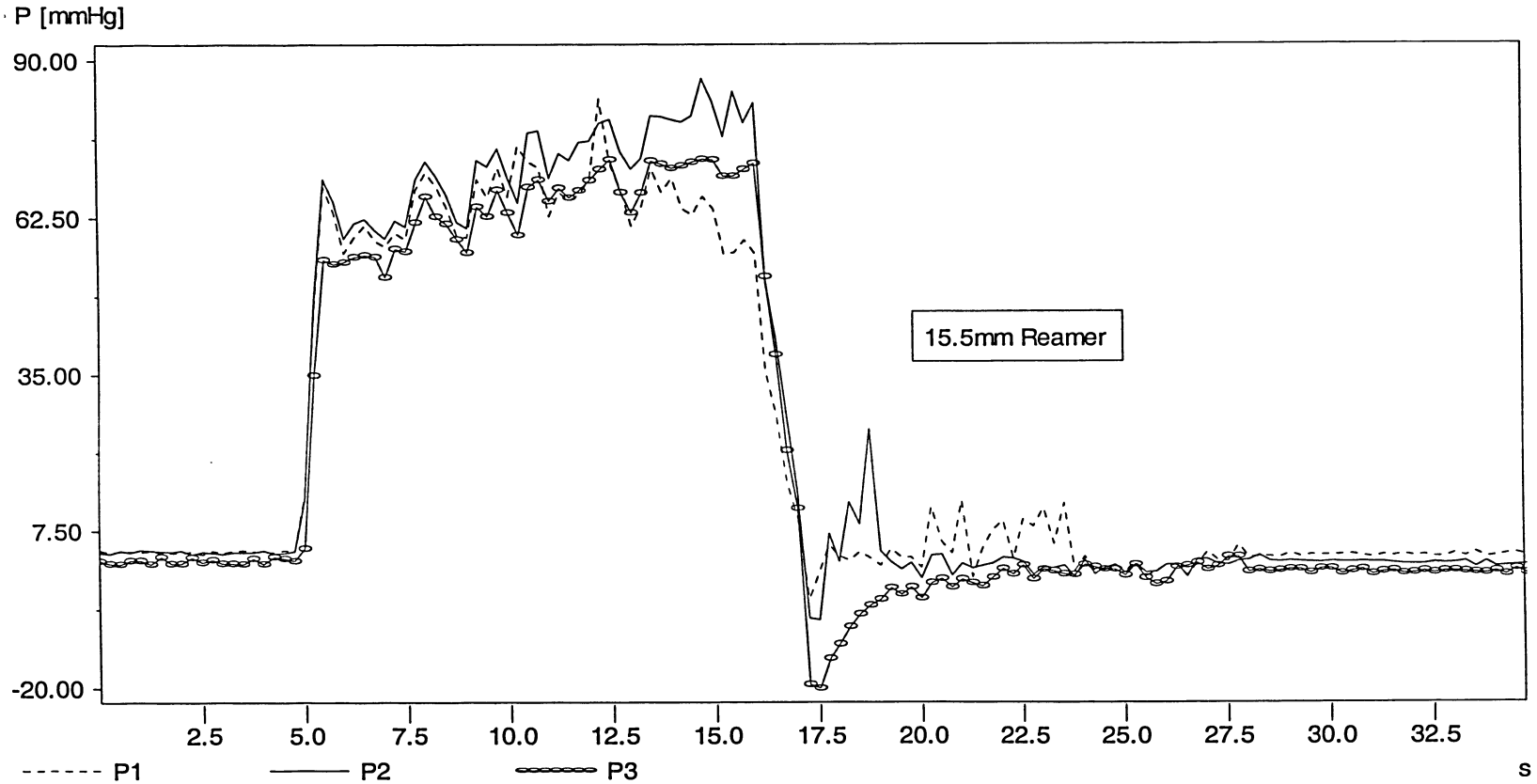

Figure B.21. Pressure variation using 15.5 mm clogged reamer, 200 RPM, 20 $\frac{mm}{sec}$ and low viscosity synthetic marrow (82.6 cP). P1, P2 and P3 are respectively corresponded to pressure transducer #1, 2 and 3. The reamer was clogged by fully covering the reamer flutes with silicon sealant.

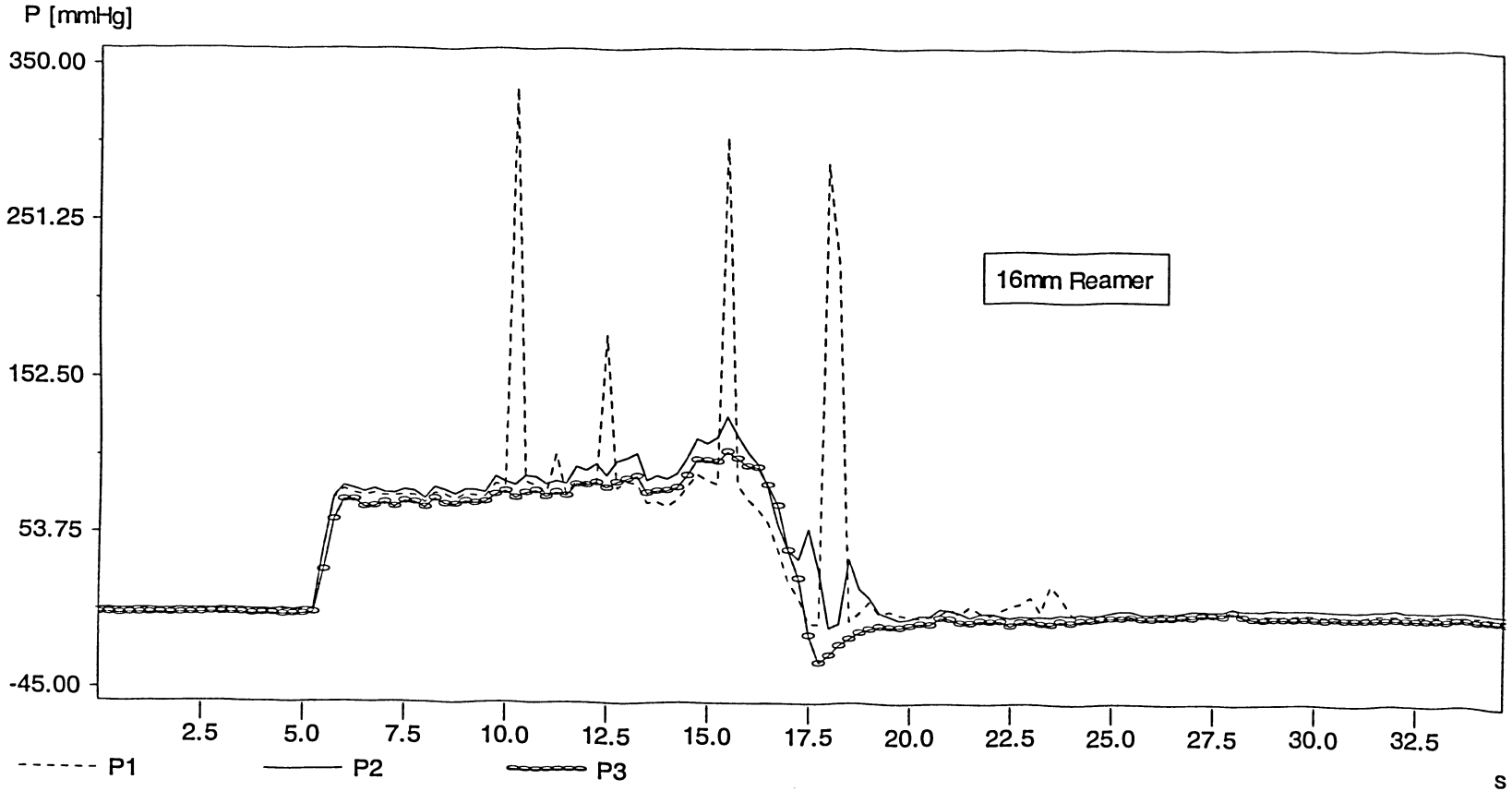

Figure B.22. Pressure variation using 16 mm clogged reamer, 200 RPM, 20 $\frac{mm}{sec}$ and low viscosity synthetic marrow (82.6 cP). P1, P2 and P3 are respectively corresponded to pressure transducer #1, 2 and 3. The reamer was clogged by fully covering the reamer flutes with silicon sealant.

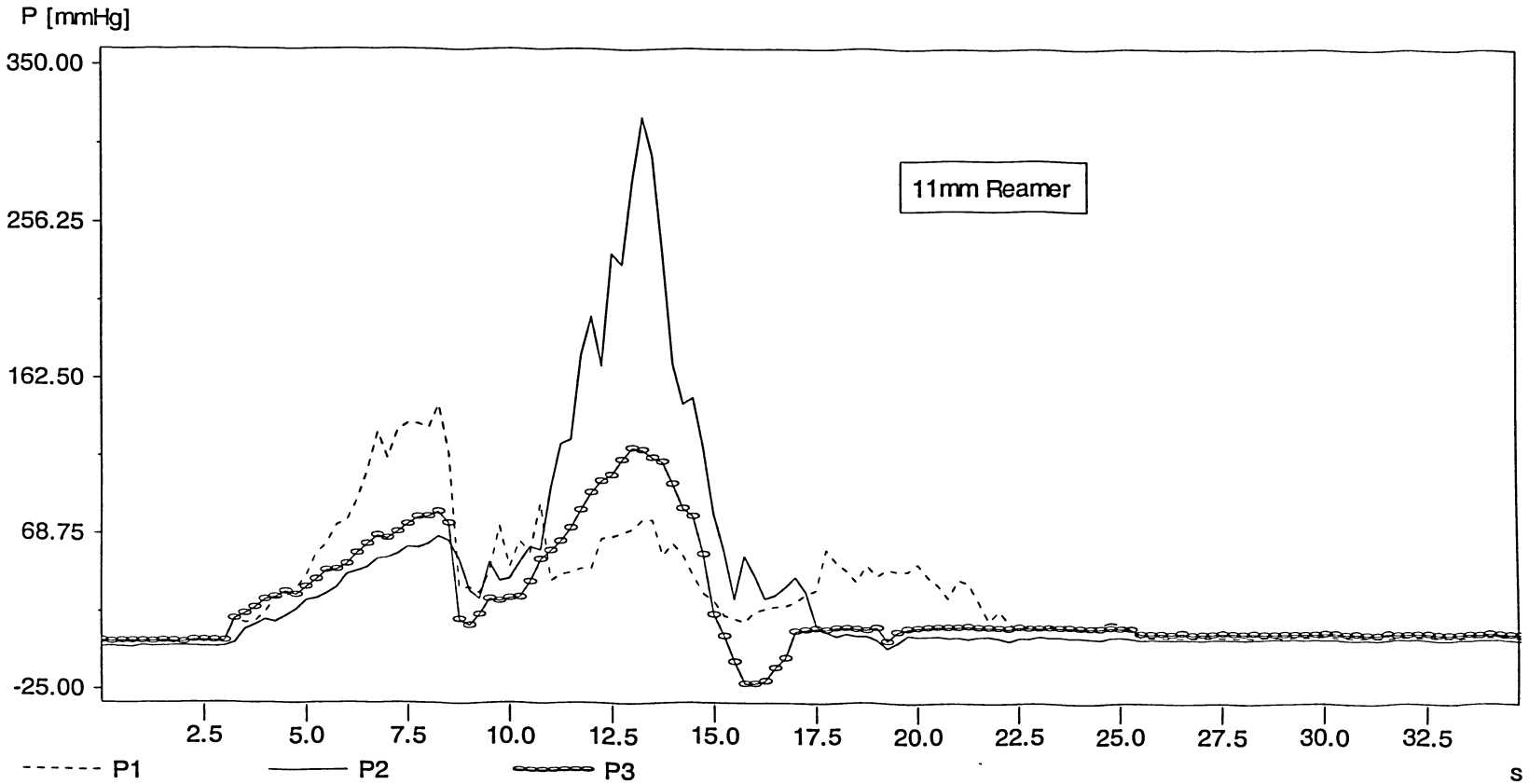

Figure B.23. Pressure variation using 11 mm unclogged reamer, 200 RPM, 20 $\frac{mm}{sec}$ and high viscosity synthetic marrow (396 cP). P1, P2 and P3 are respectively corresponded to pressure transducer #1, 2 and 3.

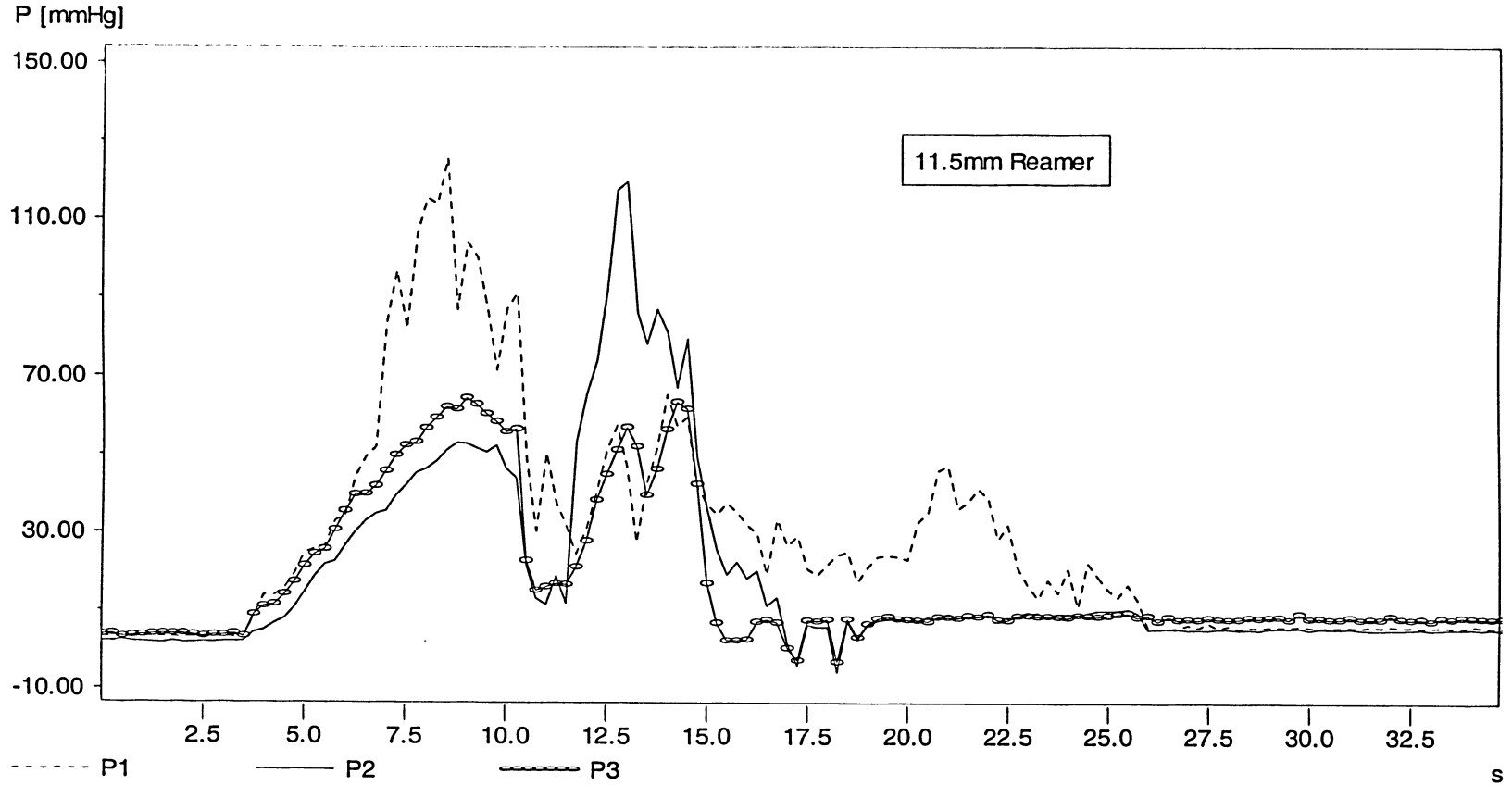

Figure B.24. Pressure variation using 11.5 mm unclogged reamer, 200 RPM, 20 $\frac{mm}{sec}$ and high viscosity synthetic marrow (396 cP). P1, P2 and P3 are respectively corresponded to pressure transducer #1, 2 and 3.

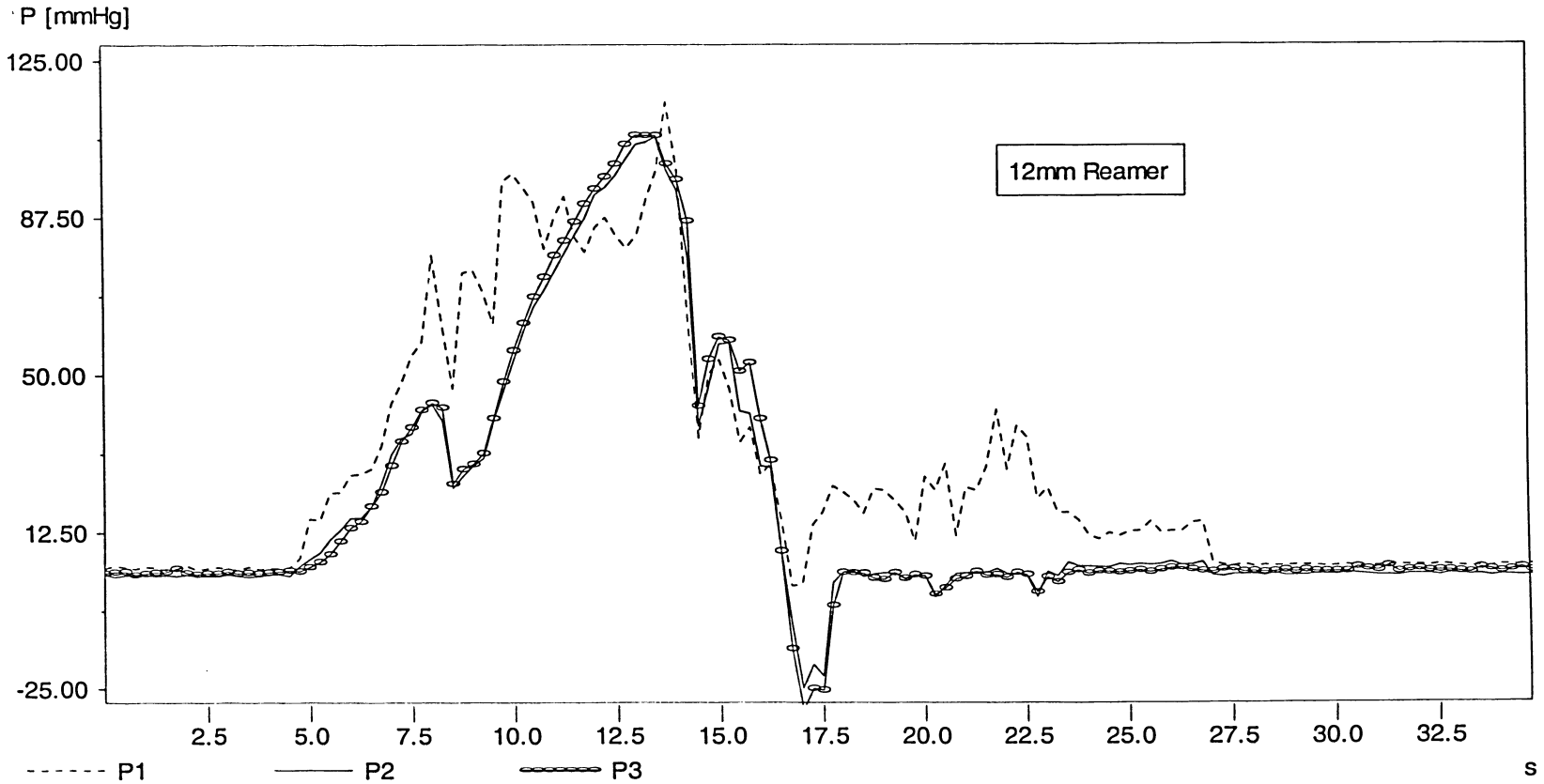

Figure B.25. Pressure variation using 12 mm unclogged reamer, 200 RPM, 20 $\frac{mm}{sec}$ and high viscosity synthetic marrow (396 cP). P1, P2 and P3 are respectively corresponded to pressure transducer #1, 2 and 3.

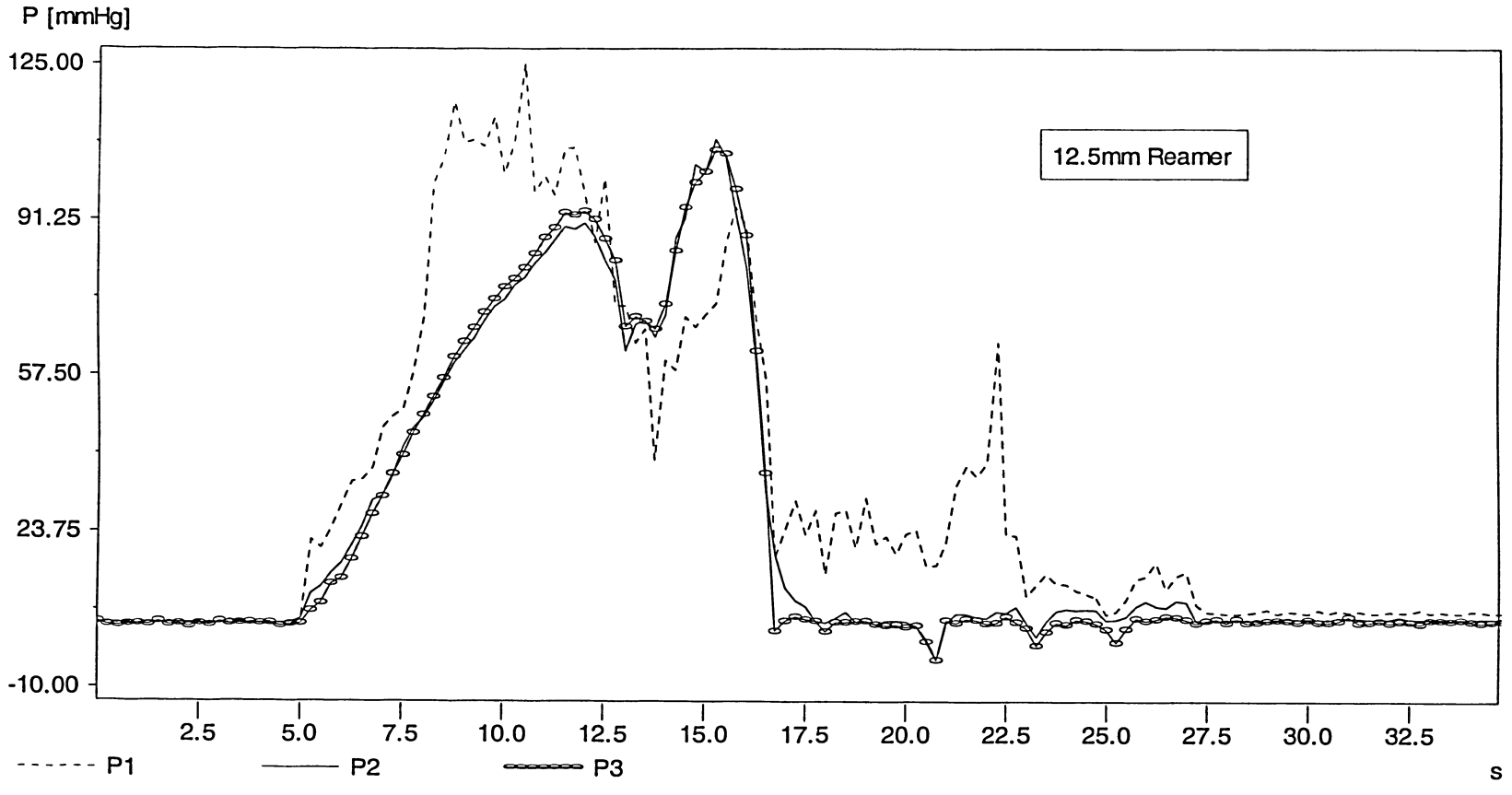

Figure B.26. Pressure variation using 12.5 mm unclogged reamer, 200 RPM, 20 $\frac{mm}{sec}$ and high viscosity synthetic marrow (396 cP). P1, P2 and P3 are respectively corresponded to pressure transducer #1, 2 and 3.

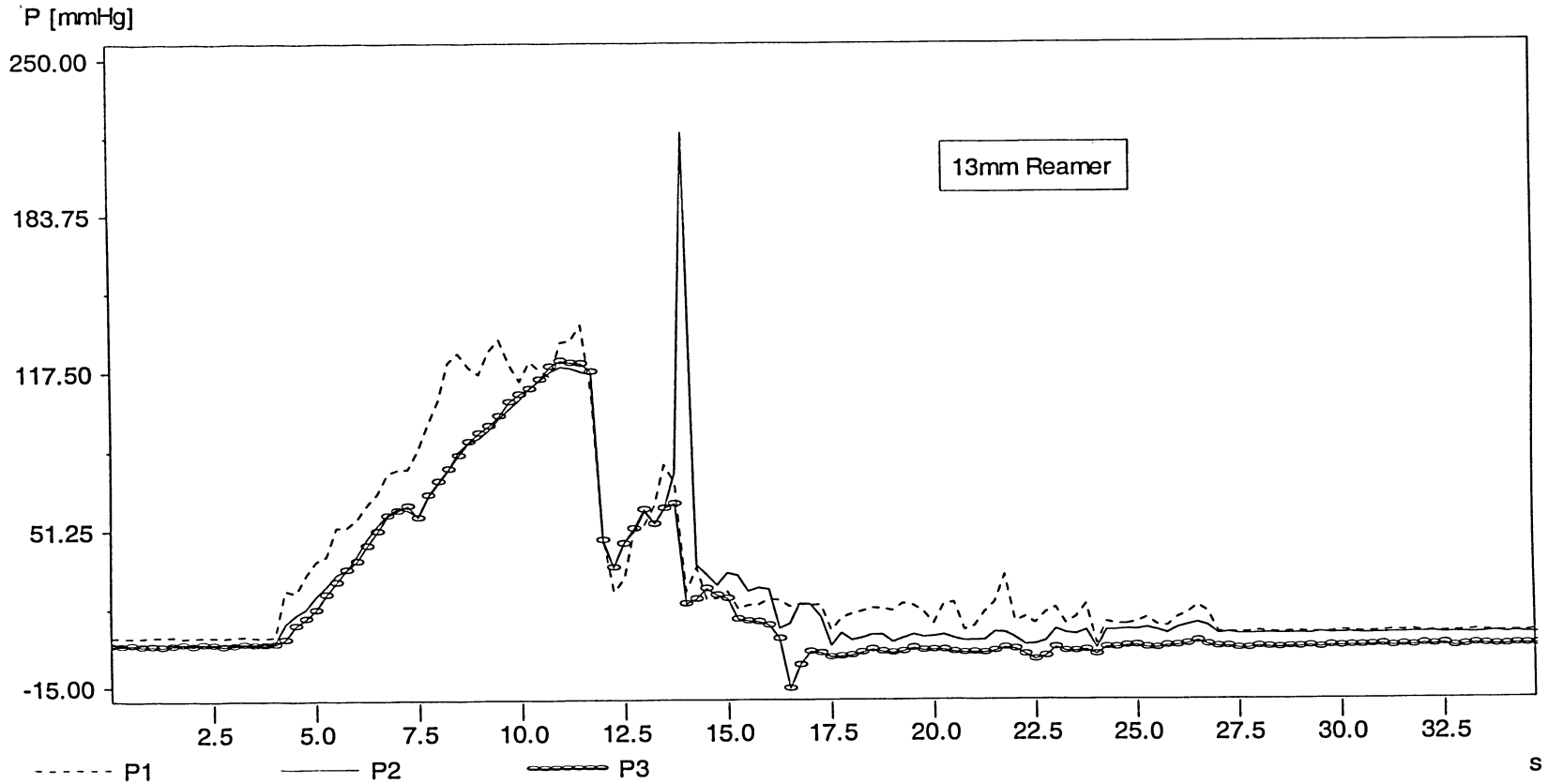

Figure B.27. Pressure variation using 13 mm unclogged reamer, 200 RPM, 20 $\frac{mm}{sec}$ and high viscosity synthetic marrow (396 cP). P1, P2 and P3 are respectively corresponded to pressure transducer #1, 2 and 3.

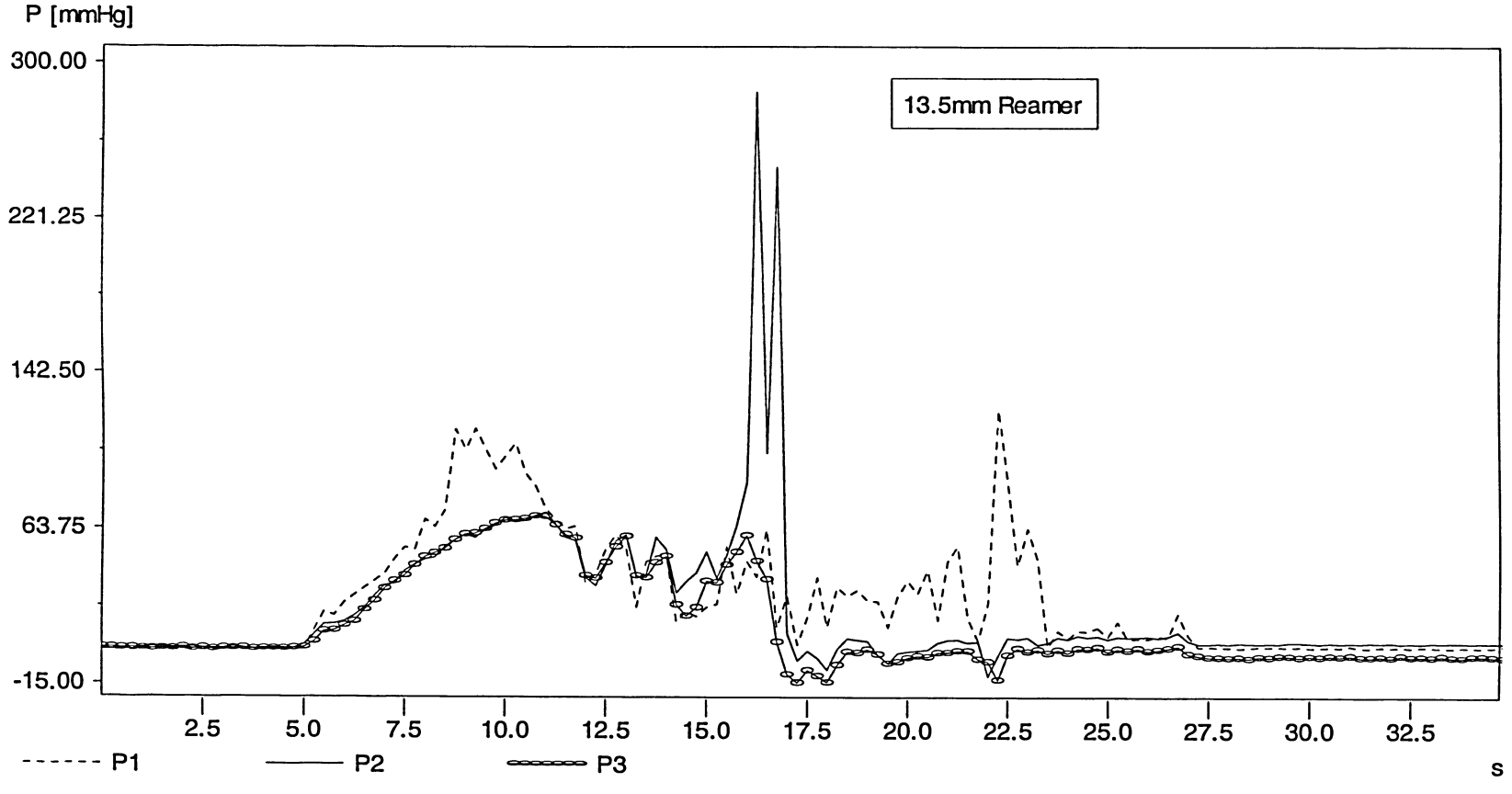

Figure B.28. Pressure variation using 13.5 mm unclogged reamer, 200 RPM, 20 $\frac{mm}{sec}$ and high viscosity synthetic marrow (396 cP). P1, P2 and P3 are respectively corresponded to pressure transducer #1, 2 and 3.

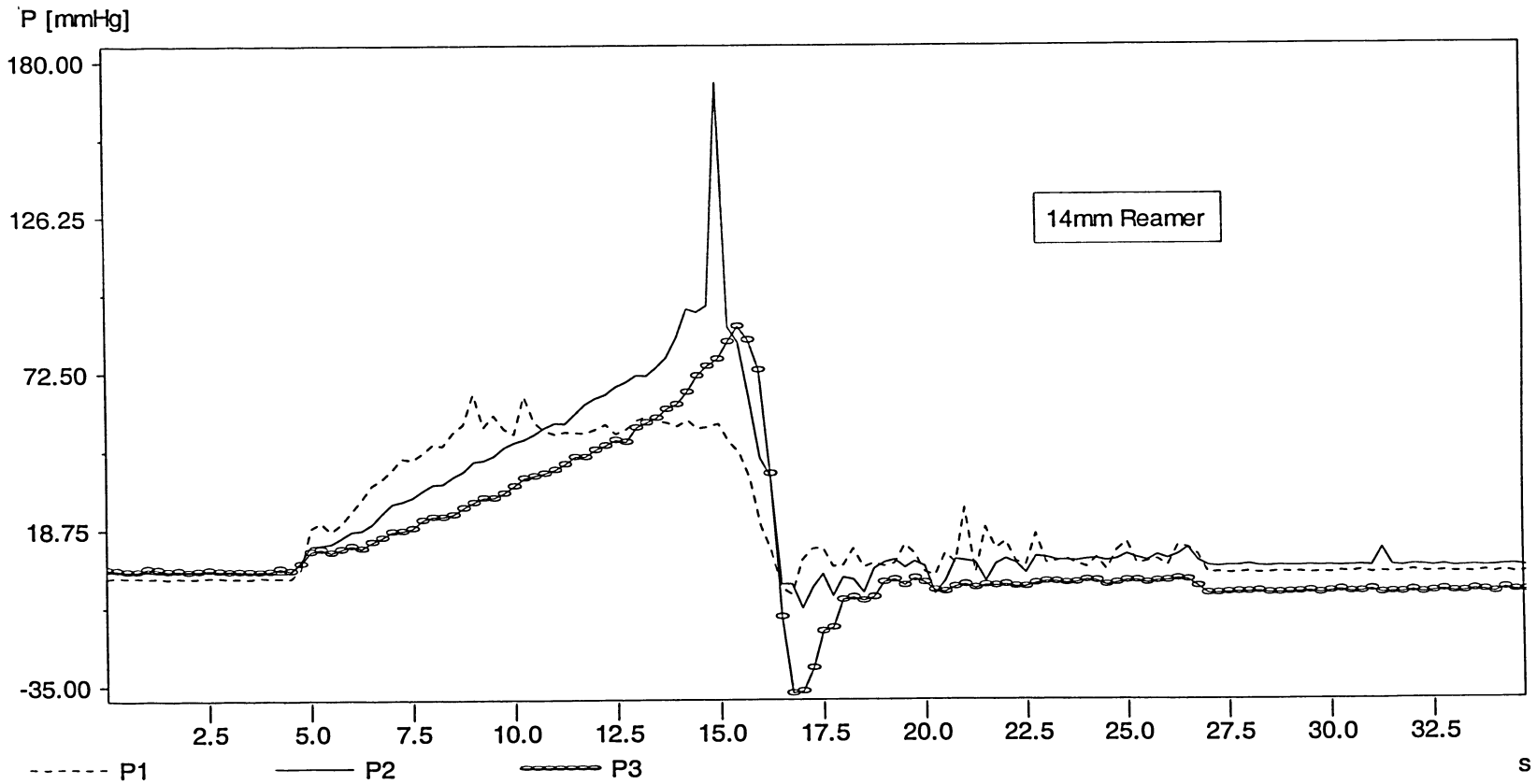

Figure B.29. Pressure variation using 14 mm unclogged reamer, 200 RPM, 20 $\frac{mm}{sec}$ and high viscosity synthetic marrow (396 cP). P1, P2 and P3 are respectively corresponded to pressure transducer #1, 2 and 3.

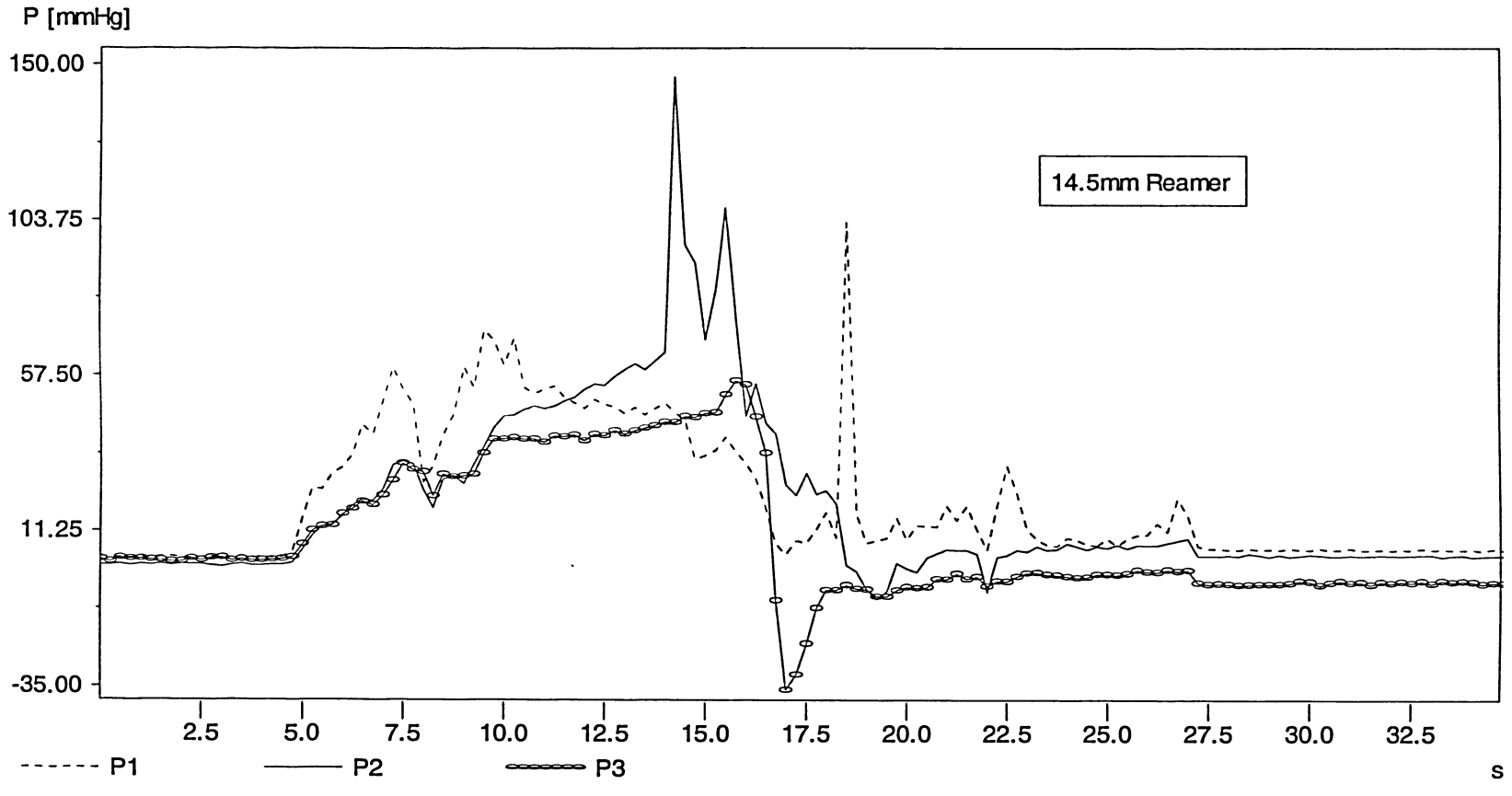

Figure B.30. Pressure variation using 14.5 mm unclogged reamer, 200 RPM, 20 $\frac{mm}{sec}$ and high viscosity synthetic marrow (396 cP). P1, P2 and P3 are respectively corresponded to pressure transducer #1, 2 and 3.

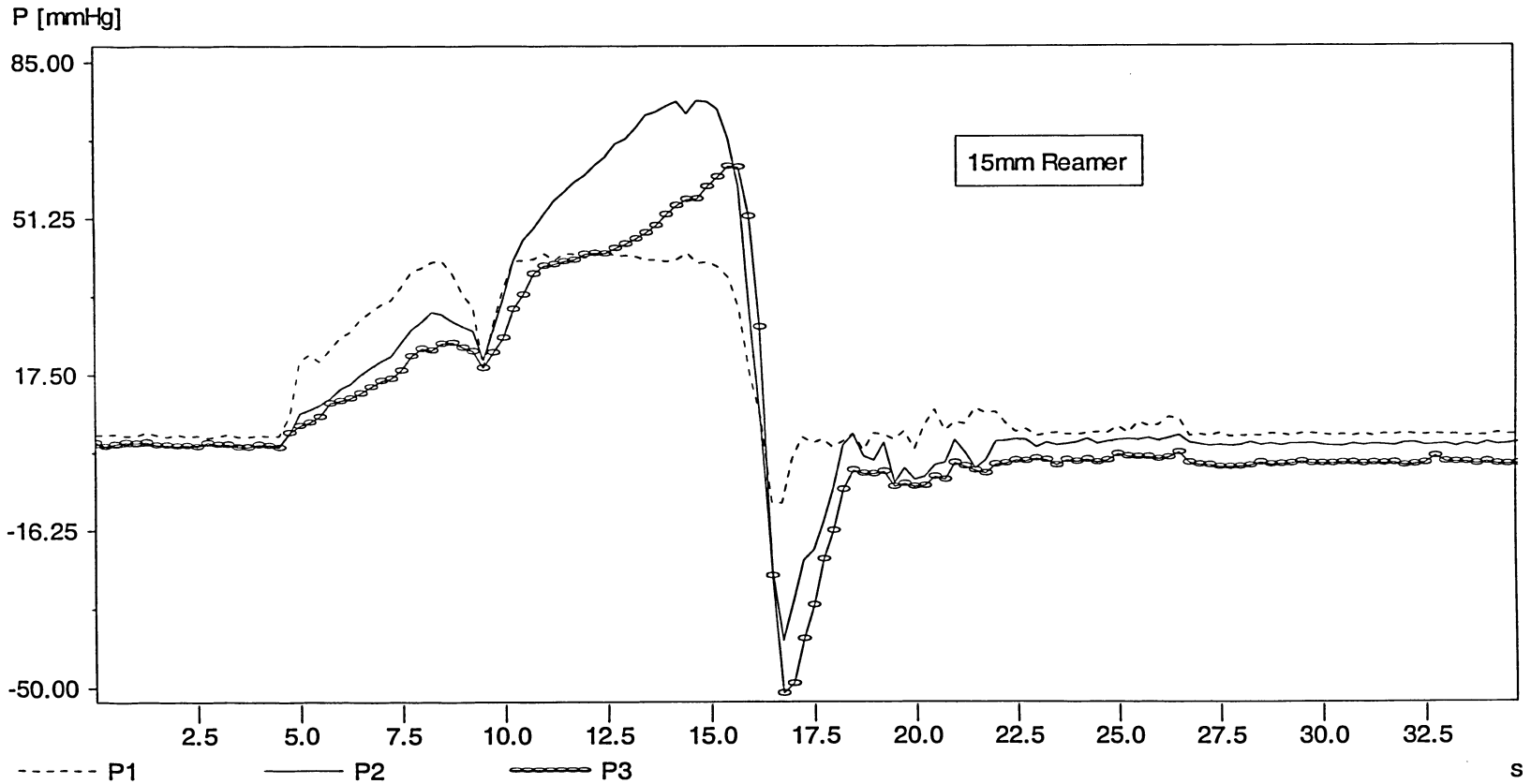

Figure B.31. Pressure variation using 15 mm unclogged reamer, 200 RPM, 20 $\frac{mm}{sec}$ and high viscosity synthetic marrow (396 cP). P1, P2 and P3 are respectively corresponded to pressure transducer #1, 2 and 3.

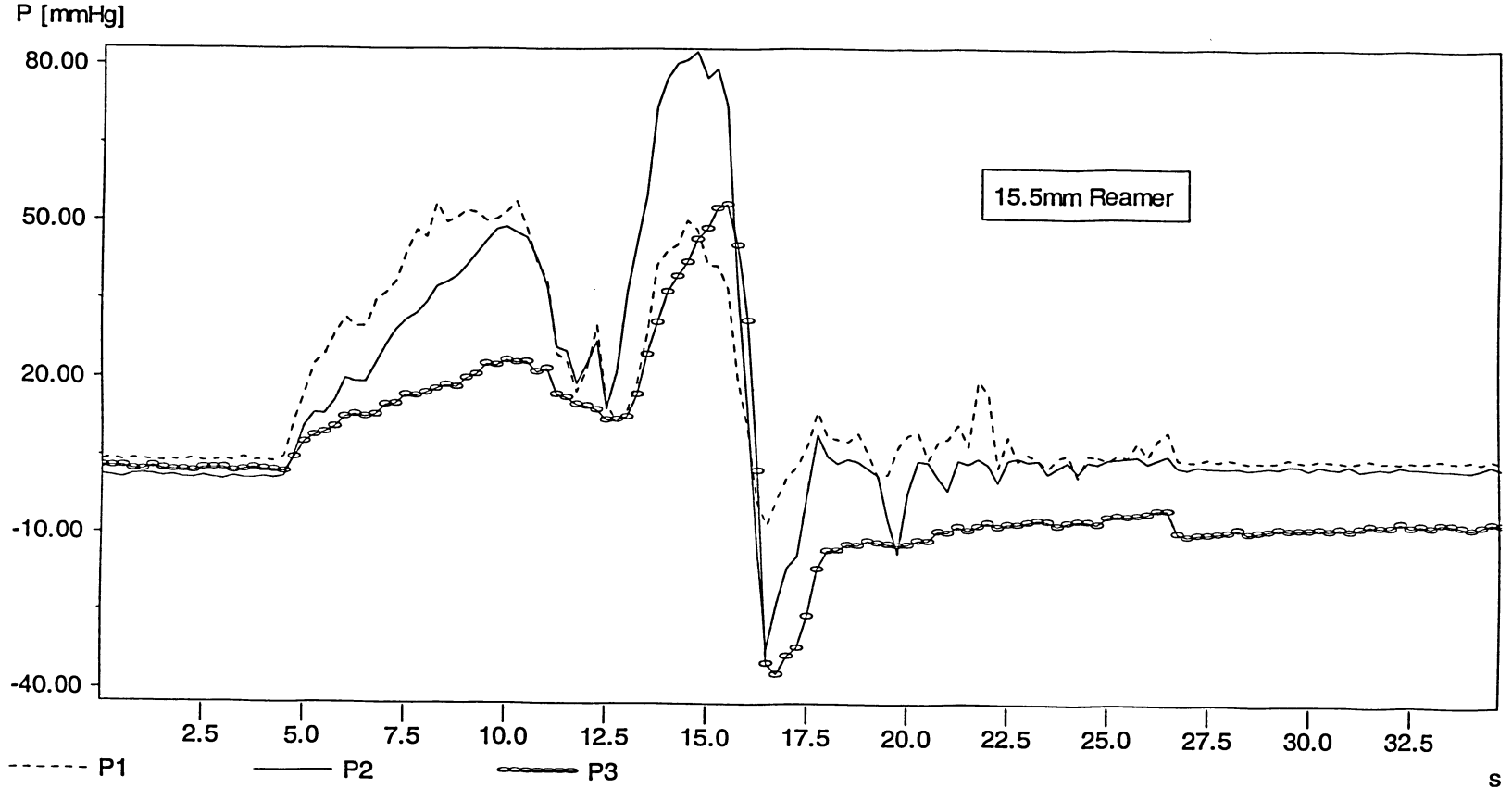

Figure B.32. Pressure variation using 15.5 mm unclogged reamer, 200 RPM, 20 $\frac{mm}{sec}$ and high viscosity synthetic marrow (396 cP). P1, P2 and P3 are respectively corresponded to pressure transducer #1, 2 and 3.

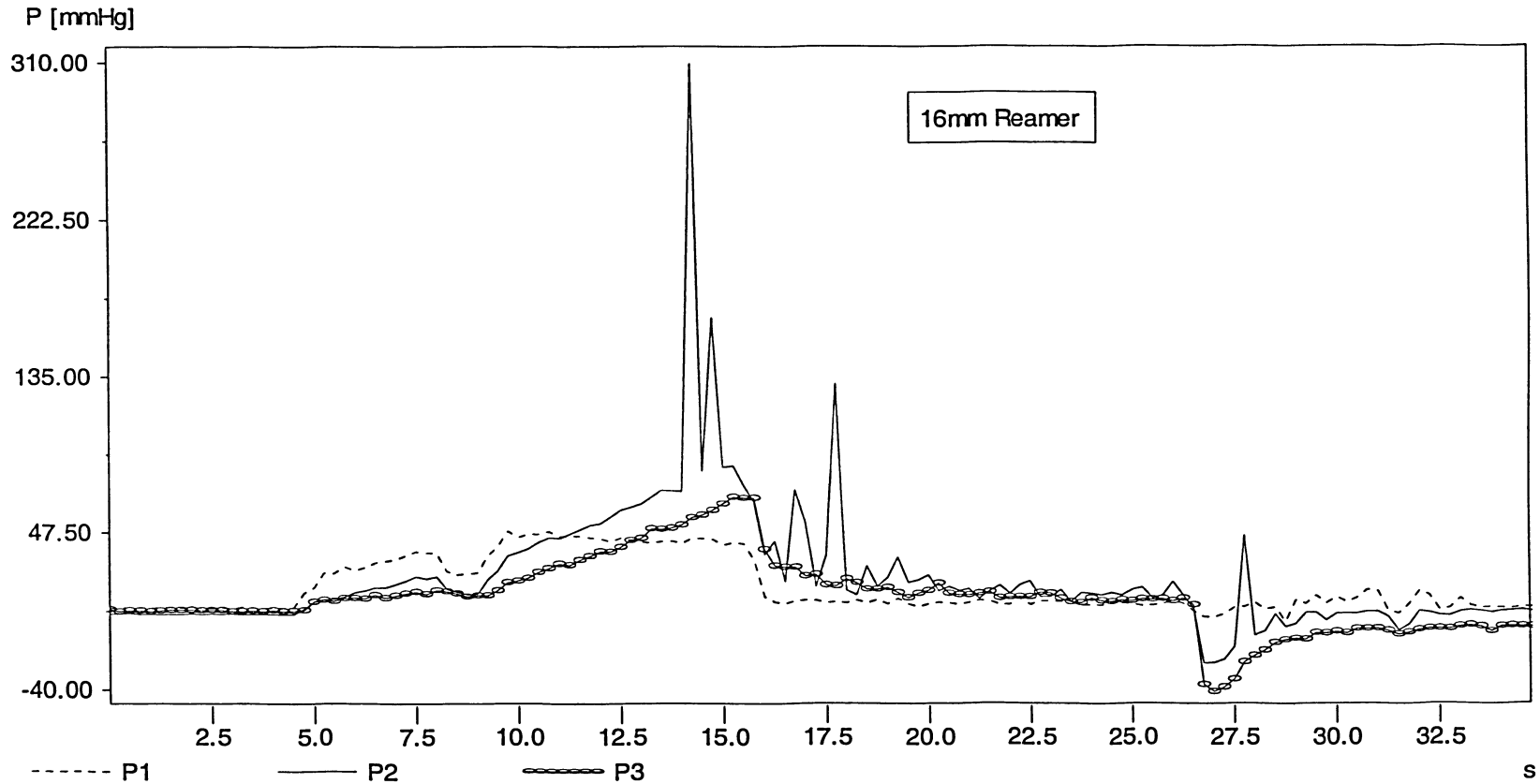

Figure B.33. Pressure variation using 16 mm unclogged reamer, 200 RPM, 20 $\frac{mm}{sec}$ and high viscosity synthetic marrow (396 cP). P1, P2 and P3 are respectively corresponded to pressure transducer #1, 2 and 3.

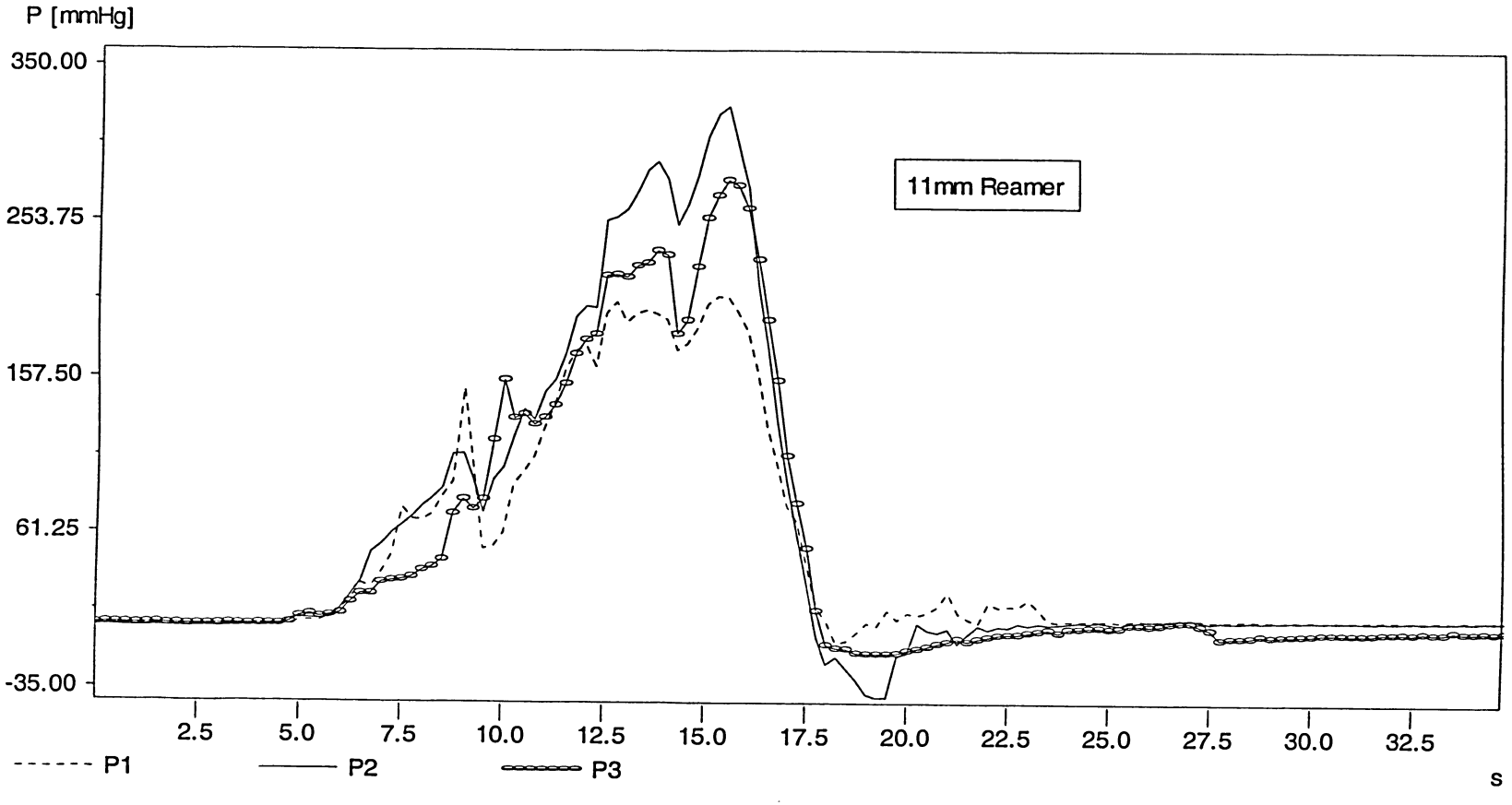

Figure B.34. Pressure variation using 11 mm clogged reamer, 200 RPM, 20 $\frac{mm}{sec}$ and high viscosity synthetic marrow (396 cP). P1, P2 and P3 are respectively corresponded to pressure transducer #1, 2 and 3. The reamer was clogged by fully covering the reamer flutes with silicon sealant.

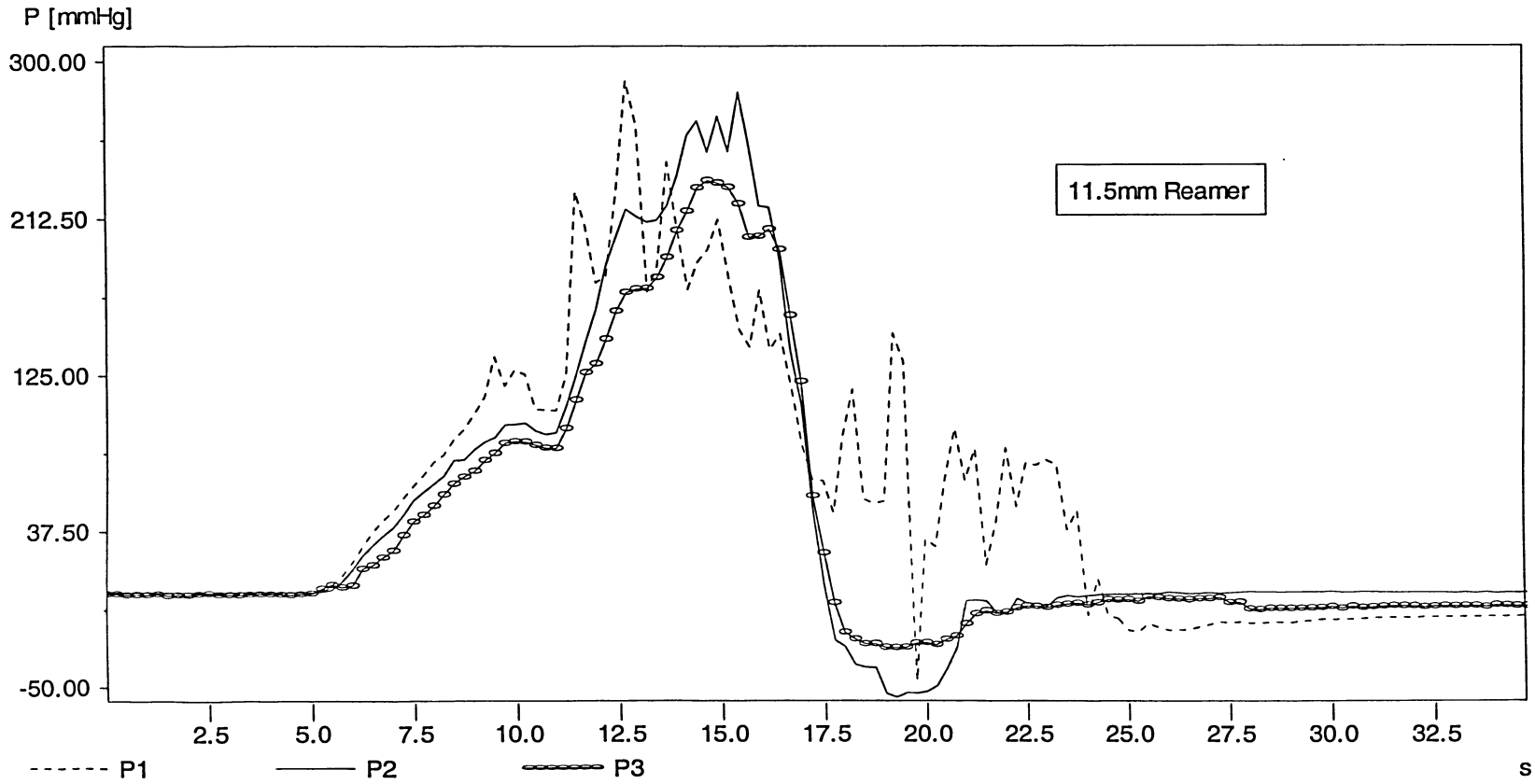

Figure B.35. Pressure variation using 11.5 mm clogged reamer, 200 RPM, 20 $\frac{mm}{sec}$ and high viscosity synthetic marrow (396 cP). P1, P2 and P3 are respectively corresponded to pressure transducer #1, 2 and 3. The reamer was clogged by fully covering the reamer flutes with silicon sealant.

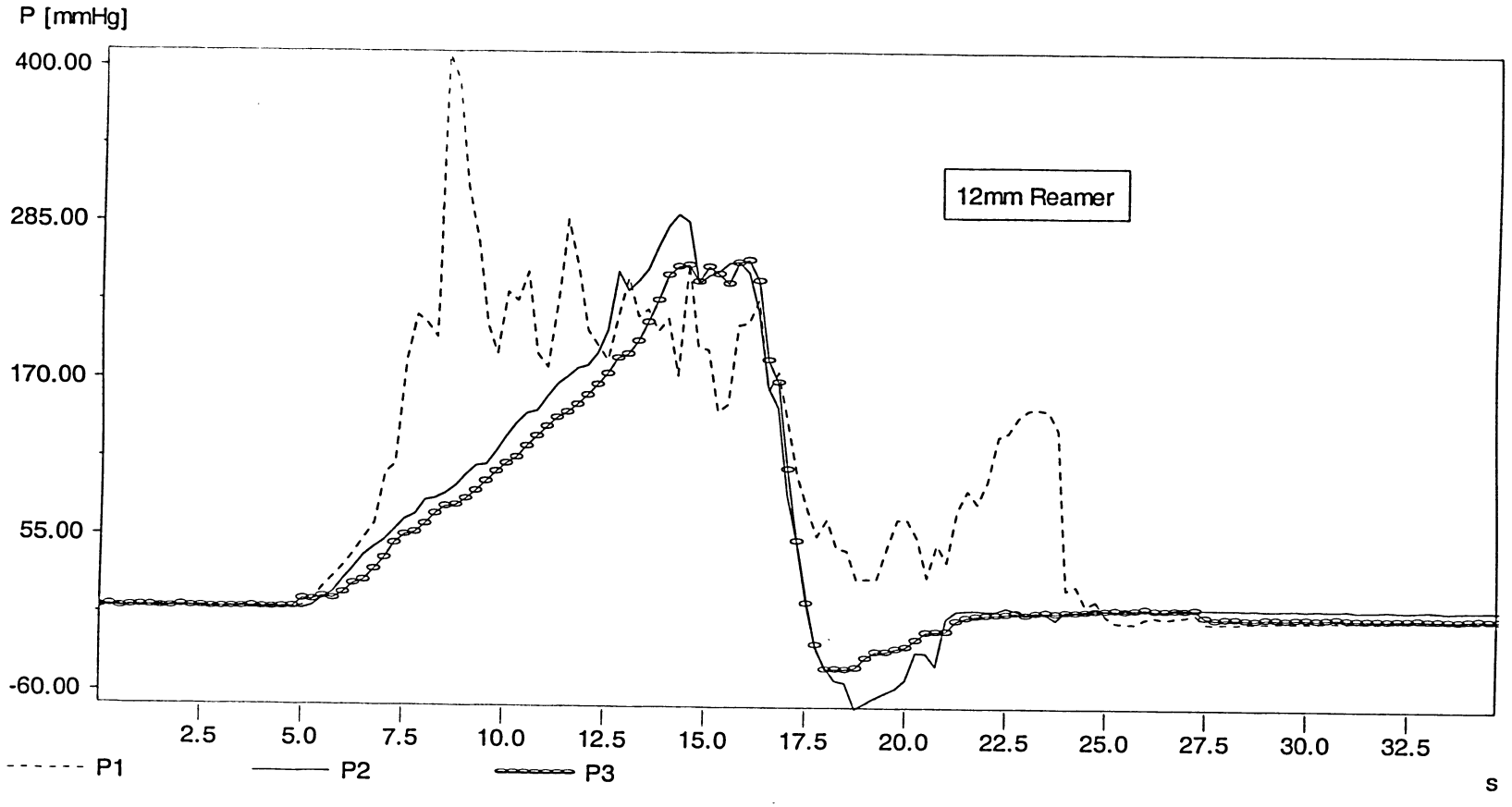

Figure B.36. Pressure variation using 12 mm clogged reamer, 200 RPM, 20 $\frac{mm}{sec}$ and high viscosity synthetic marrow (396 cP). P1, P2 and P3 are respectively corresponded to pressure transducer #1, 2 and 3. The reamer was clogged by fully covering the reamer flutes with silicon sealant.

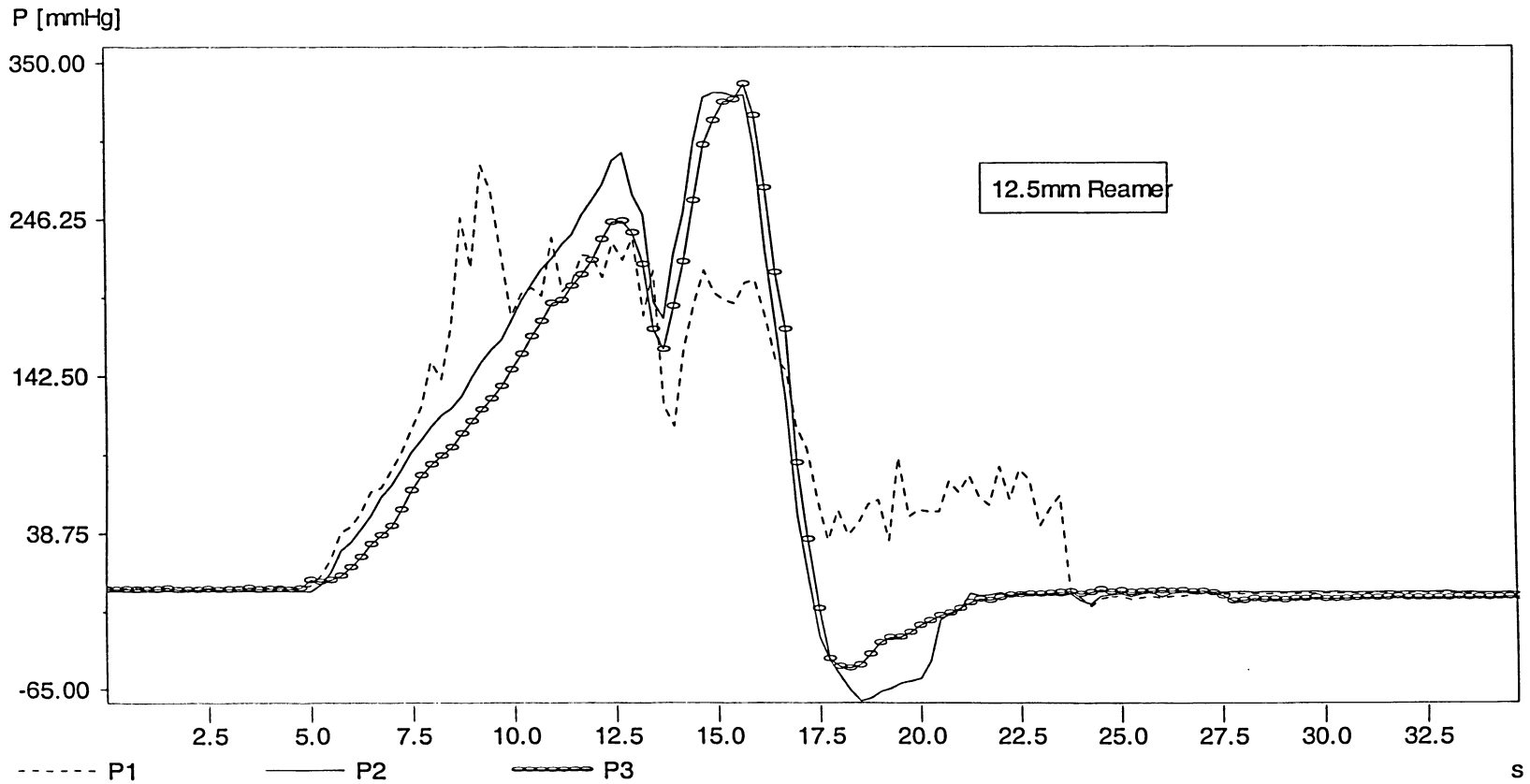

Figure B.37. Pressure variation using 12.5 mm clogged reamer, 200 RPM, 20 $\frac{mm}{sec}$ and high viscosity synthetic marrow (396 cP). P1, P2 and P3 are respectively corresponded to pressure transducer #1, 2 and 3. The reamer was clogged by fully covering the reamer flutes with silicon sealant.

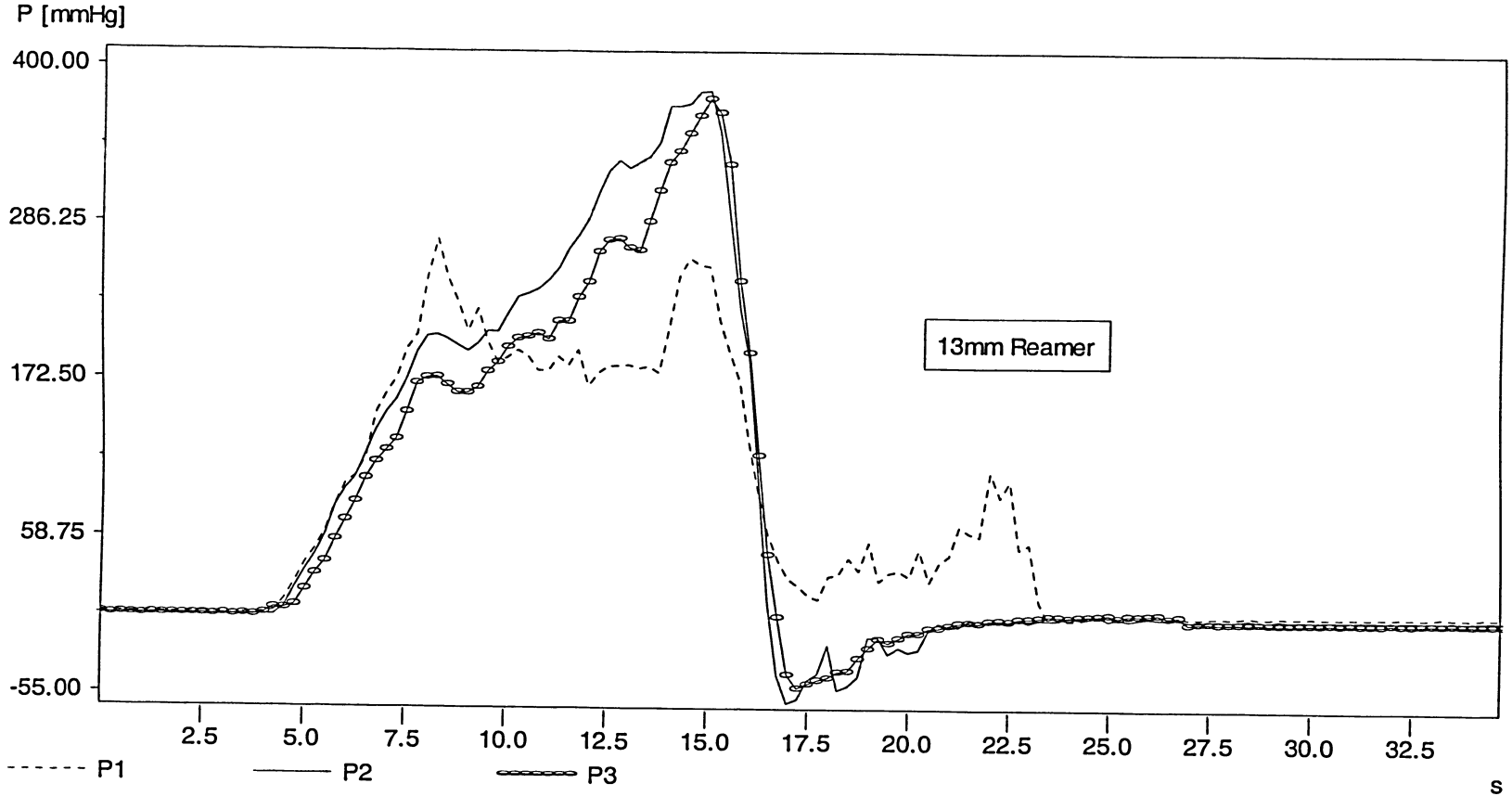

Figure B.38. Pressure variation using 13 mm clogged reamer, 200 RPM, 20 $\frac{mm}{sec}$ and high viscosity synthetic marrow (396 cP). P1, P2 and P3 are respectively corresponded to pressure transducer #1, 2 and 3. The reamer was clogged by fully covering the reamer flutes with silicon sealant.

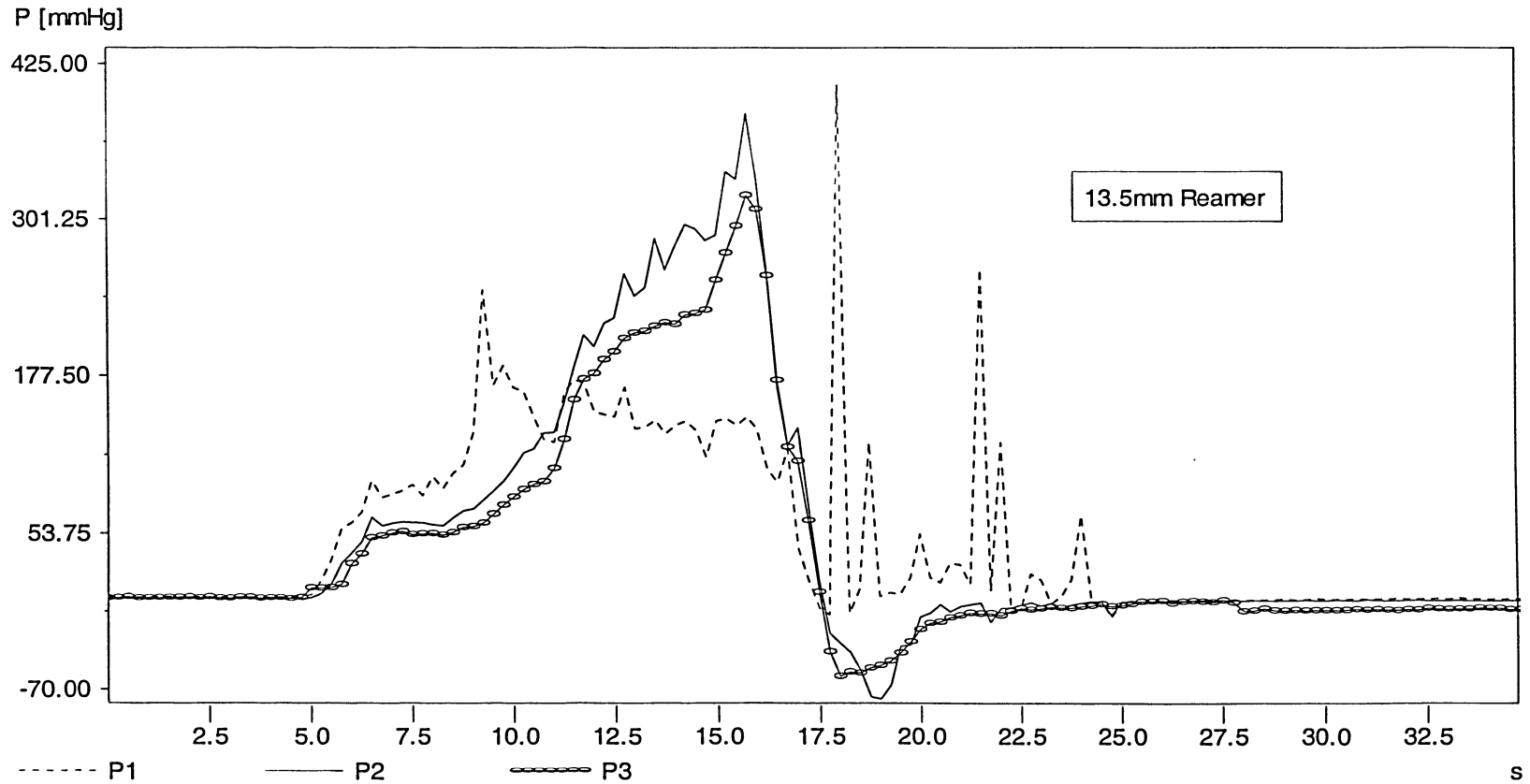

Figure B.39. Pressure variation using 13.5 mm clogged reamer, 200 RPM, 20 $\frac{mm}{sec}$ and high viscosity synthetic marrow (396 cP). P1, P2 and P3 are respectively corresponded to pressure transducer #1, 2 and 3. The reamer was clogged by fully covering the reamer flutes with silicon sealant.

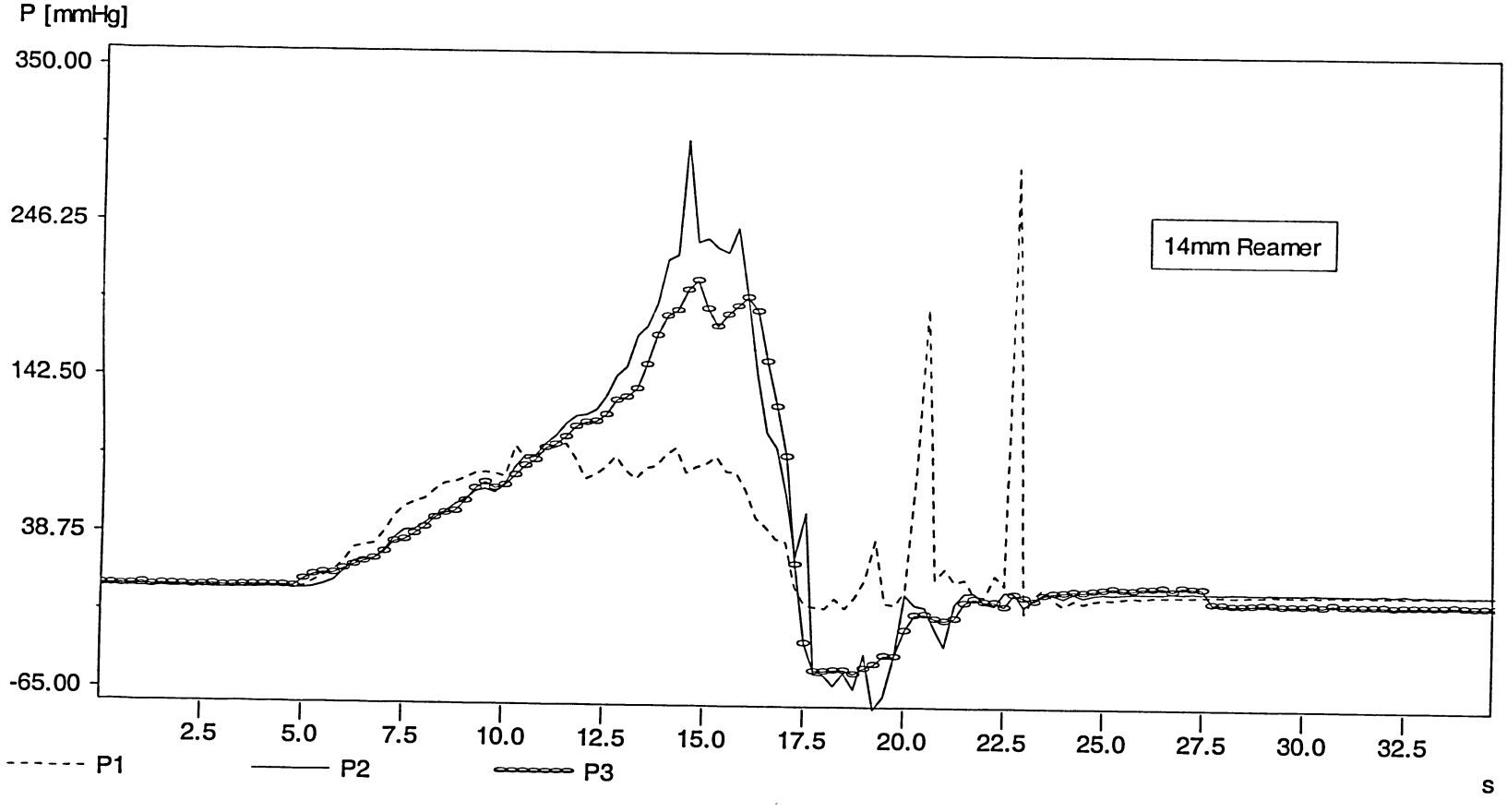

Figure B.40. Pressure variation using 14 mm clogged reamer, 200 RPM, 20 $\frac{mm}{sec}$ and high viscosity synthetic marrow (396 cP). P1, P2 and P3 are respectively corresponded to pressure transducer #1, 2 and 3. The reamer was clogged by fully covering the reamer flutes with silicon sealant.

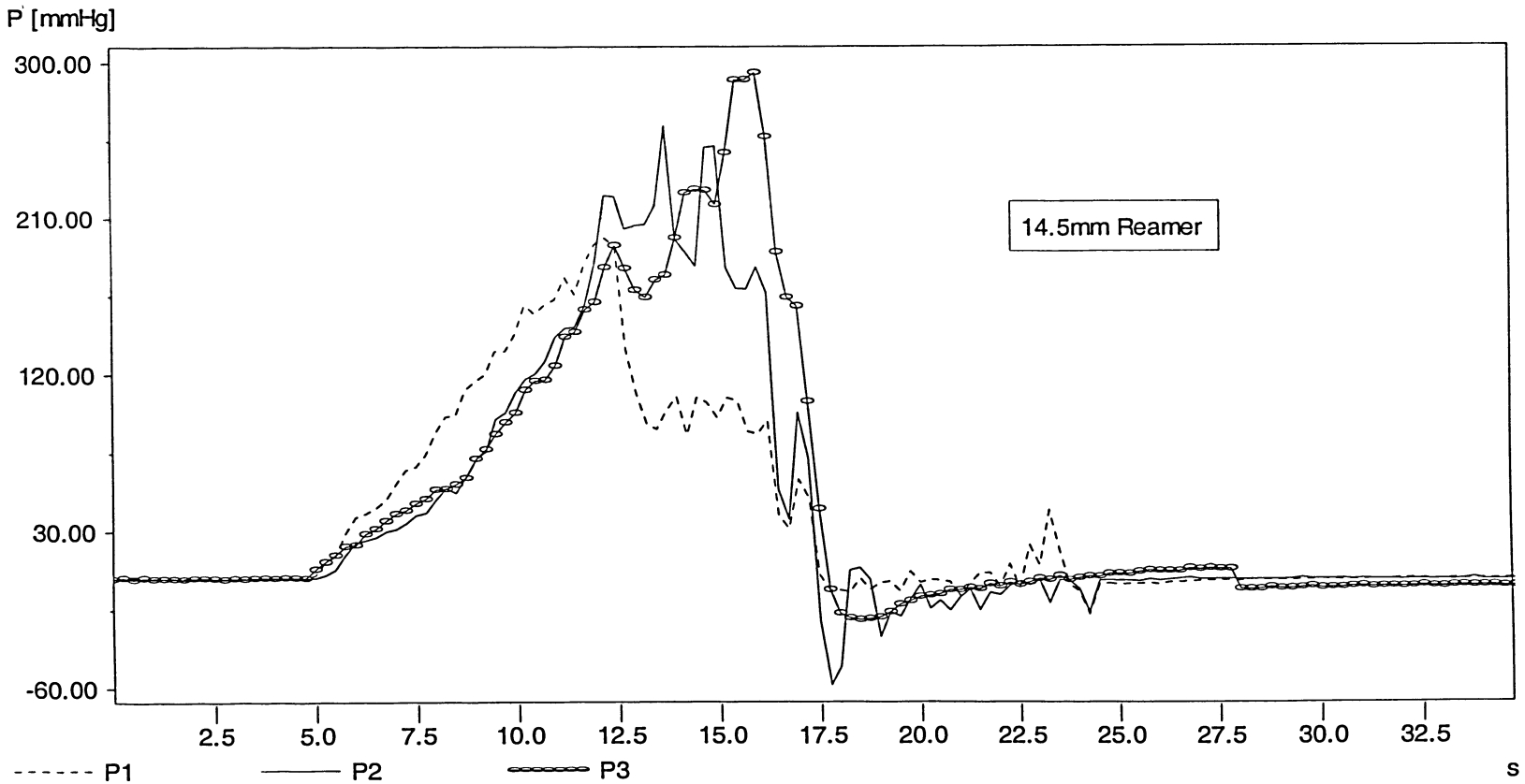

Figure B.41. Pressure variation using 14.5 mm clogged reamer, 200 RPM, 20 $\frac{mm}{sec}$ and high viscosity synthetic marrow (396 cP). P1, P2 and P3 are respectively corresponded to pressure transducer #1, 2 and 3. The reamer was clogged by fully covering the reamer flutes with silicon sealant.

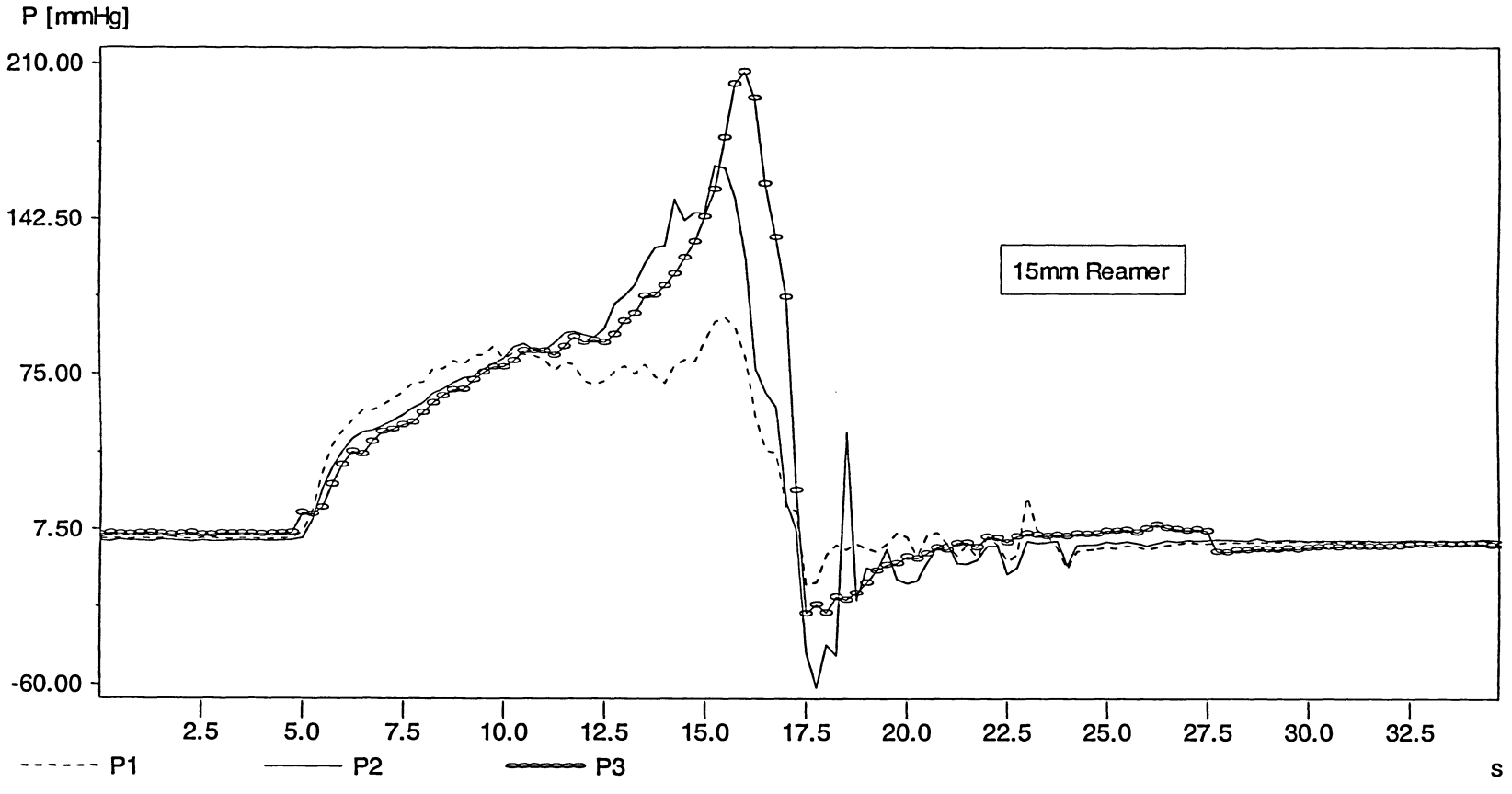

Figure B.42. Pressure variation using 15 mm clogged reamer, 200 RPM, 20 $\frac{mm}{sec}$ and high viscosity synthetic marrow (396 cP). P1, P2 and P3 are respectively corresponded to pressure transducer #1, 2 and 3. The reamer was clogged by fully covering the reamer flutes with silicon sealant.

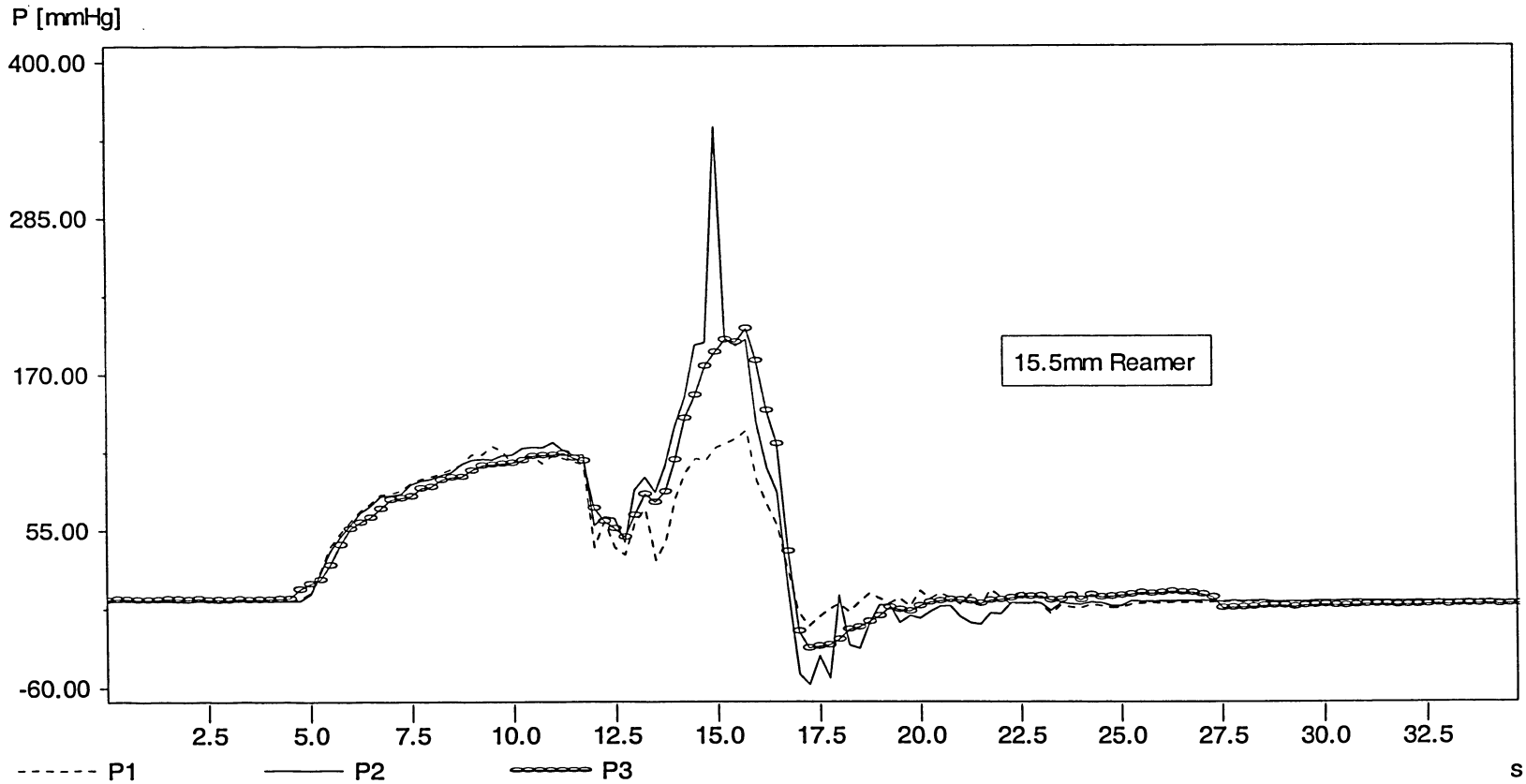

Figure B.43. Pressure variation using 15.5 mm clogged reamer, 200 RPM, 20 $\frac{mm}{sec}$ and high viscosity synthetic marrow (396 cP). P1, P2 and P3 are respectively corresponded to pressure transducer #1, 2 and 3. The reamer was clogged by fully covering the reamer flutes with silicon sealant.

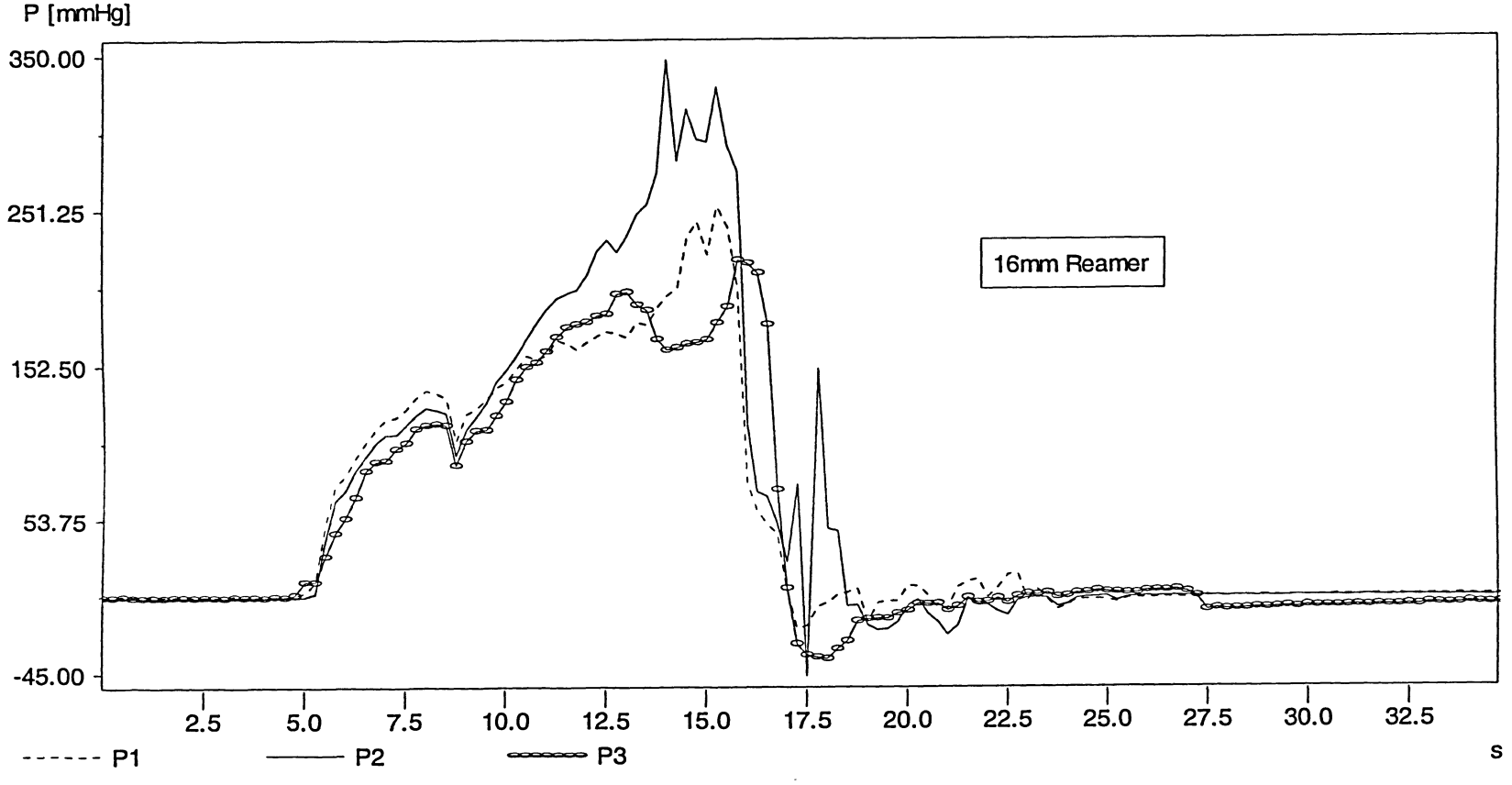

Figure B.44. Pressure variation using 16 mm clogged reamer, 200 RPM, 20 $\frac{mm}{sec}$ and high viscosity synthetic marrow (396 cP). P1, P2 and P3 are respectively corresponded to pressure transducer #1, 2 and 3. The reamer was clogged by fully covering the reamer flutes with silicon sealant.

Appendix C

Correlation Analysis

R_value 50_10	**P_1**	**P_2**	**P_3**	**F_x**	**F_y**	**F_z**	**Torque**	**P_{avg}**
P_1	1.0000							
P_2	0.7446	1.0000						
P_3	0.5851	0.8423	1.0000					
F_x	0.1433	0.4016	0.4222	1.0000				
F_y	0.0234	0.0192	-0.0863	0.1175	1.0000			
F_z	0.0785	0.3771	0.3687	0.6290	0.1139	1.0000		
Torque	0.2882	0.4901	0.4817	0.6133	0.0065	0.7954	1.0000	
P_{avg}	0.8090	0.9568	0.9318	0.3831	-0.0275	0.3320	0.4813	1.0000

Table C.1- Correlation coefficients for bone #1 (Reamed at 50 RPM and 10 $\frac{mm}{sec}$ advancement speed)

R^2 *50_10*	**P_1**	**P_2**	**P_3**	**F_x**	**F_y**	**F_z**	**Torque**	**P_{avg}**
P_1	100.00							
P_2	55.44	100.00						
P_3	34.23	70.95	100.00					
F_x	2.05	16.13	17.83	100.00				
F_y	0.05	0.04	0.74	1.38	100.00			
F_z	0.62	14.22	13.59	39.56	1.30	100.00		
Torque	8.31	24.02	23.20	37.61	0.00	**63.27**	100.00	
P_{avg}	65.45	91.55	86.83	**14.68**	**0.08**	**11.02**	**23.16**	100.00

Table C.2- Coefficients of determination for bone #1 (Reamed at 50 RPM and 10 $\frac{mm}{sec}$ advancement speed)

P_value 50_10	**P_1**	**P_2**	**P_3**	**F_x**	**F_y**	**F_z**	**Torque**	**P_{avg}**
P_1	1.0000							
P_2	0	1.0000						
P_3	0	0	1.0000					
F_x	0	0	0	1.0000				
F_y	0.5042	0.5845	0.0136	0.0008	1.0000			
F_z	0.0249	0	0	0	0.0011	1.0000		
Torque	0	0	0	0	0.8536	**0**	1.0000	
P_{avg}	0	0	0	**0**	**0.4317**	**0**	**0**	1.0000

Table C.3- p-values, Probability of error involved with accepting/rejecting the Null Hypothesis for bone #1 (Reamed at 50 RPM and 10 $\frac{mm}{sec}$ advancement speed)

R_value 50_50	P_1	P_2	P_3	F_x	F_y	F_z	Torque	P_{avg}
P_1	1.0000							
P_2	0.7919	1.0000						
P_3	0.3469	0.6573	1.0000					
F_x	-0.2828	-0.0868	0.1433	1.0000				
F_y	-0.2407	-0.2116	-0.0172	0.1288	1.0000			
F_z	-0.0556	-0.0141	0.0340	-0.2010	0.0479	1.0000		
Torque	-0.3375	-0.1994	-0.0770	0.3384	-0.0261	0.4741	1.0000	
P_{avg}	0.7660	0.9412	0.8436	-0.0451	-0.1609	-0.0049	-0.2119	1.0000

Table C.4-Correlation coefficients for bone #2 (Reamed at 50 RPM and 50 $\frac{mm}{sec}$ advancement speed)

R^2 *50_50*	P_1	P_2	P_3	F_x	F_y	F_z	Torque	P_{avg}
P_1	100.00							
P_2	62.71	100.00						
P_3	12.03	43.20	100.00					
F_x	8.00	0.75	2.05	100.00				
F_y	5.79	4.48	0.03	1.66	100.00			
F_z	0.31	0.02	0.12	4.04	0.23	100.00		
Torque	11.39	3.98	0.59	11.45	0.07	**22.48**	100.00	
P_{avg}	58.68	88.59	71.17	**0.20**	**2.59**	**0.00**	**4.49**	100.00

Table C.5-Coefficients of determination for bone #2 (Reamed at 50 RPM and 50 $\frac{mm}{sec}$ advancement speed)

P_value 50_50	P_1	P_2	P_3	F_x	F_y	F_z	Torque	P_{avg}
P_1	1.0000							
P_2	0	1.0000						
P_3	0	0	1.0000					
F_x	0	0	0	1.0000				
F_y	0	0	0.3932	0	1.0000			
F_z	0.0057	0.4836	0.0913	0	0.0175	1.0000		
Torque	0	0	0.0001	0	0.1951	**0**	1.0000	
P_{avg}	0	0	0	**0.0253**	**0**	**0.8092**	**0**	1.0000

Table C.6-p-values, Probability of error involved with accepting/rejecting the Null Hypothesis for bone #2 (Reamed at 50 RPM and 50 $\frac{mm}{sec}$ advancement speed)

R_value 200_10	P_1	P_2	P_3	F_x	F_y	F_z	Torque	P_{avg}
P_1	1.0000							
P_2	0.7005	1.0000						
P_3	0.7335	0.8260	1.0000					
F_x	0.0393	0.3403	0.2258	1.0000				
F_y	-0.13	-0.181	-0.107	-0.524	1.0000			
F_z	-0.076	0.2275	0.1917	0.6026	-0.235	1.0000		
Torque	-0.094	-0.151	0.0095	0.1281	-0.24	0.2388	1.0000	
P_{avg}	0.9060	0.9180	0.9144	0.2111	-0.156	0.1084	-0.095	1.0000

Table C.7- Correlation coefficients for bone #3 (Reamed at 200 RPM and 10 $\frac{mm}{sec}$ advancement speed)

R^2 (%) *200_10*	P_1	P_2	P_3	F_x	F_y	F_z	Torque	P_{avg}
P_1	100.00							
P_2	49.07	100.00						
P_3	53.80	68.23	100.00					
F_x	0.15	11.58	5.10	100.00				
F_y	1.69	3.28	1.14	27.46	100.00			
F_z	0.58	5.18	3.67	36.31	5.52	100.00		
Torque	0.88	2.28	0.01	1.64	5.76	**5.70**	100.00	
P_{avg}	82.08	84.27	83.61	**4.46**	**2.43**	**1.18**	**0.90**	100.00

Table C.8- Coefficients of determination for bone #3 (Reamed at 200 RPM and 10 $\frac{mm}{sec}$ advancement speed)

P_value 200_10	P_1	P_2	P_3	F_x	F_y	F_z	Torque	P_{avg}
P_1	1.0000							
P_2	0	1.0000						
P_3	0	0	1.0000					
F_x	0.2894	0	0	1.0000				
F_y	0.0004	0	0.0039	0	1.0000			
F_z	0.0395	0	0	0	0	1.0000		
Torque	0.0114	0	0.7972	0.0005	0	**0**	1.0000	
P_{avg}	0	0	0	**0**	**0**	**0.0034**	**0.0100**	1.0000

Table C.9- p-values, Probability of error involved with accepting/rejecting the Null Hypothesis for bone #3 (Reamed at 200 RPM and 10 $\frac{mm}{sec}$ advancement speed)

R_value 200_50	P_1	P_2	P_3	F_x	F_y	F_z	Torque	P_{avg}
P_1	1.0000							
P_2	0.6434	1.0000						
P_3	0.4003	0.4926	1.0000					
F_x	-0.1031	-0.1129	-0.1976	1.0000				
F_y	-0.0191	-0.1707	-0.0729	0.1334	1.0000			
F_z	-0.2383	-0.2321	0.1823	0.0375	0.0128	1.0000		
Torque	-0.2788	-0.2348	0.1089	-0.0923	-0.0532	0.8714	1.0000	
P_{avg}	0.7487	0.8696	0.8243	-0.1762	-0.1200	-0.0775	-0.1253	1.0000

Table C.10- Correlation coefficients for bone #4 (Reamed at 200 RPM and 50 $\frac{mm}{sec}$ advancement speed)

R^2 *200_50*	P_1	P_2	P_3	F_x	F_y	F_z	Torque	P_{avg}
P_1	100.00							
P_2	41.40	100.00						
P_3	16.02	24.27	100.00					
F_x	1.06	1.27	3.90	100.00				
F_y	0.04	2.91	0.53	1.78	100.00			
F_z	5.68	5.39	3.32	0.14	0.02	100.00		
Torque	7.77	5.51	1.19	0.85	0.28	**75.93**	100.00	
P_{avg}	56.06	75.62	67.95	**3.10**	**1.44**	**0.60**	**1.57**	100.00

Table C.11- Coefficients of determination for bone #4 (Reamed at 200 RPM and 50 $\frac{mm}{sec}$ advancement speed)

P_value 200_50	P_1	P_2	P_3	F_x	F_y	F_z	Torque	P_{avg}
P_1	1.0000							
P_2	0	1.0000						
P_3	0	0	1.0000					
F_x	0	0	0	1.0000				
F_y	0.4815	0	0.0070	0.0000	1.0000			
F_z	0	0	0	0.1657	0.6354	1.0000		
Torque	0	0	0.0001	0.0006	0.0491	**0**	1.0000	
P_{avg}	0	0	0	**0**	**0**	**0.0042**	**0**	1.0000

Table C.12- p-values, Probability of error involved with accepting/rejecting the Null Hypothesis for bone #4 (Reamed at 200 RPM and 50 $\frac{mm}{sec}$ advancement speed)

Appendix D

Force Profiles

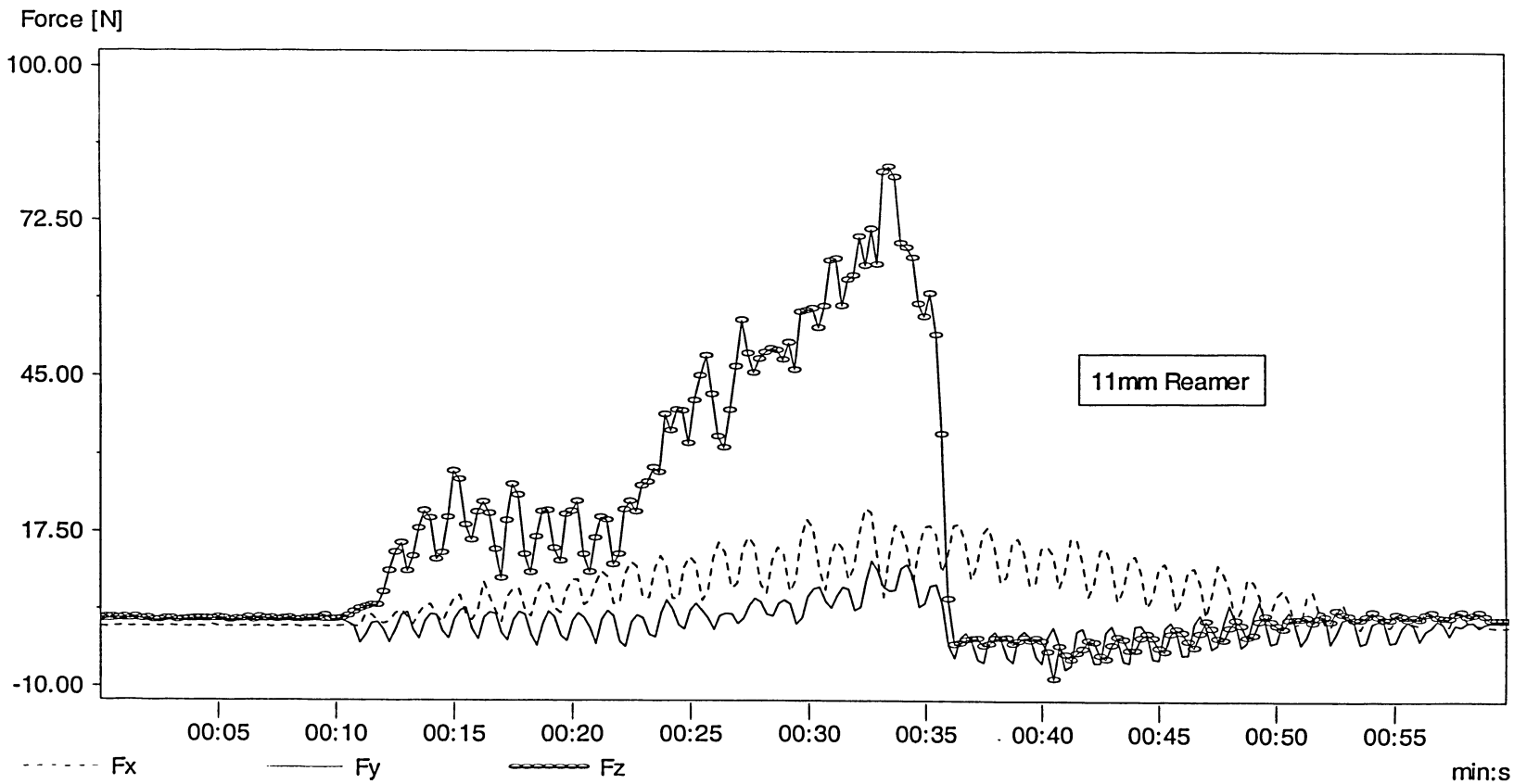

Figure D.45. Force profiles using 11mm reamer, 50 RPM, 10 $\frac{mm}{sec}$ and 82.6 cP synthetic marrow viscosity. F_x, F_y and F_z are respectively corresponded to forces applied to the closed end of the bone in x, y, and z directions.

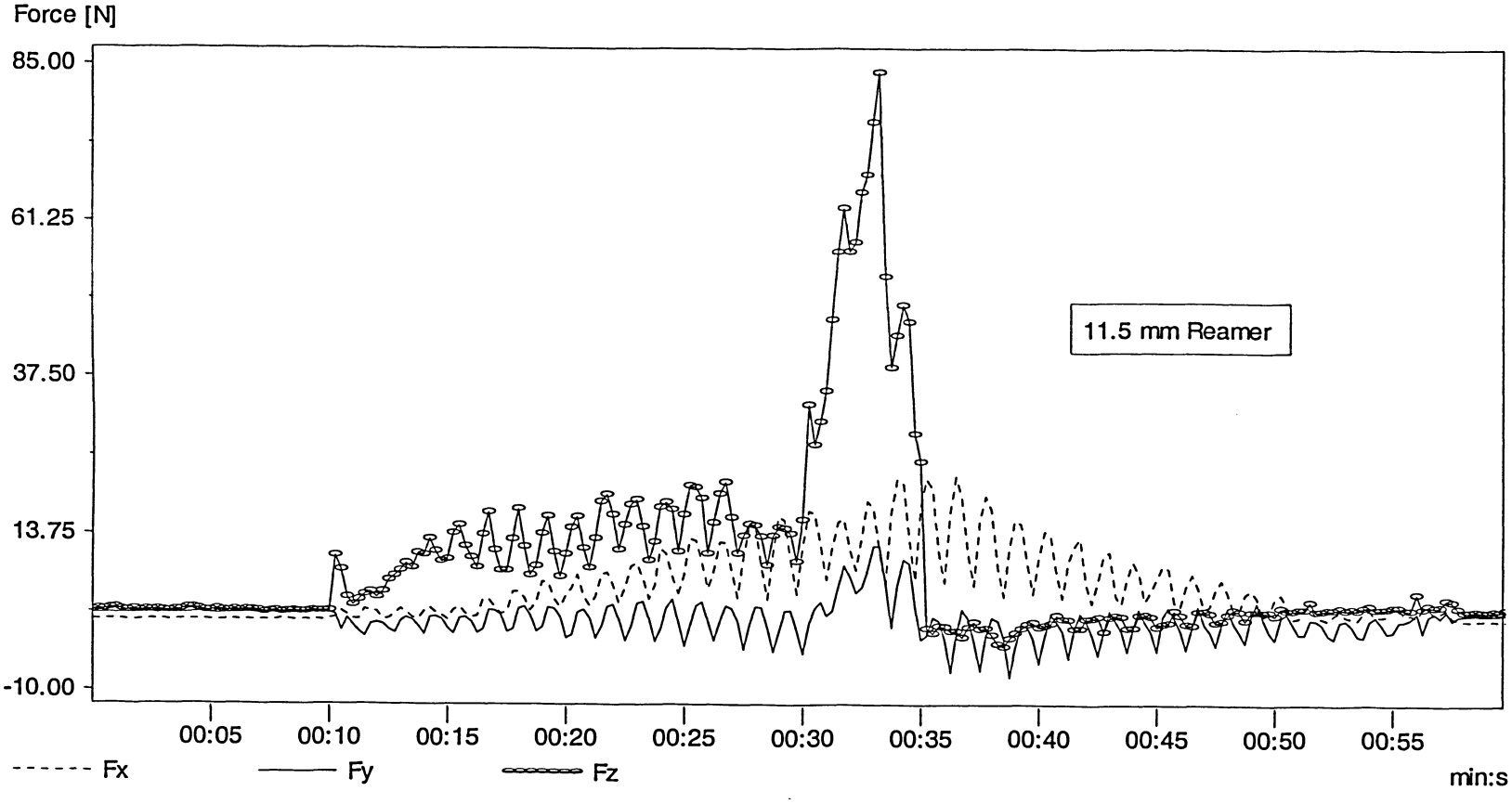

Figure D.46. Force profiles using 11.5 mm reamer, 50 RPM, 10 $\frac{mm}{sec}$ and 82.6 cP synthetic marrow viscosity. F_x, F_y and F_z are respectively corresponded to forces applied to the closed end of the bone in x, y, and z directions.

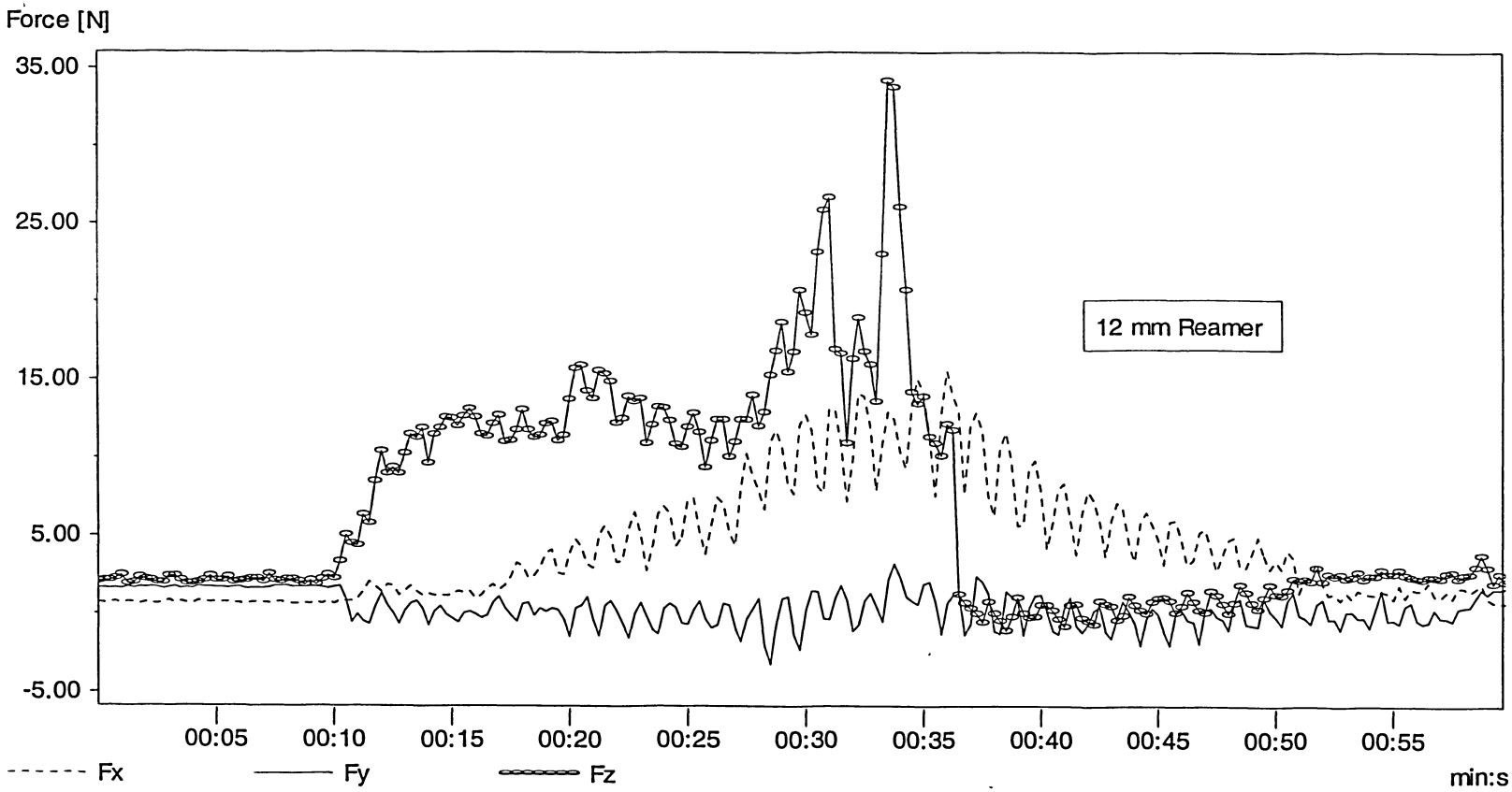

Figure D.47. Force profiles using 12mm reamer, 50 RPM, 10 $\frac{mm}{sec}$ and 82.6 cP synthetic marrow viscosity. F_x, F_y and F_z are respectively corresponded to forces applied to the closed end of the bone in x, y, and z directions.

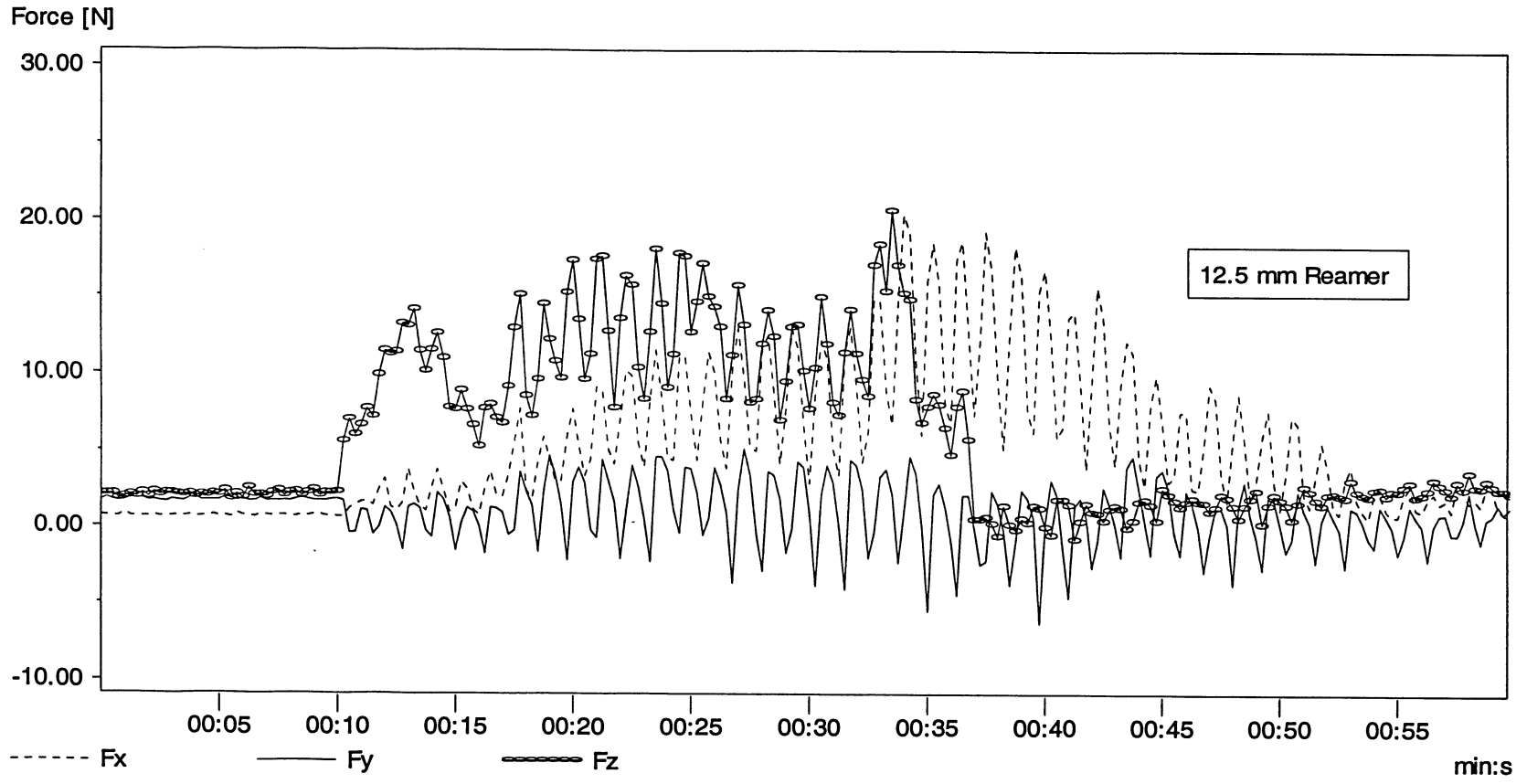

Figure D.48. Force profiles using 12.5 mm reamer, 50 RPM, 10 $\frac{mm}{sec}$ and 82.6 cP synthetic marrow viscosity. F_x, F_y and F_z are respectively corresponded to forces applied to the closed end of the bone in x, y, and z directions.

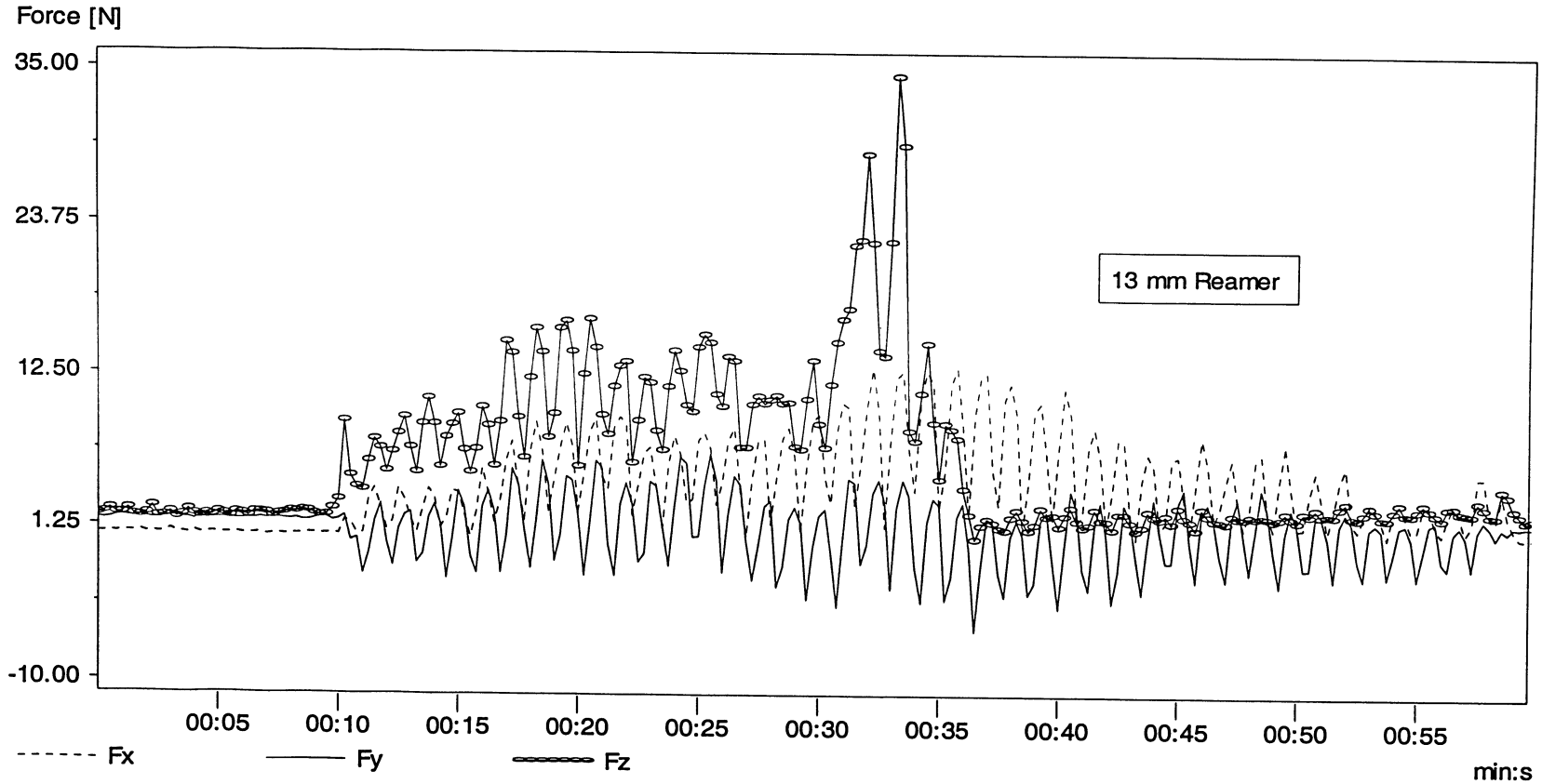

Figure D.49. Force profiles using 13mm reamer, 50 RPM, 10 $\frac{mm}{sec}$ and 82.6 cP synthetic marrow viscosity. F_x, F_y and F_z are respectively corresponded to forces applied to the closed end of the bone in x, y, and z directions.

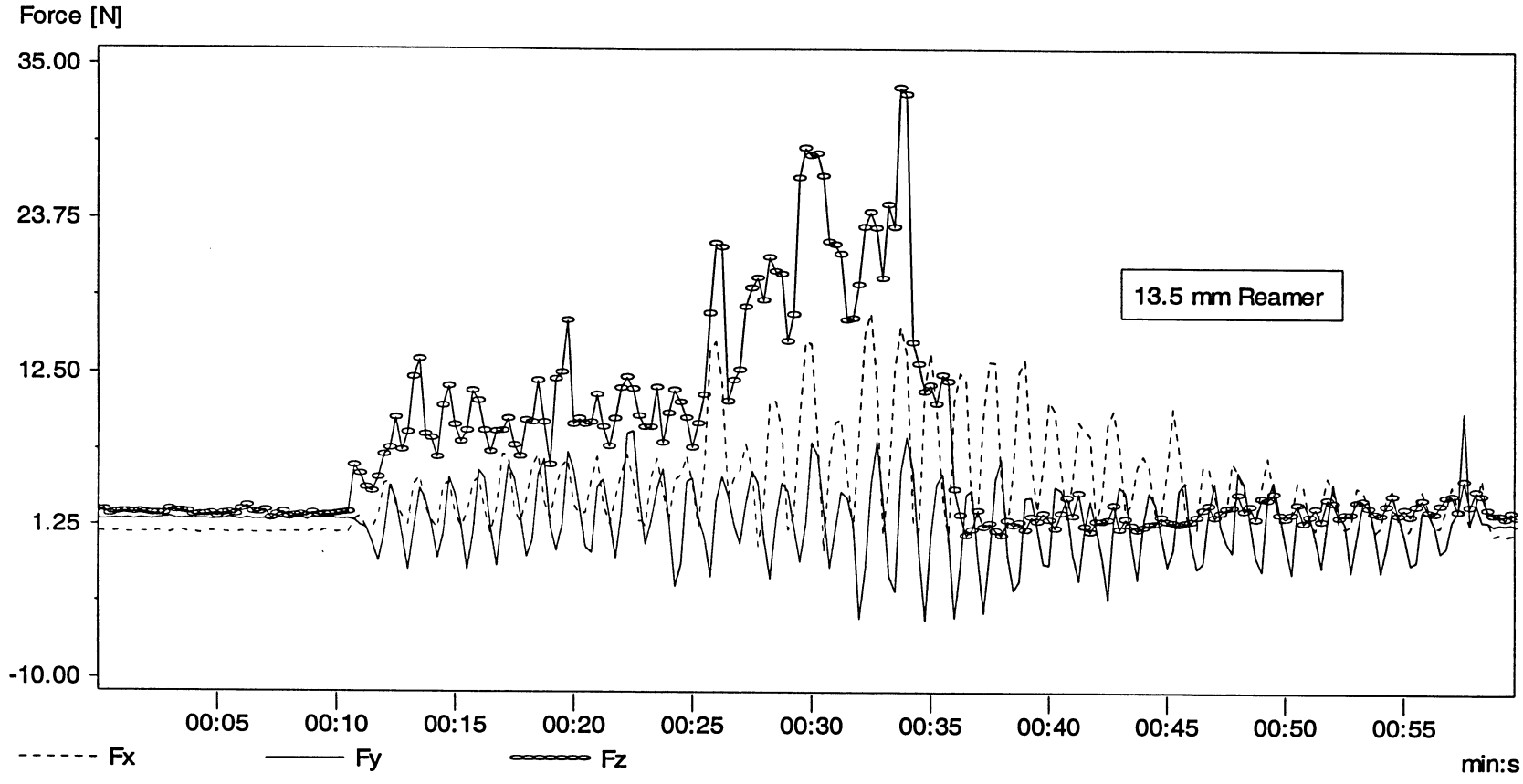

Figure D.50. Force profiles using 13.5 mm reamer, 50 RPM, 10 $\frac{mm}{sec}$ and 82.6 cP synthetic marrow viscosity. F_x, F_y and F_z are respectively corresponded to forces applied to the closed end of the bone in x, y, and z directions.

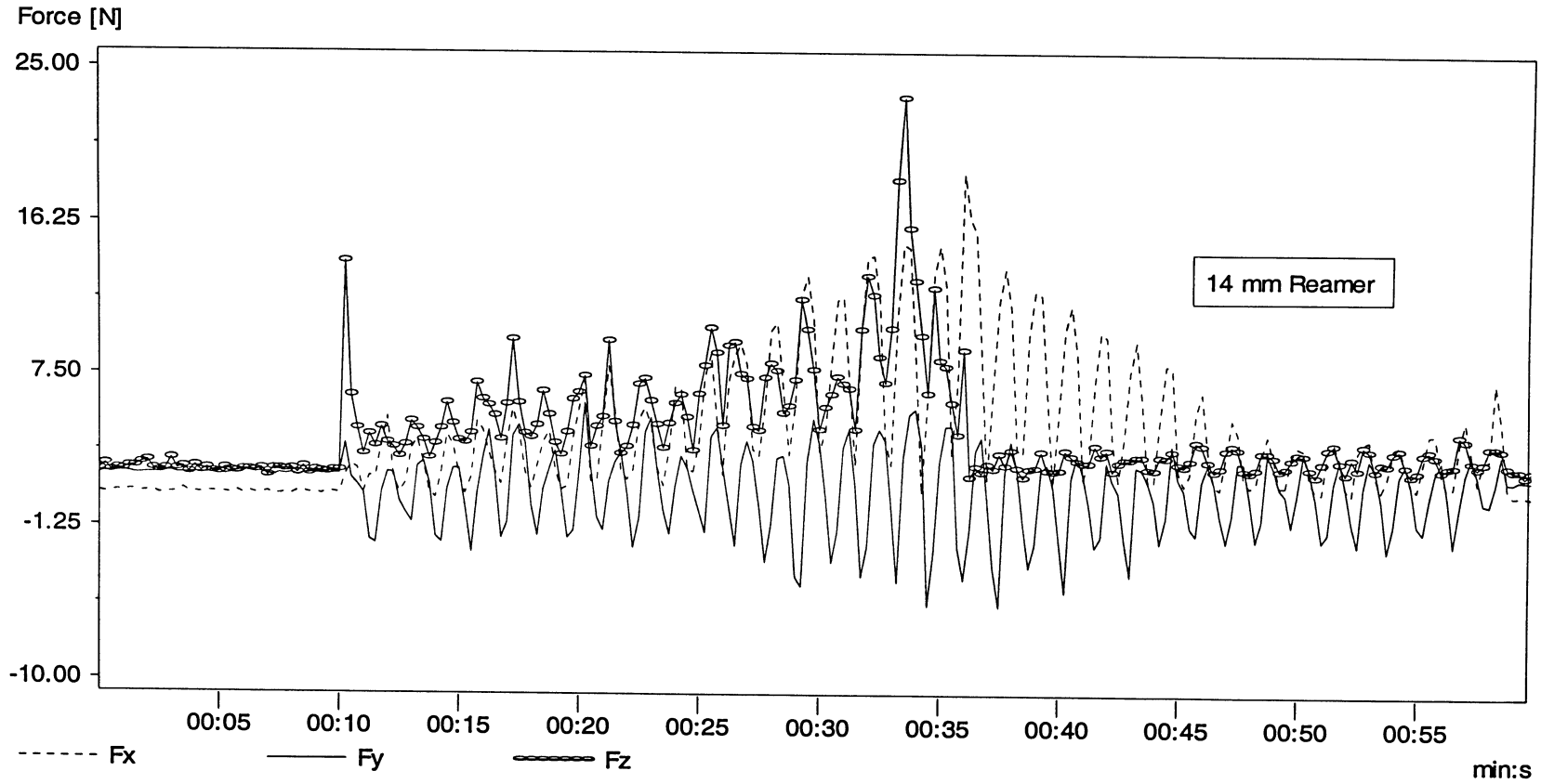

Figure D.51. Force profiles using 14 mm reamer, 50 RPM, 10 $\frac{mm}{sec}$ and 82.6 cP synthetic marrow viscosity. F_x, F_y and F_z are respectively corresponded to forces applied to the closed end of the bone in x, y, and z directions.

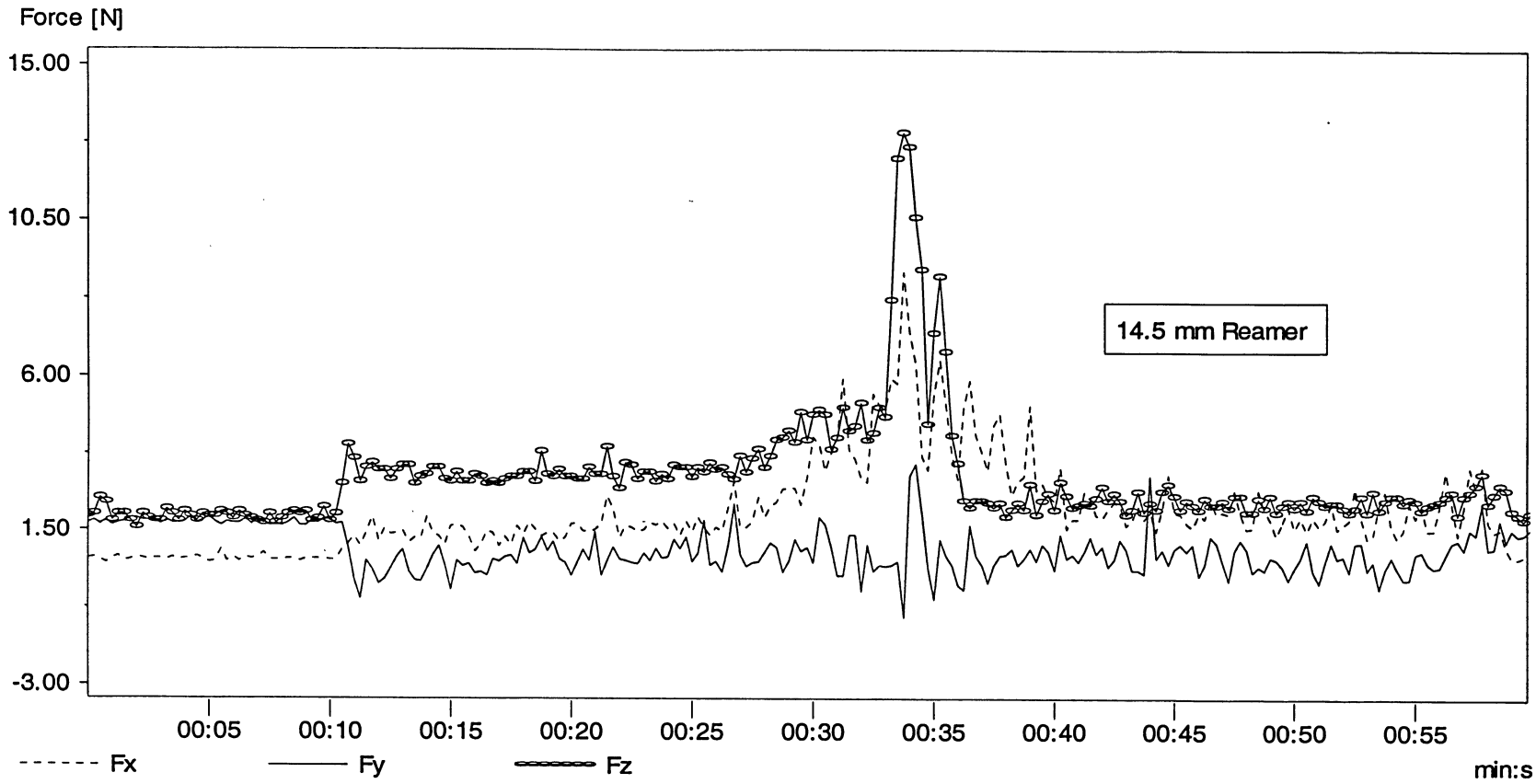

Figure D.52. Force profiles using 14.5 mm reamer, 50 RPM, 10 $\frac{mm}{sec}$ and 82.6 cP synthetic marrow viscosity. F_x, F_y and F_z are respectively corresponded to forces applied to the closed end of the bone in x, y, and z directions.

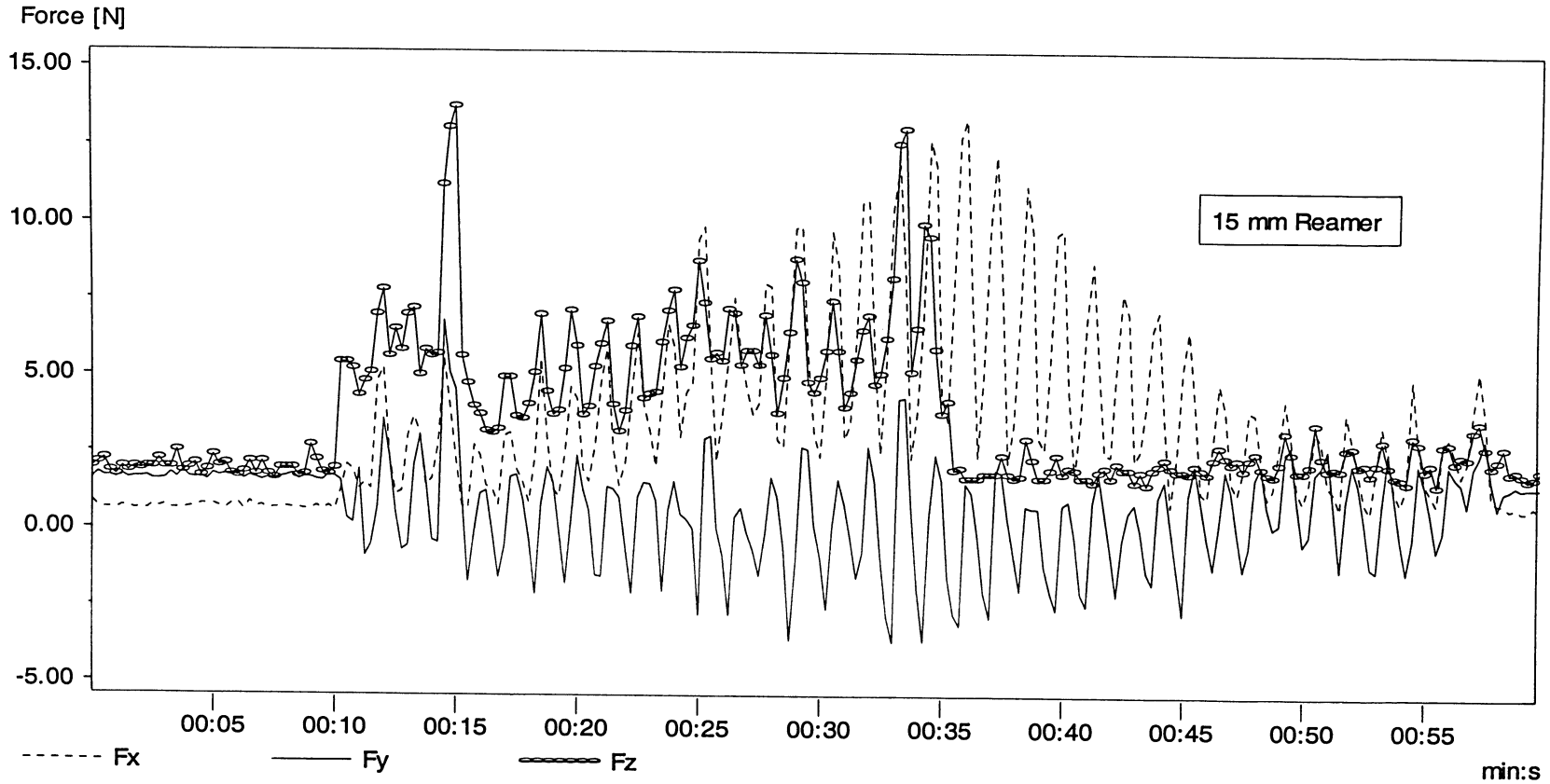

Figure D.53. Force profiles using 15 mm reamer, 50 RPM, 10 $\frac{mm}{sec}$ and 82.6 cP synthetic marrow viscosity. F_x, F_y and F_z are respectively corresponded to forces applied to the closed end of the bone in x, y, and z directions.

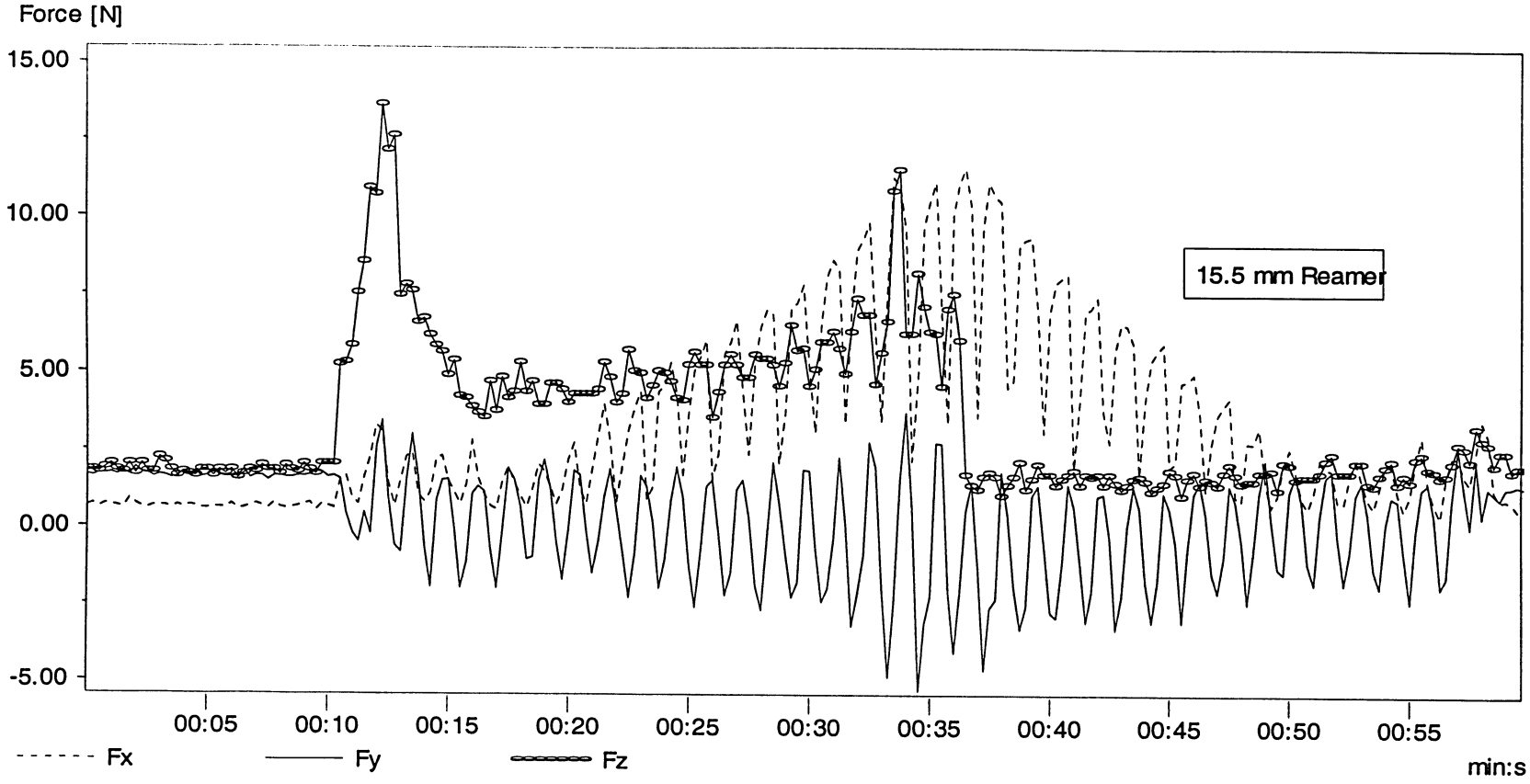

Figure D.54. Force profiles using 15.5 mm reamer, 50 RPM, 10 $\frac{mm}{sec}$ and 82.6 cP synthetic marrow viscosity. F_x, F_y and F_z are respectively corresponded to forces applied to the closed end of the bone in x, y, and z directions.

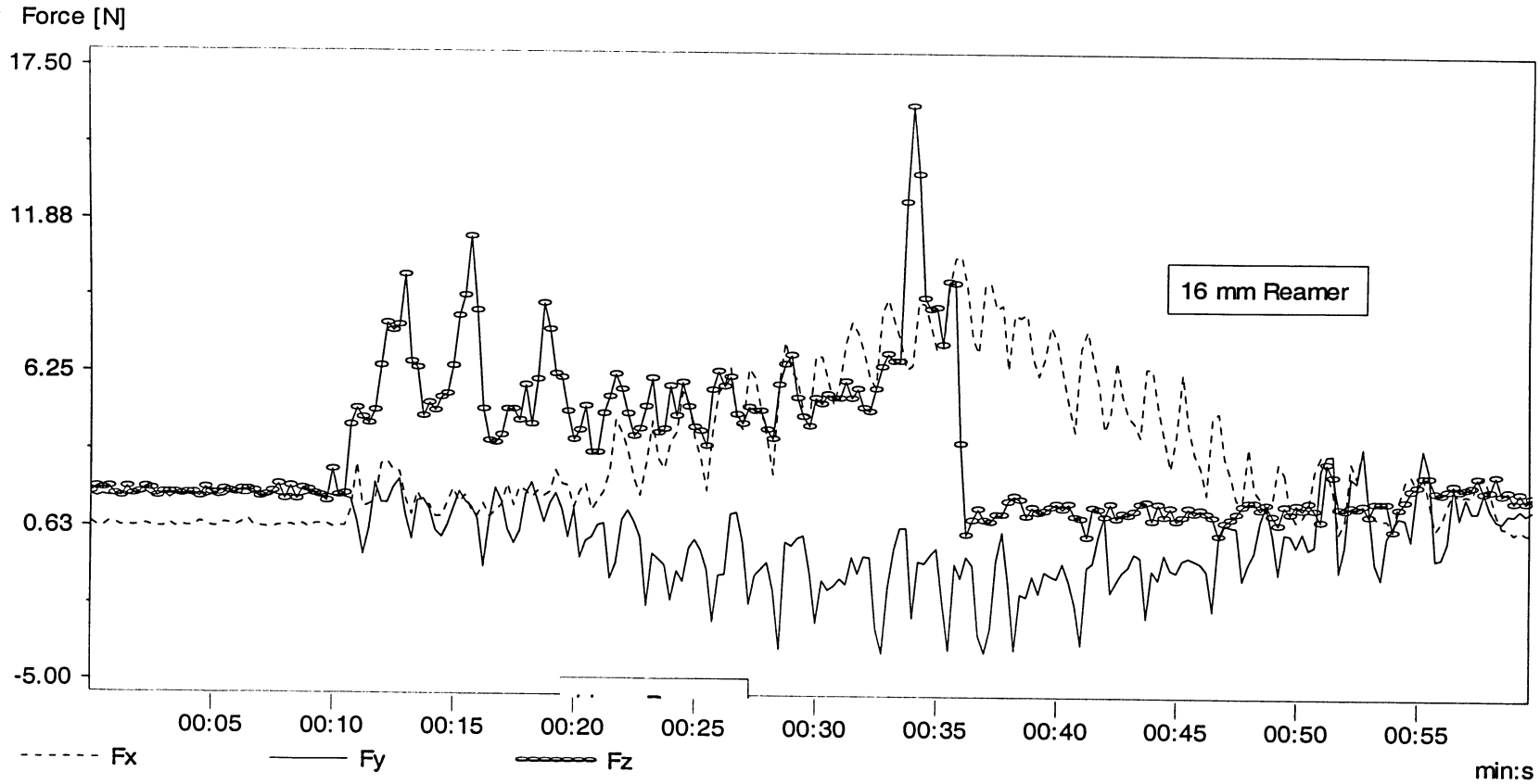

Figure D.55. Force profiles using 16 mm reamer, 50 RPM, 10 $\frac{mm}{sec}$ and 82.6 cP synthetic marrow viscosity. F_x, F_y and F_z are respectively corresponded to forces applied to the closed end of the bone in x, y, and z directions.

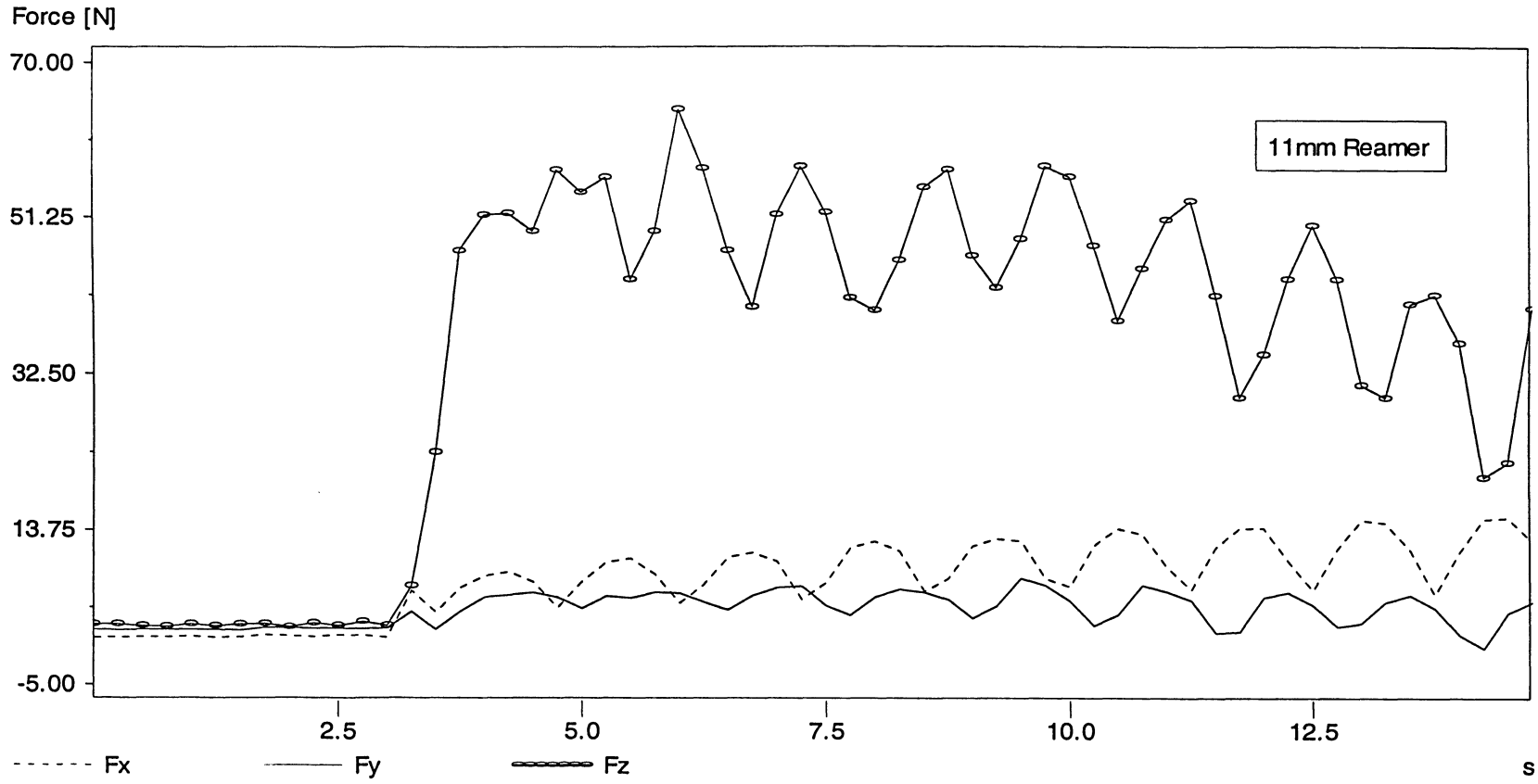

Figure D.56. Force profiles using 11 mm reamer, 50 RPM, 50 $\frac{mm}{sec}$ and 82.6 cP synthetic marrow viscosity. F_x, F_y and F_z are respectively corresponded to forces applied to the closed end of the bone in x, y, and z directions.

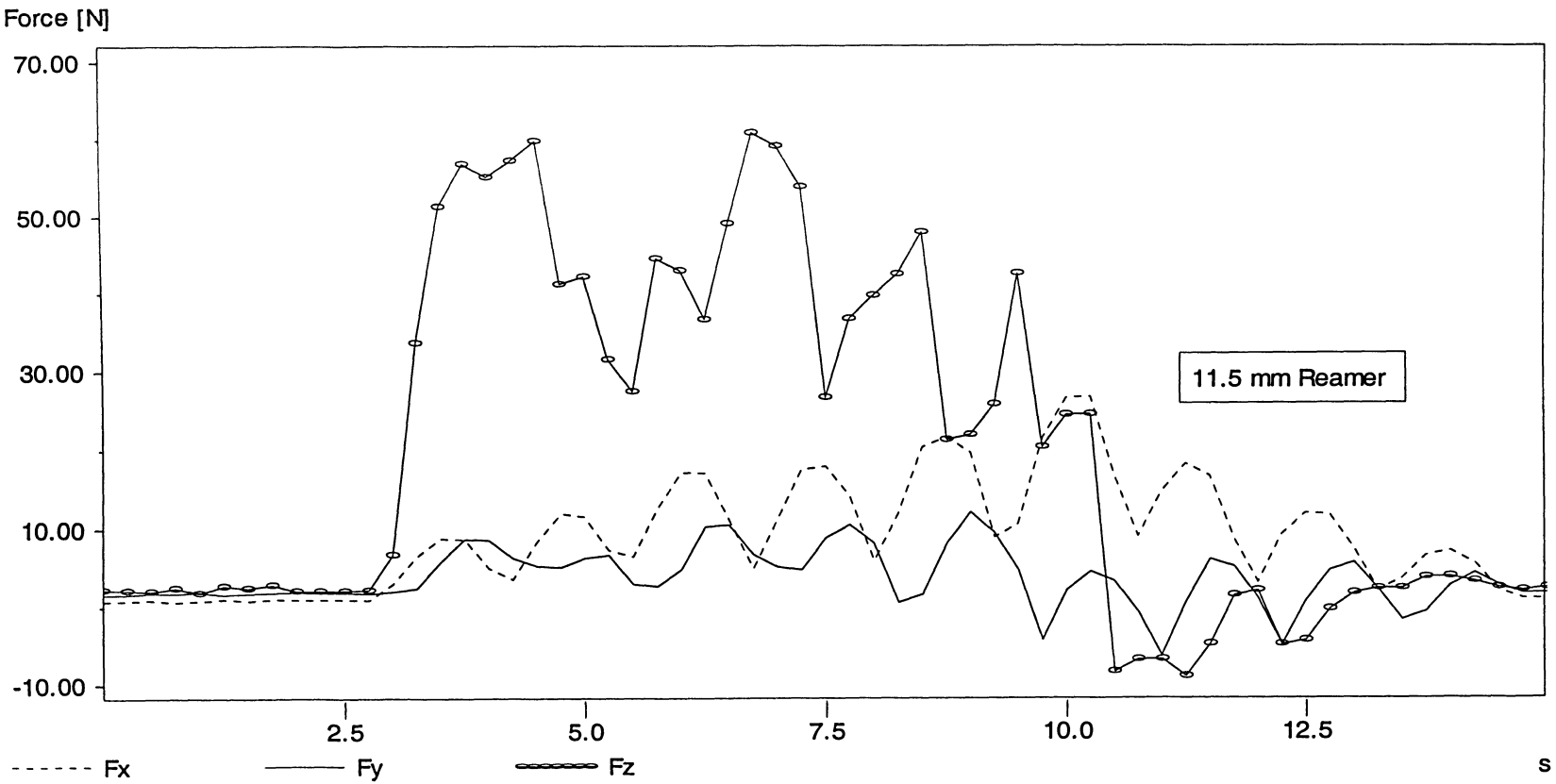

Figure D.57. Force profiles using 11.5 mm reamer, 50 RPM, 50 $\frac{mm}{sec}$ and 82.6 cP synthetic marrow viscosity. F_x, F_y and F_z are respectively corresponded to forces applied to the closed end of the bone in x, y, and z directions.

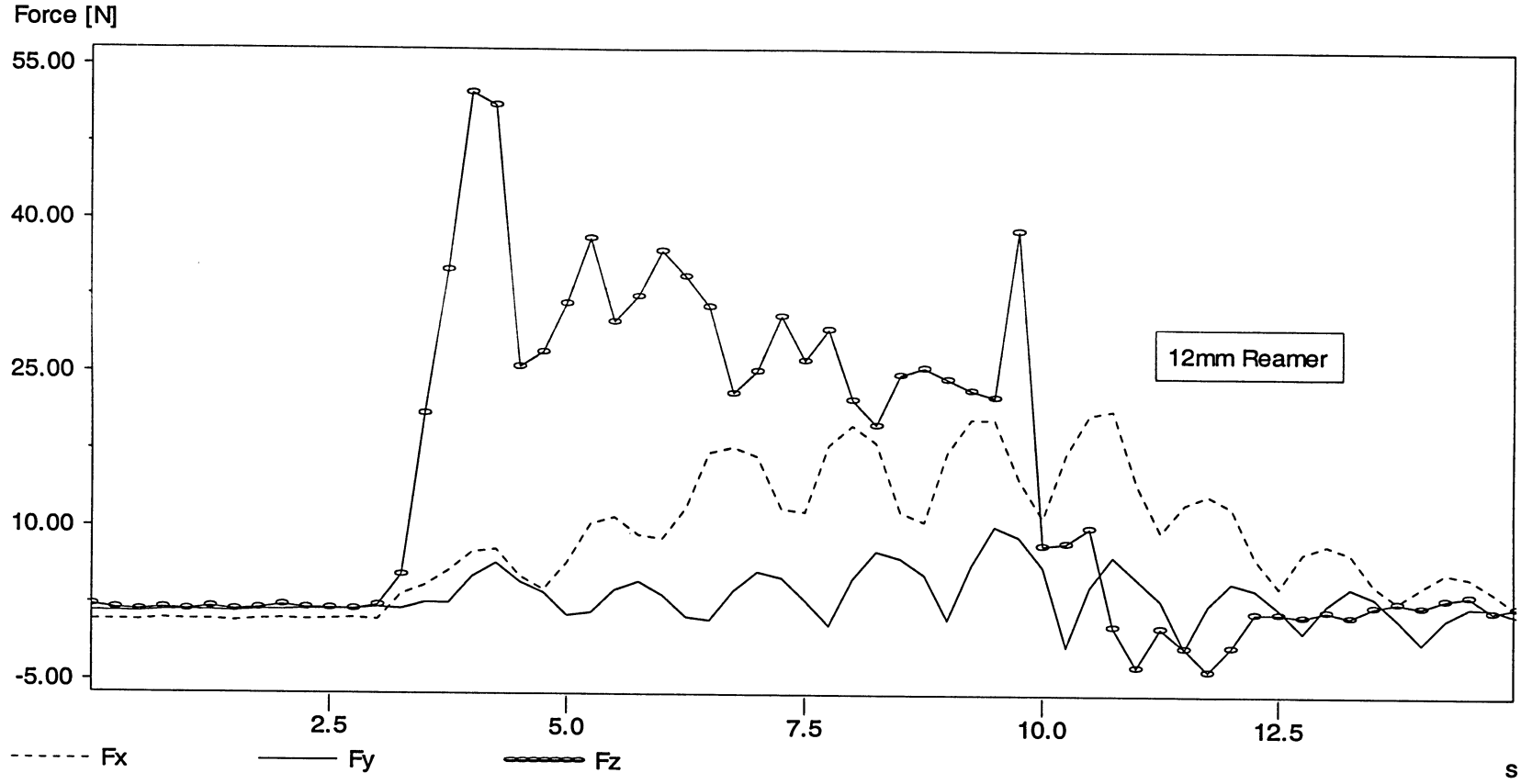

Figure D.58. Force profiles using 12 mm reamer, 50 RPM, 50 $\frac{mm}{sec}$ and 82.6 cP synthetic marrow viscosity. F_x, F_y and F_z are respectively corresponded to forces applied to the closed end of the bone in x, y, and z directions.

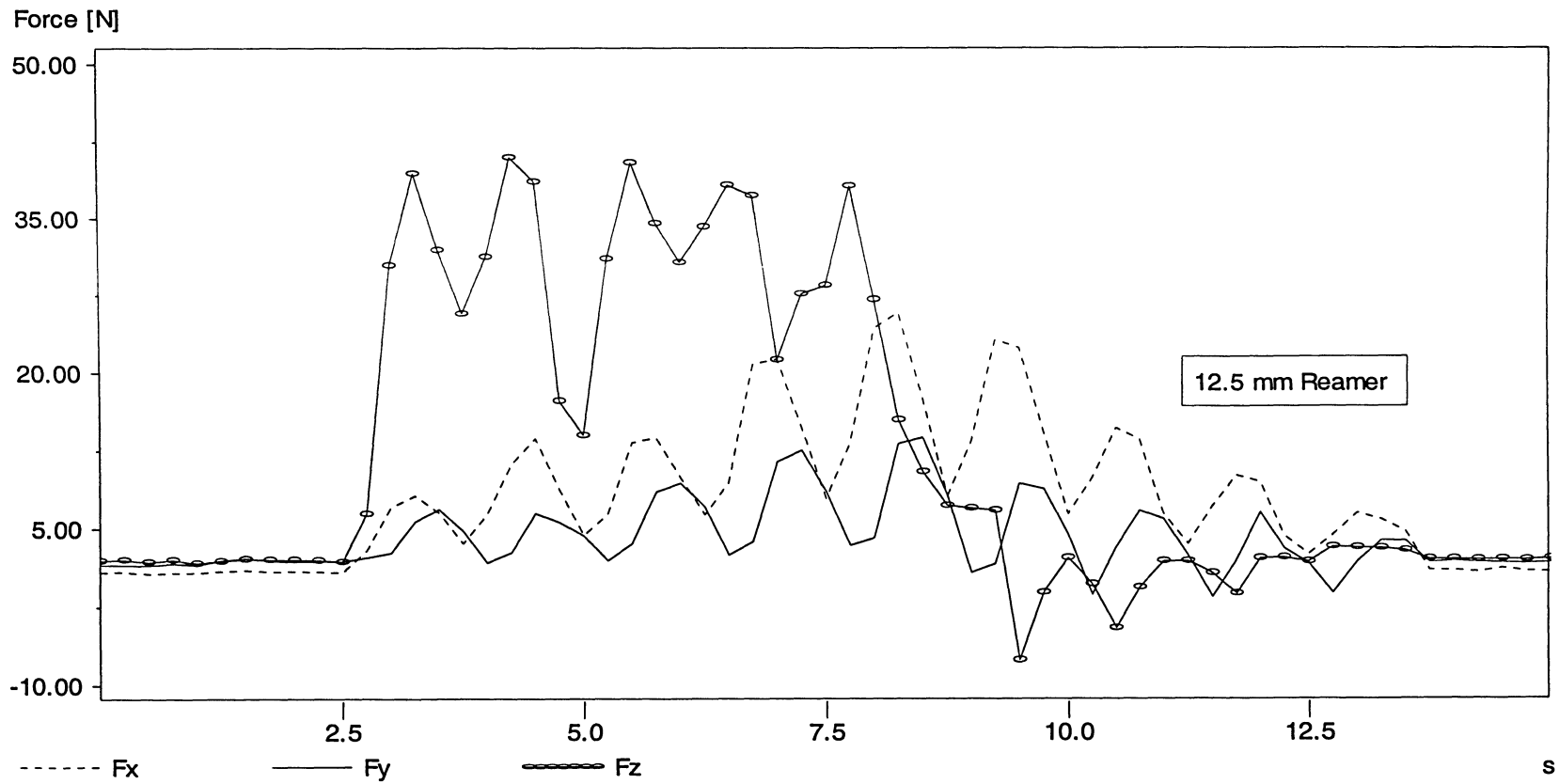

Figure D.59. Force profiles using 12.5 mm reamer, 50 RPM, 50 $\frac{mm}{sec}$ and 82.6 cP synthetic marrow viscosity. F_x, F_y and F_z are respectively corresponded to forces applied to the closed end of the bone in x, y, and z directions.

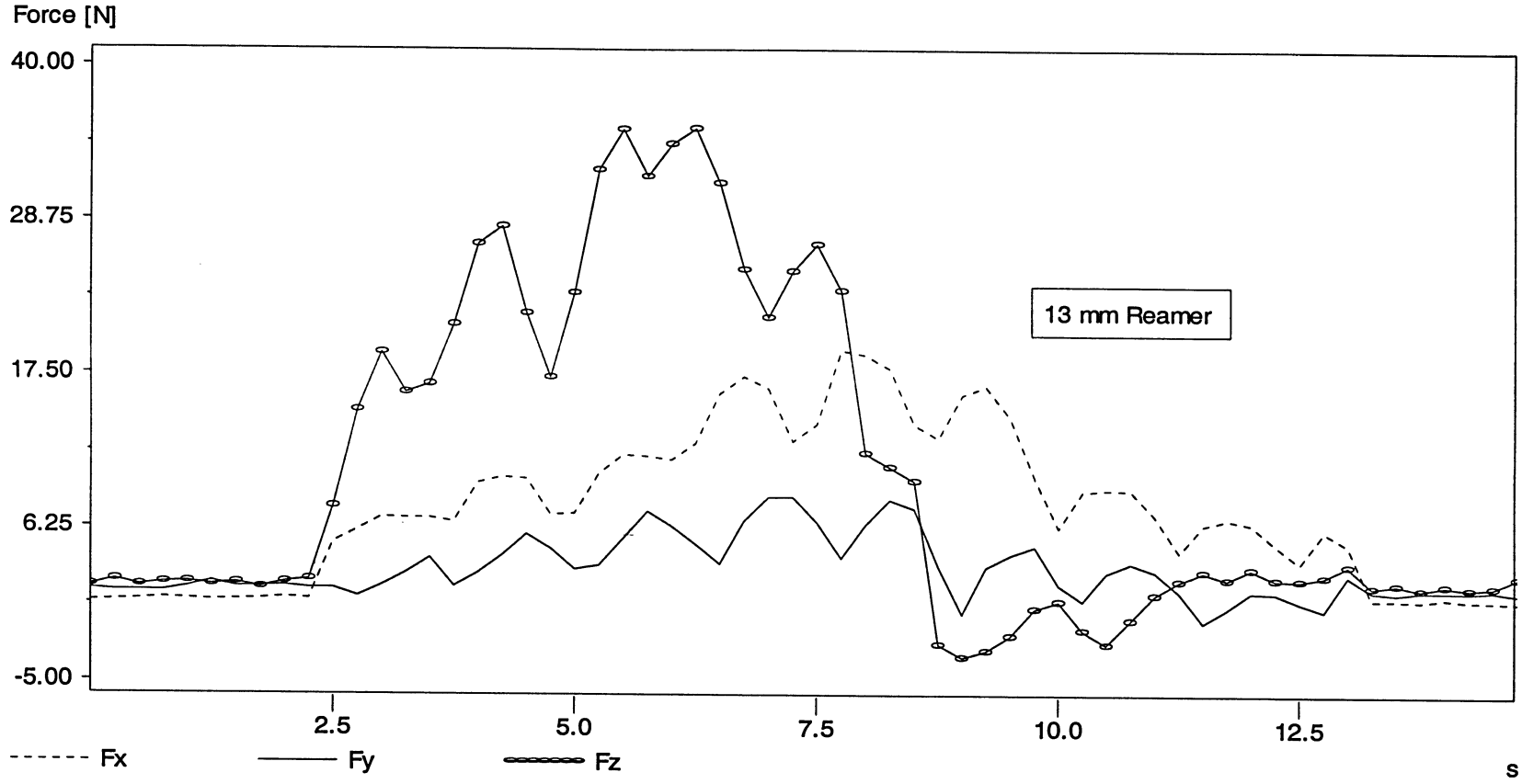

Figure D.60. Force profiles using 13 mm reamer, 50 RPM, 50 $\frac{mm}{sec}$ and 82.6 cP synthetic marrow viscosity. F_x, F_y and F_z are respectively corresponded to forces applied to the closed end of the bone in x, y, and z directions.

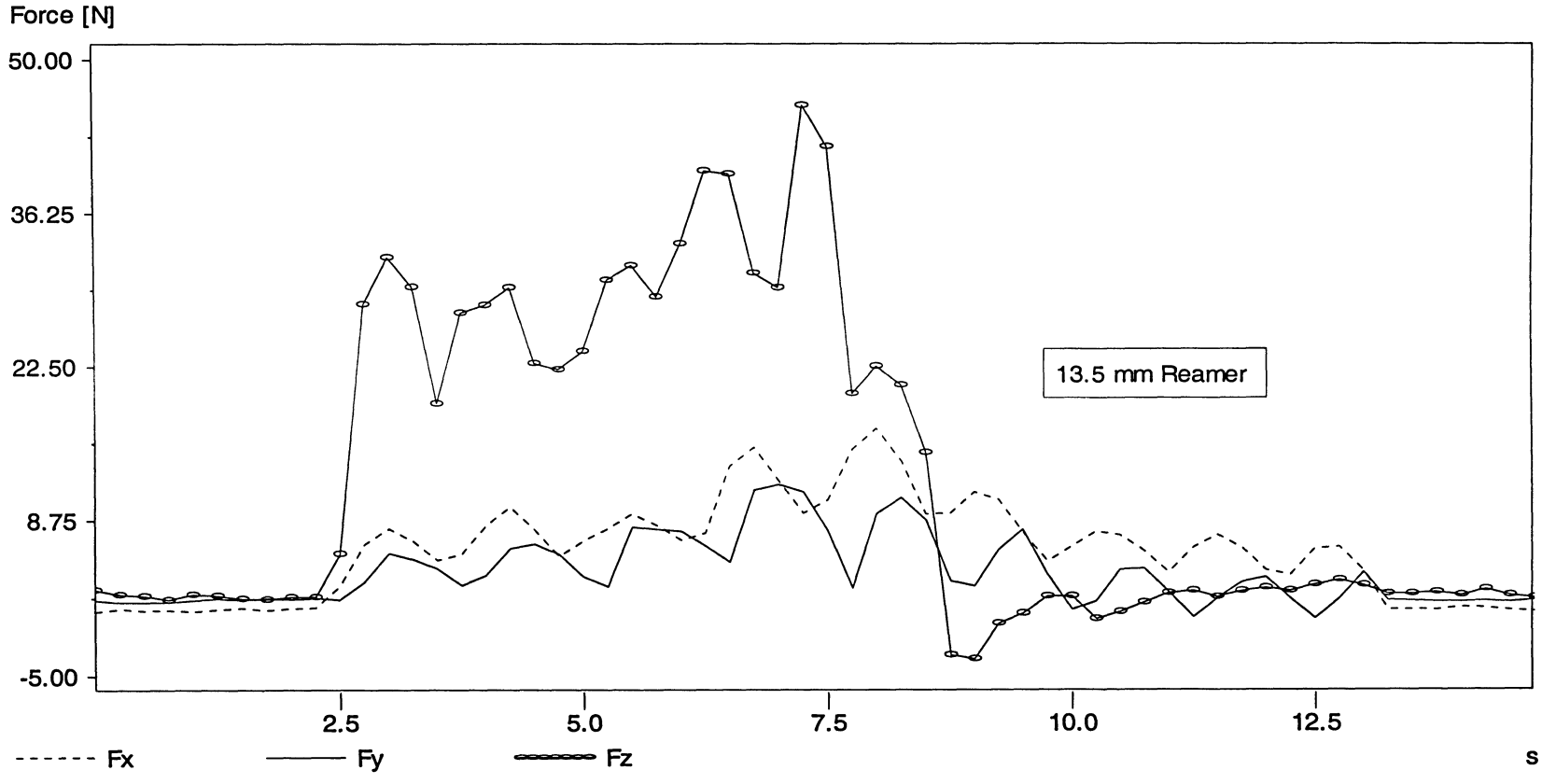

Figure D.61. Force profiles using 13.5 mm reamer, 50 RPM, 50 $\frac{mm}{sec}$ and 82.6 cP synthetic marrow viscosity. F_x, F_y and F_z are respectively corresponded to forces applied to the closed end of the bone in x, y, and z directions.

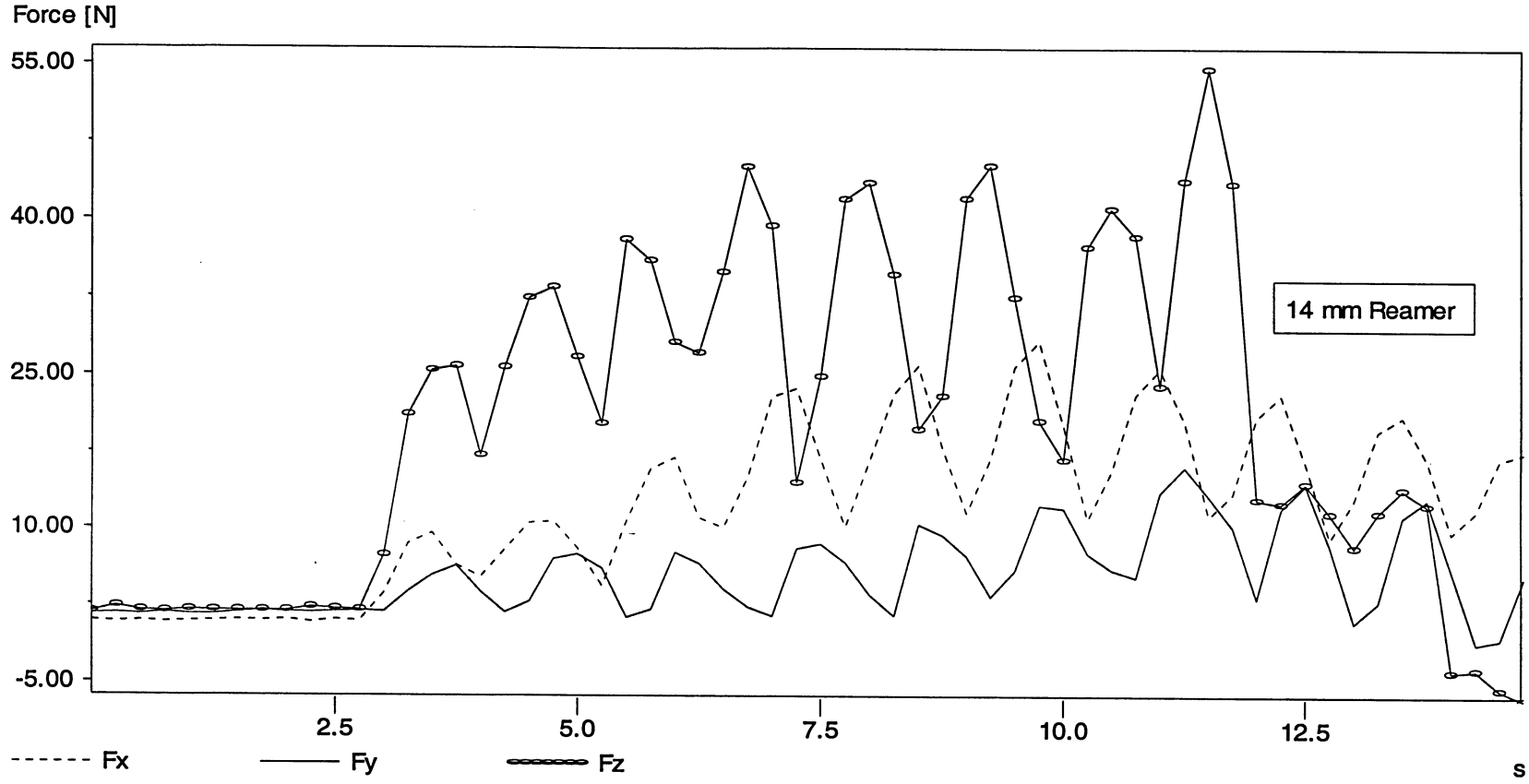

Figure D.62. Force profiles using 14 mm reamer, 50 RPM, 50 $\frac{mm}{sec}$ and 82.6 cP synthetic marrow viscosity. F_x, F_y and F_z are respectively corresponded to forces applied to the closed end of the bone in x, y, and z directions.

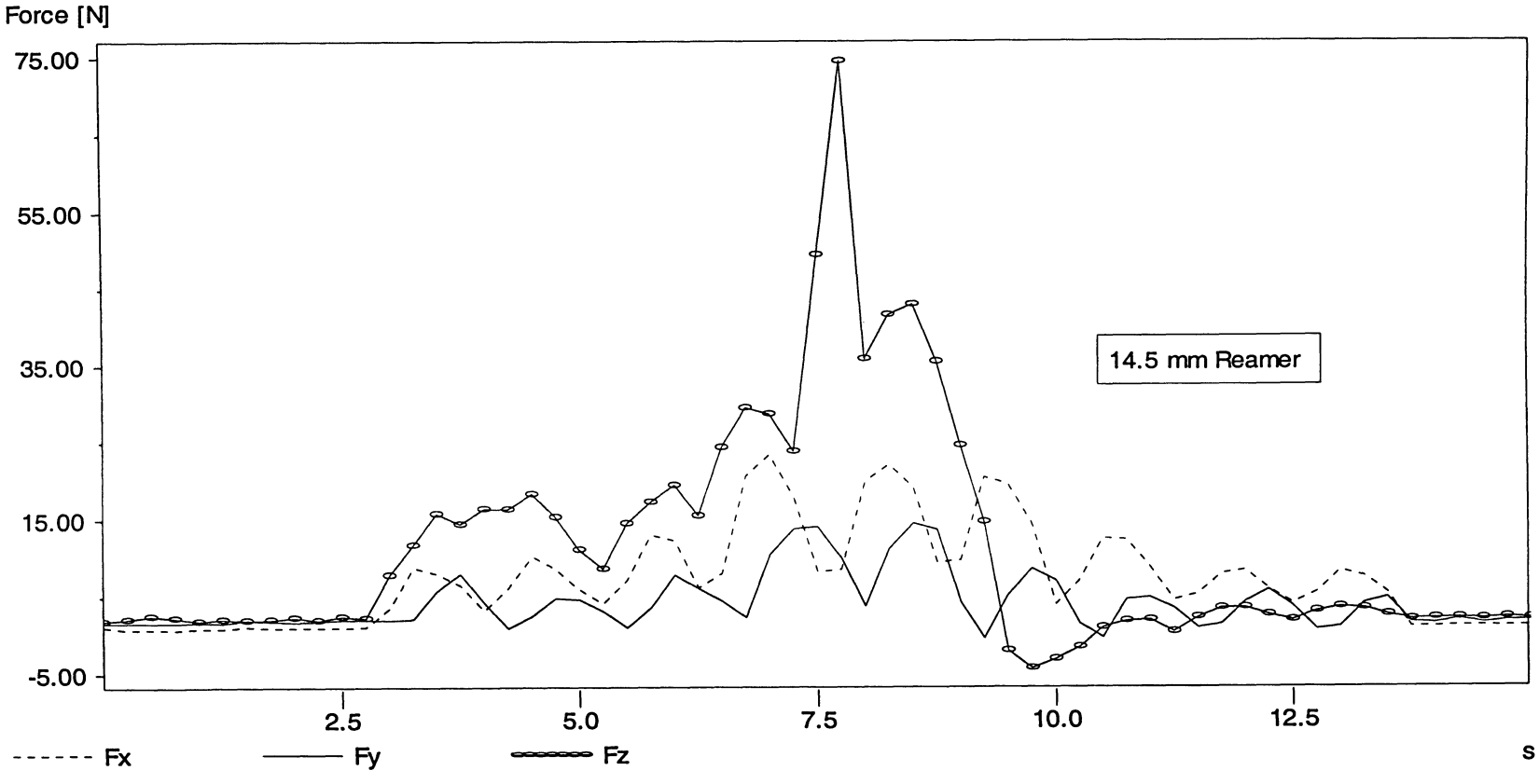

Figure D.63. Force profiles using 14.5 mm reamer, 50 RPM, 50 $\frac{mm}{sec}$ and 82.6 cP synthetic marrow viscosity. F_x, F_y and F_z are respectively corresponded to forces applied to the closed end of the bone in x, y, and z directions.

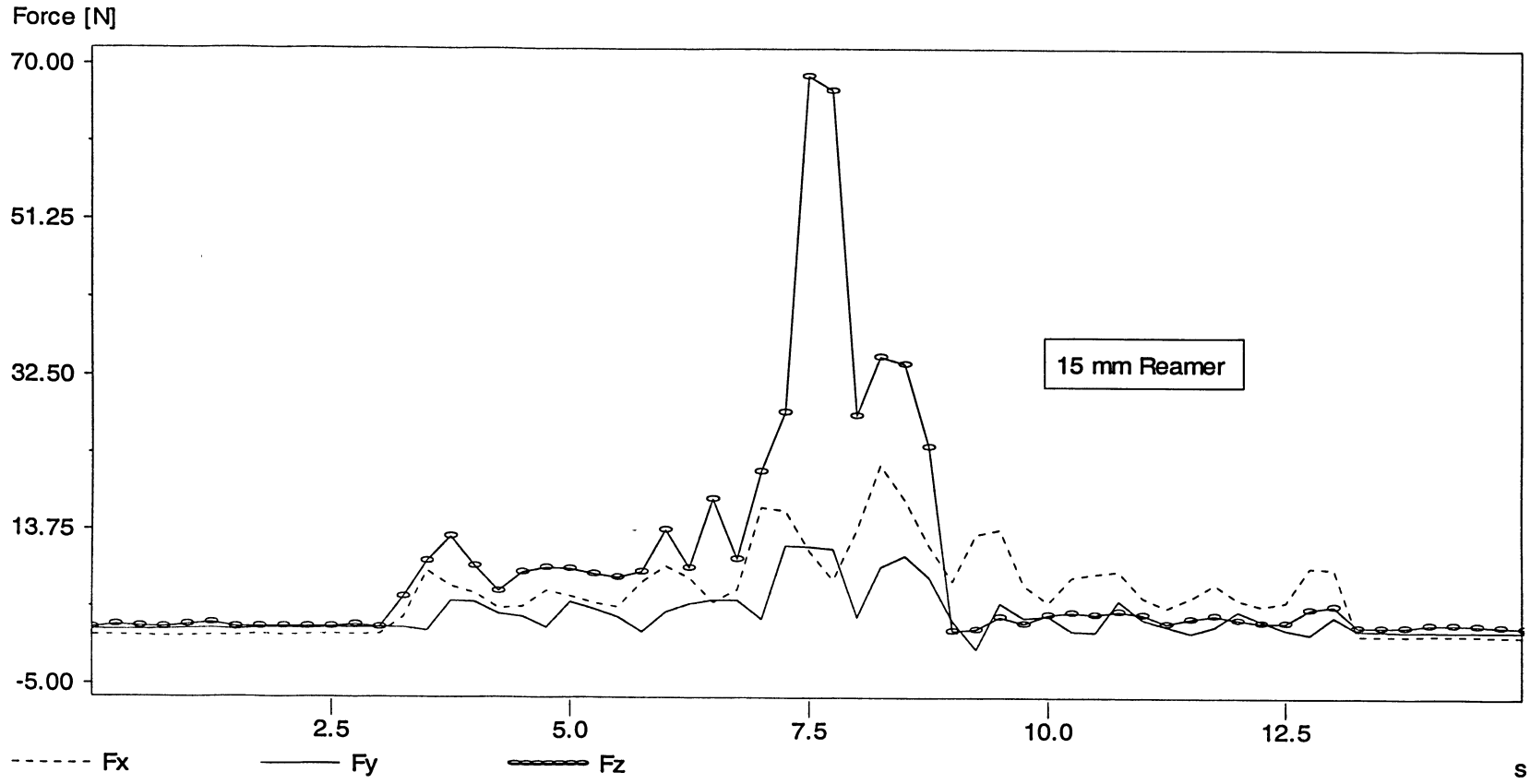

Figure D.64. Force profiles using 15 mm reamer, 50 RPM, 50 $\frac{mm}{sec}$ and 82.6 cP synthetic marrow viscosity. F_x, F_y and F_z are respectively corresponded to forces applied to the closed end of the bone in x, y, and z directions.

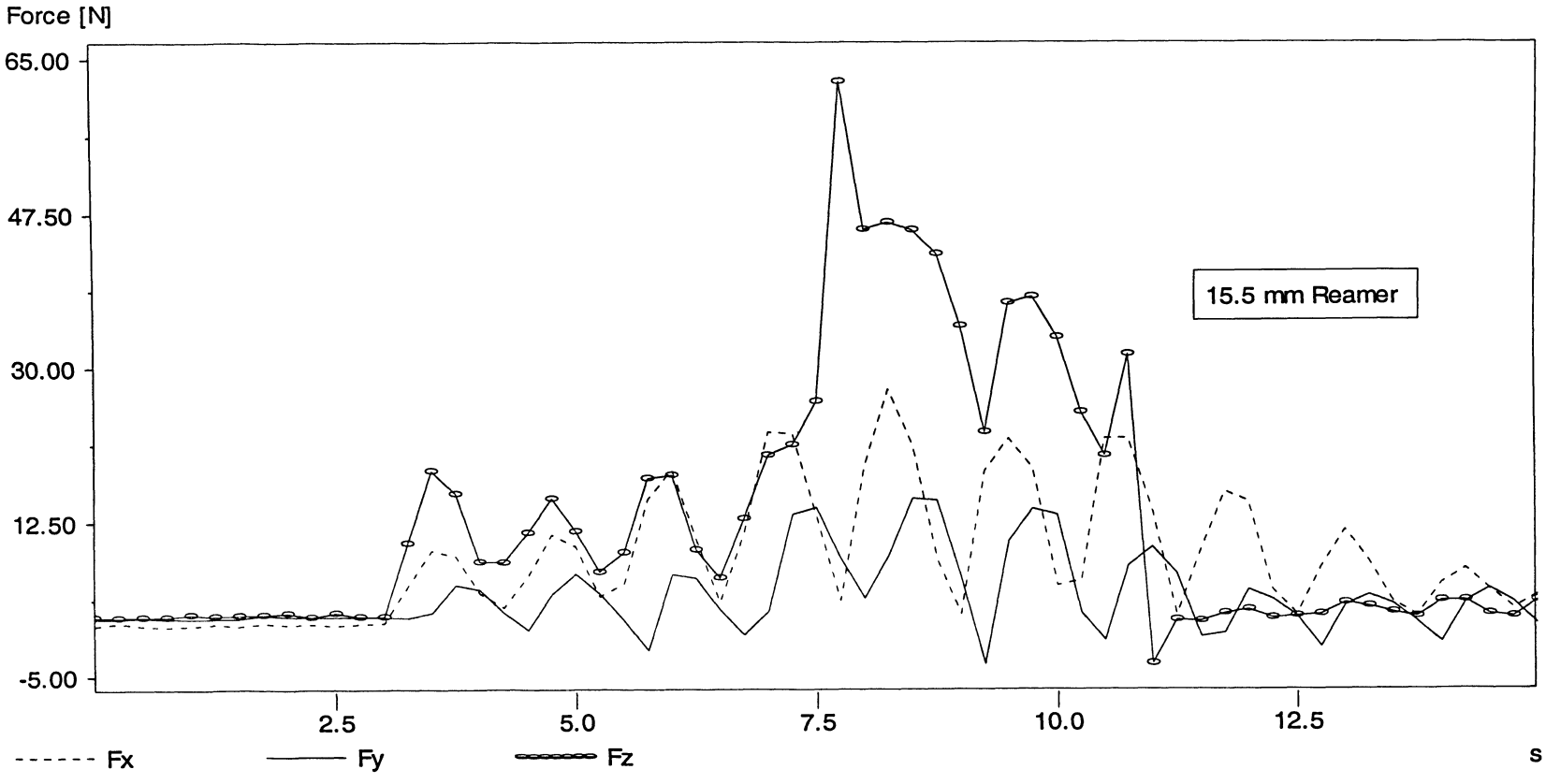

Figure D.65. Force profiles using 15.5 mm reamer, 50 RPM, 50 $\frac{mm}{sec}$ and 82.6 cP synthetic marrow viscosity. F_x, F_y and F_z are respectively corresponded to forces applied to the closed end of the bone in x, y, and z directions.

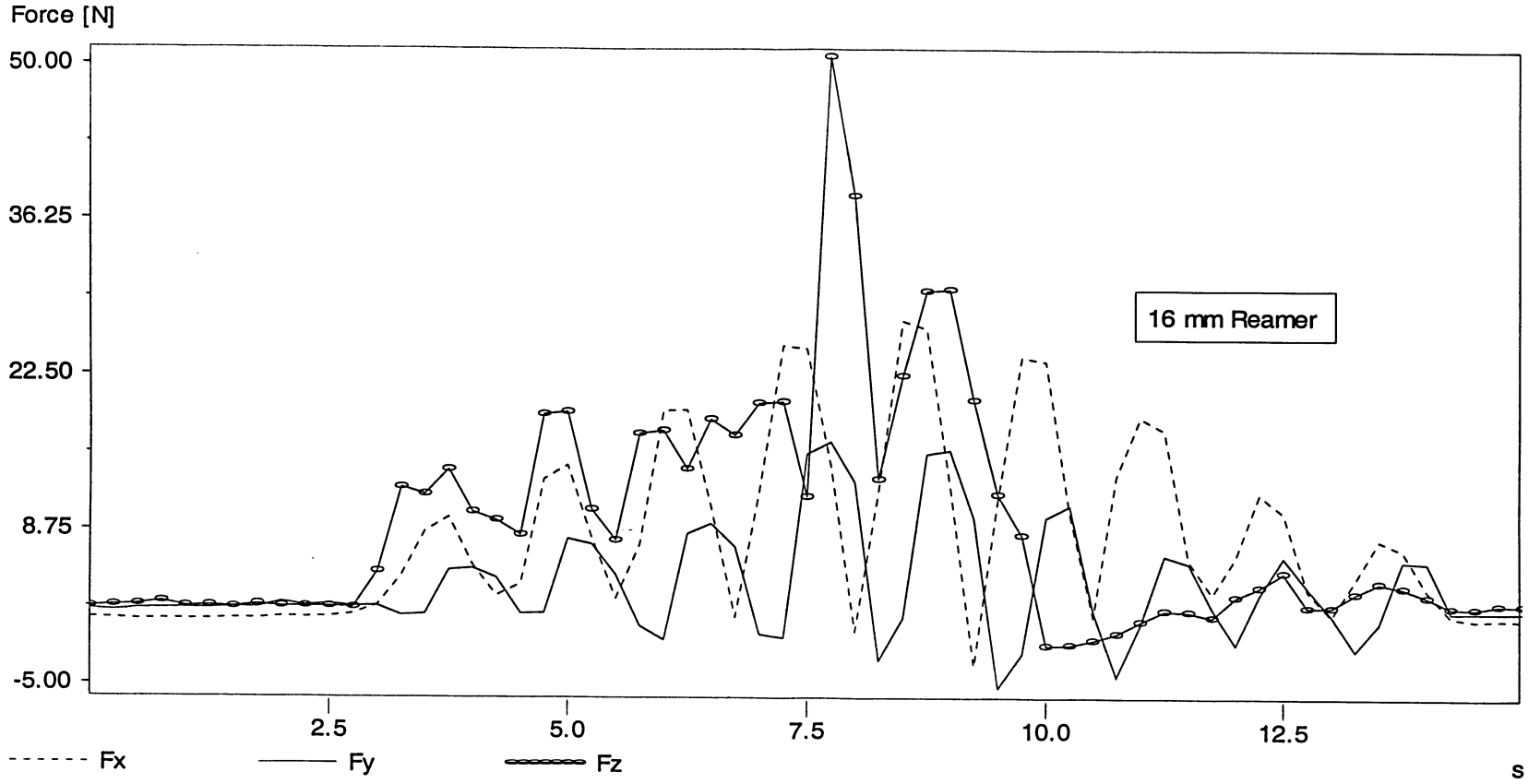

Figure D.66. Force profiles using 16 mm reamer, 50 RPM, 50 $\frac{mm}{sec}$ and 82.6 cP synthetic marrow viscosity. F_x, F_y and F_z are respectively corresponded to forces applied to the closed end of the bone in x, y, and z directions.

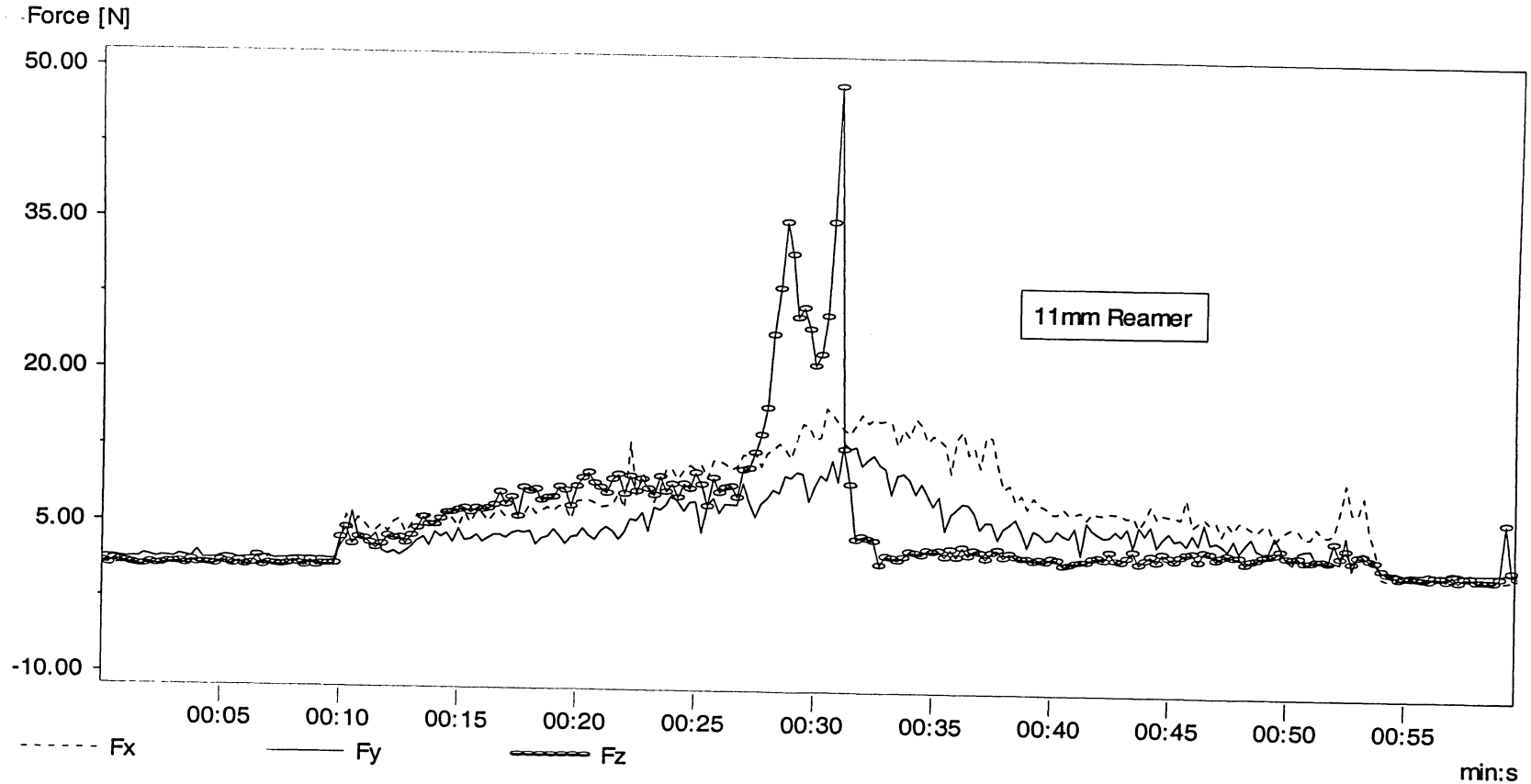

Figure D.67. Force profiles using 11mm reamer, 200 RPM, 10 $\frac{mm}{sec}$ and 82.6 cP synthetic marrow viscosity. F_x, F_y and F_z are respectively corresponded to forces applied to the closed end of the bone in x, y, and z directions.

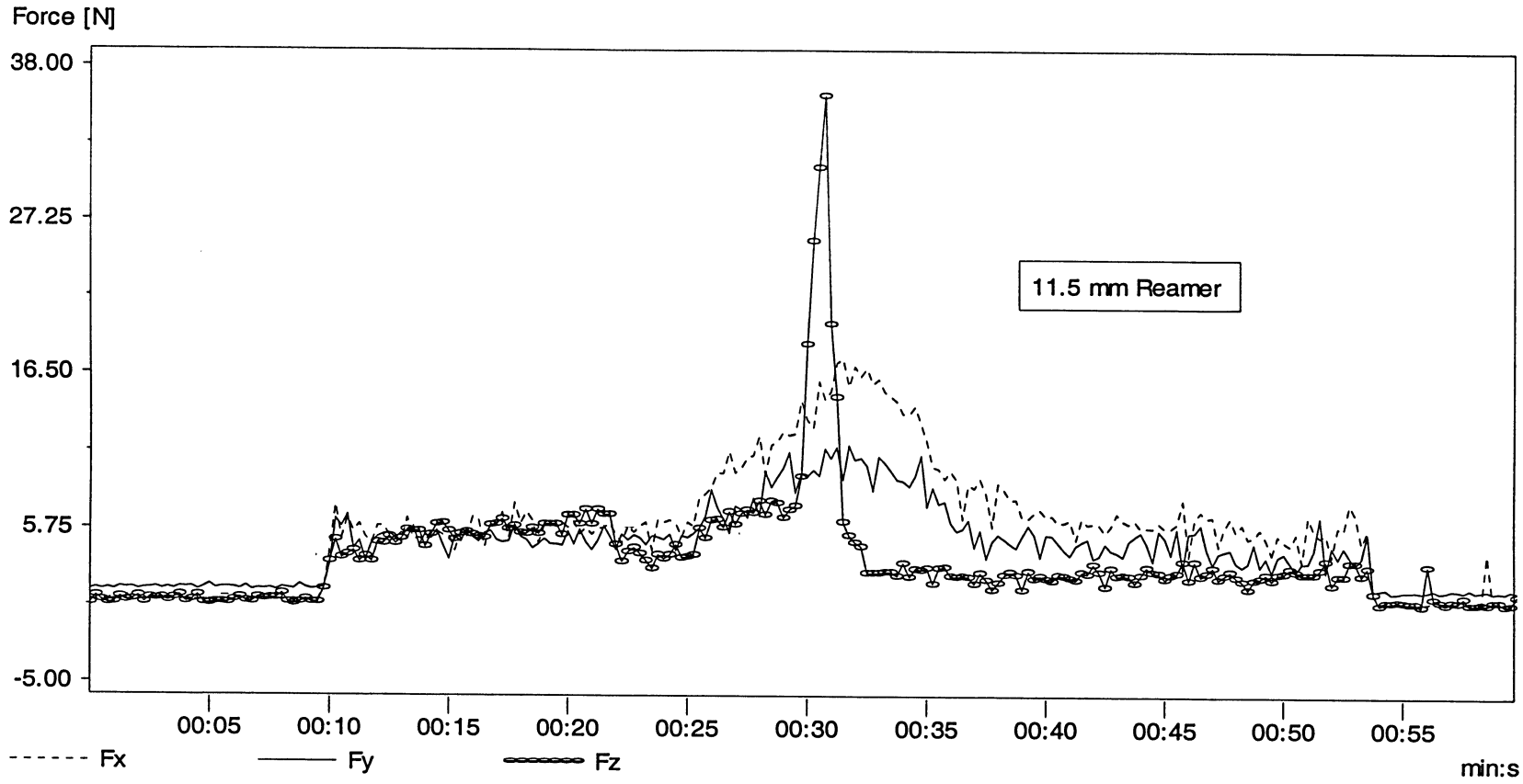

Figure D.68. Force profiles using 11.5 mm reamer, 200 RPM, 10 $\frac{mm}{sec}$ and 82.6 cP synthetic marrow viscosity. F_x, F_y and F_z are respectively corresponded to forces applied to the closed end of the bone in x, y, and z directions.

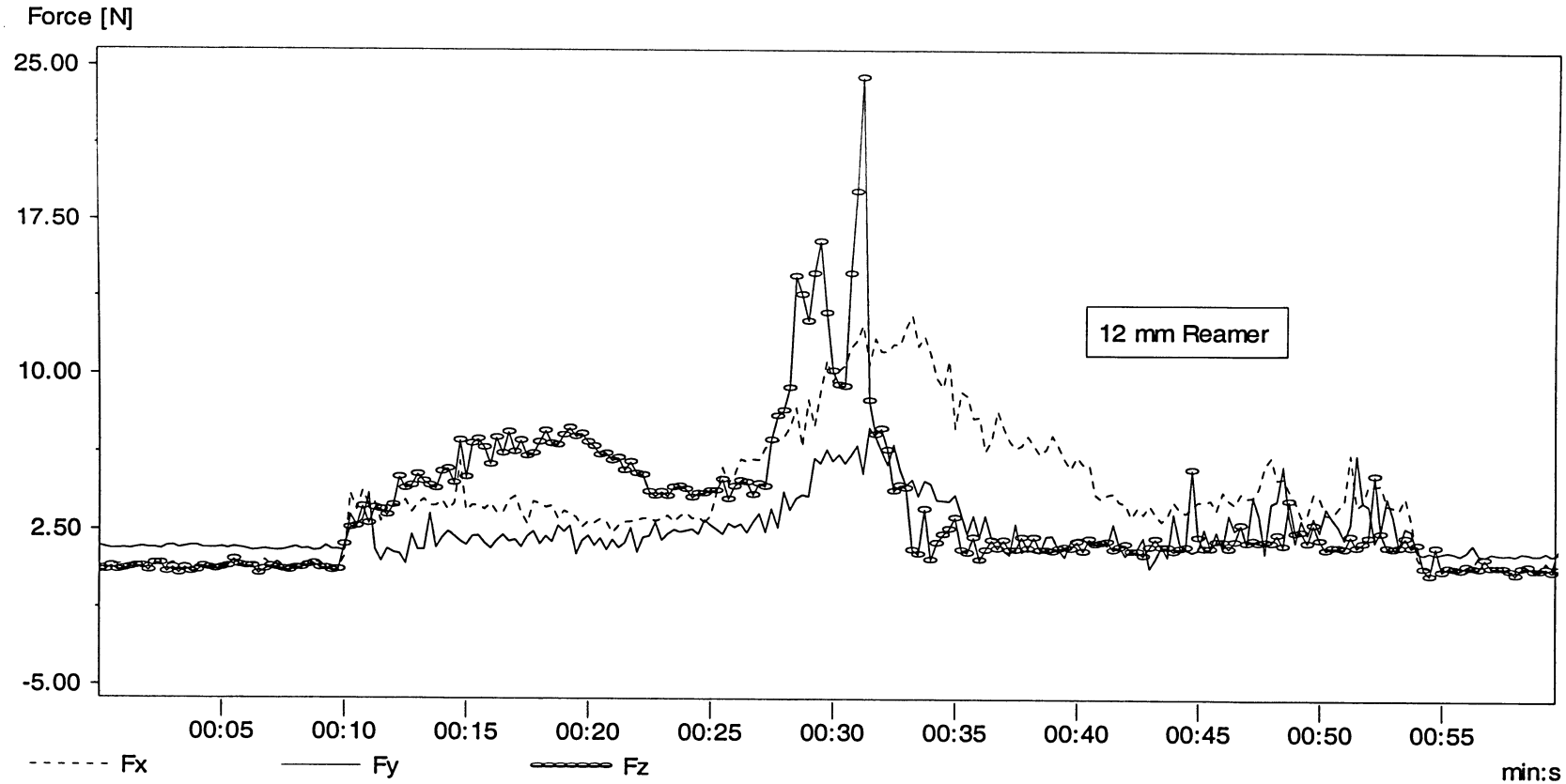

Figure D.69. Force profiles using 12 mm reamer, 200 RPM, 10 $\frac{mm}{sec}$ and 82.6 cP synthetic marrow viscosity. F_x, F_y and F_z are respectively corresponded to forces applied to the closed end of the bone in x, y, and z directions.

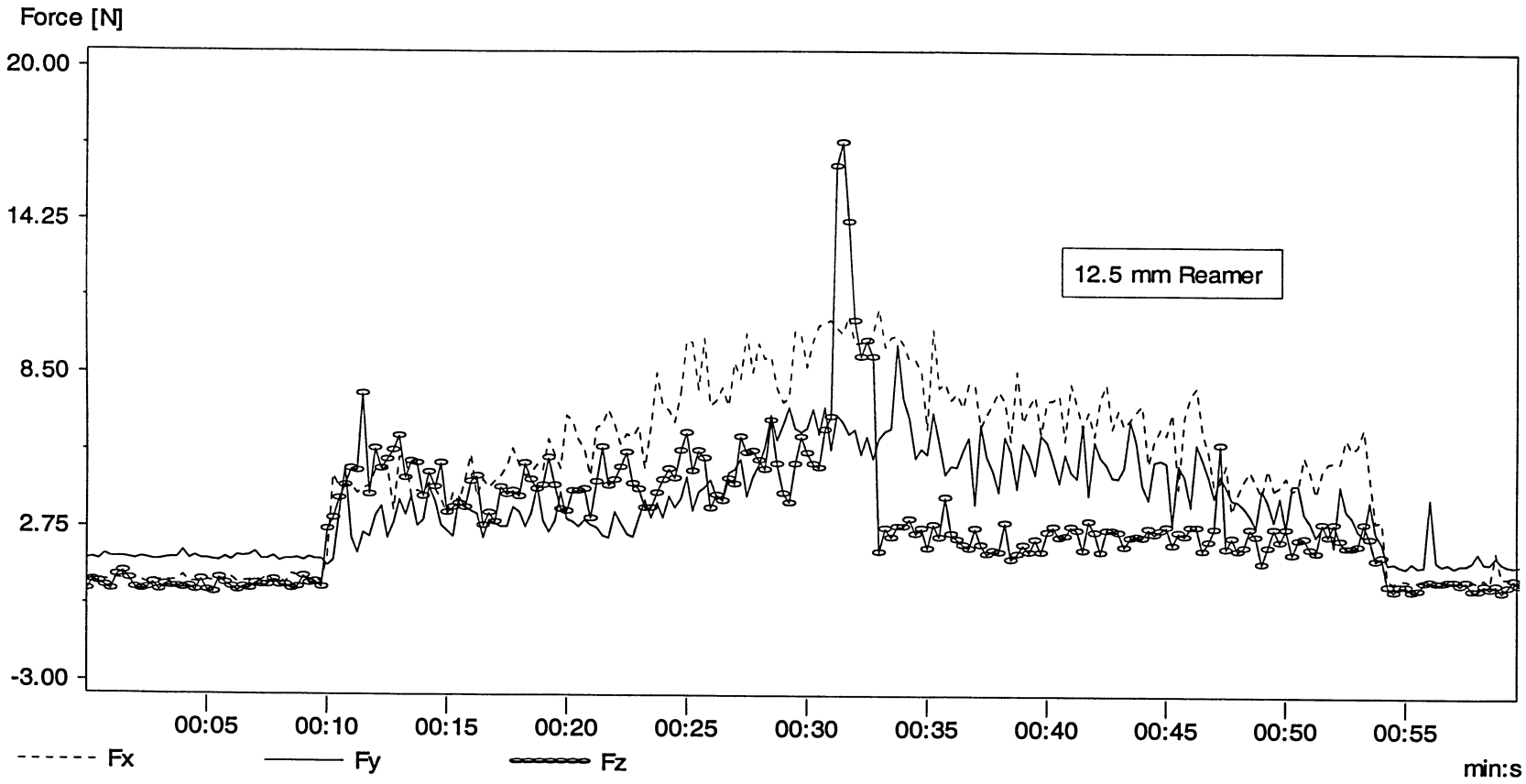

Figure D.70. Force profiles using 12.5 mm reamer, 200 RPM, 10 $\frac{mm}{sec}$ and 82.6 cP synthetic marrow viscosity. F_x, F_y and F_z are respectively corresponded to forces applied to the closed end of the bone in x, y, and z directions.

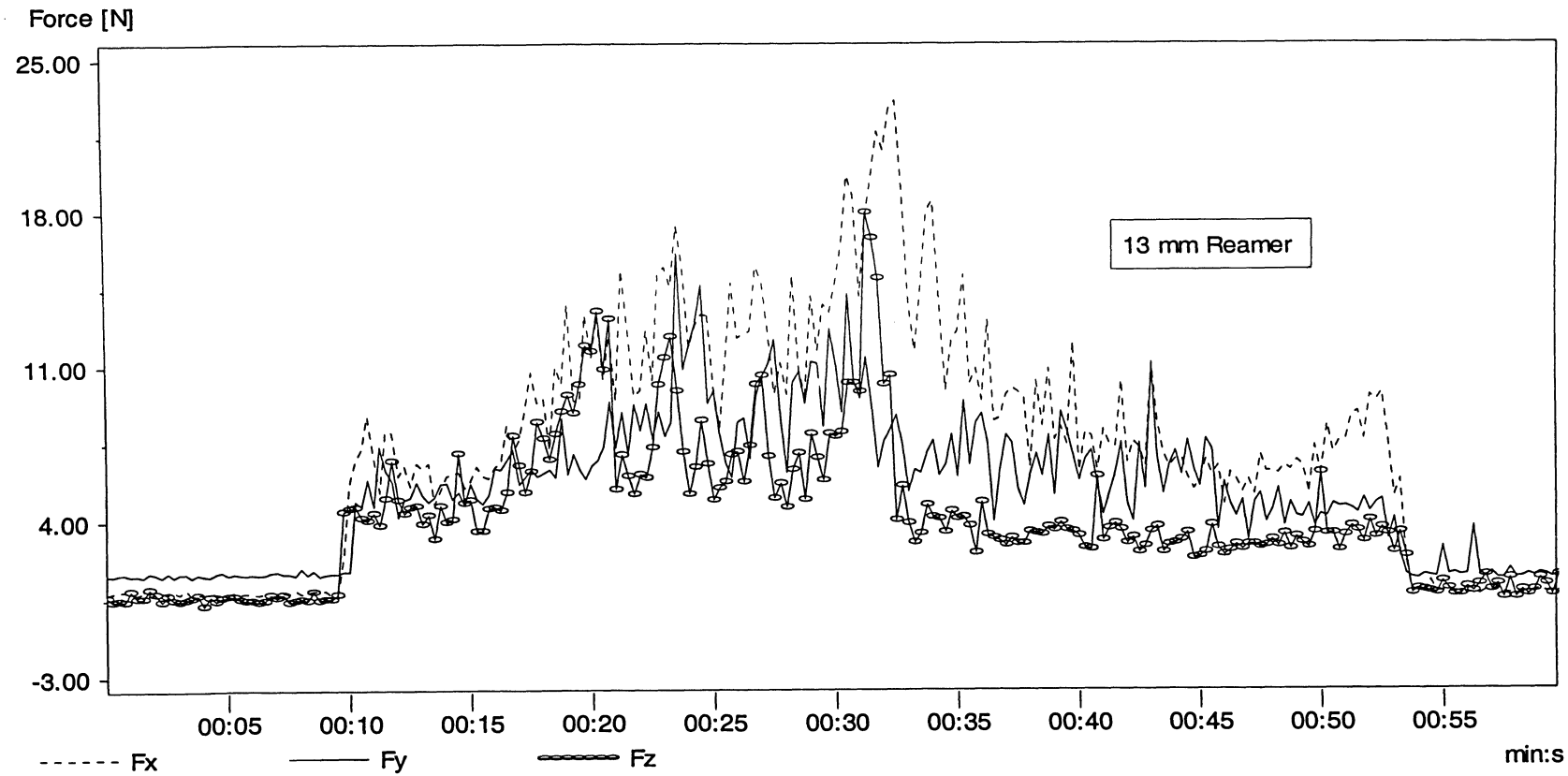

Figure D.71. Force profiles using 13 mm reamer, 200 RPM, 10 $\frac{mm}{sec}$ and 82.6 cP synthetic marrow viscosity. F_x, F_y and F_z are respectively corresponded to forces applied to the closed end of the bone in x, y, and z directions.

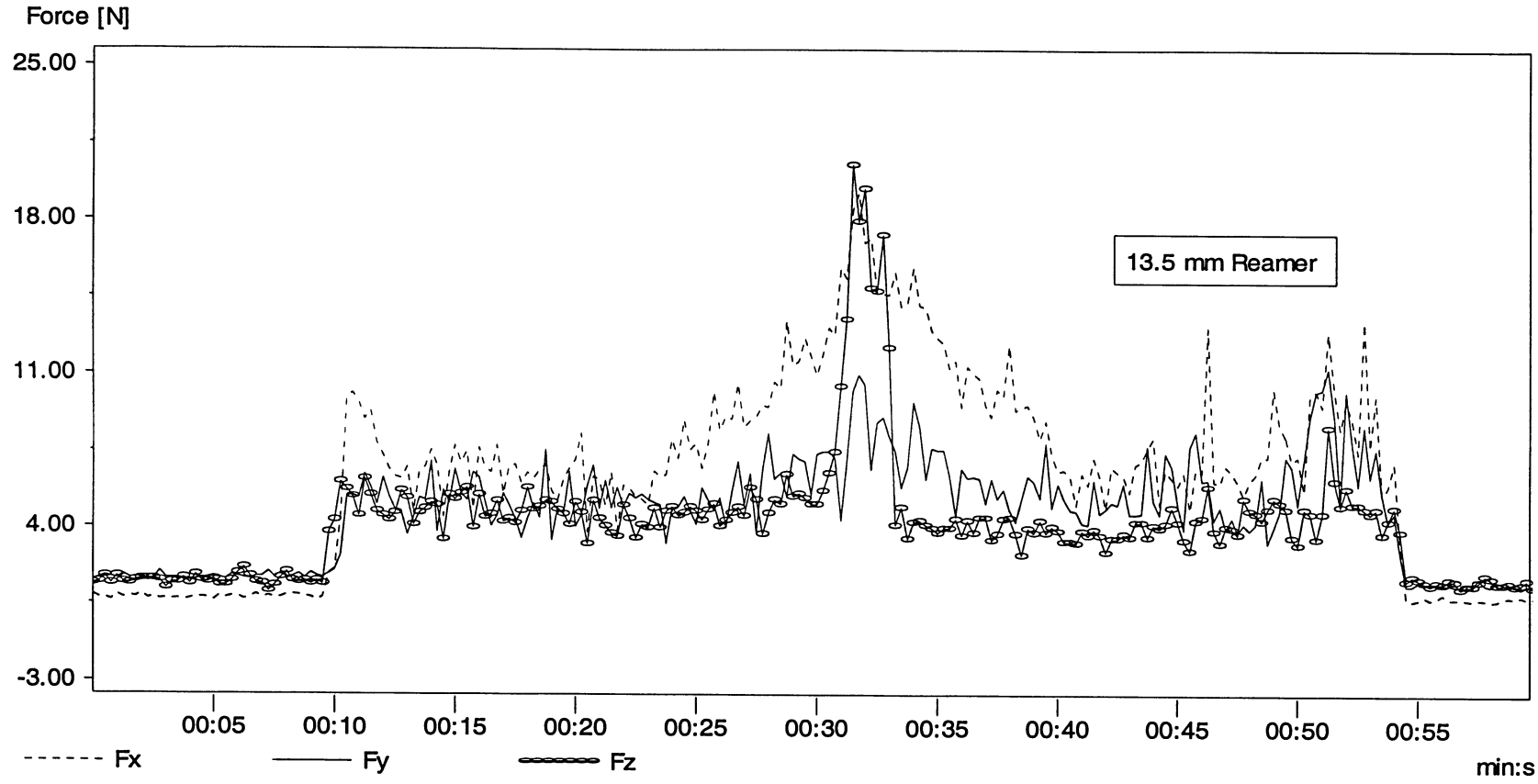

Figure D.72. Force profiles using 13.5 mm reamer, 200 RPM, 10 $\frac{mm}{sec}$ and 82.6 cP synthetic marrow viscosity. F_x, F_y and F_z are respectively corresponded to forces applied to the closed end of the bone in x, y, and z directions.

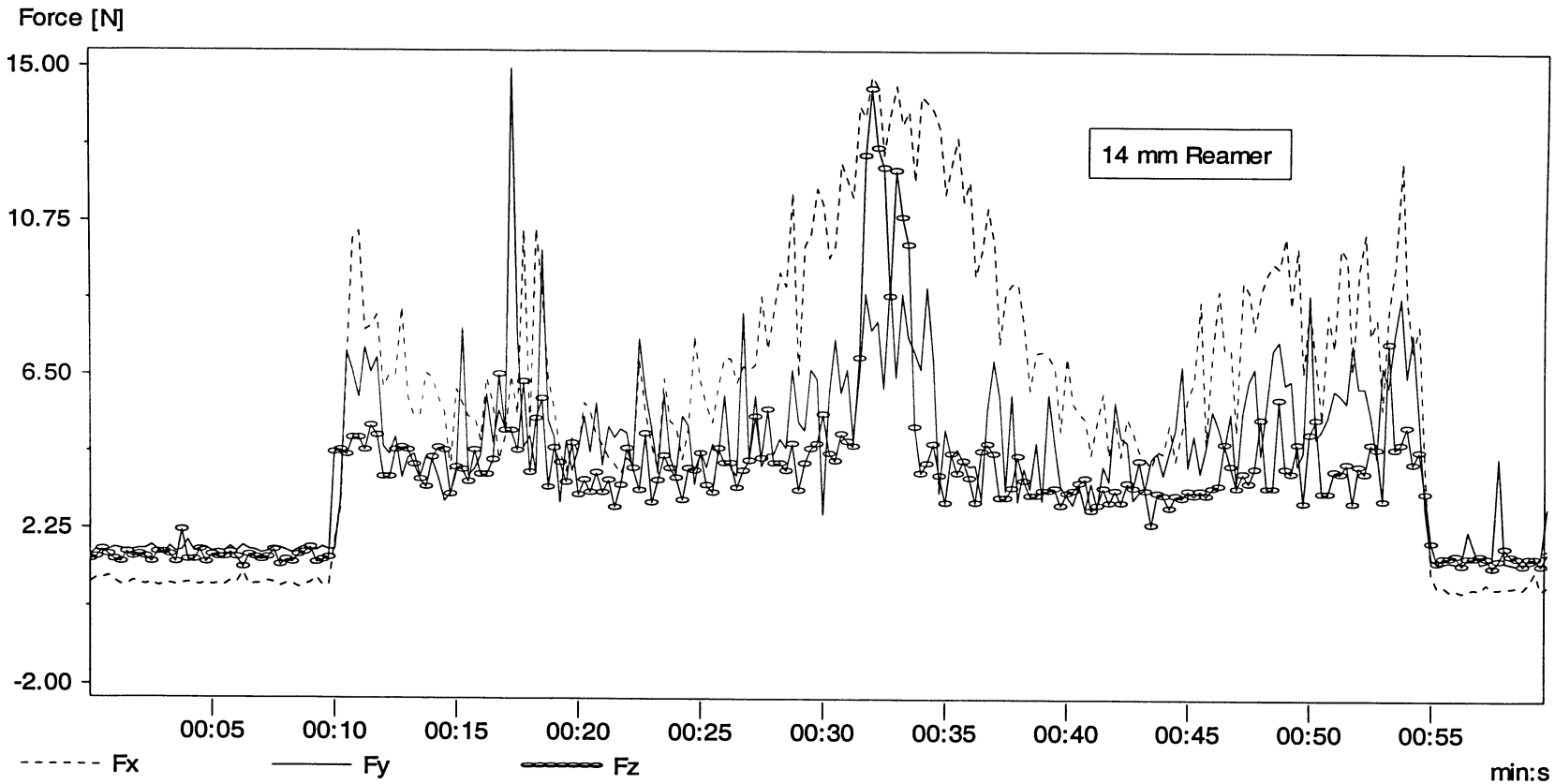

Figure D.73. Force profiles using 14 mm reamer, 200 RPM, 10 $\frac{mm}{sec}$ and 82.6 cP synthetic marrow viscosity. F_x, F_y and F_z are respectively corresponded to forces applied to the closed end of the bone in x, y, and z directions.

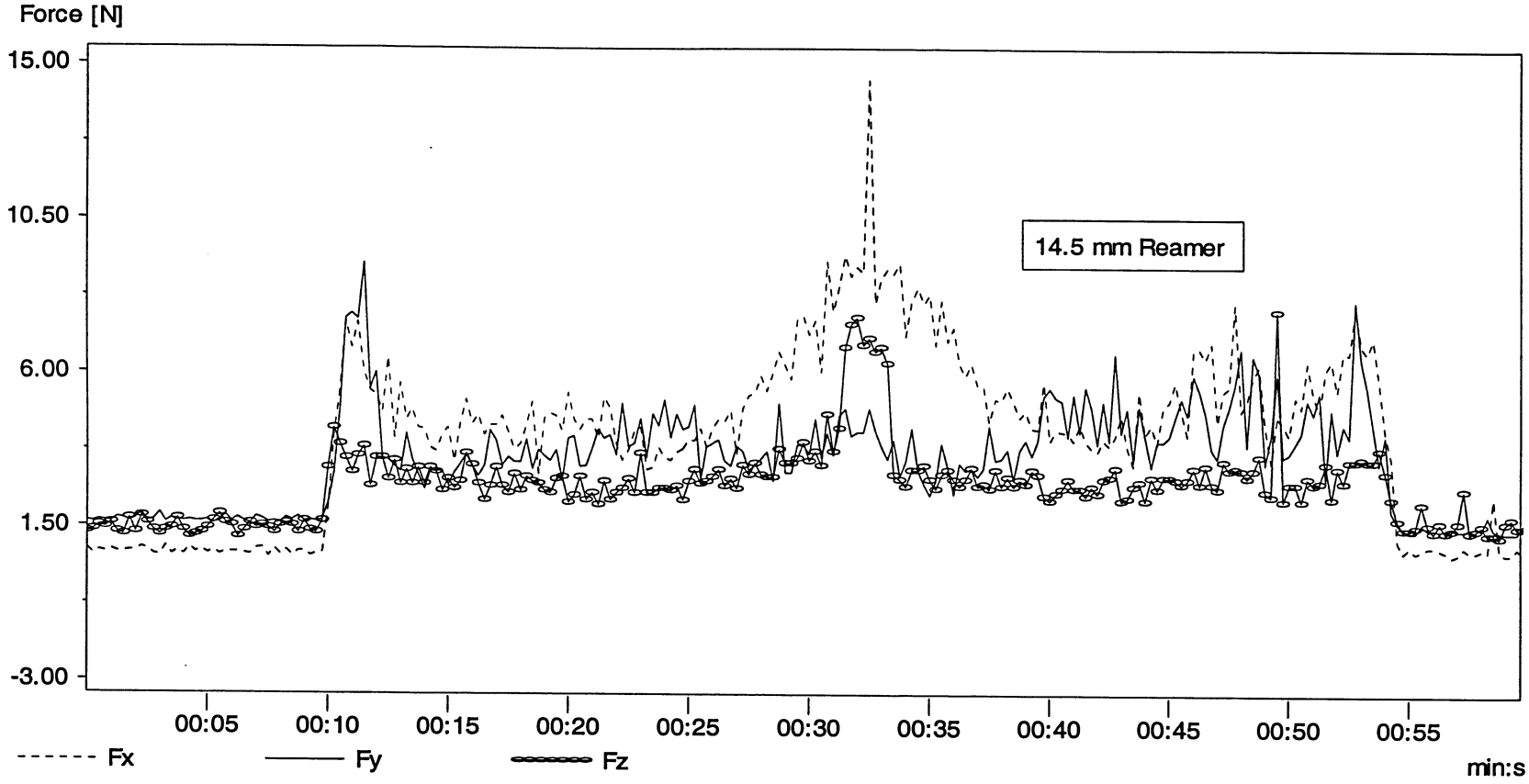

Figure D.74. Force profiles using 14.5 mm reamer, 200 RPM, 10 $\frac{mm}{sec}$ and 82.6 cP synthetic marrow viscosity. F_x, F_y and F_z are respectively corresponded to forces applied to the closed end of the bone in x, y, and z directions.

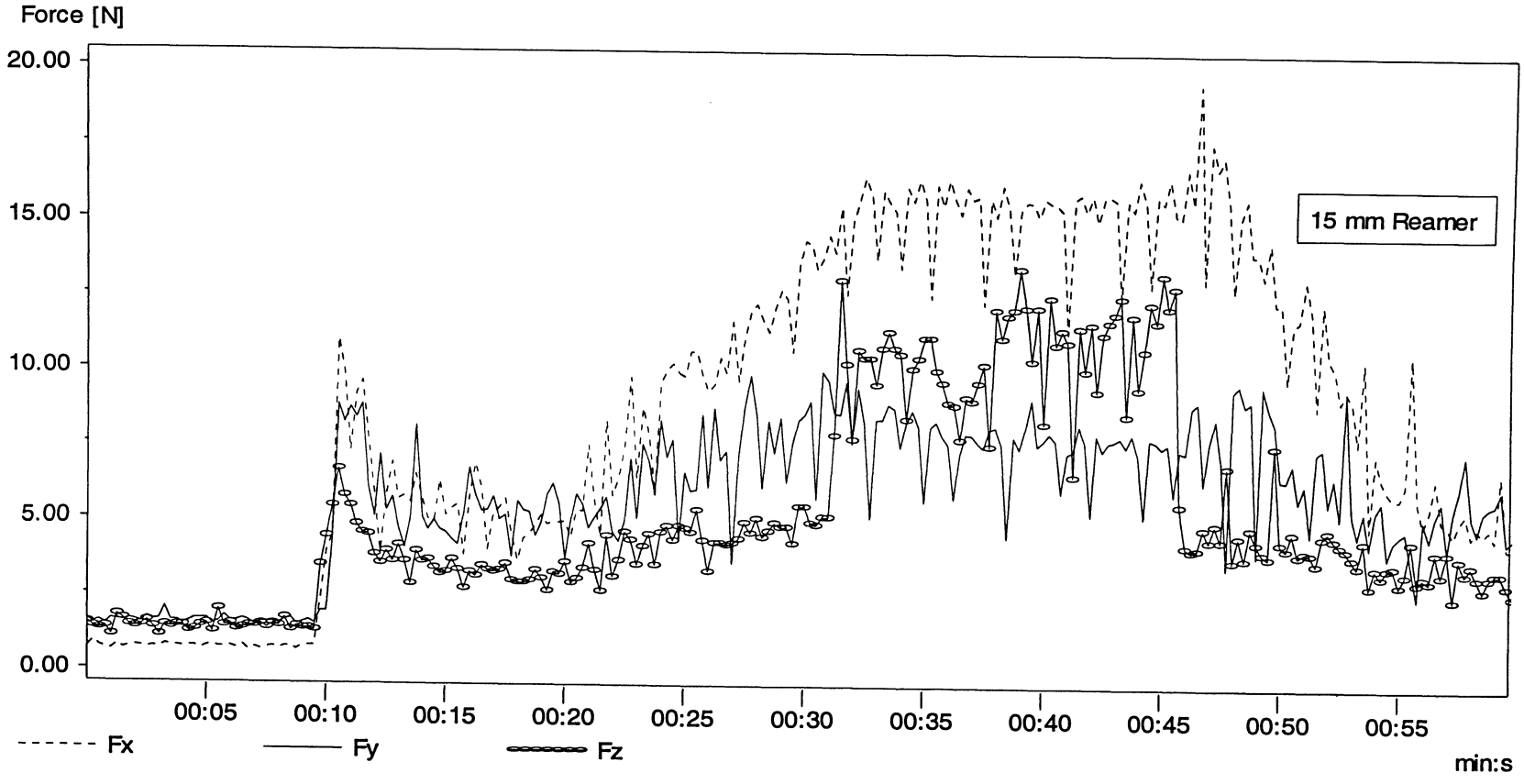

Figure D.75. Force profiles using 15 mm reamer, 200 RPM, 10 $\frac{mm}{sec}$ and 82.6 cP synthetic marrow viscosity. F_x, F_y and F_z are respectively corresponded to forces applied to the closed end of the bone in x, y, and z directions.

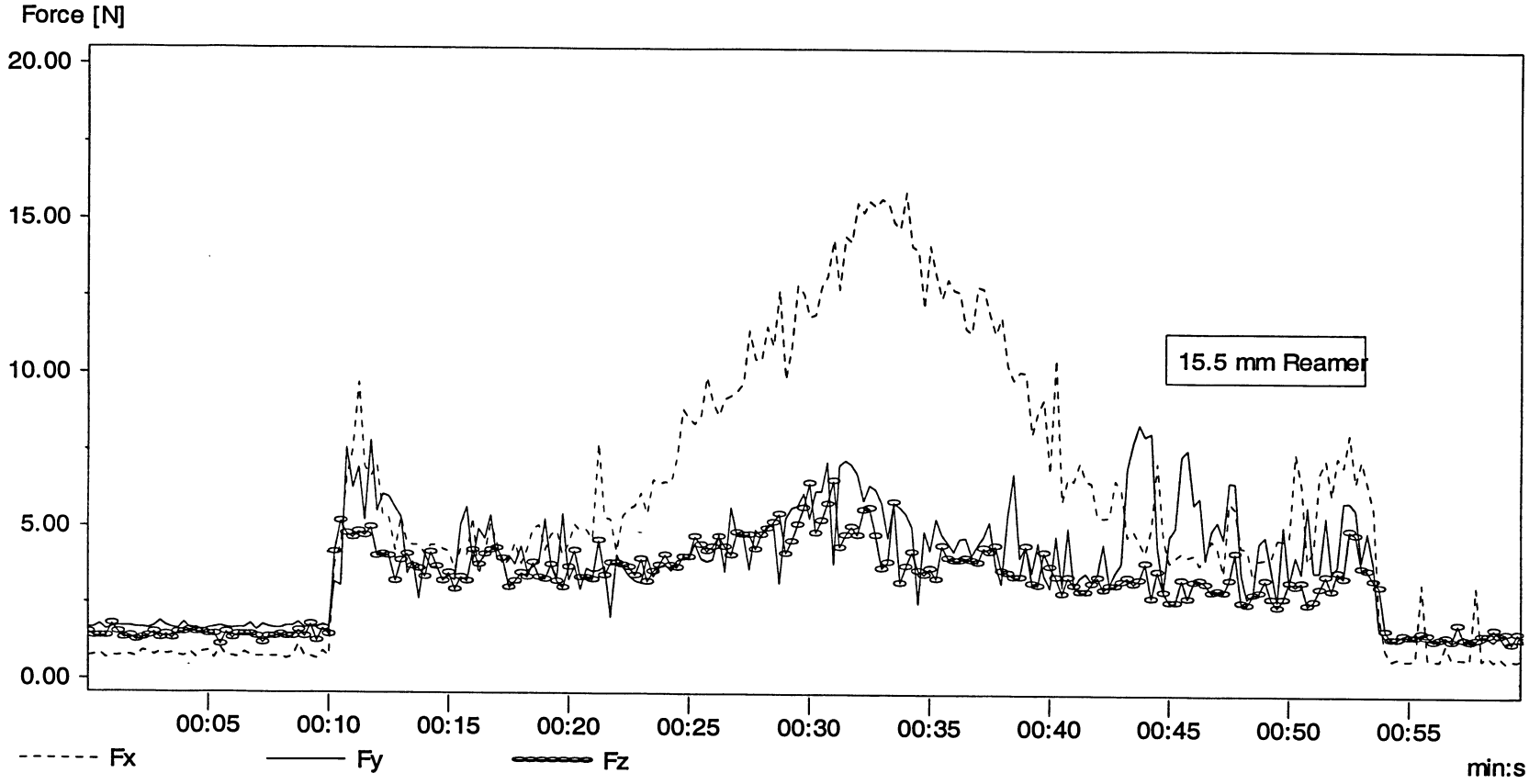

Figure D.76. Force profiles using 15.5 mm reamer, 200 RPM, 10 $\frac{mm}{sec}$ and 82.6 cP synthetic marrow viscosity. F_x, F_y and F_z are respectively corresponded to forces applied to the closed end of the bone in x, y, and z directions.

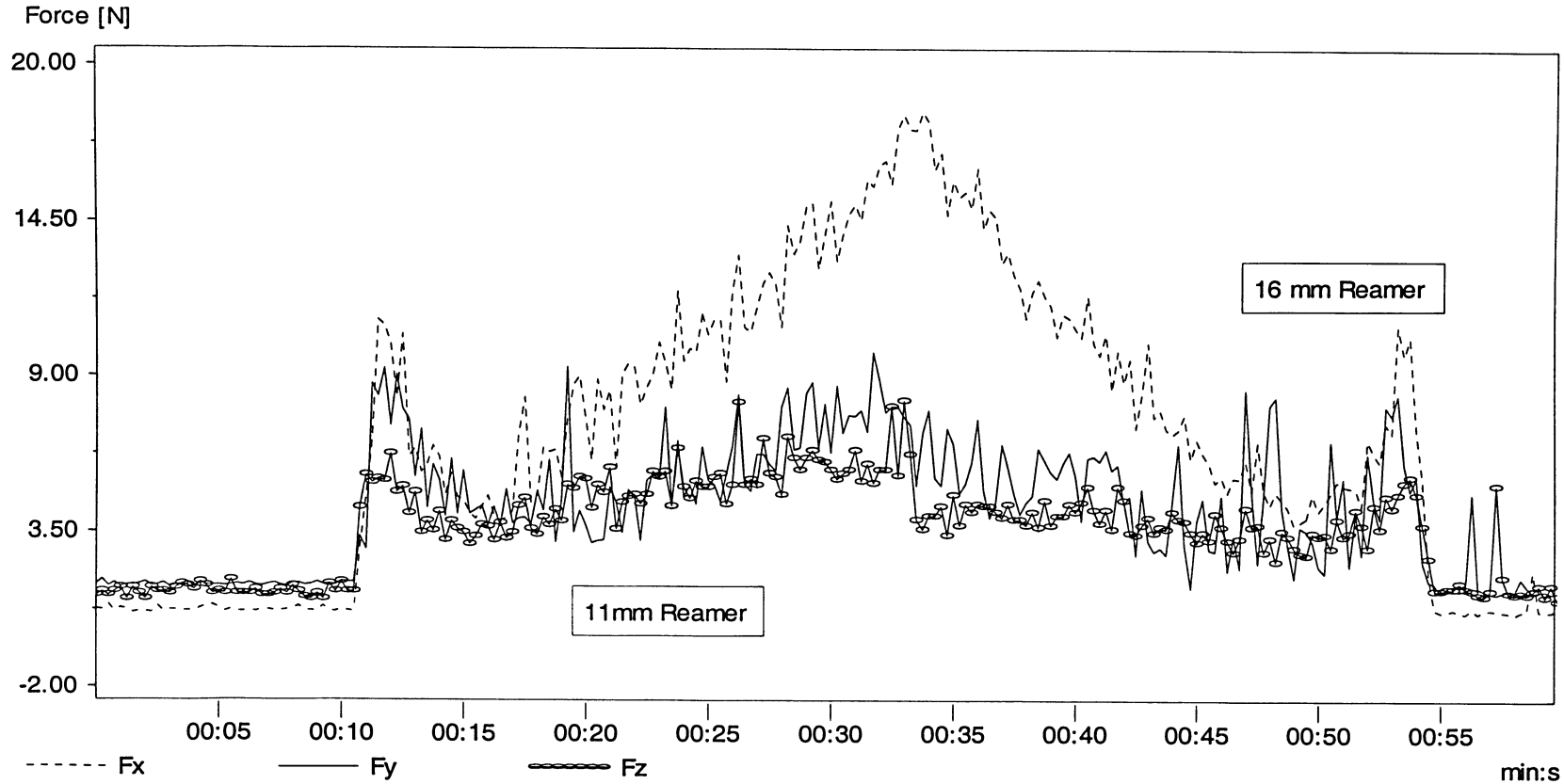

Figure D.77. Force profiles using 16 mm reamer, 200 RPM, 10 $\frac{mm}{sec}$ and 82.6 cP synthetic marrow viscosity. F_x, F_y and F_z are respectively corresponded to forces applied to the closed end of the bone in x, y, and z directions.

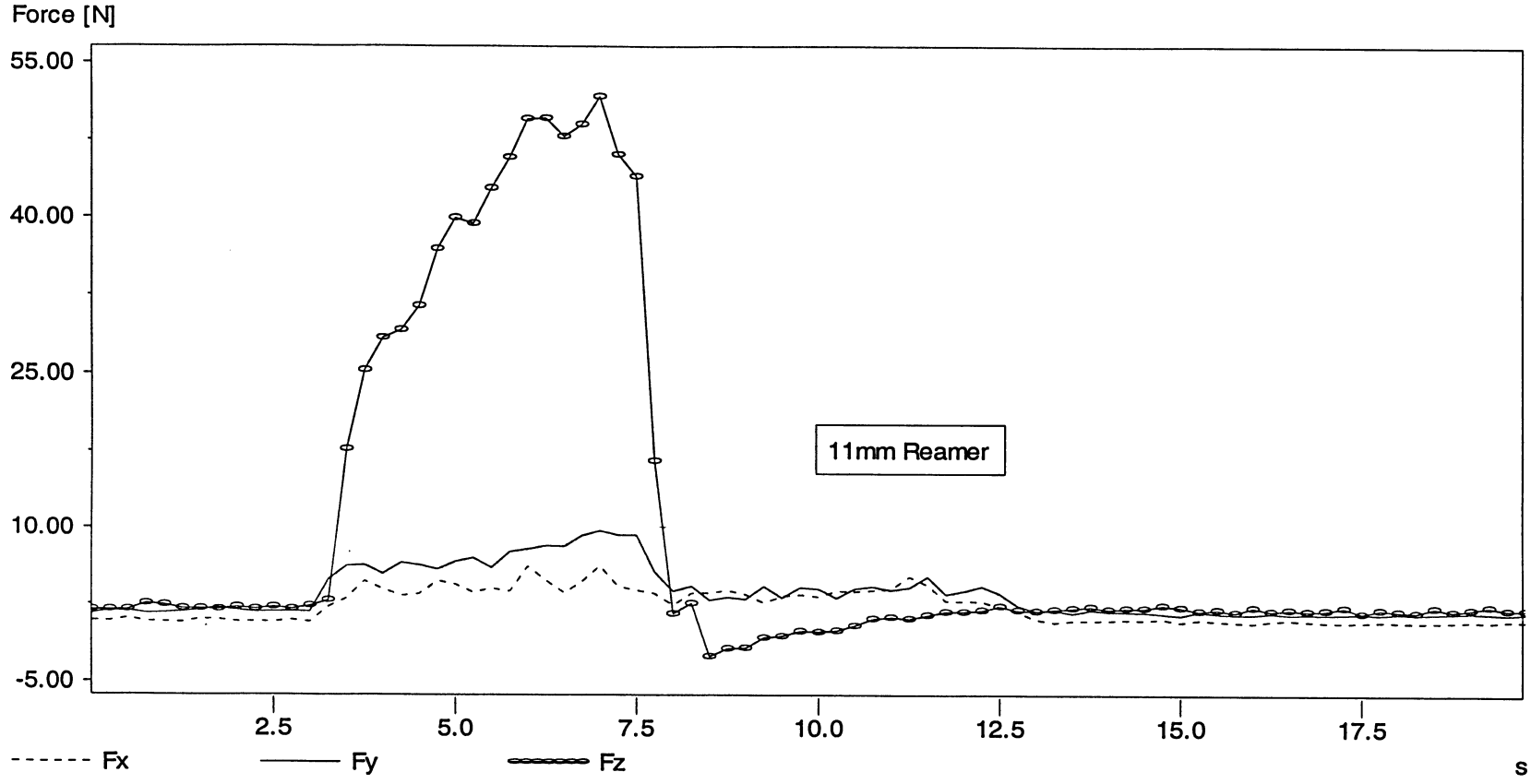

Figure D.78.Force profiles using 11mm reamer, 200 RPM, 50 $\frac{mm}{sec}$ and 82.6 cP synthetic marrow viscosity. F_x, F_y and F_z are respectively corresponded to forces applied to the closed end of the bone in x, y, and z directions.

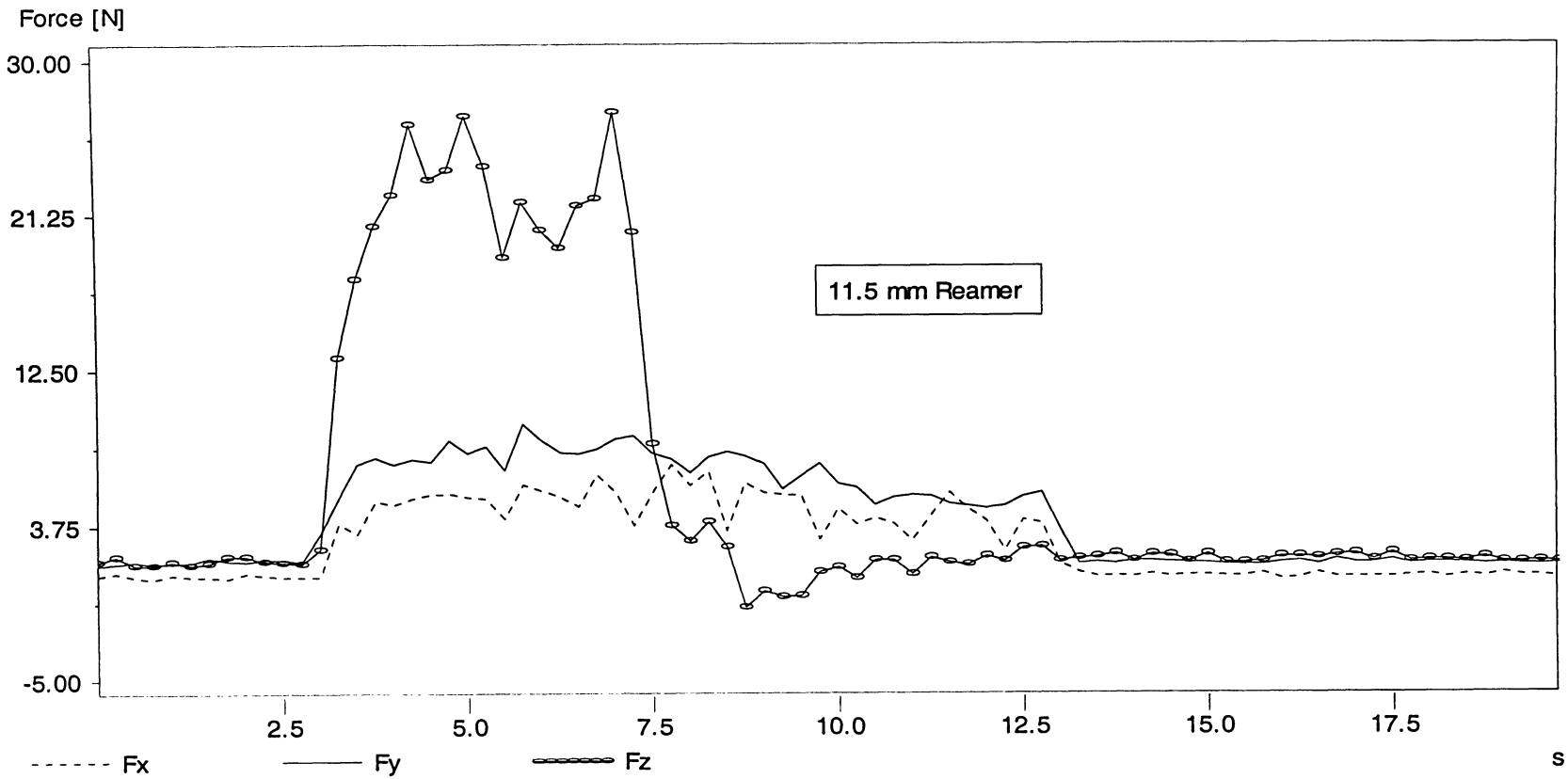

Figure D.79. Force profiles using 11.5 mm reamer, 200 RPM, 50 $\frac{mm}{sec}$ and 82.6 cP synthetic marrow viscosity. F_x, F_y and F_z are respectively corresponded to forces applied to the closed end of the bone in x, y, and z directions.

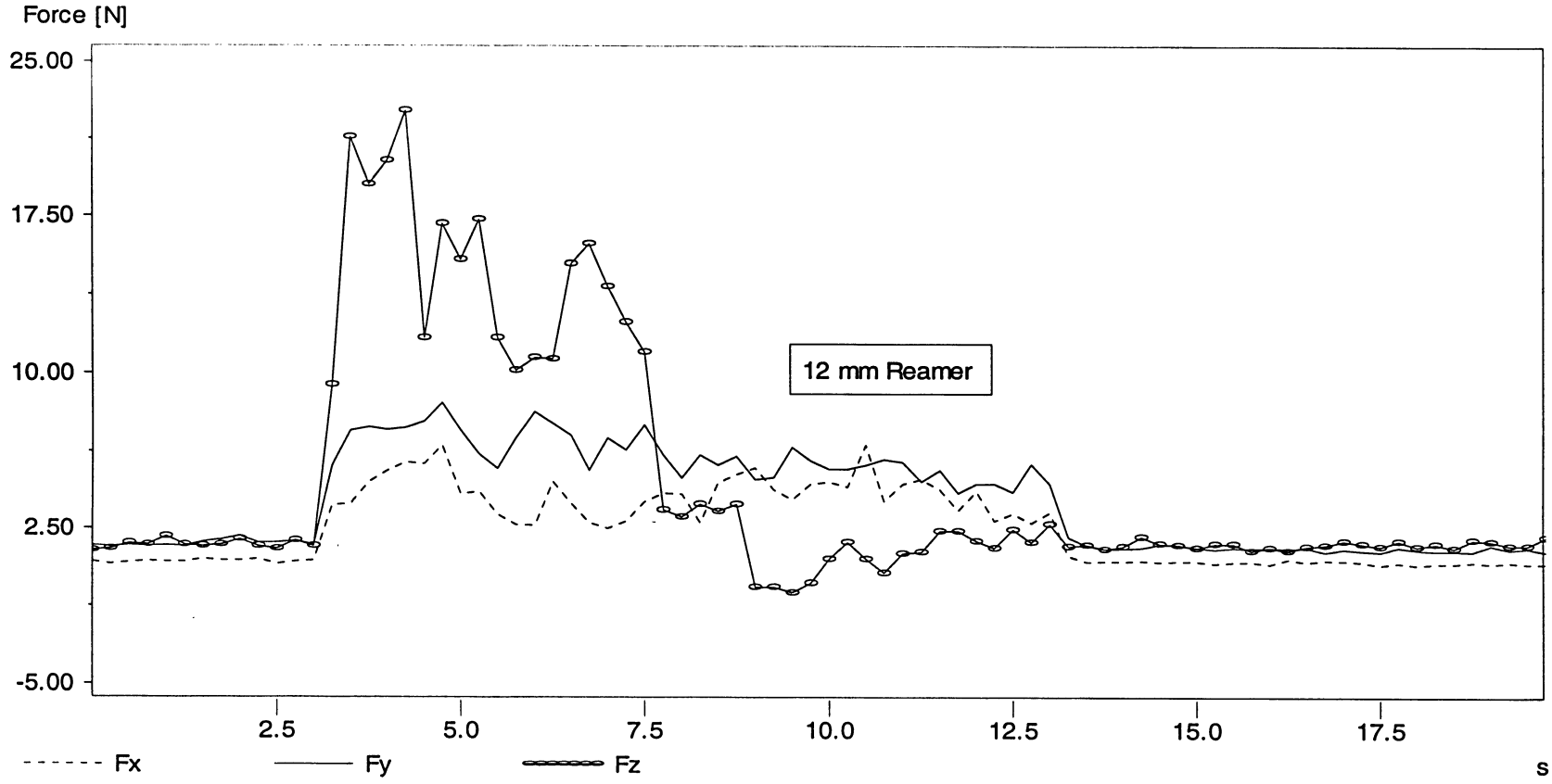

Figure D.80. Force profiles using 12 mm reamer, 200 RPM, 50 $\frac{mm}{sec}$ and 82.6 cP synthetic marrow viscosity. F_x, F_y and F_z are respectively corresponded to forces applied to the closed end of the bone in x, y, and z directions.

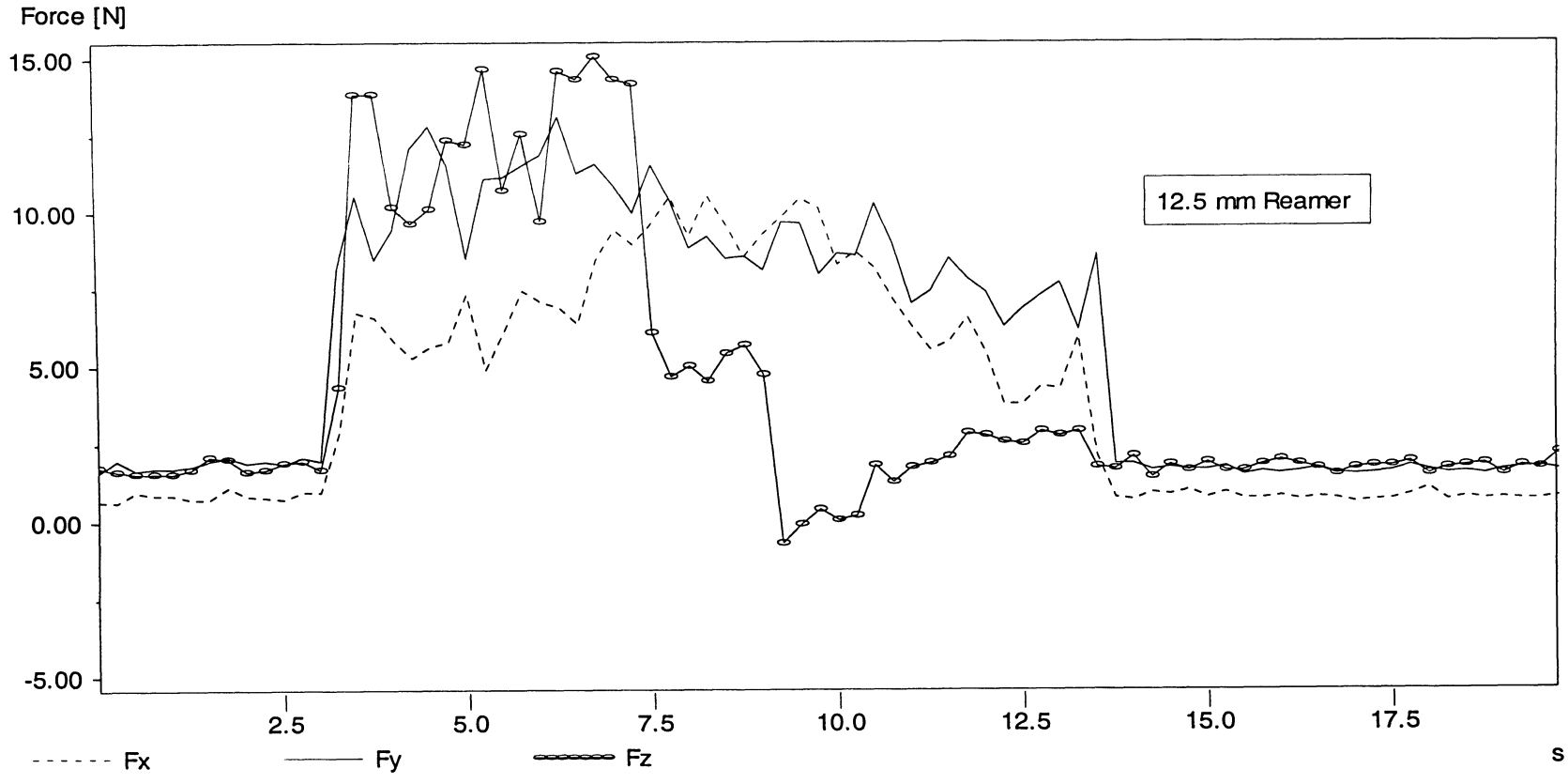

Figure D.81. Force profiles using 12.5 mm reamer, 200 RPM, 50 $\frac{mm}{sec}$ and 82.6 cP synthetic marrow viscosity. F_x, F_y and F_z are respectively corresponded to forces applied to the closed end of the bone in x, y, and z directions.

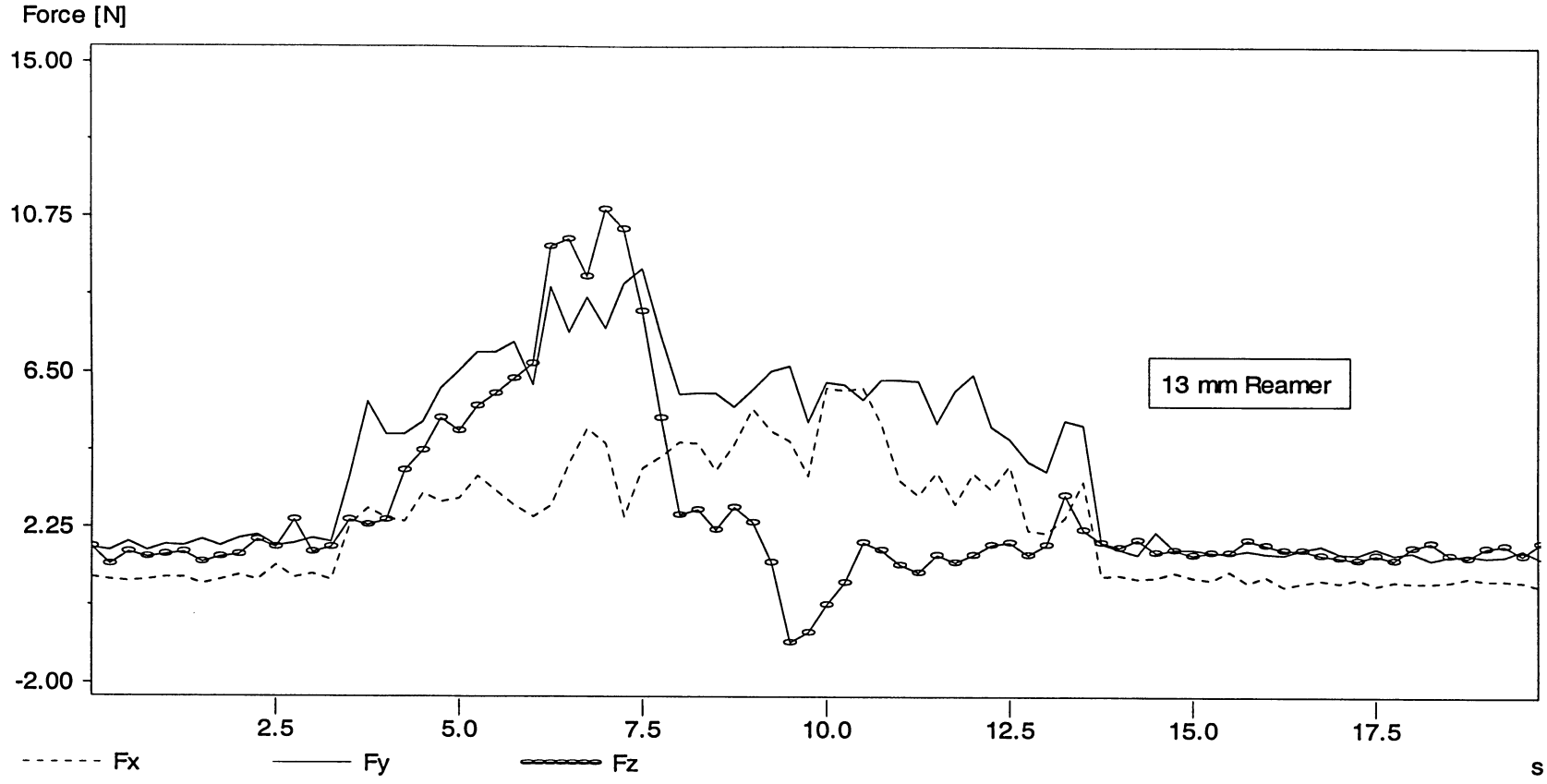

Figure D.82. Force profiles using 13 mm reamer, 200 RPM, 50 $\frac{mm}{sec}$ and 82.6 cP synthetic marrow viscosity. F_x, F_y and F_z are respectively corresponded to forces applied to the closed end of the bone in x, y, and z directions.

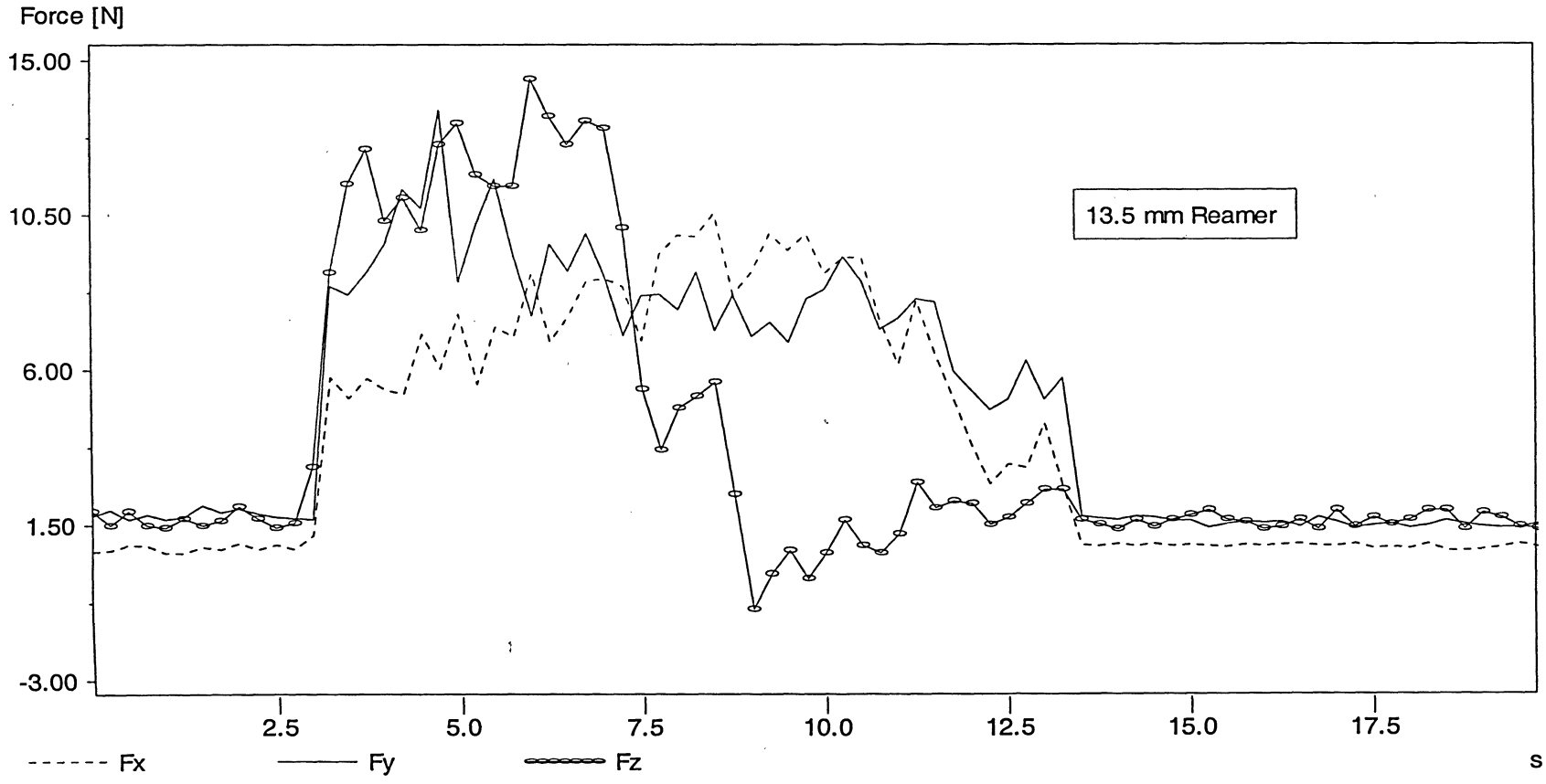

Figure D.83. Force profiles using 13.5 mm reamer, 200 RPM, 50 $\frac{mm}{sec}$ and 82.6 cP synthetic marrow viscosity. F_x, F_y and F_z are respectively corresponded to forces applied to the closed end of the bone in x, y, and z directions.

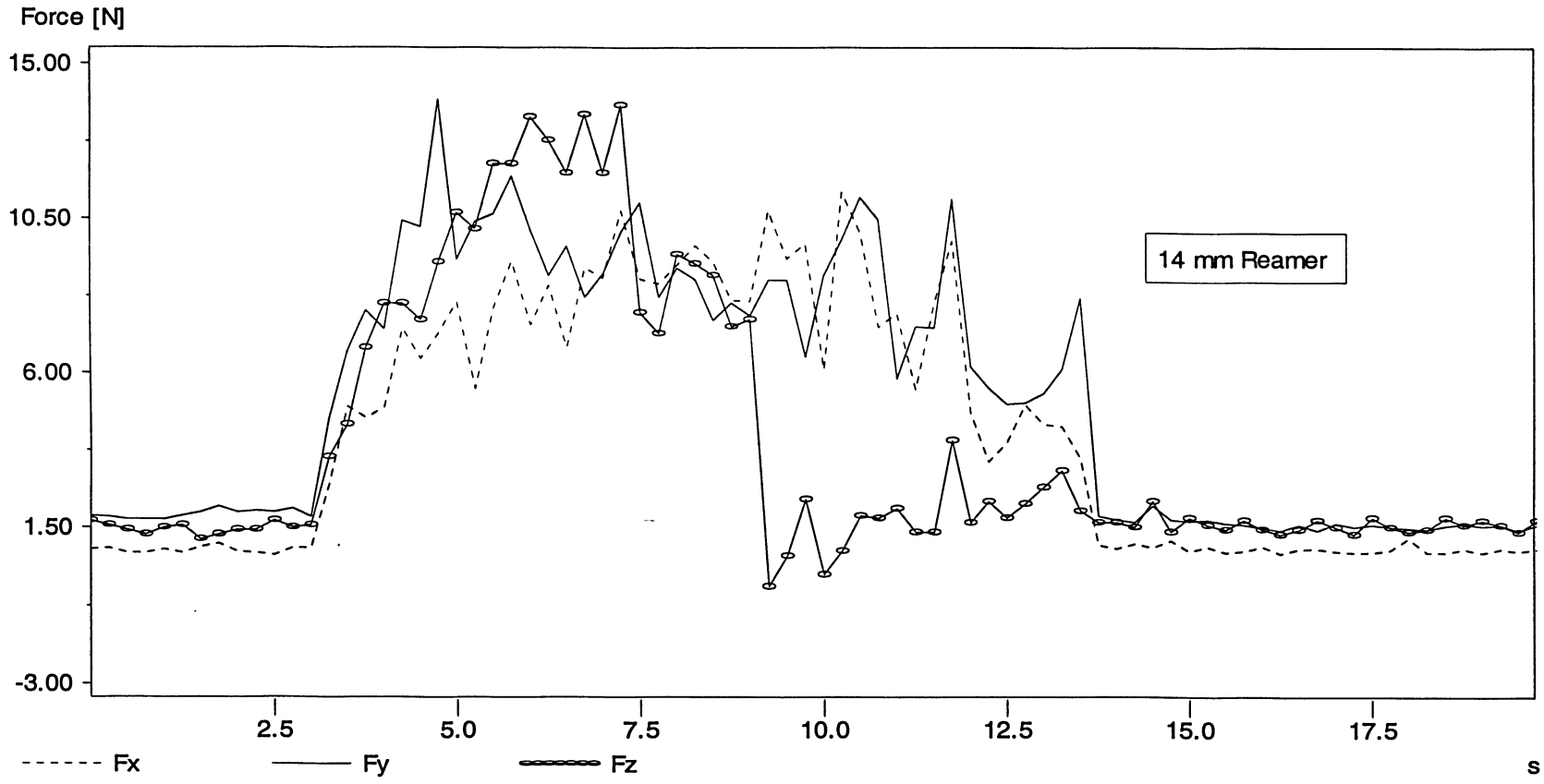

Figure D.84. Force profiles using 14 mm reamer, 200 RPM, 50 $\frac{mm}{sec}$ and 82.6 cP synthetic marrow viscosity. F_x, F_y and F_z are respectively corresponded to forces applied to the closed end of the bone in x, y, and z directions.

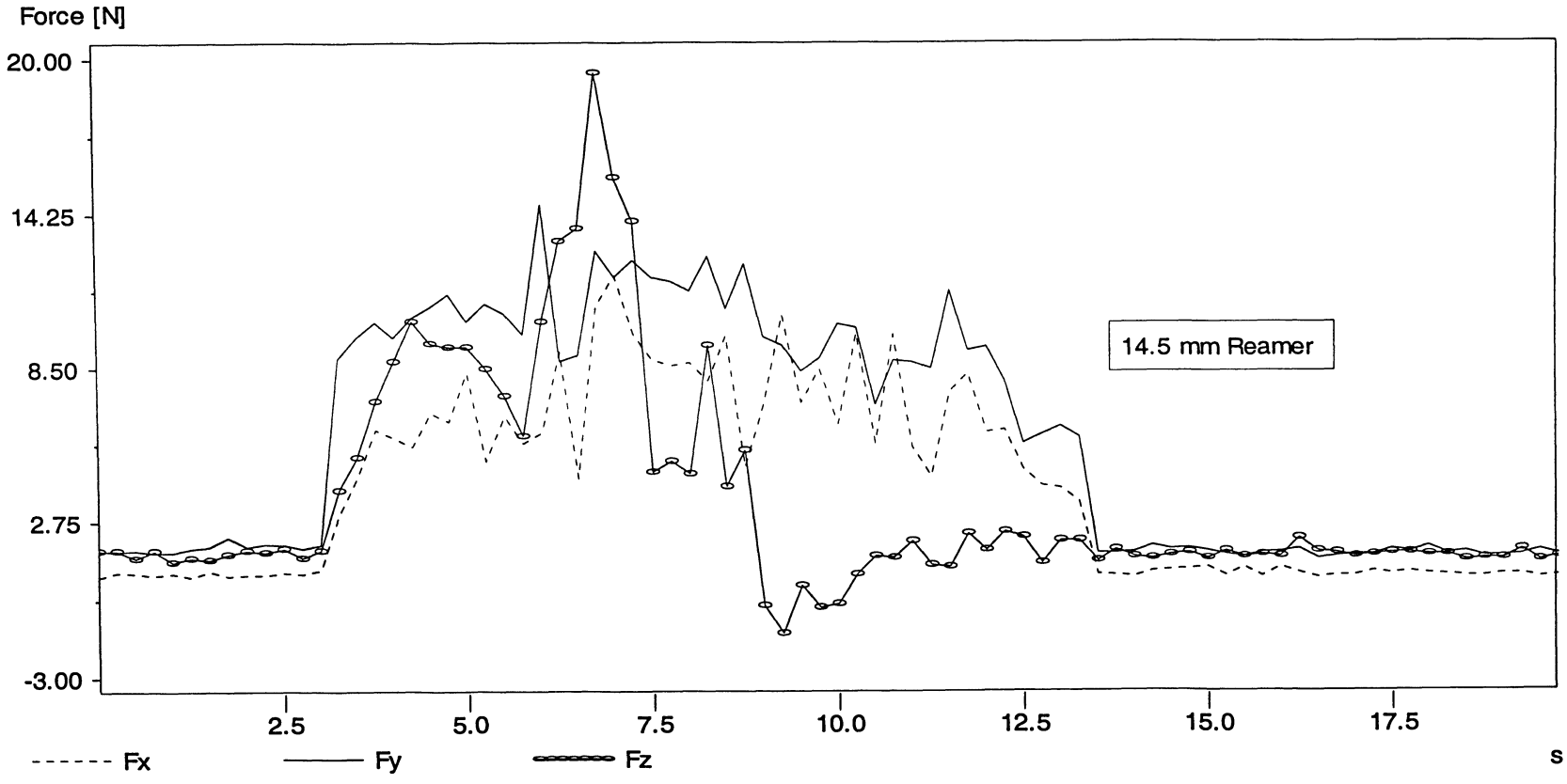

Figure D.85. Force profiles using 14.5 mm reamer, 200 RPM, 50 $\frac{mm}{sec}$ and 82.6 cP synthetic marrow viscosity. F_x, F_y and F_z are respectively corresponded to forces applied to the closed end of the bone in x, y, and z directions.

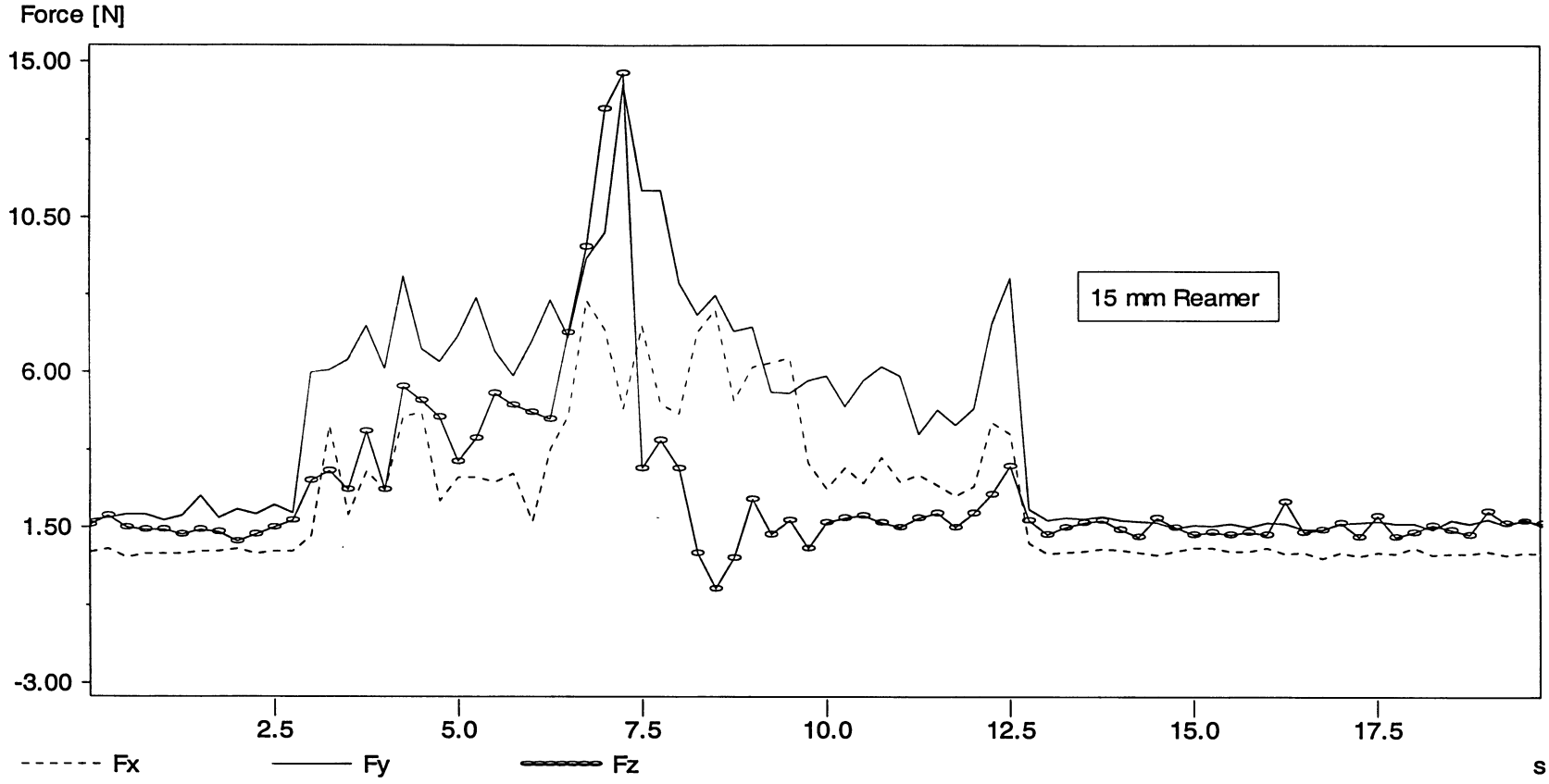

Figure D.86. Force profiles using 15 mm reamer, 200 RPM, 50 $\frac{mm}{sec}$ and 82.6 cP synthetic marrow viscosity. F_x, F_y and F_z are respectively corresponded to forces applied to the closed end of the bone in x, y, and z directions.

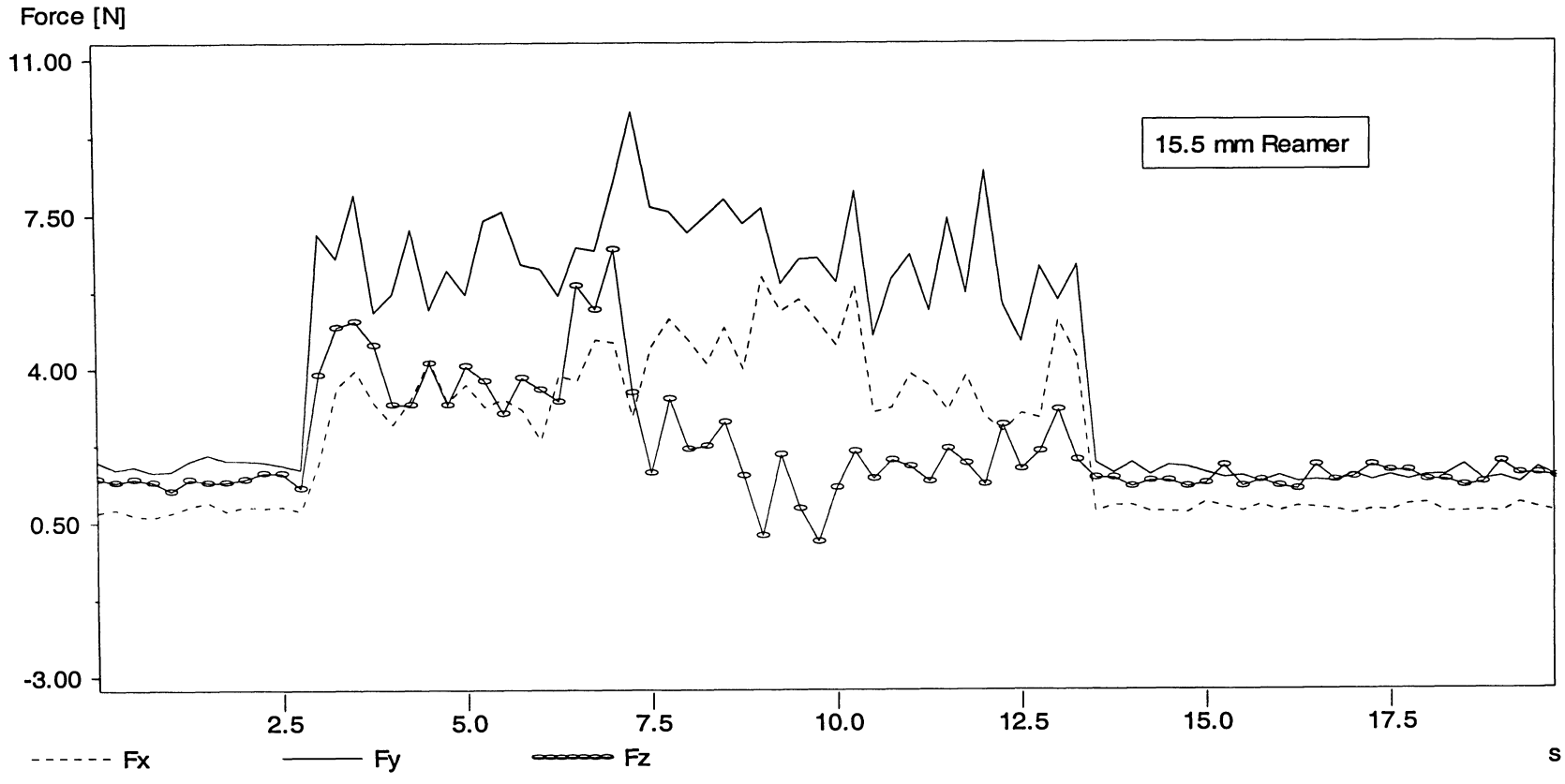

Figure D.87. Force profiles using 15.5 mm reamer, 200 RPM, 50 $\frac{mm}{sec}$ and 82.6 cP synthetic marrow viscosity. F_x, F_y and F_z are respectively corresponded to forces applied to the closed end of the bone in x, y, and z directions.

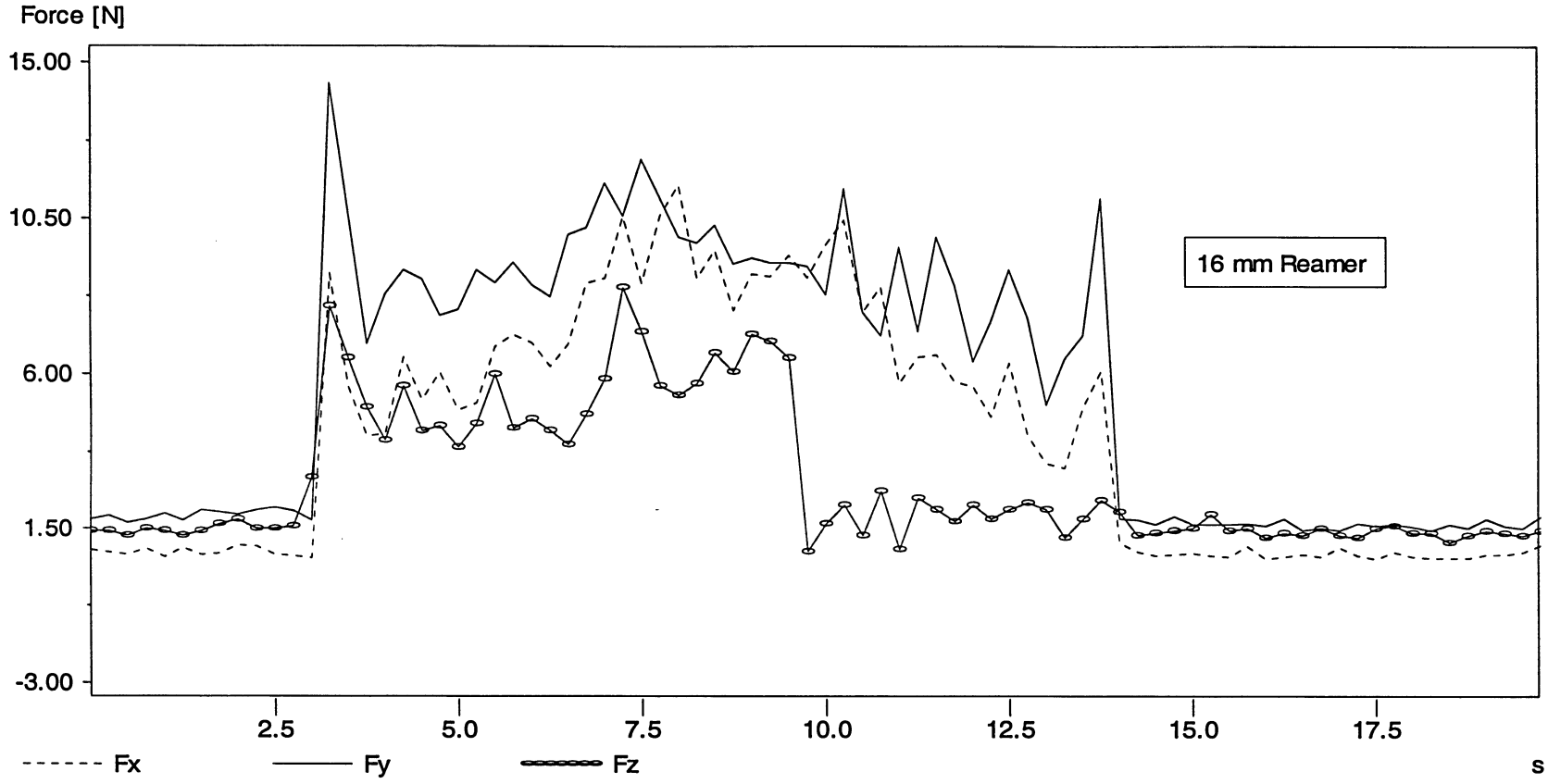

Figure D.88. Force profiles using 16mm reamer, 200 RPM, 50 $\frac{mm}{sec}$ and 82.6 cP synthetic marrow viscosity. F_x, F_y and F_z are respectively corresponded to forces applied to the closed end of the bone in x, y, and z directions.

Appendix E

Reamer Specifications

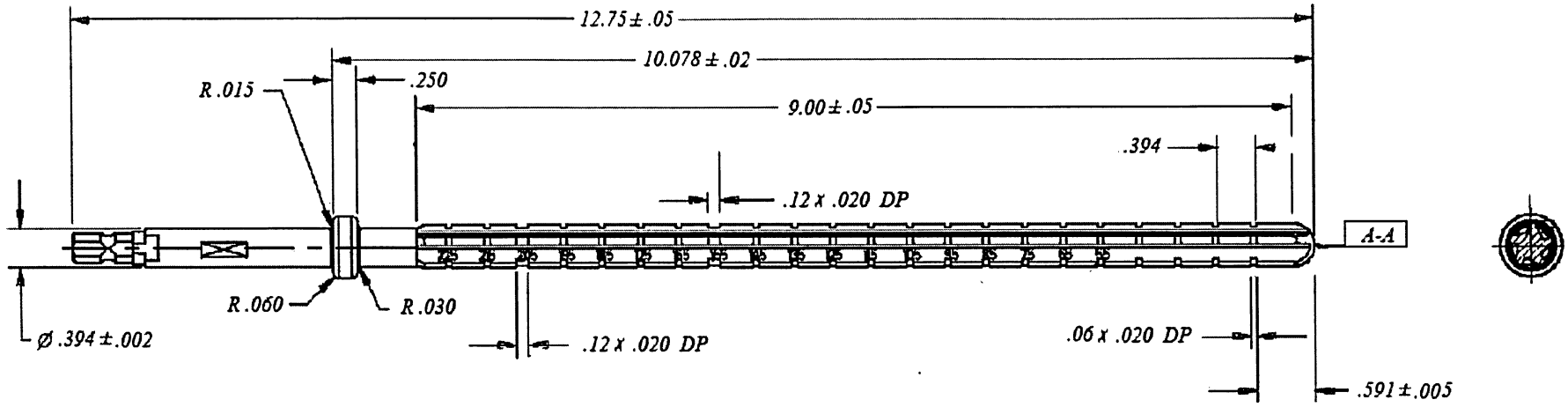

Reamer Size [mm]	A	B	F
12	0.472	0.166	0.6
12.5	0.492	0.173	0.7
13	0.511	0.180	0.7
13.5	0.531	0.187	0.7
14	0.551	0.194	0.7
14.5	0.571	0.201	0.8
15	0.590	0.208	0.8
15.5	0.610	0.215	0.8
16	0.630	0.222	0.8

Note: All dimensions are in inches, except otherwise mentioned.

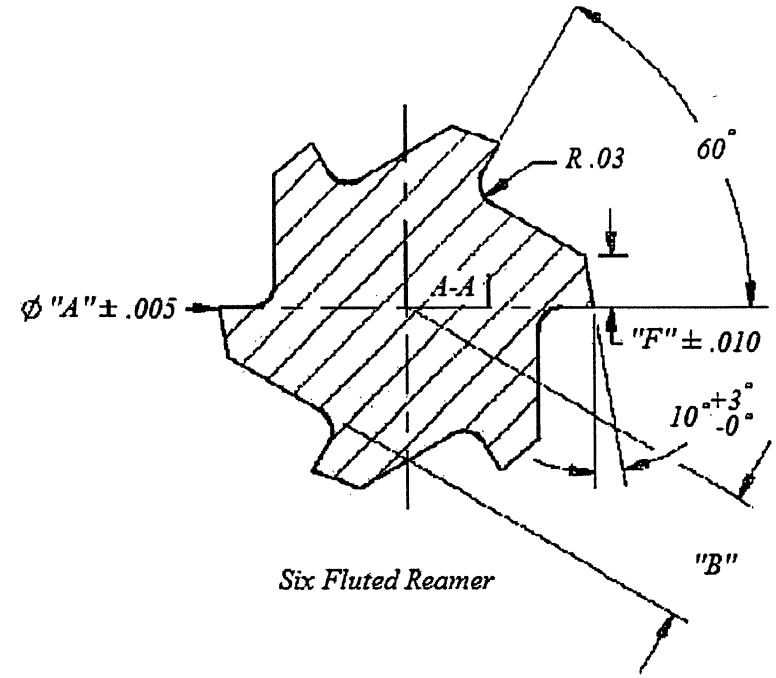

Six Fluted Reamer